Polarimetry In Radar Backscattering from Soil and Vegetated Surfaces

Tien-Hao Liao

A dissertation
submitted in partial fulfillment of the
requirement for the degree of

Doctor of Philosophy

University of Washington

2015

Reading Committee:
Leung Tsang, Chair
Akira Ishimaru
Thomas A. Cwik
Kung-Hau Ding

Program Authorized to Offer Degree:
Electrical Engineering

University of Washington

Abstract

Polarimetry In Radar Backscattering from Soil and Vegetated Surfaces

Tien-Hao Liao

Chair of the Supervisory Committee:
Professor Leung Tsang
Department of Electrical Engineering

The unique contributions of this thesis include (1) 3D numerical simulation using Maxwell Method (NMM3D) for soil surface for L-, C-, X-, and Ku-bands. (2) Multiple scattering models with cyclical correction for vegetated surface with large optical thickness and albedo (3) Simulate polarimetry SAR speckle using fully numerical method (NMM3D) for soil surface. (4) Combine NMM3D with distorted Born approximation to give coherency matrix for both polarimetry SAR and interferometric SAR.

The thesis starts with the large scale computation of rough surface for the interests increased in the earth observation using high frequency bands. The numerical methods shows the merits not only agrees the co- and cross-polarization backscatters but also acts as polarimetric SAR simulator to capture the radar speckle characteristics from soil. For the vegetation model, first we introduce the multiple scattering model which uses the scattering path to account trace the multiple scattering effects. Cyclical correction is applied to account the coherent addition at backscattering direction. Second, NMM3D is processed as coherency matrix and is combined with distorted Born approximation. The detail derivation is included for coherency matrix for both PolSAR and PolInSAR. Finally, cross-polarization and polarization ratio are validated with measurement data from SMAPVEX12 to address their importance for the focus of future study.

To my family

Acknowledgement

I would like to thank my advisor, Professor Leung Tsang for his supports during my Ph.D. program. He always told us, “Nature is very complicated”. To study remote sensing, one can easily get lost either in complicated models or in large amount of observation data. I am grateful that I have a great guider in this research field.

I also want to thank those who financially support me through my Ph.D. program. This includes research project from NASA Soil Moisture Active Passive mission and NASA Earth Observing System Simulator Suite Project funded within the Advanced Information System Technology program of NASA's Earth Science Technology Office. I also thank the electrical engineering department to offer me teaching assistantships for many quarters. I appreciate the chance of teaching and would like also thank those responses I got from my lovely students.

I also thank my lab colleagues to spend time discussing about the research. I would especially thank Xiaolan Xu, Shaowu Huang, and Shurun Tan. I really got many useful advises from them.

To my family, my mom, my dad, and my young brother, they are always the strongest support behind me. With their encouragement, I have no doubt to proceed my Ph.D. degree. I especially want to share the happiness with my grandfather who was a diligent farmer for his whole life. He always encouraged me to study as much as I can. I am sure he will the happiest man to know this news from top of the sky.

Finally, I would like to thank this beautiful city, Seattle. I love here in all respects. The sweet memory and revolutionary ideas I learned are going to be the treasure in my life.

Tien-Hao Liao

Seattle, Washington

June 2015

TABLE OF CONTENTS

List of Tables

List of Figures

Chapter 1

Introduction

SAR Polarimetry has become increasingly used for remote sensing of earth surfaces for monitoring water resources, forests, agriculture and natural disasters. Physical microwave scattering models are used to simulate the SAR polarimetric signatures and to study the microwave interactions with soil surfaces, vegetation and forests. In the past, the physical models and SAR simulators are based on simple analytical models and on assumed stochastic distributions of the signals. With the advancement of the computing technology such as NSR XSEDE, large scale computation is available to conduct full numerical simulation of Maxwell's equations. In this thesis, both numerical and theoretical study for land surface are included. This covers the fully numerical study of soil rough surface and vegetated surface.

In chapter 2, we extend 3D numerical method of Maxwell equation (NMM3D) for rough soil surface scattering to from L-band to C-, X-, and Ku-bands. NMM3D has been applied to L-band bare soil study as well as L-band satellite mission (NASA Soil Moisture Active Passive). Here we further apply the near field precondition to the speed up the computation. This will be useful as the surface gets rougher which requires more simulation time. Besides, large amount of measurement data from POLARSCAT were applied for the validation. We illustrate the results for co-polarization, cross-polarization, and polarization ratio (HH/VV). We single out the polarization ratio to address its importance to indicate the dependence over frequency.

In chapter 3, we demonstrate the radar backscattering study on vegetated surface. Beyond the distorted Born approximation, we further introduce the physical model to take into account the multiple scattering effects. The energy transport in a vegetation layer over the soil surface is examined by solving the vector radiative transfer equation using a numerical iterative approach. This approach allows a higher order that includes the multiple scattering effects. Multiple

scattering effects are important when the optical thickness and scattering albedo of the vegetation layer are large. When both the albedo and the optical thickness exceed 0.4, higher orders contribute significantly. Later, the model is applied to corn field and results are validated with SMAPVEX12 corn data. We also perform the soil moisture using pre-computed lookup table (called datacube in the thesis).

In chapter 4, we study the polarimetry SAR and interferometric SAR for soil and vegetated surface. Electromagnetic scattering from soil surfaces has stochastic fluctuations known as speckle because of the stochastic nature of rough surface heights. In simulating SAR signatures, we stochastically generate random rough surface and then we solve Maxwell equations numerically for each sample as we do in chapter 2. Scattering matrices ($S_{VV}, S_{HH}, S_{VH}, S_{HV}$) are computed. Various theoretical distributions are compared with results from NMM3D. We will show that numerical results from NMM3D is capable as being SAR simulator for soil surface. We then derive the coherency matrix and interferometric coherency matrix for Vegetated Surfaces using distorted Born approximation combined with NMM3D. The coherency matrix is the correlation of the scattered fields of different combinations of polarizations. The interferometric coherence is the correlation as weighted by the product of vertical structure function and the interferometric phase. With the coherency matrix from NMM3D, we combine it with distorted born approximation for volume scattering, double bounce, and surface scattering. Coherency matrix are then computed for these three scattering mechanisms for both PolSAR and PolInSAR. The polarimetric feature from coherency matrix is useful to classify the land surface and to retrieve geophysical parameters. The interferometric coherency matrix is capable to study the relation between the vegetation biomass and the interferogram. Finally, we show the validation with SMAPVEX12 data to address the importance of cross-polarizaiton and polarization ratio.

Chapter 2

Radar Backscatteirng of soil surface from L- to Ku-band

2.1 Basckscattering of rough surface

Radar remote sensing of land surfaces satellites are moving forward with rapid pace. These include Soil Moisture Active Passive (SMAP) [1][2] for L-band (1.26GHz) and Global Precipitation Measurement (GPM) for Ku-band (13.6GHz). Besides, there are L-band Advanced Land Observing Satellite-2 (ALOS2), C-band Radarsat2, X-band TerraSAR-X, TanDEM-X, Ku-band ISS-RapidScat, OuikSCAT and future L-band missions such as NI-SAR and TanDEM-L. For bare soils, rough surface creates backscattering as shown in Figure 2.1 that contains information of the soil moisture. For vegetated surface, rough soil surface underneath the canopy can provide either direct backscattering or strong reflection from vegetation (double bounce). For the study of backscattering from bare surface, there are empirical, analytical, and numerical models. For analytical models, small perturbation method (SPM) [3], small slope approximation (SSA) [4], and advanced integral equation method (AIEM) [5] are well-known and applied. For empirical model, there are Oh's empirical [6] and semi-empirical model [7] as well as Dubois model [8]. For numerical methods, there are method of moment (MoM) [9][10][11][12], stabilized extended boundary condition method (SEBCM) [13], finite element method (FEM) [14]. 3D Numerical Method of Maxwell equation (NMM3D) is 3D full-wave solutions of Maxwell's equations for rough surface using Monte-Carlo simulations. NMM3D was developed with hybrid UV/PBTG/SMCG method for parallel computing [12]. Results of NMM3D were shown in good agreement with POLARSCAT ground-based measurement for L-band soil surface application for both co-polarization and cross-polarization. It is also adopted in active algorithm in SMAP mission [11][12].

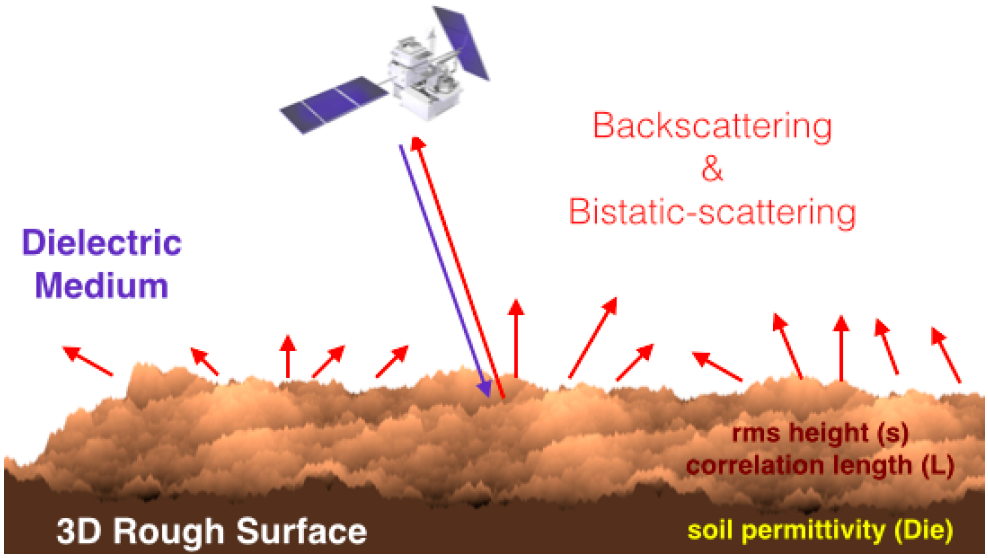

Figure 2.1 Radar backscattering and bistatic scatterin of dielectric rough surface

In previous study of NMM3D [12], there was detailed description about hybrid UV/PBTG/SMCG method including applying these methods for different regions in the MoM impedance matrix. Careful accuracy assessments were also conducted to assure the results are correct. These assessments include : (a) convergence test with discrete samplings (16 points and 32 points per wavelength) (b) convergence test against the number of realizations (up to 1000) (c) convergence test with respect to the size of sample surface(8 by 8 λ^2, 16 by 16 λ^2, and 32 by 32 λ^2) (d) energy conservation test for each realization (up to rms height = 0.336λ) (e) test of reciprocity (HV=VH) for each realization. Besides the accuracy assessments for the electromagnetic model itself, the results were compared with L-band POLARSCAT data ranging from 20 to 50 degrees. Both co-polarization and cross-polarization were in good agreement. Although the computation is intensive and was only run on supercomputing facilities such as NSF XSEDE (previous NSF TeraGrid), results were calculated only one time and transformed to look up table for further application. Lookup tables are used in the soil moisture retrieval by the SMAP mission: NMM3D lookup tables has been applied to time series retrieval for both bare soil and vegetated surface [15][16]. It is also used by the SMAP radar-only algorithm for soil moisture retrieval in vegetated surfaces including corn field, soybean field, wheat field, canola field, and grassland [17][18]. Coherent reflectivity was also calculated by NMM3D for double-bounce scattering for double-bounce scattering used in

vegetated surface model [11][18].

In this chapter parameters of NMM3D for characterizing rough soil surface such as rms height, correlation length, and soil permittivity (soil moisture) are obtained based on ground measurement data from various field campaigns since 1999. These data shown in table II gives us clear picture about reasonable input parameters for the model. In previous study [12], results were emphasized on L-band. Here the simulation and comparison is conducted for L-, C-, X-, and Ku-bands. At these frequencies backscattering coefficients are computed by various models and compared with one another. These comparisons include frequency dependence, incident angle dependence, and soil moisture dependence. For co-polarization comparison, NMM3D is compared with SPM 1st order, SSA, AIEM, and Oh's model. For cross-polarization comparison, NMM3D is compared with SPM 4th order, SSA, and Oh's model. For polarization ratio, HH/VV, the measurement data from POLARSCAT Data-1(L-, C-, X- bands) [6] is compared with backscatters from NMM3D as well as SPM 1st order, SSA, AIEM, and Oh's model to address the important feature of frequency dependence. Besides model comparison, model results are also validated with POLARSCAT measurement data for 1.25GHz, 4.75GHz and 9.5GHz for multiple incidence angle ranging from 20^o to 50^o.

The key advancement in this chapter is the enhancement of the computation speed for NMM3D. Based on the NMM3D with hybrid UV/PBTG/SMCG fast method, a physically-based near-field precondition is implemented to further improve computation efficiency. The physically-based near-field precondition matrix is applied to the impedance matrix without losing accuracy. Faster simulation is achieved consistently. Computation efficiency of cross-comparison is also presented for original and preconditioned NMM3D.

2.2 Numerical Maxwell's Method in 3D

NMM3D is the method of moment (MoM) based numerical method using Monte-Carlo simulation. For each realization, a unique height profile $z = f(x, y)$ from Gaussian random process is generated based on given rms height, correlation length, and correlation function.

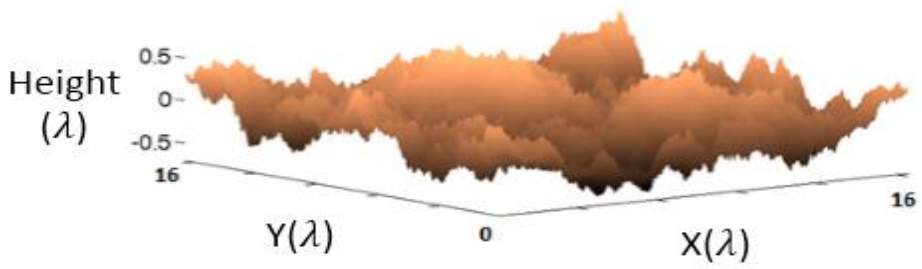

Figure 2.2 Computer generated 3D profiles for NMM3D simulation (Exponential correlation function)

Figure 2.2 shows the surface profile for exponential correlation function for 256 by 256 grid points with surface size of 16 by 16 λ^2. Exponential correlation function was applied for L-band rough surface model for NMM3D in previous study. In this study, exponential correlation function is applied for NMM3D as well as for other models. With the surface height profile, a two dielectric problem known as Poggio-Miller-Chang-Harrington-Wu (PMCHW) [19] is shown in integral forms in (2.1)-(2.5). The Rao-Wilton-Glisson (RWG) basis function and the Galerkin's method are applied to discretize the surface integral equation. A tapered plane wave is used to avoid diffraction from the edge of a finite-size surface [11].

$$\hat{n} \times (L_1 + L_2)\bar{J}_s(\bar{r}) - \hat{n} \times (K_1 + K_2)\bar{M}_s(\bar{r}) = \hat{n} \times \bar{E}_i(\bar{r}) \tag{2.1}$$

$$\hat{n} \times (K_1 + K_2)\bar{J}_s(\bar{r}) + \hat{n} \times \left(\frac{1}{\eta_1^2}L_1 + \frac{1}{\eta_2^2}L_2\right)\bar{M}_s(\bar{r}) = \hat{n} \times \bar{H}_i(\bar{r}) \tag{2.2}$$

$$L_\varsigma \bar{X}(\bar{r}) = \int_S ds' \left[-i\omega\mu_\varsigma \bar{X}(\bar{r}') - \frac{i}{\omega\mu_\varsigma}\nabla\nabla' \cdot \bar{X}(\bar{r}')\right] g_\varsigma(\bar{r}, \bar{r}') \tag{2.3}$$

$$K_\varsigma \bar{X}(\bar{r}) = \int_S ds' \left[\bar{X}(\bar{r}') \times \nabla g_\varsigma(\bar{r}, \bar{r}')\right] \tag{2.4}$$

$$g_\varsigma(\bar{r}, \bar{r}') = \frac{e^{ik_\varsigma|\bar{r}-\bar{r}'|}}{4\pi|\bar{r}-\bar{r}'|} \tag{2.5}$$

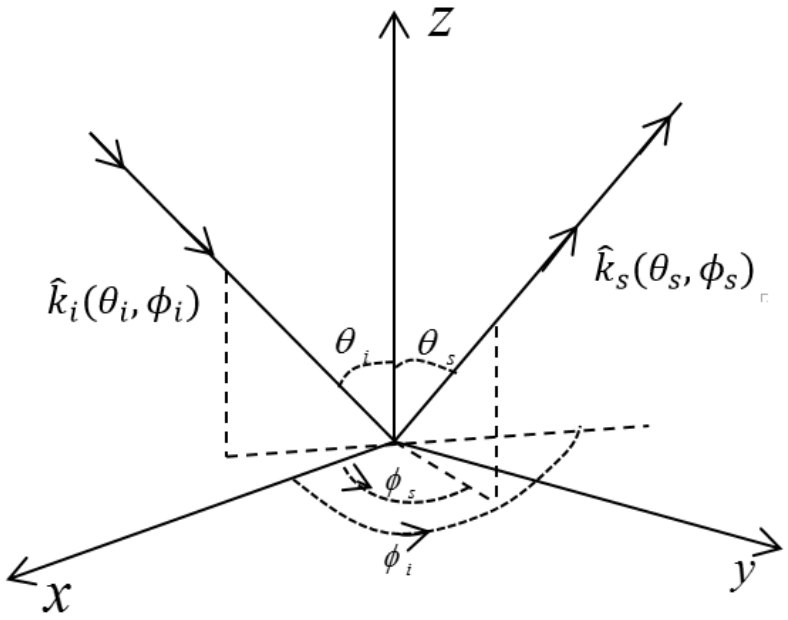

Figure 2.3 Definition of bistatic scattering of rough surface with incident direction (θ_i, ϕ_i) and scattering direction (θ_s, ϕ_s)

Figure 2.3 shows the incident and scattering angles with wave vector $\hat{k}_i(\theta_i, \varphi_i)$ and $\hat{k}_s(\theta_s, \varphi_s)$. θ_i and φ_i are elevation and azimuthal angles for the incident wave. θ_s and φ_s are elevation and azimuthal angles for the scattered wave. The equations are also shown in (2.6) and (2.7).

$$\hat{k}_i(\theta_i, \varphi_i) = sin\theta_i cos\varphi_i \hat{x} + sin\theta_i sin\varphi_i \hat{y} - cos\theta_i \hat{z} \tag{2.6}$$

$$\hat{k}_s(\theta_s, \varphi_s) = sin\theta_s cos\varphi_s \hat{x} + sin\theta_s sin\varphi_s \hat{y} + cos\theta_s \hat{z} \tag{2.7}$$

Bistatic scattering coefficient is determined in (2.8) by incident and scattered electric fields. Then it is decomposed into coherent and incoherent components as shown in (2.9) [11]. After the subtraction of coherent component, bistatic scattering coefficient, $\gamma_{\beta\alpha}^{incoh}(\theta_s, \varphi_s; \theta_i, \varphi_i)$, is shown in (2.10) for incident α-polarized and scattered β-polarized wave based on computed incoherent electric field, $E_{\beta\alpha,n}^{incoh}(\theta_s, \varphi_s; \theta_i, \varphi_i)$, from each realization. N stands for number of total realizations and P_α^i stands for incident power of α-polarized wave. The multiplication of $cos\theta_i$ and $\gamma_{\beta\alpha}^{incoh}(\theta_s, \varphi_s; \theta_i, \varphi_i)$ gives scattering cross section. Eq. (2.11) shows scattering cross section at backscattering direction.

$$\gamma_{\beta\alpha}(\theta_s,\varphi_s;\theta_i,\varphi_i)=\lim_{r\to\infty}\frac{4\pi r^2\left|E_\beta^s\right|^2}{\left|E_\alpha^i\right|^2 A cos\theta_i} \tag{2.8}$$

$$\gamma_{\beta\alpha}(\theta_s,\varphi_s;\theta_i,\varphi_i)=\gamma_{\beta\alpha}^{coh}(\theta_s,\varphi_s;\theta_i,\varphi_i)+\gamma_{\beta\alpha}^{incoh}(\theta_s,\varphi_s;\theta_i,\varphi_i) \tag{2.9}$$

$$\gamma_{\beta\alpha}^{incoh}(\theta_s,\varphi_s;\theta_i,\varphi_i)=\frac{1}{N}\frac{1}{2\eta P_\alpha^i}\sum_{n=1}^{N}\left|E_{\beta\alpha,n}^{incoh}(\theta_s,\varphi_s;\theta_i,\varphi_i)\right|^2 \tag{2.10}$$

$$\sigma_{\beta\alpha}(\theta_i,\phi_i)=cos\theta_i\gamma_{\beta\alpha}^{incoh}(\theta_i,\pi+\varphi_i;\theta_i,\varphi_i) \tag{2.11}$$

For the impedance matrix of NMM3D, a different fast method is applied based on interaction strength shown in Figure 2.4. For the strong interaction, close to diagonal, MoM is applied directly and the impedance matrix elements which consumes most memory are saved. For intermediate interaction, next to diagonal, interpolation Green's function method is applied. For weak interaction, far from diagonal, sparse matrix canonical grid (SMCG) is applied by using fast Fourier transform (FFT). The boundaries of these three regions are adjustable to balance the results accuracy and memory efficiency.

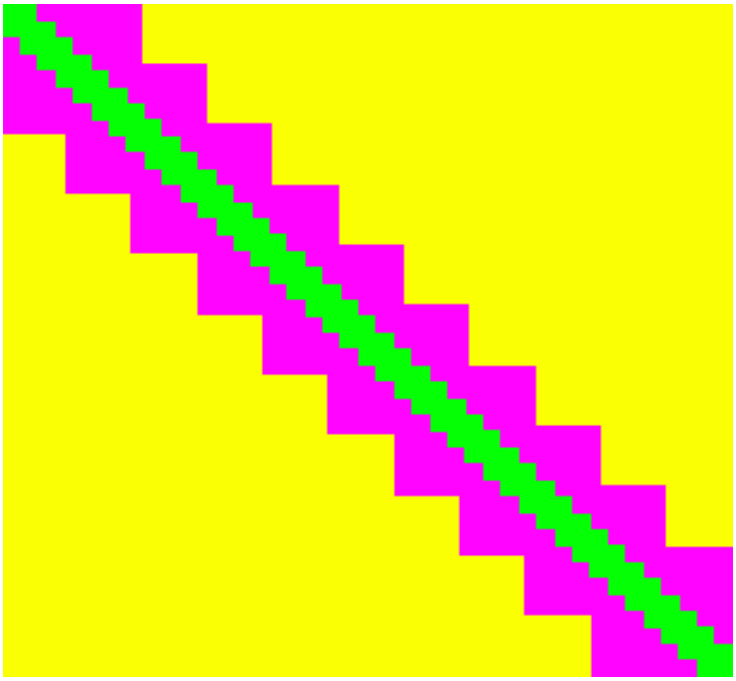

Figure 2.4 Strong, intermediate, and weak interaction regions from diagonal to off-diagonal for impedance matrix of NMM3D

2.3 Near field precondition of NMM3D

In NMM3D, the computation efficiency is improved through significantly reducing the CPU time needed for a single iteration. However, for the rougher surface it still takes more iterations for generalized minimal residual method (GMRES) to converge compared to the smooth surface. This results in longer simulation time. To further speed up the computation, near-field precondition is introduced to NMM3D. Naenna and Johnson [20] have studied physical-based preconditioner for MoM in 2D scattering problem for rough surface and it shows large reduction of iterations for surface with large rms height. This suggests that it might be applied well also in 3D scattering problem of rough surface as we are doing with NMM3D.

In this study, the physical-based precondition is implemented for NMM3D and it is compatible with existed fast method. Near-field precondition is based on physical behaviors of electromagnetic field [21]. In (2.1) and (2.2), Poggio-Miller-Chang-Harrington-Wu (PMCHW) equation is written in terms of tangential electric and magnetic fields. Due to the loss in dielectric medium, both electric and magnetic fields exponentially decay with the distance between source and observation points. The closer the distance the stronger interaction on the fields. This suggests us that the distance-related matrix could be a preconditioner. Besides, NMM3D has regular and finer meshes, 16 or 32 points per wavelength, which will include numerous interactions by basis function pairs within one wavelength. For the above reasons, near-field precondition is capable to be applied to NMM3D, in particular to solve the rough surface scattering problem. We list the steps to apply near field precondition to NMM3D as follows. We also explain how to implement it in parallel computing.

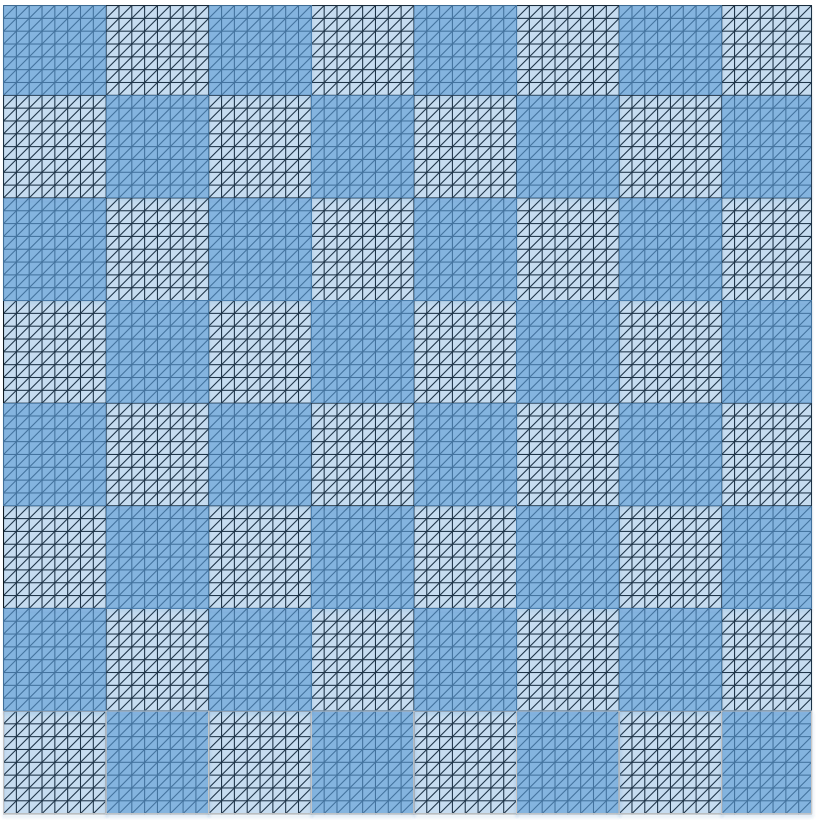

Figure 2.5 RWG meshes in blocks. This example case shows 64 by 64 grid points and 8 by 8 grid points in one block.

Figure 2.5 shows RWG meshes for $4\lambda \times 4\lambda$ of surface size with 16 points per wavelength in NMM3D. 8 by 8 grid points are grouped in blocks for parallelization. In NMM3D, the calculation related to one block is assigned to one processor in parallel computing. For a given grid point in a block (reference grid point), near field region is specified in both x and y direction for grid points within Nfp grids as shown in Figure 2.6. e.g. We take Nfp=4 for the case of 16 points per wavelength to do precondition. This is about quarter wavelength. Edges related to grid points in near field region are considered for near field interaction. In Figure 2.6 two cases for near field region are shown. Figure 2.6a is the general case and Figure 2.6b is a special case for reference grid point close to boundary that results in smaller near field region.

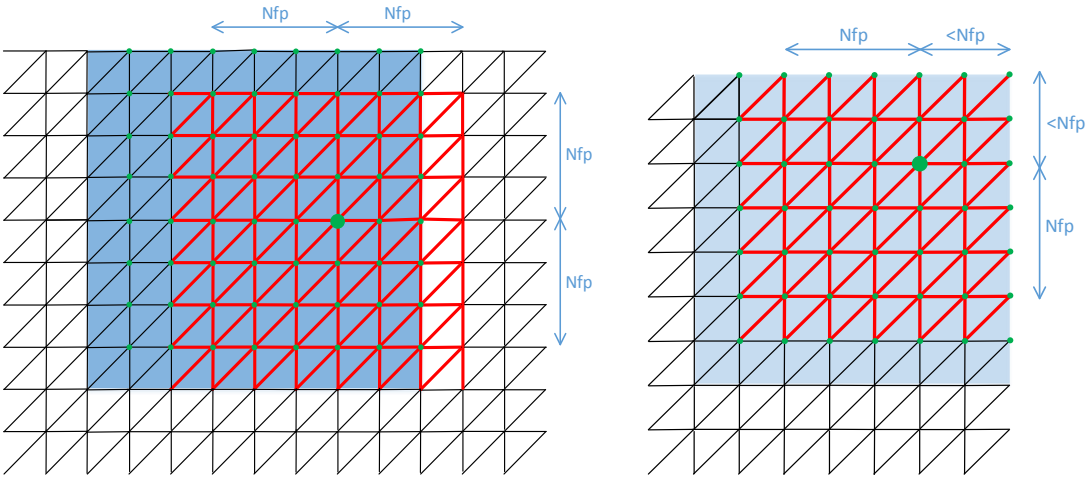

(a) (b)

Figure 2.6 Near field interaction range w.r.t. one reference grid point within one block. Green dots show reference grid points in the block. Red edge shows basis functions within near field region. Nfp shows near field region size. (a) general case (b) example case for block close or along boundary

$$L_\zeta^g(m,n) = \sum_{p=1}^{2}\sum_{q=1}^{2} \int_{T_m^p} \int_{T_n^q} - ik_\zeta \eta_\zeta \left[\frac{l_m}{2A_m^p} \bar{\rho}_m^{-p} \cdot \frac{l_n}{2A_n^q} \bar{\rho}_n^{-q} + \frac{(-1)^{p+q}}{i^2 k_\zeta^2} \frac{l_m}{A_m^p} \frac{l_n}{A_n^q} \right] g_\zeta(\bar{r}, \bar{r}') ds' ds \quad (2.12)$$

$$K_\zeta^g(m,n) = \sum_{p=1}^{2}\sum_{q=1}^{2} \int_{T_m^p} \int_{T_n^q} - \left[\left(\frac{l_m}{2A_m^p} \bar{\rho}_m^{-p} \times \bar{r} \right) \cdot \frac{l_n}{2A_n^q} \bar{\rho}_n^{-q} + \frac{l_m}{2A_m^p} \bar{\rho}_m^{-p} \cdot \left(\frac{l_n}{2A_n^q} \bar{\rho}_n^{-q} \times \bar{r}' \right) \right] G_\zeta(\bar{r}, \bar{r}') ds' ds \quad (2.13)$$

$$G_\zeta(\bar{r}, \bar{r}') = \frac{\left(ik_\zeta |\bar{r} - \bar{r}'| - 1 \right)}{4\pi |\bar{r} - \bar{r}'|^3} e^{ik_\zeta |\bar{r} - \bar{r}'|} \quad (2.14)$$

For each grid point, we compute the interaction among pairs of edges by (2.12) and (2.13). This calculation is the same as those done in strong interaction region. A block matrix for near field region is then formed as (2.15) with matrix size much less than original impedance matrix.

$$\bar{\bar{B}}^g = \begin{bmatrix} \bar{\bar{L}}_1^g + \bar{\bar{L}}_2^g & -\left(\bar{\bar{K}}_1^g + \bar{\bar{K}}_2^g\right) \\ \bar{\bar{K}}_1^g + \bar{\bar{K}}_2^g & \frac{1}{\eta_1^2}\bar{\bar{L}}_1^g + \frac{1}{\eta_2^2}\bar{\bar{L}}_2^g \end{bmatrix} \tag{2.15}$$

The block matrix is then inversed as (2.16). Since the matrix is small, the inversion process can be done quickly. However, the block-wise quasi-symmetrical property for the original block matrix does not exist after inversion. The inversed block matrix is then mapped back to the location in the original impedance matrix as shown in (2.17)-(2.19).

$$\bar{\bar{Q}}^g = \left[\bar{\bar{B}}^g\right]^{-1} \tag{2.16}$$

$$\bar{\bar{Q}}^g = \begin{bmatrix} \bar{\bar{Q}}_{11}^g & \bar{\bar{Q}}_{12}^g \\ \bar{\bar{Q}}_{21}^g & \bar{\bar{Q}}_{22}^g \end{bmatrix} \tag{2.17}$$

$$R_{ij}^{g(s,t)}(m_{g(s,t)}, n_{g(s,t)}) = Q_{ij}^g(m,n) \tag{2.18}$$

$$R_{ij}^{g_b(s,t)}(m_{g_b(s,t)}, n_{g_b(s,t)}) = Q_{ij}^g(m,n) \tag{2.19}$$

For each reference grid point, there is one inversed block matrix. The contribution from all reference grid points are later summed up. Eq. (2.20) shows the summation of all the blocks. Finally, a sparse matrix is generated for the preconditioner as (2.21). Only one-time computation of the preconditioner is needed for both vertical and horizontal incidences in one realization. e.g. We consider 8 by 8 grid points for one block. NA8 stands for block number in x direction, so does NB8 for y direction. NG is the total number of grid points in one block, 64 for typical case.

$$\bar{\bar{N}}_{ij} = \sum_{s=1}^{NB8}\sum_{t=1}^{NA8}\sum_{b=1}^{NG} \bar{\bar{R}}_{ij}^{g_b(s,t)} \tag{2.20}$$

$$\bar{\bar{N}} = \begin{bmatrix} \bar{\bar{N}}_{11} & \bar{\bar{N}}_{12} \\ \bar{\bar{N}}_{21} & \bar{\bar{N}}_{22} \end{bmatrix} \tag{2.21}$$

$\bar{\bar{N}}$ is applied to the original MoM matrix equation as (2.22).

$$\bar{\bar{N}}\bar{\bar{Z}}\bar{I} = \bar{\bar{N}}\bar{V} \tag{2.22}$$

Since $\bar{\bar{N}}$ is sparse matrix, the computation of $\bar{\bar{N}}\bar{\bar{Z}}$ and $\bar{\bar{N}}\bar{V}$ is in order O(N). Let $\bar{\bar{Z}}' = \bar{\bar{N}}\bar{\bar{Z}}$ and $\bar{V}' = \bar{\bar{N}}\bar{V}$. Then GMRES iterative solver is applied to (2.23). Since $\bar{\bar{Z}}'$ has much smaller condition number than $\bar{\bar{Z}}$, it converges much faster.

$$\bar{\bar{Z}}'\bar{I} = \bar{V}' \tag{2.23}$$

Table 2.1

Computer efficiency comparison : 256 processors, 16λ by 16λ, 16 points/λ, 40^o incidence, rms height=0.084λ, correlation length=0.84λ, dielectric constat=30+4.5i, NMM3D (run on Kraken XT5 2.6GHz), preconditioned NMM3D(run on Stampede 2.7GHz

	NMM3D	Preconditioned NMM3D
0.01 residual for V-pol	263 iterations	12 iterations
Time for one realization	12min	2.5min
Memory per processor	0.676GBytes	0.402GBytes

In Table 2.1, the comparison is shown for surface size of 16 by $16\lambda^2$ with 16 points per wavelength. With the precondition, it takes only 12 iterations to converge for V-polarized incidence. The convergence is more than 20 times faster than that without precondition, which requires 263 iterations. For a single realization, preconditioned case is close to 5 times faster.

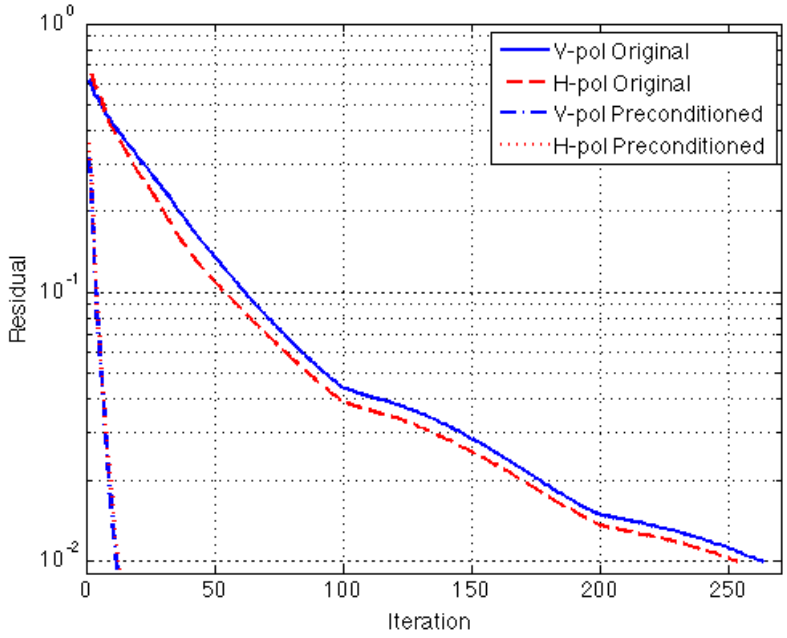

Figure 2.7 Comparison of iterations required to achieve 10^{-2} residual, detailed parameters in Table 2.1

In Figure 2.7, it is obvious that how the solutions converge for both.

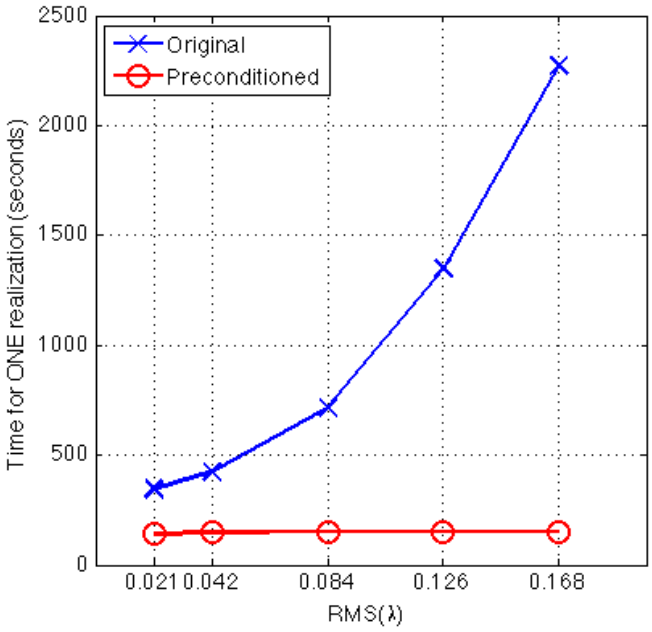

Figure 2.8 Comparison of simulation time for one realization, correlation length to rms height ratio = 10, rest parameters are the same as in Table 2.1

In Figure 2.8, simulation time for one realization is shown by varying rms height with fixed correlation to rms height ratio. The preconditioned case gives the same simulation time, independent of rms height change. In contrast, the simulation time of original NMM3D increases with rms height. For instance, when rms height is equal to 0.168λ, preconditioned case is more than 10 times faster. Thus, the preconditioner is critical for solving problem with larger surface roughness. In Figure 2.9, emissivity for the same variation is computed to show the results are consistent for both.

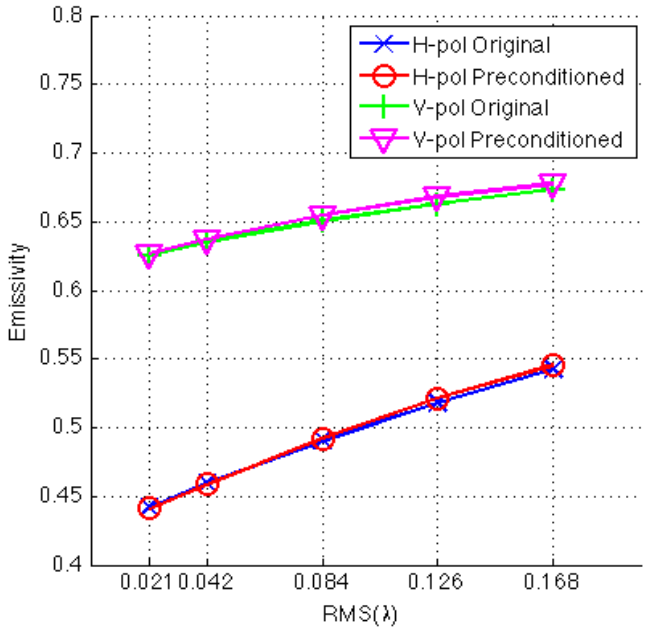

Figure 2.9 Comparison of emissivity. Correlation length to rms height ratio = 10, rest parameters are the same as in Table 2.1

2.4 Physical Parameters of Rough Soil Surface

For modeling rough soil surface, the primary input parameters are rms height, correlation length, and soil permittivity. For soil permittivity, the measurement is usually done for soil moisture instead. For a given frequency and soil texture, the relationship between soil moisture and soil permittivity can be determined by the empirical 'dielectric' model such as Mironov's model [22] In this thesis, we will also apply it to calculate soil permittivity. Since 1999, many field campaigns have been conducted for vegetated surfaces to collect vegetation biomass data as well as soil surface data. They are Southern Great Plain (SGP99), Soil Moisture Experiment in 2002 (SMEX02), Cloud and Land Surface Interaction Campaign in 2007 (CLASIC07), SMAP Validation Experiment 2008 (SMAPVEX08), and SMAPVEX12. Large amount of data were collected, including rms height, correlation length, soil moisture, and soil texture. 112 fields are picked up here from vegetated surface and are listed in Table 2.2.

Table 2.2

Physical parameter from field campaigns

s(cm)	#	L(cm)	#	L/s	#	Clay fraction	#	Soil Moisture (cm^3/cm^3)	#
<0.5	**10**	<5	**6**	<5	**2**	<0.1	**15**	<0.1	**112**
0.5~1	**63**	5~10	**51**	5~10	**32**	0.1~0.2	**38**	0.1~0.2	**351**
1~1.5	**31**	10~20	**38**	10~20	**57**	0.2~0.3	**32**	0.2~0.3	**496**
1.5~2	**8**	20~30	**8**	20~30	**11**	0.3~0.5	**10**	0.3~0.4	**151**
>2	**0**	>30	**9**	>30	**10**	>0.5	**17**	>0.4	**52**

# denotes number of data. s for rms height and L for correlation length

Since mostly rough surface is applied with canopy on top rather than alone, these data shows practical input parameter range how we will apply them into the model. In Table 2.2, each physical parameter is listed in 5 groups. Clay fraction is listed as it is required for Mironov's model. For soil moisture, there are overall 1162 measured data in these 112 fields. Rms height varies mostly between 0.5cm and 1.5cm and correlation length varies mostly between 5cm and 20cm. However, instead of applying correlation length, correlation length to rms height ratio is considered. The ratio varies mostly between 5 and 20. The clay fraction varies mostly between 0.1 and 0.3. For soil moisture, it varies mostly between 0.1 and $0.4 cm^3/cm^3$. Soil moisture and soil dielectric constant mapping conducted in this study is shown in Table 2.3 for 5.4GHz, 9.65GHz, 13.4GHz with soil moisture from 0.15 to 0.5 cm^3/cm^3. In addition to physical parameters, correlation function is also important. In L-band, exponential correlation function is applied well as shown in previous NMM3D validation [12]. In this study, exponential correlation function is also applied for analytical and numerical model except small slope approximation (SSA) and small perturbation method up to 4^{th} order (SPM 4^{th}). For these two, they are implemented with modified exponential correlation function instead.

Table 2.3

Dielectric constant for soil (clay fraction = 0.3)

Soil Moisture	5.4 GH	9.65 GHz	13.4 GHz
0.15	6.2+1.16i	5.72+1.56i	5.29+1.73i
0.2	8.54+1.78i	7.78+2.44i	7.1+2.74i
0.3	14.33+3.4i	12.85+4.74i	11.49+5.36i
0.4	21.6+5.51i	19.18+7.75i	16.92+8.8i
0.5	30.36+8.12i	26.75+11.48i	23.37+13.04i

2.5 Experimental Results and Analysis

2.5.1 Backscatters of Co-polarization and Cross-polarization

In this section, co- and cross-polarization of NMM3D results are compared with those from the other models for C-, X-, and Ku-bands. L-band comparison has been done extensively in previous study[11][12], so we focus on higher frequencies. Models include SPM [3], SSA [4], advanced integral equation method (AIEM) [5], and Oh's empirical model[6]. For SPM, we apply SPM 1st order for co-polarization, VV and HH. However to account for cross-polarization we need to apply higher order SPM since cross-polarization is not provided in 1st order. SPM is applied from 2nd up to 4th order only for the cross-polarization. Higher orders, up to 4, contribute very little to co-polarization, so SPM 1st order is considered for co-polarization. SPM could be applied to relatively smooth surface, rms height smaller than $\lambda/8\cos\theta_i$. AIEM is previously studied up to $k\sigma = 5.13$ for Gaussian correlated surface.[5] SSA could be applied for large rms height as long as slope is small. For Oh's empirical model, it is based on POLARSCAT data-1 measurement, including sites with rms height from 0.32cm to 3.02cm for L,C,X bands. In this study, the range mentioned above for analytical methods is less important. Cross-comparison of models are more important as well as how close the results to the measurement. For this reason, Oh's model is treated most of the time as reference in this study.

The surface size for NMM3D considered in these comparisons is 16 by 16 squared wavelength (λ^2) with 16 points per wavelength. Preconditioned NMM3D is applied. We run NMM3D with 256 CPU cores on NSF Extreme Science and Engineering Discovery Environment (XSEDE) clusters.

This includes TACC Stampede (2.7GHz Xeon E5-2680) and NICS Darter (2.6GHz Xeon E5-2600). Up to 50 realizations were simulated for each case.

For co-polarization comparison, NMM3D with SPM 1st order, SSA, AIEM, and Oh's model were compared. For cross-polarization, NMM3D with SPM 4th, SSA, and Oh's model were compared. Among these models, Oh's model is treated as reference as it is constructed based on L, C, X band measurement for incident angle from 10 to 70 degrees.[6] By comparing co- and cross-polarization results with Oh's model, it shows how good these models predict the backscattering. For Ku-band, Oh's model is also applied for quick comparison as the extension, however this should be less emphasized.

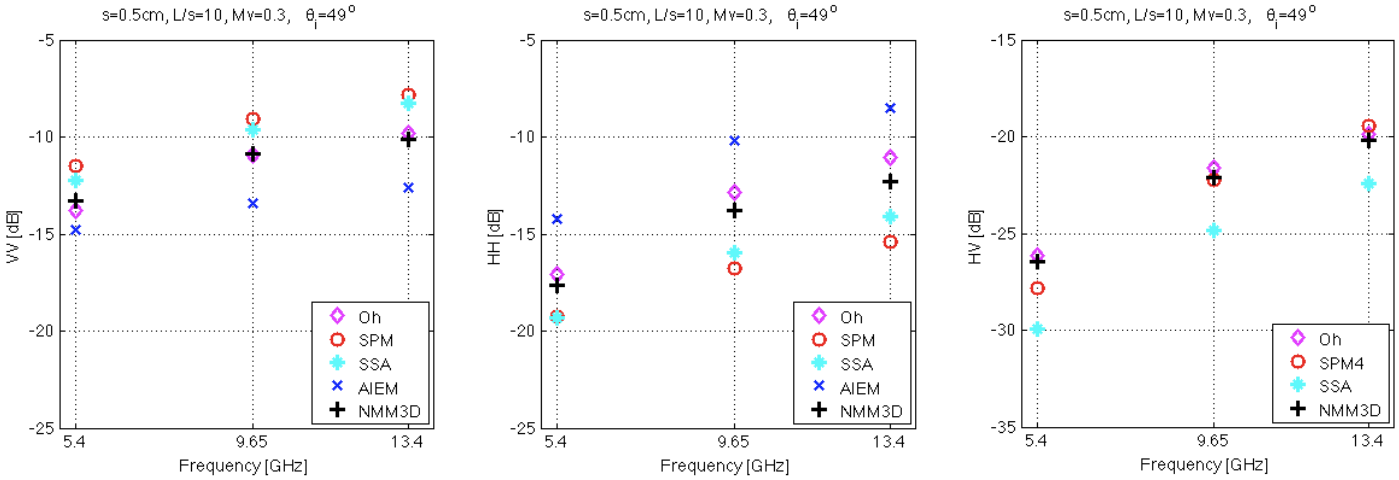

Figure 2.10 Frequency dependence of co- and cross-polarization from 5.4GHz to 13.4GHz (s=0.5cm, L/s=10, mv=0.3, $\theta_i = 49^o$)

In Figure 2.10, frequency dependence of VV, HH, and HV are shown for 49 degrees. 49 degree incidence is covered by C-band Radarsat-2($29^o \sim 50^o$), X-band TerraSAR-X($20^o \sim 55^o$), and Ku-band ISS-RapidScat(49^o). Surface rms height is 0.5cm with correlation length to rms height ratio equal to 10. Results from NMM3D stay close to those from Oh's model for both co- and cross-polarization. HH and HV show larger dynamic range, about 5 to 7dB, than VV, about 3dB. Meanwhile, AIEM shows different trend from SSA and SPM for VV and HH. All three stay away from results from Oh's model.

In Figure 2.11, it shows soil moisture dependence of VV, HH, and HV, for C, X, and Ku bands.

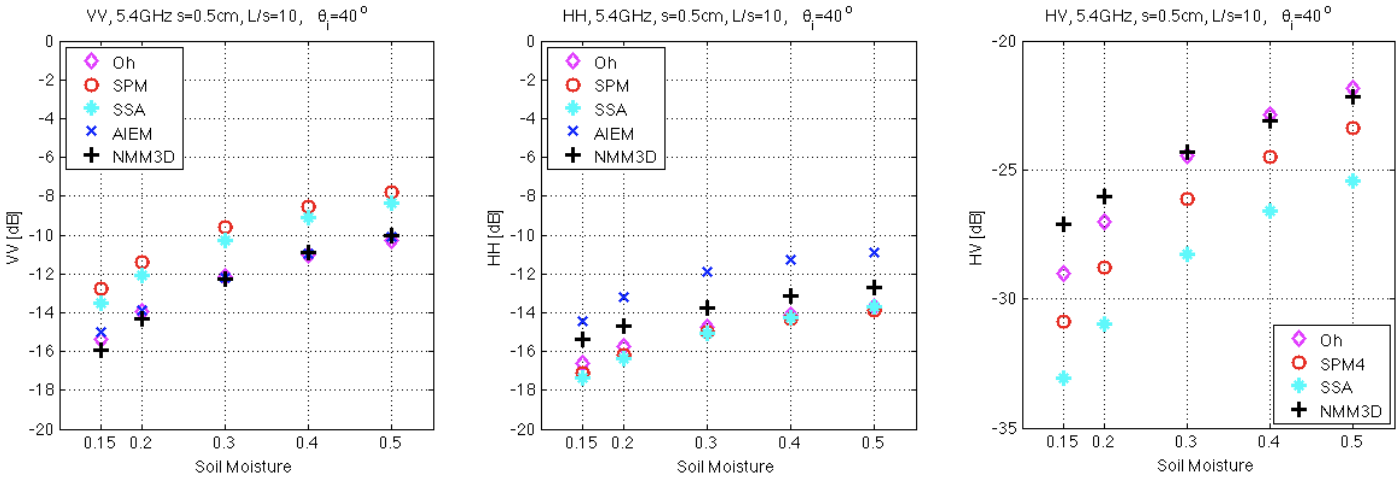

(a)

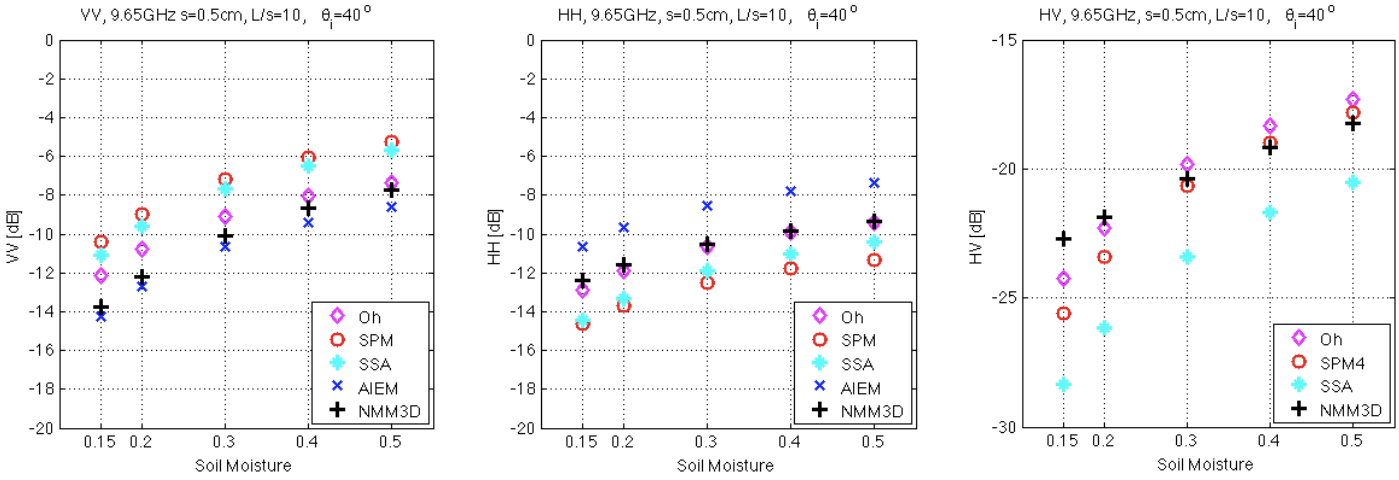

(b)

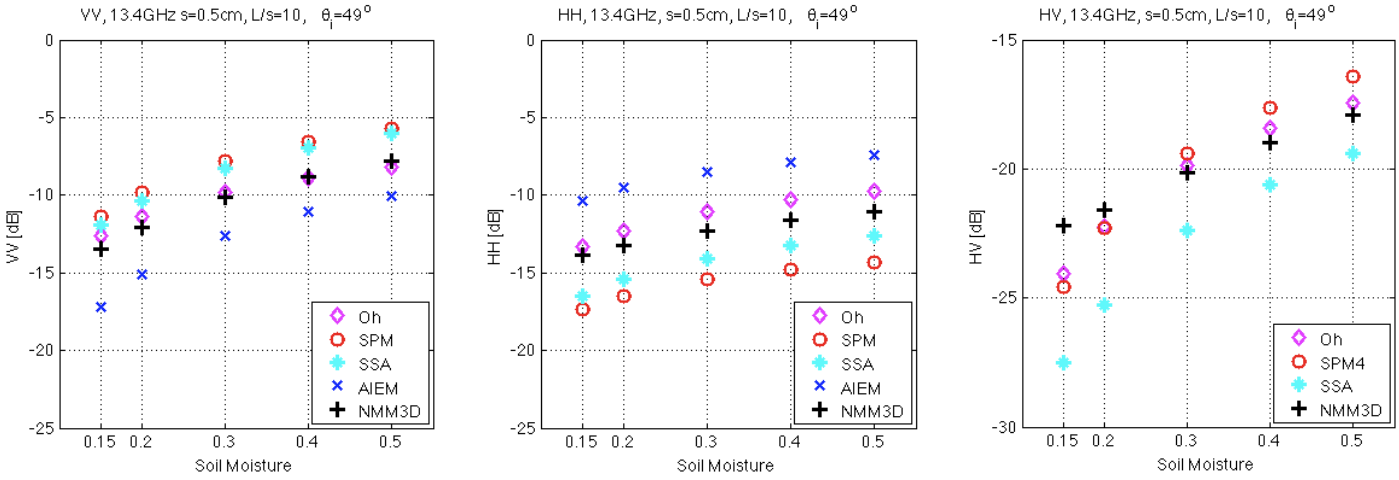

(c)

Figure 2.11 Soil moisture dependence of co- and cross-polarization (s=0.5cm, L/s=10)
(a) 5.4 GHz, $\theta_i = 40^o$ (b) 9.65 GHz, $\theta_i = 40^o$ (c) 13.4 GHz, $\theta_i = 49^o$

40 degree incidence is considered for 5.4 and 9.65GHz, 49 degree incidence for 13.4GHz. Soil moisture is considered from 0.15 to 0.5 for these cases. The soil dielectric constants used here are listed in Table 2.3. Overall, considering both co- and cross-polarization results from NMM3D still stay closer to those from Oh's model. VV and HV show larger dynamic range, about 5 to 6dB, over HH for all 3 frequencies for NMM3D.

In Figure 2.12, it shows angular dependence of co- and cross-polarization from NMM3D POLARSCAT data-1 for C-band(4.75GHz) and X-band(9.5GHz).

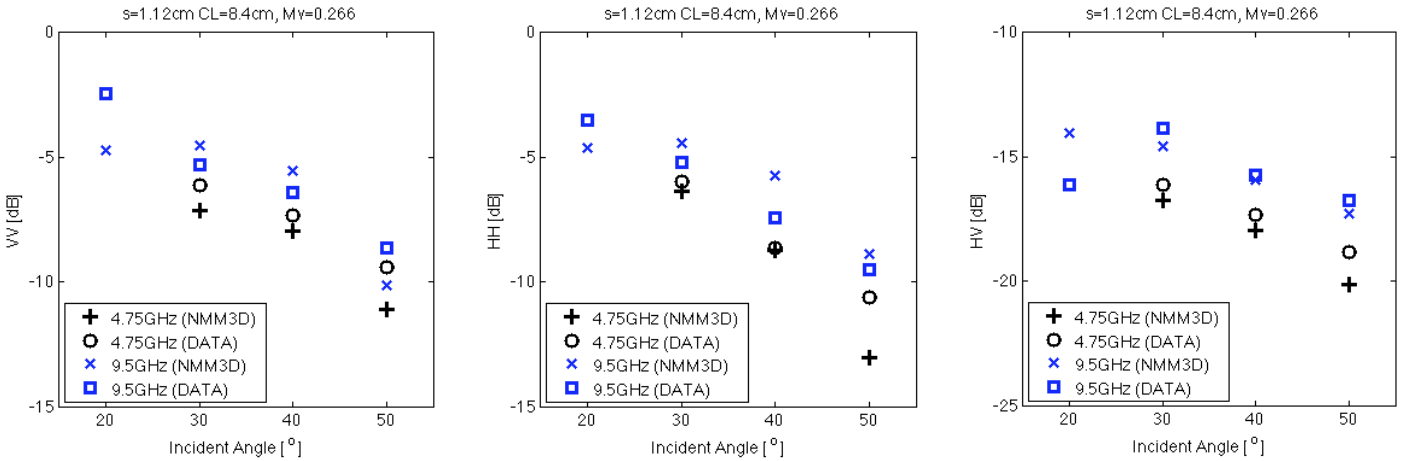

Figure 2.12 Angular dependence of co- and cross-polarization validation comparison with POLARSCAT DATA1, $\theta_i = 30^o \sim 50^o$ for C-band (4.75GHz) , $\theta_i = 20^o \sim 50^o$ X-band (9.5GHz)

Site with rms, 1.12cm, with soil moisture, 0.266, is considered. Within the angular range for Radarsat2 and TerraSAR-X earlier, we validate data of $30^o \sim 50^o$ for C-band and $20^o \sim 50^o$ for X-band. Roughly the decreasing trend for 30 to 50 degrees are similar for C and X band observed from data. Both NMM3D and data show stronger dependence on angles for VV and HH. HV is less dependent on the angle change. In Figure 2.13, results from various models were compared with POLARSCAT data for L-band(1.25GHz), C-band(4.75GHz) and X-band(9.5GHz).

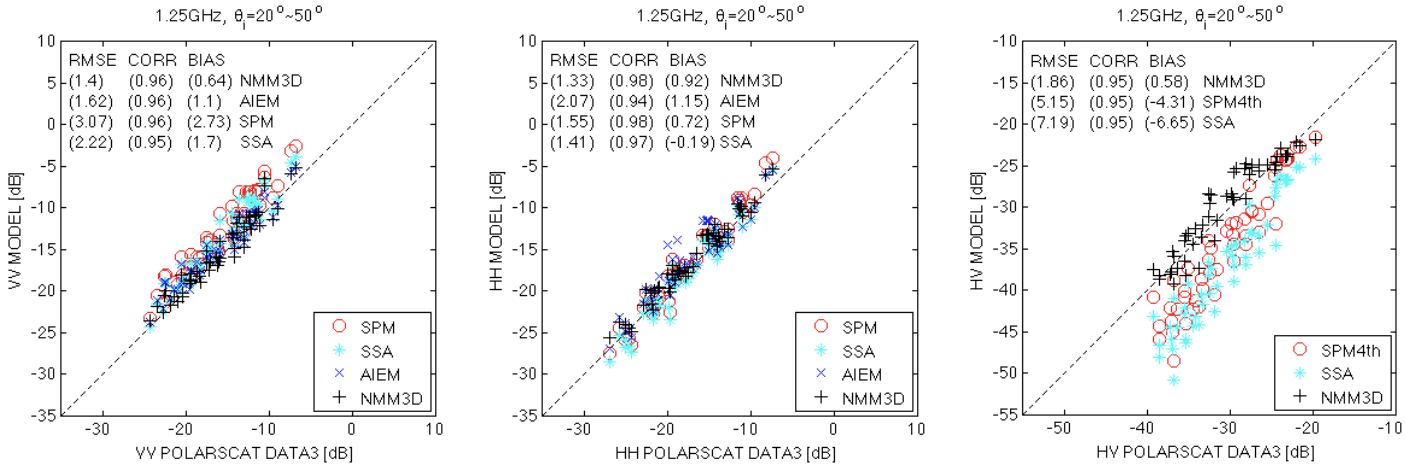

(a)

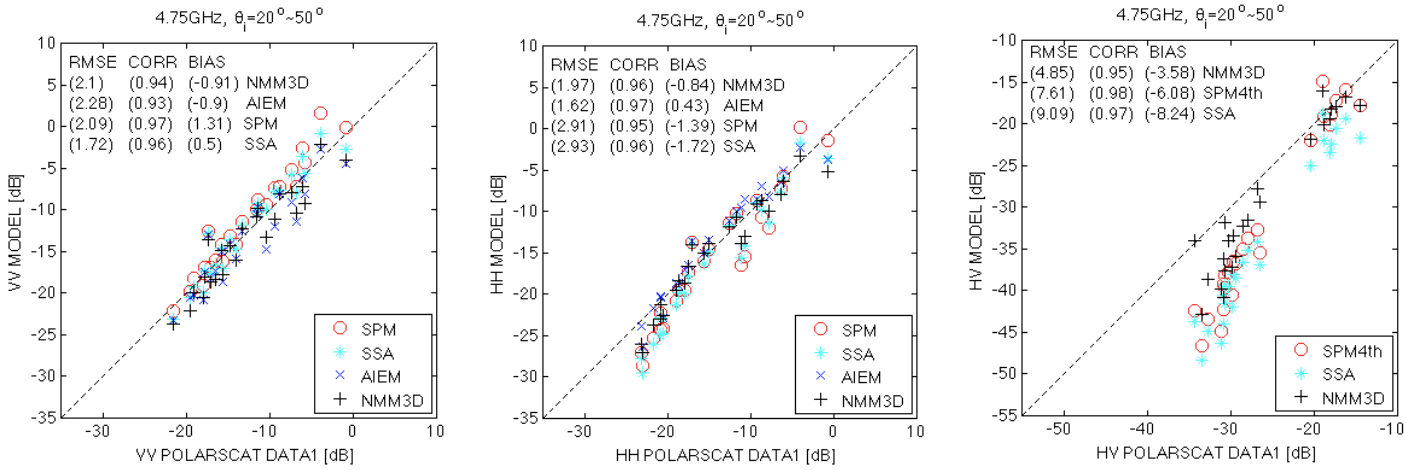

(b)

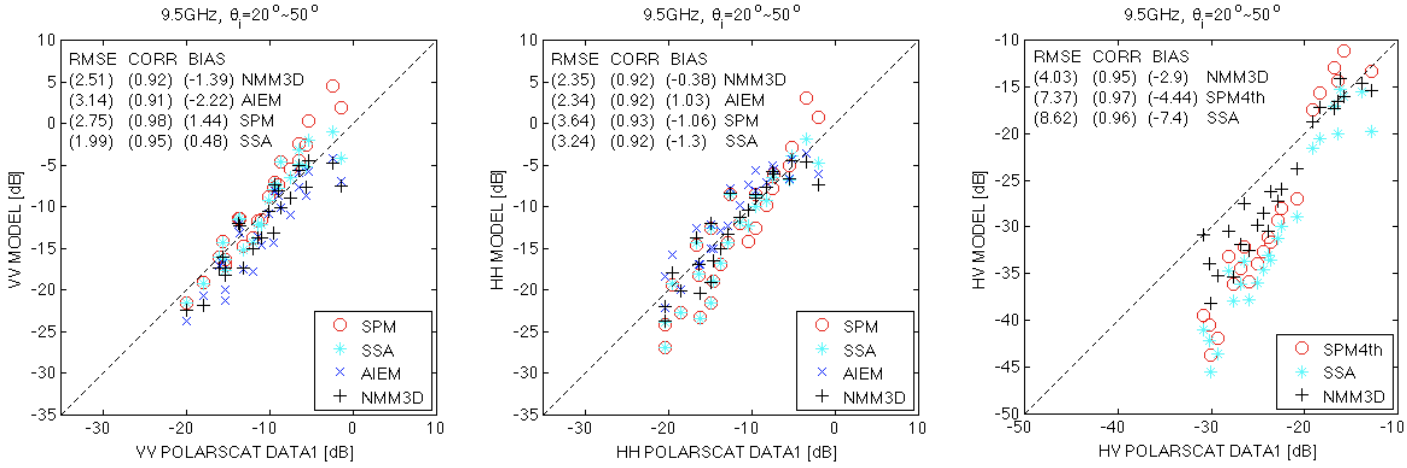

(c)

Figure 2.13 Co- and cross-polarization validation with POLARSCAT DATA1 (a) L-band (1.25GHz) , $\theta_i = 20^o \sim 50^o$ (b) C-band (4.75GHz) , $\theta_i = 20^o \sim 50^o$ (c) X-band (9.65GHz) , $\theta_i = 20^o \sim 50^o$

Detail parameters considered for C- and X- bands in the validation are listed in Table 2.4.

Table 2.4

Physical parameter of validation sites for C-band(4.75GHz) & X-band(9.5GHz)

s(cm)	L(cm)	Frequency (GHz)	Incident Angle	Soil Moisture (cm^3/cm^3)
0.4	8.4	4.75, 9.5	$20^o, 30^o, 40^o, 50^o$	0.253, 0.126
0.32	9.9	4.75, 9.5	$20^o, 30^o, 40^o, 50^o$	0.262, 0.09
1.12	8.4	4.75, 9.5	$20^o, 30^o, 40^o, 50^o$	0.266, 0.14

For L-band validation, the site information is listed in previous study.[12] Root mean square error(RMSE), correlation(CORR), and mean bias error(BIAS) are calculated accordingly to emphasize the comparison. Correlation is good, above 0.9, for all the validation. Overall, NMM3D performs well for L-, C- and X- bands on root mean square error and has less bias considering all 3 polarizations. It is worth mentioning SPM4th and SSA underestimate HV while NMM3D could provide larger HV close the measurement. In Figure 2.14a, the energy conservation is shown as increasing soil moisture for cases considered in Figure 2.11a and Figure 2.11b. It's roughly within 2% error for soil moisture up to 0.5 for both C- and X- bands. In Figure 2.14b, we compare HV and VH from NMM3D to examine the reciprocity. The good agreement for HV and VH means the reciprocity still holds as NMM3D applies to C- and X- bands. This is essential if we apply NMM3D for polarimetric SAR study.[23]

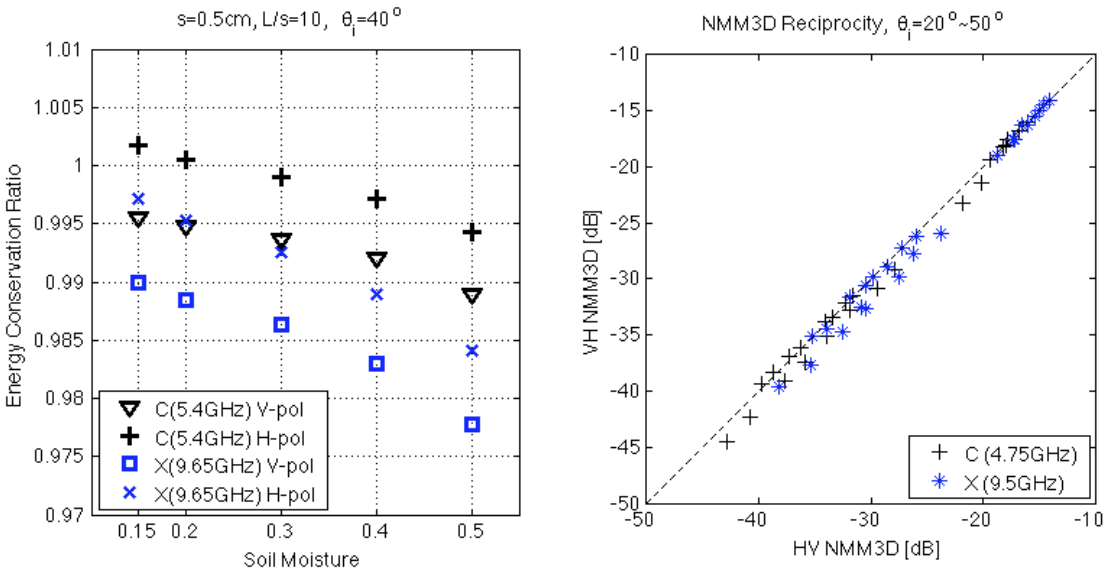

(a) (b)

Figure 2.14 Test of simulation results of C-band and X-band from NMM3D (a) Energy conservation (b) Backscattering reciprocity for HV and VH

2.5.2 Polarization ratio, HH/VV

In this section, polarization ratio, HH/VV, is studied and it shows the feature on frequency dependence and soil moisture dependence. In Figure 2.15, it shows the trends of HH/VV over frequencies for different incidence, from 20 to 50 degrees. 3 fields from POLARSCAT data-1 are considered and the corresponding regression lines are plotted as well. It is obvious that as incident angle increases, the dynamic range also increases. For 50 degree incidence, the regression shows about 4dB increase from 1.5GHz to 9.5GHz. For 20 degree incidence, there is less than 1 dB increase. To emphasize the situation with stronger dependence, we calculate only larger angles and compare HH/VV among models.

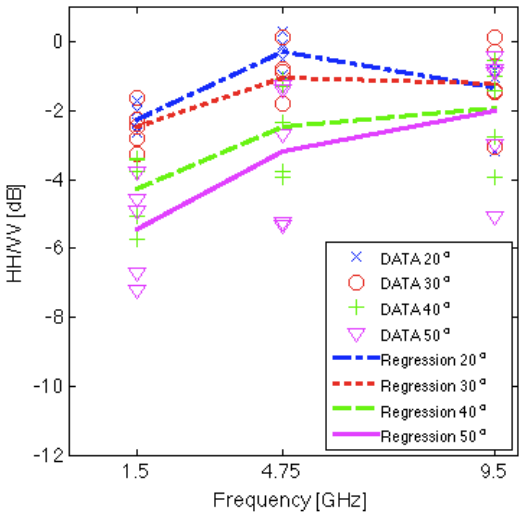

Figure 2.15 Frequency dependence of polarization ratio, HH/VV, from POLARSCAT DATA1 (s=0.32,0.4,1.12cm, Mv=0.09~0.266)

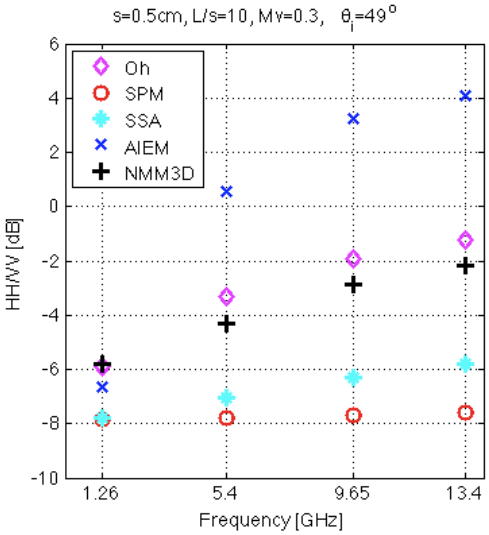

Figure 2.16 Model comparison of polarization ratio, HH/VV, over L, C, X, and Ku bands, (s=0.5cm, L/s=10,Mv=0.3, $\theta_i = 49^o$)

In Figure 2.16, same parameters are considered as those in Figure 2.11. It shows HH/VV from L- to Ku- bands. Again, Oh's model is treated as reference and results from NMM3D stays pretty close to it while AIEM overestimates and SSA underestimates the values. It is worth pointing out that SPM shows no dependence on frequency change. This can be explained by the SPM formula at backscattering direction as shown in (2.24) [24]. Terms related to roughness is from the spectral density, $W(-2\bar{k}_{i\perp})$, and it is the same for both VV and HH. Scattering amplitude, $f_{\beta\alpha}(-\bar{k}_{i\perp}, \bar{k}_{i\perp})$, does not include roughness effect. After taking the ratio of HH and VV, roughness effect cancelled out and gives no dependence on roughness. For the same field, surface gets rougher as frequency increases. However, HH/VV for SPM does not sense this change since roughness effect is gone by the cancellation.

$$\sigma_{\beta\alpha}^{SPM} = 4\pi k^2 \cos^2\theta_i \, W(-2\bar{k}_{i\perp}) \left| f_{\beta\alpha}(-\bar{k}_{i\perp}, \bar{k}_{i\perp}) \right|^2 \qquad (2.24)$$

In Figure 2.17, we demonstrate the soil moisture dependence of HH/VV for C-, X-, and Ku-bands.

HH/VV from NMM3D stays closer to those from Oh's model. AIEM predicts larger values and keeps increase as the frequency increases. SPM and SSA predict lower ratio and they stay closer to each other.

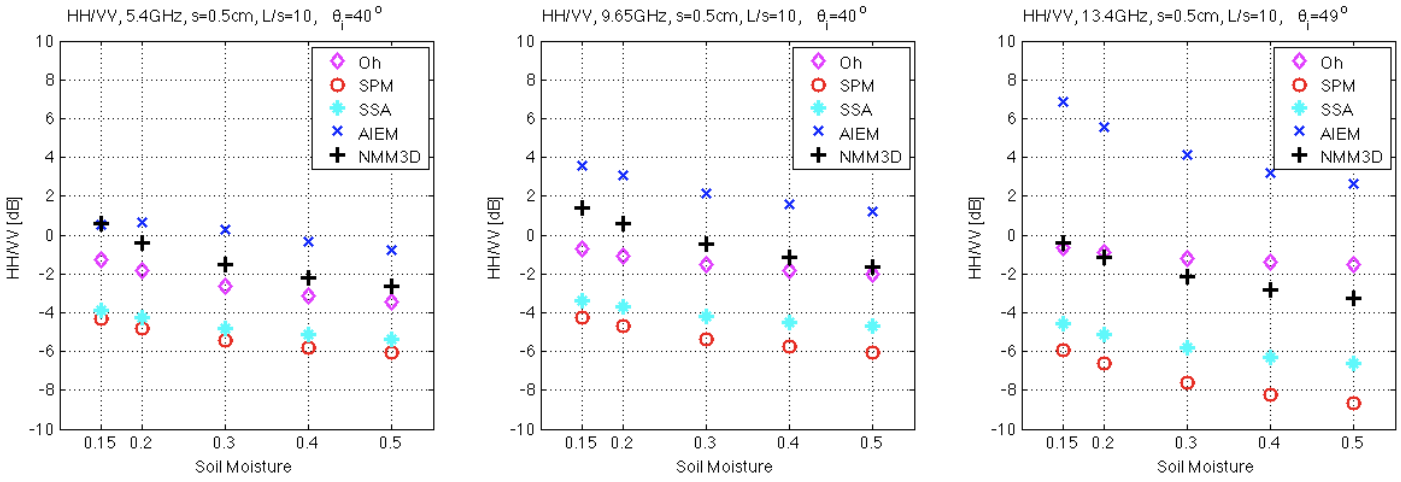

(a) (b) (c)

Figure 2.17 Model comparison of soil moisture dependence of polarization ratio HH/VV (s=0.5cm, L/s=10) (a) 5.4 GHz, $\theta_i = 40^o$ (b) 9.65 GHz, $\theta_i = 40^o$ (c) 13.4 GHz, $\theta_i = 49^o$

In Figure 2.18, it shows the validation of HH/VV with POLARSCAT data for L-, C- and X- bands. HH/VV from NMM3D shows least root mean square error and bias. Also it shows better correlation. From both frequency dependence and soil moisture dependence, we see NMM3D can be applied well to predict polarization ratio, HH/VV. It shows much different dependence from other models and is pretty close to measurement data based empirical model, Oh's model. Also, HH/VV could be a good estimate to be included for the retrieval of the soil moisture.

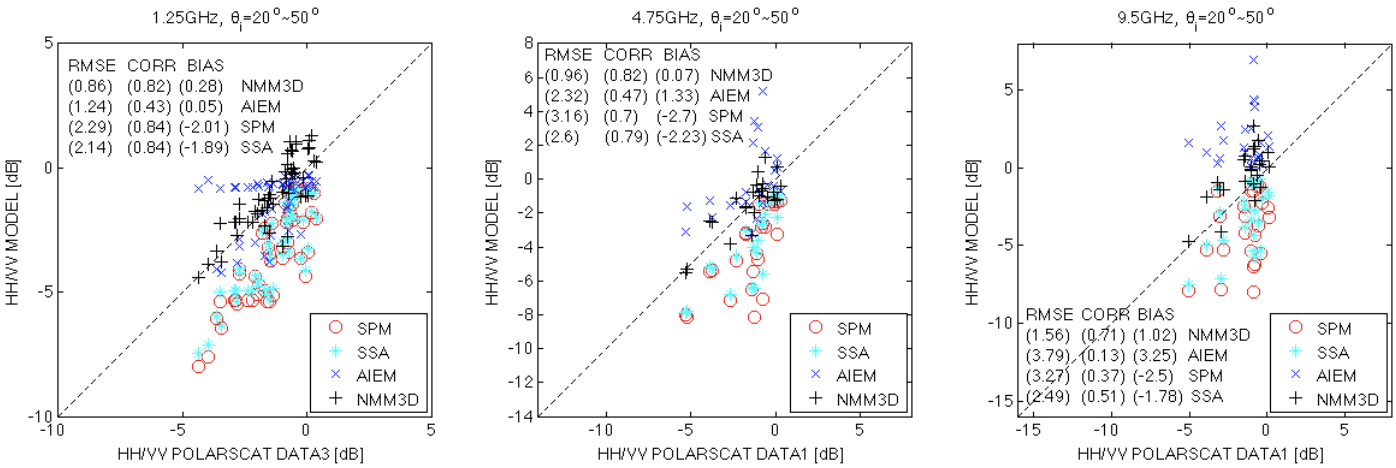

Figure 2.18 Model comparison for validation of polarization ratio, HH/VV, with POLARSCAT DATA1 for C-band (4.75GHz) and X-band (9.5GHz)

2.6 Summary

In this chapter, the near-field precondition method is introduced to NMM3D and it provides faster and consistent simulation time that is independent of roughness. This will be useful as we move forward to larger roughness and larger surface size. Besides, the study of backscattering from soil rough surface is extended from L-band to C-, X-, and Ku-bands. Cross-comparison among various models for co-polarization, cross-polarization are also made as well as polarization ratio, HH/VV. Frequency dependence, incident angle dependence, and soil moisture dependence are applied to examine these quantities. Measurement data from POLARSCAT were applied to the validation. In model comparison, measurement data based empirical model, Oh's model, is treated as reference to see how model results are close to measurement for L-, C-, X-bands. NMM3D performs pretty well considering all the concerned quantities among various models. The polarization ratio, HH/VV is shown to have frequency dependence from measurement data. Some inherent properties of SPM which causes no dependence on surface roughness and it leads to no dependence on frequency. Among these models, NMM3D agrees well with Oh's model from L- to Ku-bands. This suggests that HH/VV could be a good estimate to be included for the soil moisture retrieval study of land surfaces. Also, NMM3D will also be useful for L-, C-, X-, and Ku-bands.

Chapter 3

Multiple Scattering Model for Vegetated Surface

3.1 Backscattering from vegetated surface

When scattering albedo and optical thicknesses of a vegetation layer over soil are significant, both the albedo and the optical thickness larger than 0.4, the effects of multiple scattering need to be taken into account as will be shown in this study. The scattering albedo and the optical thickness of a vegetated surface generally increases with frequency except for the resonance of large structure at low frequencies. In this study, the multiple scattering effects in radar scattering from the vegetation layer overlying a soil surface from L-band to Ku-band for applications to the soil moisture science with the NASA Soil Moisture Active Passive mission and Global Precipitation Measurement, respectively.

The vector radiative transfer (RT) theory with inclusion of cyclical correction is the basis of the approach. In radar backscattering, the results of radiative transfer theory are different from the wave approach. This is because the radiative transfer theory only includes the ladder terms of the Feynman diagrams [25,26]. It was shown that the cyclical terms of the Feynman diagrams need to be included in the backscattering direction. The inclusion results in backscattering enhancement which has a peak in the backscattering direction [25-29]. The physical interpretation is that the forward path and the reverse path give constructive interference for the two scattered fields. However, when the observation direction deviates from the backscattering direction, the phase of these paths fluctuates from particle to particle, and the coherent addition of fields quickly degrades to the incoherent addition of energy. This results in the finite angular width of the backscattering enhancement. Previous papers have used the wave approach summing up all the ladder and cyclical terms in volume scattering [25, 26]. The enhancement also occurs when there are interactions with

surface scattering [26, 29]. It can also be included in the distorted Born approximation [29]. However, the distorted Born approximation only accounts for single volume scattering. In this study, the cyclical correction is applied for the higher order cyclical terms of volume scattering as well as volume-to-surface interactions for a vegetation layer above a soil surface.

In passive remote sensing, multiple scattering effects were studied by Ferrazzoli et al. [30]. It should be noted that cyclical terms are not important for passive remote sensing because the angular width of enhancement is small and does not contribute significantly to energy transfer in passive remote sensing.

In this chapter, the iterative approach is used to solve the vector radiative transfer equations and iteration is performed for higher orders numerically until convergence is achieved. Each term is then examined and the terms that contribute to backscattering enhancement are then identified. Next the cyclical correction is applied to those cyclical terms as the backscattering enhancement and is included in the total radar backscattering.

Finally, the approach is applied to the model for the backscattering from corn fields. From the field campaign data of Soil Moisture Active Passive Validation Experiment 2012 (SMAPVEX12) [32], there are both ground measurement data of corn as well as radar measurement data from the L-band airborne UAVSAR (Uninhabited Airborne Vehicle Synthetic Aperture Radar, http://uavsar.jpl.nasa.gov). The multiple scattering model is trained to best match both data. Since the UAVSAR offers a finite number of independent polarimetric channels, the vegetation parameter in the model has to condense into one parameter - vegetation water content (VWC) – during the comparison of backscatters from UAVSAR and the multiple scattering model. Empirical formulas are applied to establish the allometric relationship between the geometry of corn (stalks and leaves) and VWC. The rational of employing VWC and allometric relationship in the context of comparing with UAVSAR and applying to SMAP is fully described in [33]. With the reasonable allometric relationship the backscatter was computed using the multiple scattering model. Corn is found to have strong backscatter due to multiple scattering, particularly for the later growth stage. The model results were validated with UAVSAR sigma0 measurements from the SMAPVEX12 field campaign data. The investigation is aimed at improving soil moisture retrieval, the model's performance was validated further in terms of soil moisture retrieval. Soil moisture and the bias in VWC are retrieved using the time-series approach [33]. The results of this study

are applicable to L-, C-, X-, Ku- bands such as SMAP mission (L-band) [2] and the GPM (Ku-band).

3.2 Distorted born approximation

Physical modeling approach of vegetation and forests based on the distorted Born approximation is widely applied. There are three scattering terms in the distorted Born approximation: the volume scattering, the double bounce and the surface scattering (Figure 3.1). In the distorted Born approximation [29], the incident wave propagates with an attenuation and the attenuation is obtained from the Foldy approximation [26]. The attenuated wave then impinges on the scatterer which scatters backward giving volume scattering or scatters in the double bounce direction (Figure 3.1). Thus the distorted Born approximation is a single scattering approximation. To distinguish between single scattering and multiple scattering, one uses the optical thickness which is the product of attenuation and distance. The validity of distorted Born approximation is when optical thickness is less than 0.2.

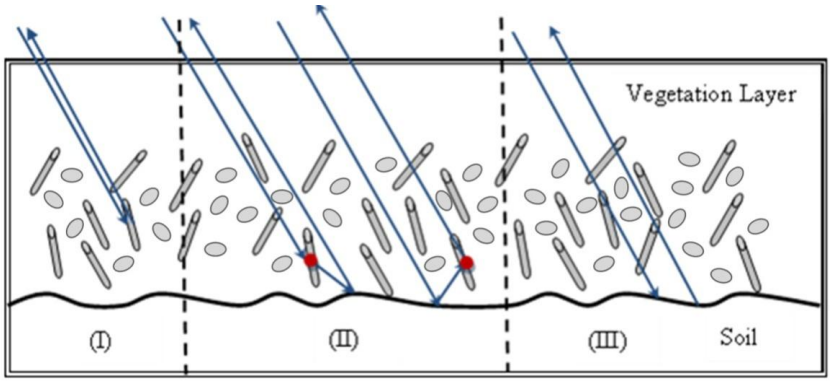

Figure 3.1 Attenuation associated with the propagation through the canopy, and three scattering processes in distorted Born Approximation (I) volume scattering (II).double bounce

3.3 Vector Radiative Transfer equation

3.3.1 Vector radiative transfer and iterative method

The vector radiative transfer (RT) equation [26, 34] under the active configuration with a single reflective boundary at the bottom, which is the typical case of the vegetation layer where the top boundary reflection is negligible. It can be expressed as

$$\cos\theta \frac{d\bar{I}(\theta,\phi,z)}{dz} = -\bar{\bar{\kappa}}_e(\theta,\phi)\cdot\bar{I}(\theta,\phi,z) + \bar{S}(\theta,\phi,z) \tag{3.1}$$

$$-\cos\theta \frac{d\bar{I}(\pi-\theta,\phi,z)}{dz} = -\bar{\bar{\kappa}}_e(\pi-\theta,\phi)\cdot\bar{I}(\pi-\theta,\phi,z) + \bar{W}(\theta,\phi,z) \tag{3.2}$$

where $\bar{I}(\theta,\phi,z)$ and $\bar{I}(\pi-\theta,\phi,z)$ denote, upward- and downward-going specific intensities, respectively and are 4 by 1 column matrices containing the four Stokes parameters. $\bar{\bar{\kappa}}_e(\theta,\phi)$ is the extinction matrix. $\bar{S}(\theta,\phi,z)$ and $\bar{W}(\theta,\phi,z)$ are source terms representing scattering from other directions into the direction of propagation. The specific intensity $\bar{I}(\theta,\phi,z)$ and two source terms $\bar{S}(\theta,\phi,z)$ and $\bar{W}(\theta,\phi,z)$ can be described by their three independent variables of vertical coordinate z, inclination angle θ, between 0 and $\pi/2$, and azimuth angle ϕ, between 0 and 2π. The boundary conditions are expressed as

$$\bar{I}(\pi-\theta,\phi,z=0) = \bar{I}_0\delta(\cos\theta-\cos\theta_0)\delta(\phi-\phi_0) \tag{3.3}$$

$$\bar{I}(\theta,\phi,z=-d) = \bar{\bar{R}}(\theta)\bar{I}(\pi-\theta,\phi,z=-d) \tag{3.4}$$

where $\bar{\bar{R}}(\theta)$ is the reflectivity matrix for Stokes parameters, defined in pp. 285, 305 [34]. In the active RT equation, the formal source term $\bar{S}$ and $\bar{W}$ are related to $\bar{I}$ by phase matrix $\bar{\bar{P}}(\theta,\phi;\theta',\phi')$, the integration of $\theta'$and ϕ' accounts for the scattering from all directions.

$$\bar{S}(\theta,\phi,z) = \int_0^{2\pi} d\phi' \int_0^{\frac{\pi}{2}} d\theta' \sin\theta' \left[\bar{\bar{P}}(\theta,\phi;\theta',\phi')\cdot\bar{I}(\theta',\phi',z) + \bar{\bar{P}}(\theta,\phi;\pi-\theta',\phi')\cdot\bar{I}(\pi-\theta',\phi',z)\right] \tag{3.5}$$

$$\bar{W}(\theta,\phi,z) = \int_0^{2\pi} d\phi' \int_0^{\pi/2} d\theta' \sin\theta' \left[\bar{\bar{P}}(\pi-\theta,\phi;\theta',\phi') \cdot \bar{I}(\theta',\phi',z) + \bar{\bar{P}}(\pi-\theta,\phi;\pi-\theta',\phi') \cdot \bar{I}(\pi-\theta',\phi',z)\right] \tag{3.6}$$

The vector RT could be casted into two coupled integral equations using method of variation of variables,

$$\begin{aligned}
&\bar{I}(\theta,\phi,z) \\
&= \bar{\bar{E}}(\theta,\phi)\bar{\bar{D}}(-\beta(\theta,\phi)(z+d)\sec\theta) \cdot \bar{\bar{E}}^{-1}(\theta,\phi)\bar{R}(\theta) \cdot \bar{\bar{E}}(\pi-\theta,\phi)\bar{\bar{D}}(-\beta(\pi-\theta,\phi)d\sec\theta) \\
&\quad \cdot \bar{\bar{E}}^{-1}(\pi-\theta,\phi)\,\bar{I}_0\delta(\cos\theta-\cos\theta_0)\delta(\phi-\phi_0) \\
&\quad + \bar{\bar{E}}(\theta,\phi)\bar{\bar{D}}(-\beta(\theta,\phi)(z+d)\sec\theta)\sec\theta \int_{-d}^{0} dz' \left\{\bar{\bar{E}}^{-1}(\theta,\phi)\bar{R}(\theta)\right. \\
&\quad \left. \cdot \bar{\bar{E}}(\pi-\theta,\phi)\bar{\bar{D}}(-\beta(\pi-\theta,\phi)(z'+d)\sec\theta)\bar{\bar{E}}^{-1}(\pi-\theta,\phi)\bar{W}(\theta,\phi,z')\right\} \\
&\quad + \sec\theta \int_{-d}^{z} dz' \left\{\bar{\bar{E}}(\theta,\phi)\bar{\bar{D}}(\beta(\theta,\phi)(z'-z)\sec\theta)\right. \\
&\quad \left. \cdot \bar{\bar{E}}^{-1}(\theta,\phi)\bar{S}(\theta,\phi,z')\right\}
\end{aligned} \tag{3.7}$$

$$\begin{aligned}
&\bar{I}(\pi-\theta,\phi,z) \\
&= \bar{\bar{E}}(\pi-\theta,\phi)\bar{\bar{D}}(\beta(\pi-\theta,\phi)z\sec\theta) \cdot \bar{\bar{E}}^{-1}(\pi-\theta,\phi)\bar{I}_0\delta(\cos\theta-\cos\theta_0)\delta(\phi-\phi_0) \\
&\quad + \sec\theta \int_{z}^{0} dz' \left\{\bar{\bar{E}}(\pi-\theta,\phi)\bar{\bar{D}}(\beta(\pi-\theta,\phi)(z-z')\sec\theta) \cdot \bar{\bar{E}}^{-1}(\pi-\theta,\phi)\bar{W}(\theta,\phi,z')\right\}
\end{aligned} \tag{3.8}$$

where $\beta_i(\theta,\phi)$ are the eigenvalues of coherent propagation (homogenous equation) and $\bar{\bar{E}}(\theta,\phi)$ is the associated eigenmatrix, and $\bar{\bar{D}}(\beta(\theta,\phi)z\sec\theta)$ is a diagonal matrix with the iith element equal to $\exp(\beta_i(\theta,\phi)z\sec\theta)$. The general expression for $\beta_i(\theta,\phi)$ and $\bar{\bar{E}}(\theta,\phi)$ are given in pp. 141 [26] or pp. 275 [34]. When the scatterers have azimuthal symmetry, the vertically polarized waves and the horizontally polarized waves are the characteristic polarizations of the medium. In this case,

$$\bar{\bar{E}} = \bar{\bar{E}}(\theta,\phi) = \begin{bmatrix} 1 & 0 & 0 & 0 \\ 0 & 1 & 0 & 0 \\ 0 & 0 & 1 & 1 \\ 0 & 0 & i & -i \end{bmatrix} \tag{3.9}$$

$$\bar{\beta}(\theta) = \bar{\beta}(\theta,\phi) = \begin{bmatrix}\beta_1(\theta,\phi)\\ \beta_2(\theta,\phi)\\ \beta_3(\theta,\phi)\\ \beta_4(\theta,\phi)\end{bmatrix} = \frac{2\pi n_0}{k}\begin{bmatrix}2\langle \mathrm{Im}\, f_{vv}(\theta,\phi;\theta,\phi)\rangle\\ 2\langle \mathrm{Im}\, f_{hh}(\theta,\phi;\theta,\phi)\rangle\\ i(\langle f_{vv}^*(\theta,\phi;\theta,\phi) - f_{hh}(\theta,\phi;\theta,\phi)\rangle)\\ i(\langle f_{hh}^*(\theta,\phi;\theta,\phi) - f_{vv}(\theta,\phi;\theta,\phi)\rangle)\end{bmatrix} \quad (3.10)$$

where $f_{\beta\alpha}$ is the component of the scattering amplitude matrix of the scatterer, (pp. 132 [26]; pp. 7 [34]), and the angular bracket denotes configuration average over orientation and size of the scatterer. The imaginary part of $\langle f(\theta,\phi;\theta,\phi)\rangle$ is then replaced by the extinction coefficient κ_e through the optical theorem to account for the inaccuracy of approximating scattering models,

$$\kappa_e(\theta) = \frac{4\pi}{k}\langle Im\, f(\theta,\phi;\theta,\phi)\rangle \quad (3.11)$$

where extinction coefficient $\kappa_e(\theta)$ is calculated as the sum of absorption coefficient $\kappa_a(\theta)$ and scattering coefficient $\kappa_s(\theta)$, derived from the internal field and scattering amplitude $f_{\beta\alpha}$, respectively. The phase matrix $\bar{\bar{P}}(\theta,\phi;\theta',\phi')$ can also be derived from the scattering amplitude from pp.126[34].

The integral equation governing the upward- and downward-going specific intensity could be solved iteratively by treating the viewing source term $\bar{S}$ and $\bar{W}$ as small perturbations. The zeroth order solution is called the reduced intensity which is part of the homogenous solution of the differential equation with coefficients determined by enforcing boundary conditions.

$$\bar{I}^{(0)}(\pi-\theta,\phi,z) = \bar{\bar{E}}(\pi-\theta,\phi)\bar{\bar{D}}(\beta(\pi-\theta,\phi)z\sec\theta)\cdot\bar{\bar{E}}^{-1}(\pi-\theta,\phi)\bar{I}_0\delta(\cos\theta-\cos\theta_0)$$
$$\delta(\phi-\phi_0) \quad (3.12)$$

$$\bar{I}^{(0)}(\theta,\phi,z) = \bar{\bar{E}}(\theta,\phi)\bar{\bar{D}}(-\beta(\theta,\phi)(z+d)\sec\theta)\cdot\bar{\bar{E}}^{-1}(\theta,\phi)\bar{R}(\theta)\cdot\bar{\bar{E}}(\pi-\theta,\phi)$$
$$\bar{\bar{D}}(-\beta(\pi-\theta,\phi)d\sec\theta)\cdot\bar{\bar{E}}^{-1}(\pi-\theta,\phi)\,\bar{I}_0\delta(\cos\theta-\cos\theta_0)\delta(\phi-\phi_0) \quad (3.13)$$

The $(n+1)$-th order solution is related to the n-th order solution recursively,

$$\bar{I}^{(n+1)}(\pi-\theta,\phi,z) = \sec\theta\int_z^0 dz'$$
$$\left\{\bar{\bar{E}}(\pi-\theta,\phi)\bar{\bar{D}}(\beta(\pi-\theta,\phi)(z-z')\sec\theta)\cdot\bar{\bar{E}}^{-1}(\pi-\theta,\phi)\bar{W}^{(n+1)}(\theta,\phi,z')\right\} \quad (3.14)$$

$$\bar{I}^{(n+1)}(\theta,\phi,z) = \bar{\bar{E}}(\theta,\phi)\bar{\bar{D}}(-\beta(\theta,\phi)(z+d)\sec\theta)\sec\theta \int_{-d}^{0} dz' \left\{\bar{\bar{E}}^{-1}(\theta,\phi)\bar{R}(\theta)\right.$$
$$\left. \cdot \bar{\bar{E}}(\pi-\theta,\phi)\bar{\bar{D}}(-\beta(\pi-\theta,\phi)(z'+d)\sec\theta)\bar{\bar{E}}^{-1}(\pi-\theta,\phi)\bar{W}^{(n+1)}(\theta,\phi,z')\right\}$$
$$+\sec\theta \int_{-d}^{z} dz' \left\{\bar{\bar{E}}(\theta,\phi)\bar{\bar{D}}(\beta(\theta,\phi)(z'-z)\sec\theta)\cdot\bar{\bar{E}}^{-1}(\theta,\phi)\bar{S}^{(n+1)}(\theta,\phi,z')\right\} \quad (3.15)$$

where source terms $\bar{S}^{(n+1)}$ and $\bar{W}^{(n+1)}$ could be updated from lower order solution $\bar{I}^{(n)}$,

$$\bar{S}^{(n+1)}(\theta,\phi,z)$$
$$= \int_0^{2\pi} d\phi' \int_0^{\pi/2} d\theta' \sin\theta' \left[\bar{\bar{P}}(\theta,\phi;\theta',\phi')\cdot\bar{I}^{(n)}(\theta',\phi',z) + \bar{\bar{P}}(\theta,\phi;\pi-\theta',\phi')\right.$$
$$\left.\cdot\bar{I}^{(n)}(\pi-\theta',\phi',z)\right] \quad (3.16)$$

$$\bar{W}^{(n+1)}(\theta,\phi,z) = \int_0^{2\pi} d\phi' \int_0^{\frac{\pi}{2}} d\theta' \sin\theta'$$
$$\left[\bar{\bar{P}}(\pi-\theta,\phi;\theta',\phi')\cdot\bar{I}^{(n)}(\theta',\phi',z) + \bar{\bar{P}}(\pi-\theta,\phi;\pi-\theta',\phi')\cdot\bar{I}^{(n)}(\pi-\theta',\phi',z)\right] \quad (3.17)$$

Note the integrals in $\bar{S}^{(1)}(\theta,\phi,z)$ and $\bar{W}^{(1)}(\theta,\phi,z)$ are cancelled by the Dirac functions in $\bar{I}^{(0)}$, yielding explicit expressions.

The incoherent bistatic scattering coefficient and backscattering coefficient are then calculated from $\bar{I}(\theta,\phi,z=0)$ [26, 31, 34], where $\bar{I}$ is the sum of contribution from each scattering order $\bar{I}^{(n)}$ $(n = 1,2,...)$.

3.3.2 Numerical iterative approach and numerical recipe

The explicit expression for 1st order and 2nd order solution can be analytically derived by manually substituting $\bar{I}^{(0)}$ into $\bar{I}^{(1)}$, and substituting $\bar{I}^{(1)}$ into $\bar{I}^{(2)}$. This concept works for higher order, but the number of terms grows exponentially. If we use $\left[I_u^{(n)}\right]$ to denote the number of terms in $\bar{I}^{(n)}(\theta,\phi,z)$, and use $\left[I_d^{(n)}\right]$ to denote the number of terms in $\bar{I}^{(n)}(\pi-\theta,\phi,z)$, then the number of terms in $\bar{I}^{(n+1)}(\theta,\phi,z)$ denoted by $\left[I_u^{(n+1)}\right]$ will be $2\left(\left[I_u^{(n)}\right]+\left[I_d^{(n)}\right]\right)$, and the number of terms in $\bar{I}^{(n+1)}(\pi-\theta,\phi,z)$ denoted by $\left[I_d^{(n+1)}\right]$ will be $\left[I_u^{(n)}\right]+\left[I_d^{(n)}\right]$. This quickly becomes complex.

Alternatively by adopting a numerical solution, all the terms of the same scattering order could be aggregated together. There is no additional computing cost as the order goes higher.

The iteration starts with the discretized $\bar{S}^{(1)}$ and $\bar{W}^{(1)}$, then calculate the discretized $\bar{I}^{(1)}$; and finally update $\bar{S}^{(2)}$ and $\bar{W}^{(2)}$ at the sampling points, and use them to calculate $\bar{I}^{(2)}$. This procedure can be extended to any order, where we update $\bar{S}^{(n+1)}$ and $\bar{W}^{(n+1)}$ from the pre-calculated $\bar{I}^{(n)}$, and use them to predict $\bar{I}^{(n+1)}$. This process is repeated until the backscattering converges.

3.3.3 Angular integral, using Gaussian-Legendre quadrature for θ-integral and trapezoidal integral for ϕ-integral

The typical integral can be evaluated as follows:

$$\bar{S}^{(n+1)}(\theta,\phi,z) = \int_0^{2\pi} d\phi' \int_0^{\frac{\pi}{2}} d\theta' \sin\theta'$$
$$\left[\bar{\bar{P}}(\theta,\phi;\theta',\phi') \cdot \bar{I}^{(n)}(\theta',\phi',z) + \bar{\bar{P}}(\theta,\phi;\pi-\theta',\phi') \cdot \bar{I}^{(n)}(\pi-\theta',\phi',z)\right] \quad (3.18)$$

Next consider the azimuthal symmetry of $\bar{\bar{P}}(\theta,\phi;\theta',\phi')$ with respect to $\phi-\phi'$,

$$\bar{S}^{(n+1)}(\theta,\phi,z) = \int_0^{2\pi} d\phi' \int_0^{\frac{\pi}{2}} d\theta' \sin\theta'$$
$$\left[\bar{\bar{P}}(\theta,\phi-\phi';\theta',0) \cdot \bar{I}^{(n)}(\theta',\phi',z) + \bar{\bar{P}}(\theta,\phi-\phi';\pi-\theta',0) \cdot \bar{I}^{(n)}(\pi-\theta',\phi',z)\right] \quad (3.19)$$

Applying the Gaussian-Legendre quadrature for θ-integral and a trapezoidal integral for ϕ-integral, sample $\bar{S}_u^{(n+1)}(\theta,\phi,z)$ on the Gaussian-Legendre quadrature points θ_k $(k=1,\dots,N_k)$, and trapezoidal quadrature points ϕ_p $(p=0,1,\dots,N_p-1)$, where $\mu_k=\cos(\theta_k)$ is the positive half of the $2N_k$ roots of Legendre polynomial of $2N_k$-th order, and $\phi_p=p\Delta\phi$, $\Delta\phi=2\pi/N_p$. a_k is the corresponding Gaussian-Legendre quadrature weights at θ_k.

$$\bar{S}^{(n+1)}(\theta_k,\phi_p,z)$$
$$= \Delta\phi \sum_{p'=1}^{N_p} \sum_{k'=1}^{N_k} a_{k'} \left[\bar{\bar{P}}(\theta_k,\phi_p-\phi_{p'};\theta_{k'},0) \cdot \bar{I}^{(n)}(\theta_{k'},\phi_{p'},z) + \bar{\bar{P}}(\theta_k,\phi_p-\phi_{p'};\pi-\theta_{k'},0)\right.$$
$$\left. \cdot \bar{I}^{(n)}(\pi-\theta_{k'},\phi_{p'},z)\right] \quad (3.20)$$

Note $\bar{\bar{P}}(\theta,\phi;\theta',\phi')$ only needs to be stored at the grid points $\bar{\bar{P}}\left(\theta_k,\phi_p;\theta_{k'},0\right)$, and the summation over $\phi_{p'}$ forms a cyclic convolution, and could be accelerated by FFT. The evaluation of $\bar{W}^{(n+1)}(\theta,\phi,z)$ is similar.

3.3.4 Recursive *z*-integral

Three z-integrals will be utilized. In $\bar{I}^{(n+1)}(\theta,\phi,z)$ there is $\int_{-d}^{0} dz' f(z')$ and $\int_{-d}^{z} dz' f(z')$, and in $\bar{I}^{(n+1)}(\pi-\theta,\phi,z)$ there is $\int_{z}^{0} dz'$. If z is sampled uniformly, $z_q = -d + q\Delta z$, $\Delta z = d/N_q$, $q = 0,1,\dots,N_q$, also let $f_q = f\left(z_q\right)$. As a result the first integral is easily treated applying trapezoidal quadrature rule.

$$\int_{-d}^{0} dz' f(z') = \Delta z\left(\frac{1}{2}f(z_0) + \sum_{q'=1}^{N_q-1} f\left(z_{q'}\right) + \frac{1}{2}f\left(z_{N_q}\right)\right) \tag{3.21}$$

The other two integrals can be efficiently evaluated recursively,

For $\int_{-d}^{z_q} dz' f(z')$,

$$\int_{-d}^{z_0} dz' f(z') = 0, q = 0 \tag{3.22}$$

$$\int_{-d}^{z_q} dz' f(z') = \int_{-d}^{z_q-1} dz' f(z') + \frac{\Delta z}{2}\left(f_{q-1} + f_q\right), q = 1,\dots,N_q \tag{3.23}$$

For $\int_{z_q}^{0} dz' f(z')$,

$$\int_{z_{N_q}}^{0} dz' f(z') = 0, q = N_q \tag{3.24}$$

$$\int_{z_q}^{0} dz' f(z') = \frac{\Delta z}{2}\left(f_q + f_{q+1}\right) + \int_{z_{q+1}}^{0} dz' f(z'), q = N_q - 1,\dots,0 \tag{3.25}$$

3.4 Cyclical correction & backscattering enhancement

3.4.1 Scattering path notation and tracing

When the iterative approach is used to solve the vector radiative transfer equations, the iteration corresponds to the accumulation of scattering orders. Each scattering order contains many independent physical scattering terms. Each physical scattering term is associated with a unique scattering path. The scattering path is a sequence of scattering, reflection and the intensity flow connecting the event of scattering and reflection. The direction of energy flow is separated into upwelling and downwelling.

'd' and 'u' are used to denote downwelling and upwelling energy flow, 's' indicates a single scattering, and 'r' to denote a single reflection of specific intensity at the bottom boundary. For example:

- "du", which is short for "dsu", means 1st order volume scattering
- "dd", which is short for "dsdru", means 1st order double bounce scattering, scattering followed by reflection, Fig.1a
- "uu", which is short for "drusu", means 1st order double bounce scattering, reflection followed by scattering, Fig.1a
- "ud", which is short for "drusdru", means 1st order double reflection scattering, reflection followed by scattering followed by reflection.

Note that the two-character combination of "du", "dd", "uu", "ud" indicates one scattering order. The first character denotes the direction of stream flow before scattering, while the second character denotes the direction of stream flow after scattering. There is a hidden 's' (scattering) in between. The 'r' (reflection) between two succeeding scattering orders may or may not be automatically deduced between two scattering events to connect the succeeding stream flows.

One path could be a dual path of itself, or two paths could be dual to each other. A dual path means that the intensity flows in the opposite direction, and the sequence of scattering and events also take place in a reverse order. Technically, one could find the dual path of a certain path apply the following procedure to the sequence of path characters:

- Reverse the order of scattering between surface and reflection

- Reverse the direction of energy flow (change ‘d’ to ‘u’, and change ‘u’ to ‘d’)

For example,

- “dsu” and “drusdru”are self-dual
- “dsdru” and “drusu” are dual to each other, Fig.1a

When one path is self-dual, in general it denotes two physical paths in reverse order. However, in the backscattering direction, there is a special issue in the determination of its uniqueness:

- It could denote two distinct scattering paths, such as “dsd|rusu”, which is the second order scattering with once surface bounce in between, Fig.1c. Another examples of this kind of self-dual paths in second order scattering is “drusd|rusdru”
- There could be essentially only one scattering path in backscattering direction, eg. “dsu” and “drusdru” in first order scattering.

In fact for these two first order paths we could not find a corresponding backscattering path in reverse order, because from 2nd order on, the scattering events of the succeeding scatterers could always change order to form a dual scattering path even in backscattering direction.

In Figure 3.2a, the cyclical term is illustrated for 1st order scattering, where the scattering field due to the single scattering of the particle followed by the reflection of surface is exactly the same as the scattering field due to the single scattering of the particle succeeding the reflection of surface. This term corresponds to the double bounce effect. In Figure 3.2b, the cyclical term is illustrated for 4th order volume scattering, where the overall scattering field is the same if we completely reverse the sequence of particles in the scattering path. In Figure 3.2c and Figure 3.2d, the cyclical

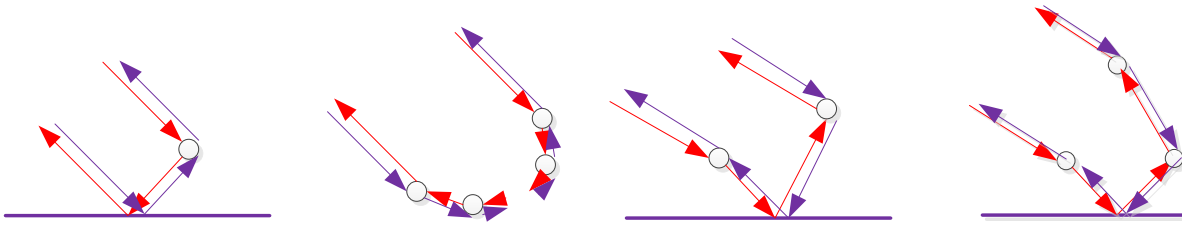

(a) cyclical terms in 1st order double bounce scattering

(b) cyclical terms in multiple volume scattering

(c) cyclical terms in 2nd order volume scattering and bounce from surface

(d) cyclical terms i order volume scatt and bounce from su

Figure 3.2 Illustration of cyclical terms

terms are illustrated for volume surface scattering interactions for 2nd order and 3rd order scattering, respectively. The inclusion of a reflective boundary significantly increases the number of cyclical terms.

3.4.2 Cyclical correction and backscattering enhancement effects

If two distinct paths are dual to each other (including those self-dual paths which denote two reverse physical paths), in backscattering direction, the scattering field has exactly the same phase. The fields add up instead of intensity adding up, this is called backscattering enhancement [24, pp. 361]. We need to augment their contribution to the backscattering by a factor of two. This is called cyclical correction, and the corresponding terms are called cyclical terms. The method of cyclical correction is only applicable to co-pol backscattering.

In fact, if a path does not have a distinct dual path, it must be self-dual. So we only need to identify all the self-dual terms, and only account for those representing a single physical scattering path (we call it I_{single}) and subtract them out from twice of the total contribution.

- backscattering without cyclical correction: $I = I_{\text{dual}} + I_{\text{single}}$
- backscattering with cyclical correction: $I_{\text{cor}} = 2I_{\text{dual}} + I_{\text{single}} = 2I - I_{\text{single}}$

Note that I_{single} contains only two terms “d s u” and “d r u s d r u”. Since these two first order terms could be analytically calculated out, (they in fact only involve the backscattering of the scatterer.) and the multiple scattering could be solved using the standard quadrature-eigenanalysis approach [31]. The cyclical correction could be immediately accounted for. However, this numerical iterative approach turns out to be a more robust (could handle all types of physical phase matrix), more stable (always produce positive numbers for backscattering and bistatic scattering) and efficient (tytpically very large orders are not considered) approach. It also offers more physical insight into the problem by allowing us to separate contribution from different scattering orders, and even the separate contribution from each scattering mechanism (path).

The numerical iterative approach documented in the previous section could be applied to each scattering path as well as to each scattering order. In this way it would be possible to keep track of each term separately. This permits the identification of cyclical terms by checking the duality of

scattering paths. Then it would be possible to correct contribution from those cyclical terms when including them into the overall backscattering.

3.5 Results discussion of multiple scattering effects

The proposed iterative numerical approach allows us to model the multiple scattering effects when the optical thickness and scattering albedo are large. The cyclical correction to the contribution from the cyclical terms allows us to consider the backscattering enhancement effects at the same time. In this section we apply this approach to the scenario of vegetation scattering. Investigation is conducted for the optical thickness dependence, dependence of backscattering on biomass, frequency and incidence angle, identification of the dominant scattering orders and mechanisms, and discussion for the significance of multiple scattering effects under various cases from L-band to Ku-band.

First, consider an assembly of dielectric cylinders with a radius of 1 cm, length of 1 m, and relative permittivity of $50 + 15i$ (typical corn stalk parameters from [35]) and an L-band sensor. The cylinders are predominantly vertical, which is typical of many crops. The probability distribution function of the Eulerian angle α and β of the cylinder axis is

$$p(\alpha,\beta) = \begin{cases} \frac{1}{2\pi}\frac{\sin\beta}{1-\cos\Delta\beta}, \text{for } 0 \le \beta \le \Delta\beta \\ 0 \qquad\qquad , otherwise \end{cases} \tag{3.26}$$

α and β are the orientation angles of the body axis of the cylinder. α is in the azimuthal direction about the cylinder and β is in the elevation angle from the vertical ($+z$ direction). In this numerical example, the backscatter is computed from the cylinder only case for $\Delta\beta = 15°$. Using these parameters it is possible to compute an averaged phase function of the cylinder over orientation, $\beta = 0°\sim15°$ and $\alpha = 0°\sim360°$, based on infinite cylinder approximation [34, pp. 41-45]. Let the cylinder density be 7.2/m^2, radar frequency 1.26GHz and incidence angle $40°$. The density was obtained from the SMPAVEX12 data. Flat ground is assumed below the vegetation layer with dielectric constant of $10.12 + 1.11i$. The dielectric constant of soil is calculated from the generalized refractive mixing dielectric model for moist soils [34] with soil moisture of 20% and clay fraction of 18%. This example represents a mature corn with the height of 1 m. Also, Table

3.7 summarizes most simulation parameters used in this study. The numerical iteration is performed up to 5th order. In Figure 3.3, the contribution from each order is compared. For horizontal polarization, 1st order backscattering dominates, contributing up to 93.7%; for vertical polarization the backscattering from the first three orders are important, with contribution percentage 53.6%, 33.0% and 10.1%, respectively.

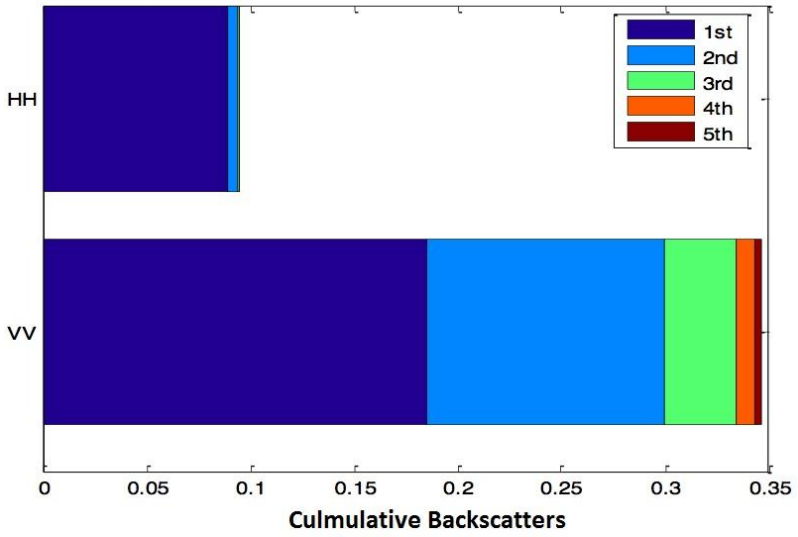

Figure 3.3 Backscatter contribution up to 5th order for a mature corn with 1 m tall at 1.26 GHz (L-band) with 40 degree incidence. Detail parameters are in Table 3.7. ($VV5^{th}$ = -4.61 dB, $HH5^{th}$ = -10.23 dB, $VV1^{st}$ = -7.32 dB, $HH1^{st}$ = -10.51 dB)

In Table 3.1, the contribution from the dominant scattering mechanisms is listed. For horizontal polarization, the first order volume-surface double bounce term dominates and contributes up to 93.4%. For vertical polarization the significant scattering mechanisms include the first order volume-surface double bounce term, the second order volume surface interaction terms in the sequence of volume-surface-volume and volume-volume-surface, and the third order volume surface interaction terms in the sequence of volume-volume-surface-volume and volume-volume-volume-surface. The cyclical correction has been included in these scattering results. The scattering albedo is 0.6816 for vertical and 0.3751 for horizontal polarization; the optical thickness in the direction of incidence is 0.8928 for vertical pol and 0.1669 for horizontal polarization. These results demonstrate that the importance of multiple scattering effects when both scattering albedo

and optical thickness are large.

Table 3.1
Backscatter contribution from the dominant scattering mechanisms. Parameters are given in Table 3.7

Order	Description	Percentage (VV)	Percentage (HH)	Possible Paths With Strong Contribution
1	volume-surface	52.9%	93.4%	drusu, dsdru
2	volume-surface-volume	16.0%	1.9%	dsd|rusu
2	volume-volume-surface	16.3%	3.6%	drusu|usu, dsd|dsdru
3	volume-volume-surface-volume	6.9%	-	dsd|rusu|usu, dsd|dsd|rusu
3	volume-volume-volume-surface	2.8%	-	drusu|usu|usu, dsd|dsd|dsdru

* "d" for down "u" for up "s" for single volume scattering "r" for reflection See the main text for more detail

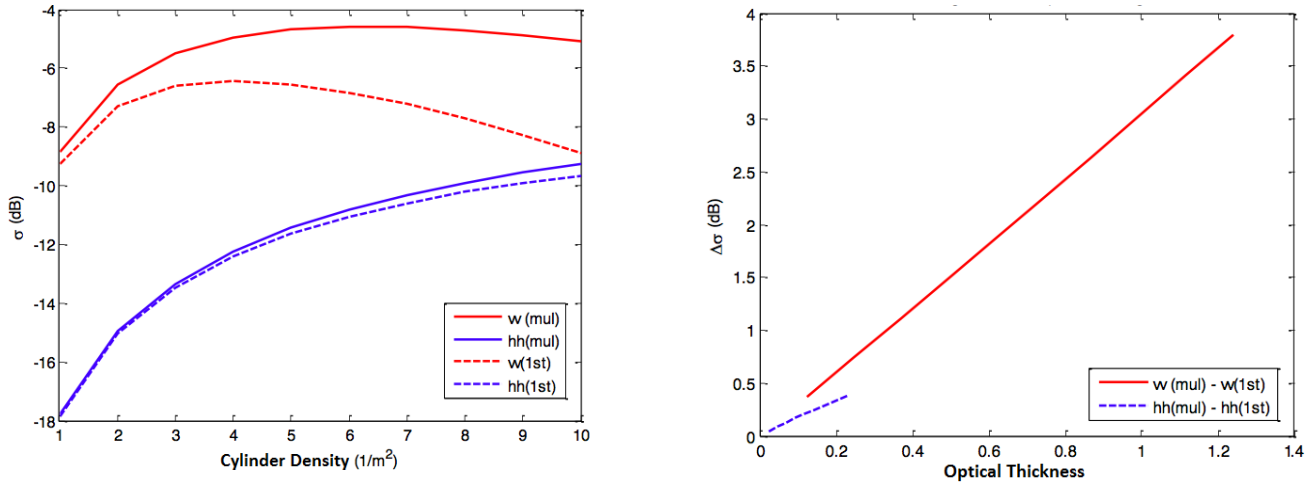

(a) (b)

Figure 3.4 Backscatter's dependence at 1.26 GHz with 40 degree incidence. (a) Backscatter's dependence on cylinder density (b) Backscatter's difference between 5th and 1st order scattering as a function of optical thickness. Detail parameters are in Table 3.7

Backscatters' dependence on vegetation biomass is illustrated in Figure 3.4 at 1.26 GHz using the same set of cylinder parameters. The optical thickness is assumed to be linearly proportional to the

cylinder densities, and thus to the the vegetation water content (or biomass assuming a fixed volumetric water percentage of a plant). In Figure 3.4a, the backscattering from 1st order results and multiple scattering results (up to 5th order) is plotted as a function of cylinder density; as the density changes from 1 to 10/m^2, the optical thickness in the direction of incidence increases from 0.124 to 1.24 for v-pol and from 0.0232 to 0.232 for h-pol. The multiple scattering effects for HH is small: there is less than 0.5dB difference between multiple scattering and 1st order scattering. The 1st order scattering result for vertical co-polarization quickly saturates at a cylinder density of 4/m^2, corresponding to 0.496 in optical thickness, and then quickly decreases. The attenuation from trunks increases faster than the scattering with the increasing of the density. In comparison, the multiple scattering result for VV keeps increasing to a larger cylinder density of about 7/m^2, or 0.868 in optical thickness, and then slowly decreases. In Figure 3.4b, the difference between backscatters of multiple scattering and 1st order scattering, $\sigma^{\mathrm{mul}}(\mathrm{dB}) - \sigma^{1\mathrm{st}}(\mathrm{dB})$, are explicitly drawn as a function of optical thickness. It is worth noting that the dependence is close to linear. This clearly shows the multiple scattering corrects the underestimated backscatter for larger optical thickness for the single scattering.

It is interesting to compare the backscattering results when using only the first two Stokes parameters (I_v and I_h) and all of the four Stokes parameters. In Table 3.2, the backscattering from the first fifth order is listed for both cases. The 1st order scattering is exactly the same; the difference in 2nd order scattering is within 10%. This indicates that when multiple scattering becomes important, the correlation between polarizations also becomes significant to contribute to the backscattering. As a result, it is necessary to employ all four Stokes parameters. However, while using only the first two Stokes parameters maintains a relatively good approximation. Note that all four Stokes parameters are used in the examples throughout the study if not explicitly stated.

Table 3.2
Comparison of backscatters from each order using first two and all four Stokes parameters, parameters are given in Figure 3.3

Order	2 Stokes VV	4 Stokes VV	2 Stokes HH	4 Stokes HH
1st	0.1853	0.1853	0.0889	0.0889
2nd	0.1055	0.1140	0.0047	0.0052
3rd	0.0342	0.0349	0.00063	0.00065
4th	0.0093	0.0093	0.00012	0.00012
5th	0.0025	0.0025	0.000026	0.000026
sum	0.3369	0.3460	0.0943	0.0949

The scattering and attenuation of leaves becomes more and more important as frequency increases. In the following examples, we introduce leaves into the geometry and scattering modeling. Circular disks are considered to model leaves [36,37], and the Generalized Rayleigh-Gans approximation (GRG) is applied to calculate the internal field and scattering field of a circular disk [37]. The radius is set to be 2.5 cm with a thickness 0.3 mm. The same probability, $p(\alpha, \beta)$, is used to quantify the leaf orientation distribution with $\Delta\beta$ equal to $45°$, which means the tilting angle of the normal direction of leaves are uniformly distributed between 0 and 45 degree. The dielectric constant of leaves is set to $35 + 10i$ [35]. The disk number density is related to the cylinder density by 100 disks per cylinder. When the cylinder density is 7.2/m^2, the disk density is 720/m^2. At 1.26 GHz, the scattering albedo of leaves is 0.0611 for v-pol and 0.0604 for h-pol; the optical thickness of a leaf in the direction of incidence is 0.0717 for v-pol and 0.1004 for h-pol. Using the same permittivity and geometric parameters, the scattering albedo of a leaf at 13.6 GHz is 0.8410 for v-pol and 0.8636 for h-pol and optical thickness in the direction of incidence is 4.5655 for v-pol and 7.4660 for h-pol. The scattering properties of cylinders using the same set of parameters at 13.6 GHz, albedo of 0.7085 for v-pol and 0.6170 for h-pol, and the optical thickness in the direction of incidence is 0.2894 for v-pol and 0.2190 for h-pol. It is obvious that at L-band, scattering from leaves is small compared to stalks/trunks (cylinders), while at Ku-band, when the scattering from cylinders enters geometric optics region, the leaf scattering and absorption far overweighs that of cylinder. The scattering and absorption optical thickness in the direction of incidence for cylinders

and disks are listed in Table 3.3.

Table 3.3
Comparison of scattering/absorption optical thickness The dielectric constants are given in Table 3.4 and geometrical parameters are given in Table 3.7

Optical thickness	1.26GHz				13.6GHz			
	τ_{sv}	τ_{sh}	τ_{av}	τ_{ah}	τ_{sv}	τ_{sh}	τ_{av}	τ_{ah}
Cylinder	0.6085	0.0626	0.2843	0.1043	0.2050	0.1351	0.0844	0.0839
Disk	0.0044	0.0061	0.0673	0.0943	3.8396	6.4476	0.7259	1.0184
Cylinder+disk	0.6129	0.0687	0.3516	0.l986	4.0446	6.5827	0.8103	1.1923

* "s" for scattering and "a" for absorption. "v" for v-pol and "h" for h-pol.

In the next example a canopy layer comprised of both cylinders (stalks) and disks (leaves) in L-band at 1.26 GHz is considered. The geometric and dielectric properties of cylinders and disks are those described previously. The number density of disk is set to be 100 times that of cylinders. When the cylinder number density is 7.2/m^2, the overall scattering albedo is 0.6355 for v-pol, and 0.2569 for h-pol; the optical thickness in the direction of incidence is 0.9644 for v-pol and 0.2673 for h-pol. Compared with the cylinder-only simulations above, the multiple backscattering up to 5th order decreases from -4.61dB to -5.18dB for v-pol by including disks, and reduces from -10.23dB to -10.53dB for h-pol; the first-order backscattering is lowered by a similar amount, i.e., from -7.32dB to -7.89dB for v-pol, and from -10.51dB to -10.83dB for h-pol.

In Figure 3.5, the backscatter is again plotted as a function of cylinder densities. For the vertical polarization, the incorporation of leaves results in more attenuation than scattering, so the backscatter is reduced. The size of the change gradually increases with the density up to 0.8dB at the cylinder density of 10/m^2. For the horizontal polarization, the impact of incorporating leaves is different between sparse and dense corn population. The backscatter is increased by about 0.4dB for a cylinder density of 1/m^2, and decreases by about 0.6dB for a cylinder density of 10/m^2.

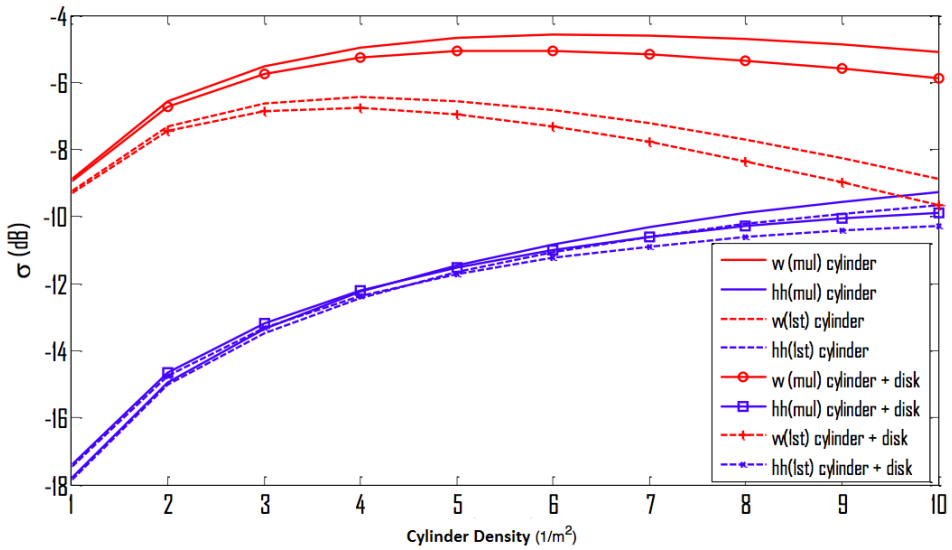

Figure 3.5 Backscatters at 1.26 GHz with 40 degree incidence as a function of optical thickness for a canopy layer comprised of cylinders and disks. Detail parameters are in Table 3.7

Frequency dependence of backscatters is examined to see how the multiple scattering results deviate from 1st order scattering. For this purpose, both cylinders and disks are included when modeling the scattering from a vegetation layer. A dual-dispersion model by Ulaby et al. [38] is used to account for the frequency dispersive dielectric constants of vegetation. In this model, the vegetation dielectric constant is a function of frequency, water content and salinity. The salinity is set to be 8.5 parts per thousand, yielding an ionic conductivity of 1.27 Siemens per meter [38]. For the moisture content of vegetation, the gravimetric moisture content of cylinder is 70%, and the gravimetric moisture content of disks is 50%. The resulting dielectric constants are listed in Table 3.4, for a set of frequencies of interest, including 1.26 GHz (L-band), 5.3 GHz(C-band), 9.6 GHz (X-band), and 13.6 GHz (Ku-band). A smooth soil surface is also assumed, with the same soil moisture of 20% and clay fraction of 18% as before. The soil permittivity from the generalized refractive mixing dielectric model for moist soils [22] is listed in Table 3.4.

Table 3.4

Dielectric constants of cylinder, disk and soil.

Frequency	cylinder	disk	soil
1.26GHz	29.47+9.38i	17.46+5.90i	10.12+1.11i
5.3GHz	25.06+8.06i	14.26+4.71i	9.68+1.92i
9.6GHz	21.91+9.42i	12.49+5.13i	8.87+2.73i
13.6GHz	19.2+10.04i	11.1+5.31i	8.06+3.13i

* The Gravimetric moisture content for cylinder and disk are 70% and 50% respectively. Soil moisture is 20% and clay fraction is 18%

Based on the same geometric parameter of cylinders and disks, and a number density of cylinder set to 5.5/m^2, and number density of disks as 550/m^2, the optical thickness in the direction of incidence and the single scattering albedo for each frequency was determined and presented in Table 3.5. The h-pol optical thickness increases quickly with frequency mainly due to leaves. The v-pol optical thickness exhibits a more complex behavior. It first decreases with frequency and then increases. This is because the decrease of cylinder scattering and increase of disk scattering at the same time.

Table 3.5

Optical thickness (40 degree incidence) and single scattering albedo. The dielectric constants are given in Table 3.4 and geometrical parameters are given in Table 3.7

Frequency	$\tau_{v,c\&d}$	$\tau_{h,c\&d}$	$\tau_{v,c}$	$\tau_{h,c}$	$\tau_{v,d}$	$\tau_{h,d}$	$\varpi_{v,c\&d}$	$\varpi_{h,c\&d}$	$\varpi_{v,c}$	$\varpi_{h,c}$	$\varpi_{v,d}$	$\varpi_{h,d}$
1.26GHz	0.7344	0.1192	0.6983	0.0686	0.0362	0.0506	0.6207	0.3084	0.6515	0.5172	0.0261	0.0258
5.3GHz	0.5069	0.4395	0.3221	0.1788	0.1847	0.2607	0.5298	0.3937	0.638	0.4628	0.341	0.3463
9.6GHz	0.6947	0.852	0.243	0.181	0.6947	0.852	0.5162	0.4982	0.6207	0.5236	0.46	0.4913
13.6GHz	0.9590	1.3182	0.2222	0.1848	0.7368	1.1334	0.5363	0.5516	0.6297	0.5444	0.5081	0.5528

* "c" for cylinder and "d" for disk. "c&d" for cylinder and disk combined "v" for v-pol and "h" for h-pol.

In Figure 3.6, the backscatter is plotted as a function of frequency. In the left panel, the multiple scattering results are compared with the 1st order results. Note that the multiple scattering effects are important for v-pol over the whole frequency range because of the relatively large optical thickness and albedo. For h-pol, the significance of the multiple scattering effects increases with

frequency. In the middle and right panels the 1st order scattering results are decomposed into a double bounce contribution and a volume scattering contribution for v-pol and h-pol, respectively. The 1st-order volume scattering keeps increasing with frequency. The double bounce contribution (mostly due to cylinders) dominants the 1st order backscattering at L-band for both v-pol and h-pol. The volume scattering (mostly due to disks) becomes comparable to the double bounce contribution in C-band, and outweighs the double bounce contribution in X-band. The double bounce contribution to the h-pol is also dominant in C-band, and decreases to the same level as volume scattering in X-band. The decrease in the h-pol double bounce contribution with frequency is caused by the attenuation from the disks.

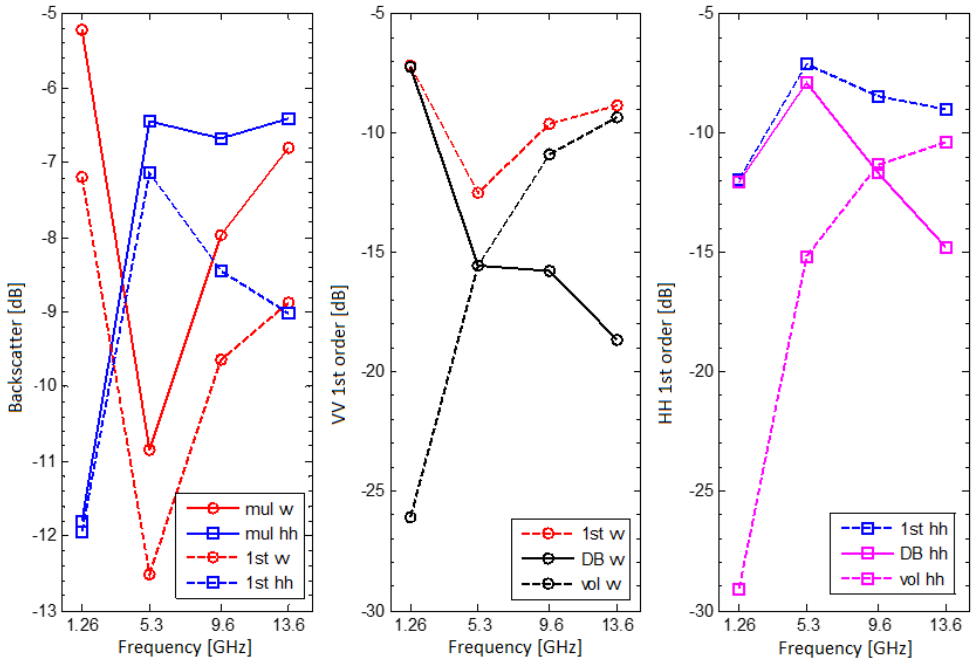

(a) (b) (c)

Figure 3.6 Backscatter's dependence on frequency at 40 degree incidence. The vegetation layer is comprised of cylinders and disks. (a) Backscatters from multiple and 1st order scattering (b) Scattering decomposition of VV (c) Scattering decomposition of HH. The dielectric constants are given in Table 4 and geometrical parameters are given in Table 3.7 Cylinder density is $5.5/m^2$ and disk density is $550/m^2$.

For the special case of 13.6 GHz, in Figure 3.7 the contribution to backscattering from different scattering orders are compared along with a list of the dominant scattering mechanisms in Table 3.6. At this frequency, the optical thickness in the direction of incidence is 0.9590 for v-pol and

1.3182 for h-pol. The scattering albedo at the angle of incidence is 0.5363 for v-pol and 0.5516 for h-pol. The contribution from 2nd and 3rd order scattering are important for both v-pol and h-pol due to the large optical thickness and scattering albedo. The first order contribution comprises only 62.6% for v-pol, and 55.6% for h-pol. Multiple scattering effects are even larger for h-pol in this example. It is also interesting to note that the contribution from the 1st order surface-volume double bounce term is even smaller than the contribution from the second order volume-volume scattering due to the large attenuation. The direct volume backscattering from disks (leaves) comprises the largest portion of the total backscattering.

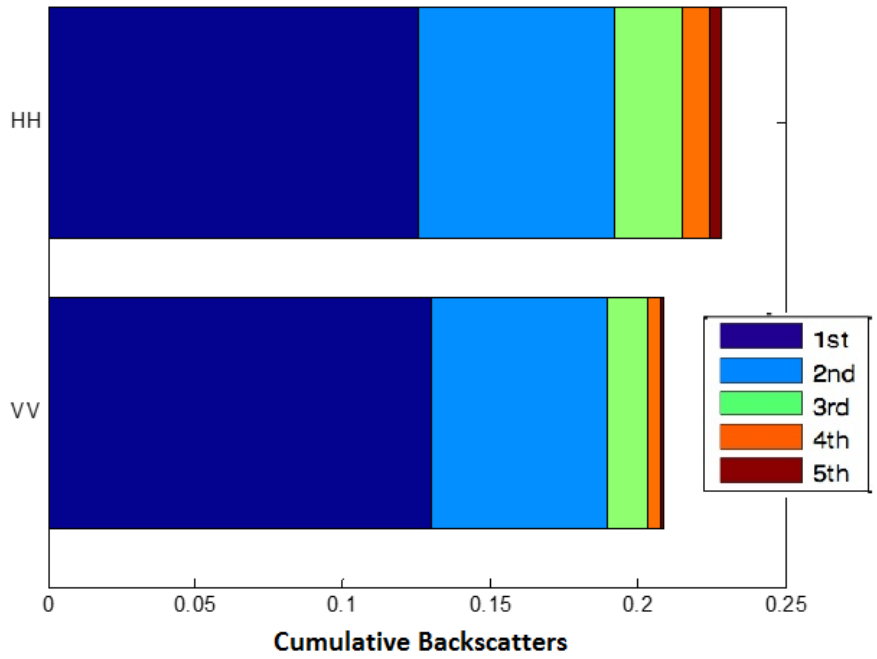

Figure 3.7 Backscatter contribution up to 5th order at 13.6GHz (Ku-band) with 40 degree incidence. Parameters are the same as given in Figure 3.6.

Table 3.6
Contribution from dominant terms at Ku-band (13.6GHz). The parameters as the same as given in Figure 3.6

order	description	Percentage (VV)	Accumulative percentage (VV)	Percentage (HH)	Accumulative percentage (HH)	Possible paths with strong contribution
1	volume	55.5%	55.5%	40.2%	40.2%	dsu
2	volume-volume	25.3%	80.8%	20.6%	60.8%	dsu|usu,dsd|dsu
1	volume-surface	6.5%	87.3%	14.6%	75.3%	drusu, dsdru

Next, we then examine the angular dependence of the backscattering. In Figure 3.8 and Figure 3.9, the backscattering is plotted as a function of incidence angle for L-band and Ku-band in the previous example, respectively. The results of multiple scattering and 1st order scattering are compared. For L-band (Figure 3.8), the horizontal backscattering decreases uniformly with incidence angle as the optical thickness increases. The effects of multiple scattering are weak due to the generally small optical thickness and albedo. The vertical backscattering on the other hand undergoes several resonances.

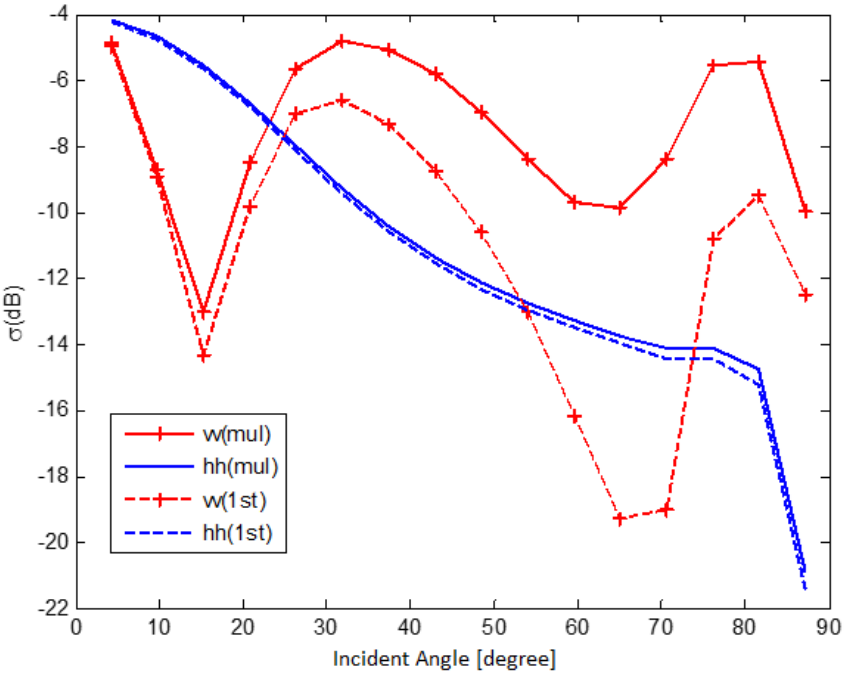

Figure 3.8 Angular dependence of backscatters at 1.26 GHz. Parameters are the same as given in Figure 3.6.

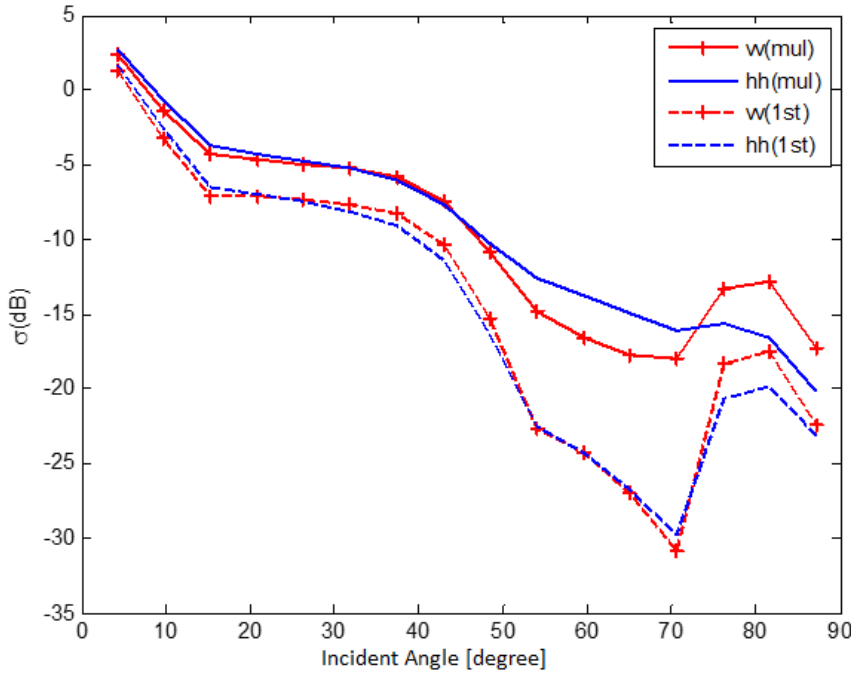

Figure 3.9 Angular dependence of backscatters at 13.6 GHz. Parameters are the same as given in Figure 3.6.

The first minimum of VV around 15 degree can be explained by the pattern of the scattering cross section of cylinder in the double bounce direction; the second minimum of VV around 70 degree could be explained by the Brewster angle effect of ground reflectivity; the final drop of both VV and HH is caused by the increase in optical thickness. The effects of multiple scattering for v-pol then become significant except at near nadir incidence angles and increase with incidence angle. At Ku-band (Figure 3.9), multiple scattering effects are generally large due to large optical thickness and scattering albedo; HH typically has a larger optical thickness than VV. For incidence angle below 10 degree, VV and HH decrease mainly due to the decrease in scattering cross section of disk in the double bounce direction. Between 10 degree and 70 degree, volume scattering from disk (leaves) dominates the backscattering, thus the overall backscattering follow the trend of the backward scattering cross section of disk (leaves). Between 70 degree and 80 degree, the backscattering increases due to the rapid increase of cylinder (stalks) backward scattering cross section and the rapid increase of surface reflectivity after passing the Brewster angle. Backscattering then drops because volume scattering saturates and the bounce terms decrease due to the large attenuation associated with large optical thickness in the last 10 degrees.

Table 3.7
Simulation parameters in Figures and Tables (ϵ is for 1.26GHz)

Figure or Table	Cylinder (=stalk)		Disk (=leaf)		Soil
Figure 3.3 Figure 3.4 (no leaf case)	radius	1 cm	NONE		Flat ground $\epsilon = 10.12 + 1.11i$
	Length	1 m			
	ϵ	$50 + 15i$			
	Density	$7.2\ m^{-2}$			
	β	$0^o \sim 15^o$			
Figure 3.5 Table 3.3 (with leaf)	radius	1 cm	radius	2.5 cm	Flat ground $\epsilon = 10.12 + 1.11i$
	Length	1 m	Thickness	0.3 mm	
	ϵ	$50 + 15i$	ϵ	$35 + 10i$	
	Density	$7.2\ m^{-2}$	Density	$720\ m^{-2}$	
	β	$0^o \sim 15^o$	β	$0^o \sim 45^o$	

3.6 Results and comparison with SMAPVEX12 measurement data

3.6.1 Forward model comparison with SMAPVEX12 corn data

In this section we validate the above modeling result using the extensive L-band airborne field campaign data from the SMAPVEX12 [32]. The SMAPVE12 data covers the entire range of VWC change and soil moisture (Mv) change cycles, offering an opportunity to validate the model over comprehensive conditions of corn growth. The following key findings from the above modeling study are critical to successful validation with the observation : Multiple scattering effects become significant for all incident angles for co-polarization as frequency increases; when both optical thickness and scattering albedo exceed 0.4, there is large deviation between multiple scattering and 1st order scattering results, while the first order scattering saturates (Figure 3.4a & Table 3.5).

Corn field (field number 83) is used here as an example of the successful validation (Figure 3.10). The soil moisture and vegetation water content (VWC) time-series are shown in Figure 3.10a. The corn field is modeled as a collection of cylinders randomly distributed with a preferred average orientation. The cylinder dimension, orientation distribution, and gravimetric moisture content are themselves a function of time (as a result of crop growth), and they are estimated from the ground measurement data collected in the SMAPVEX12 campaign. The rough soil surface is modeled as a 3D random profile with an exponential correlation function. The rms height of 1.25 cm and correlation length of 23.75 cm are based upon the experiment data for this field. The bare surface backscattering is determined using a pre-calculated lookup table applying Numerical Solutions of Maxwell Equations in 3D (NMM3D) [12,39]. The surface scattering is attenuated by the vegetation layer before being added to the total backscattering. The surface coherent reflectivity is calculated using the Kirchhoff approximation. The forward scattering model predictions using 1st order scattering and multiple scattering, both with cyclical correction included, are plotted against the measured backscatter time series in Figure 3.10b. Results of the 1st order and multiple scattering are similar for HH backscattering when VWC is small, however, they deviate by about 2dB for the largest VWC of about 3 kg/m^2; the deviation between 1st order and multiple scattering for VV backscatter is larger than that of HH and could be as large as 6.5 dB when VWC is 3 kg/m^2.

The incorporation of multiple scattering effects improves the agreement between the model predictions and measurements for both polarizations especially at the later growth stage when VWC of corn is > 3 kg/m^2.

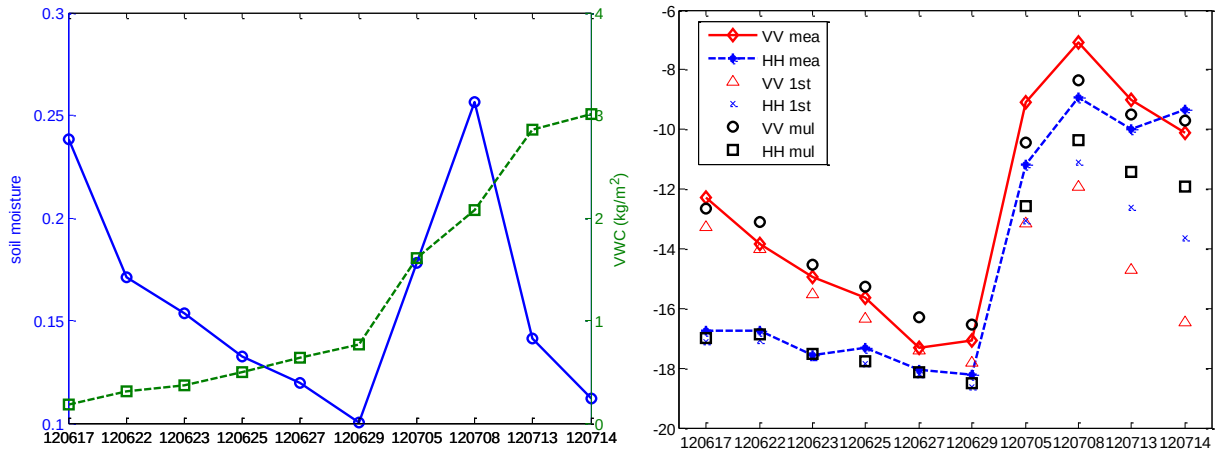

(a) soil moisture and VWC time series

(b) comparison between backscattering

Figure 3.10. Backscatters from multiple and 1st order scattering in comparison with SMAP corn data. Corns are modeled with cylinders only and parameters estimated from ground measurement of corn field 83 in SMAPVEX12 [8]. Soil parameters are given in Table 3.8.

During the SMAPVEX12 field campaign, both ground measurements and radar measurements at 1.26 GHz were obtained. Figure 3.11 shows the vegetation water content for both corn stalks and corn leaves. In the early growth stage, the VWC of the stalks and leaves are comparable. Later VWC from stalks continues to increase while VWC from leaves levels off. The regression lines in the plot are used to derive the VWC ratio for stalks and leaves. The ratio is later applied to the multiple scattering model by separating a total VWC into those of stalks and leaves. E.g. $VWC_{stalk}(VWC) = VWC\frac{VWC_{stalk,empirical}(VWC)}{VWC_{total,empirical}(VWC)}$

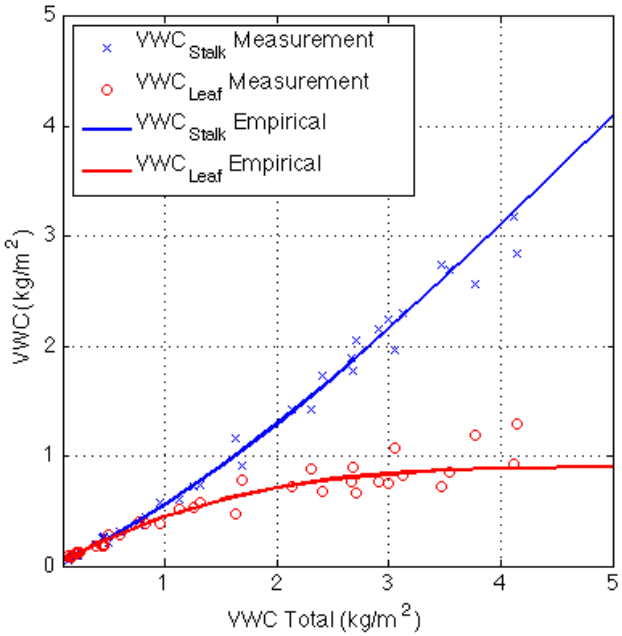

Figure 3.11 SMAPVEX12 measurement data and empirical approximation for VWC of corn stalk and leaf.

Among parameters essential to simulate the corn, radius of the stalk(r_{stalk}) and the number of leaves per corm plant(N_{LPP}) come from empirical allometric equations derived from measurement data. The length of the stalk (L_{stalk}) and the radius of the leaf (r_{leaf}) come from the allometric relationship given in (3.27) and (3.28).

$$VWC_{stalk} = \rho_{water}\pi r_{stalk}^2 L_{stalk} m_{veg,stalk} N_A \tag{3.27}$$

$$VWC_{leaf} = \rho_{water}\pi r_{leaf}^2 t_{leaf} m_{veg,leaf} N_A N_{LPP} \tag{3.28}$$

$VWC_{stalk}(kg/m^2)$ is VWC for stalks while $VWC_{leaf}(kg/m^2)$ is for leaves. ρ_{water} stands for water density (1000 kg/m^3). $r_{stalk}(m)$ is the radius of the stalk while $L_{stalk}(m)$ is the length. $m_{veg,stalk}(dimensionless)$ is the volumetric moisture content of the stalk while $m_{veg,leaf}(dimensionless)$ is for the leaf. $N_A(1/m^2)$ is the number of corn stalks per squared meter. $r_{leaf}(m)$ is the equivalent radius of the leaf. t_{leaf} is the thickness of leaves. N_{LPP} is the number of leaves per corn plant.

Table 3.8
SMAPVEX12 corn field soil parameters

Field ID	RMS height [cm]	Correlation Length [cm]	Clay fraction
24	1.79	11.75	0.048
53	0.80	7.5	0.291
54	0.82	36.75	0.132
62	1.5	14.25	0.076
71	1.57	15.5	0.063
72	1.07	15	0.049
83	1.25	23.75	0.155
93	1.73	66.75	0.377
94	1.28	23.75	0.183

We have VWC data for all 9 fields as well as soil parameters (Table 3.8), but the geometry data collection was not necessarily synchronized with UAVSAR measurements of backscattering coefficients. To improve the synchronization, we estimate these essential parameters from VWC. Because VWC is easier to measure. For cylinders, backscatter is more sensitive on the change of the radius rather than the length (power to 4 vs power to 2). We first derive empirical formula for the radius to make sure the backscatter is within the reasonable range as we observe in the measurement data. Second, corn stalk density, $N_A(\ 1/m^2)$, is fixed to 6 since it is reasonable to keep the same number of corn plants through the growth period. The number of leaves per plant (N_{LPP}) is also counted in situ. For the thickness of leaves, since the quantity is very small (0.2~0.4mm), we choose a fixed value within this range instead of varying with VWC. We use 0.35mm and this value can also be referred to the study from Chauhan and et al. [40] Then moisture contents for stalks ($m_{veg,stalk}$) and leaves ($m_{veg,leaf}$) are chosen to give the best match of the length of the stalk and the equivalent radius of the leaf with ground measurement data. Finally, we plot the length of the stalk in Figure 3.12b and the equivalent radius of the leaf in Figure 3.13a. Both agree well with the change of VWC.

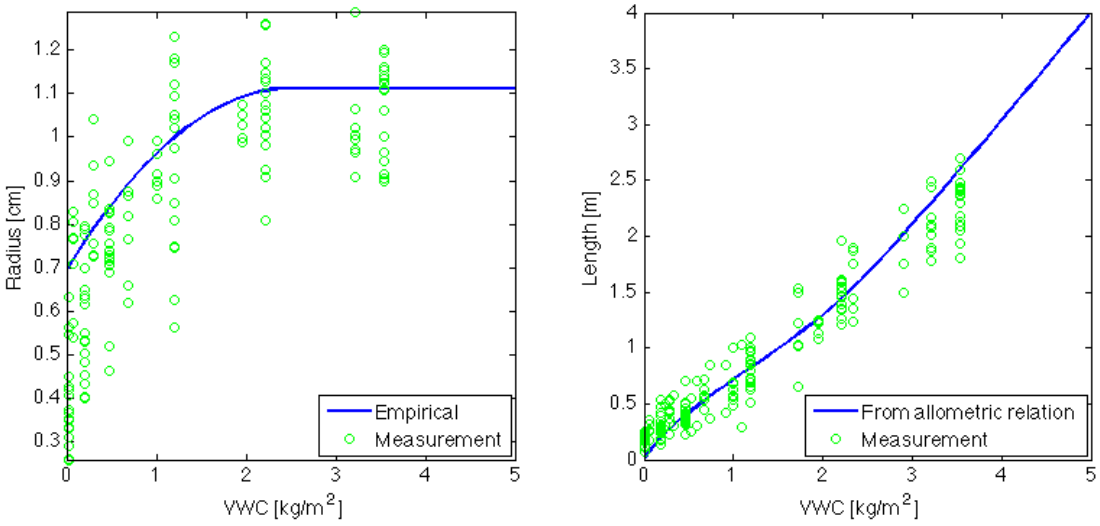

(a) (b)

Figure 3.12 (a) Corn stalk radius from SMAPVEX12 measurement data and empirical approximation (b) Corn stalk length from SMAPVEX12 measurement data and the estimation from allometric relation

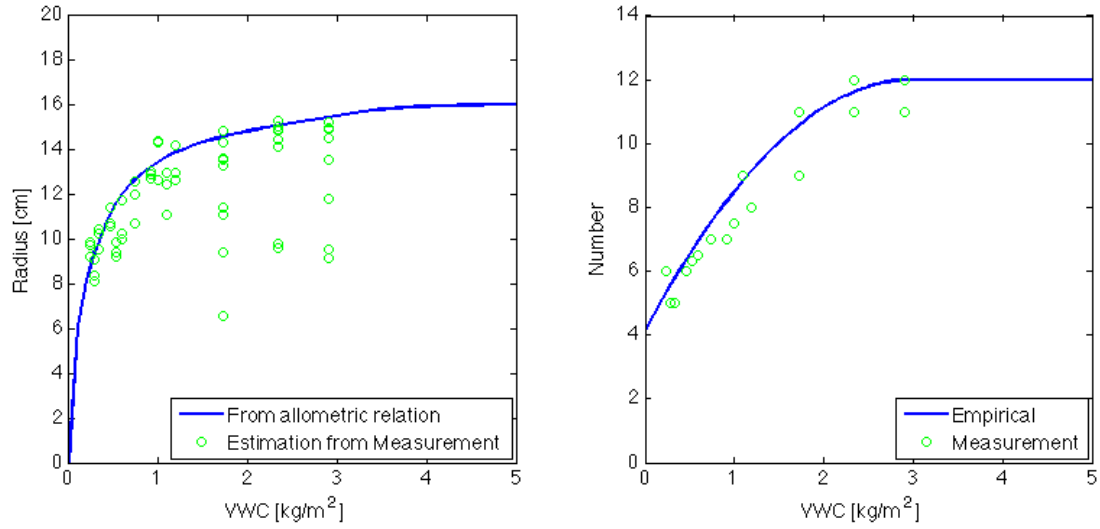

(a) (b)

Figure 3.13 (a) Estimation of corn leaf radius from SMAPVEX12 measurement data and allometric relation (b) Number of leaves per corn plant from SMAPVEX12 measurement data and empirical approximation.

The moisture content for stalks is found the same as that in [40] while the moisture content for leaves is larger. The difference is expected since we apply this value for the whole growth period. However, it is still within the reasonable range as we see in the study of corn leaf's dielectric

constant. [41] With the allometric relationship, for a given VWC input axis of the model, the plant geometry data are estimated and used to drive the model computation. VWC becomes the only kernel parameter to represent the growth of corn.

For leaves, we calculate the scattering based on infinite disk approximation. [34] Since the thickness of leaves is very small, the leaves' area is more important than the shape. As a result, this yields the same scattering as the previous used GRG method. For this reason, we approximate the leaf using thin circular disks. We plot the equivalent radius, computed from length and width of leaves based upon ground measurement in Figure 3.13a. The radius is derived assuming the length (L) and the width (W) come from the rectangular sheet. In the study of Sarabandi and et al for backscattering from leaf, rectangular sheet was analyzed [42]. The same shape was also applied to the modeling of corn leaf. [43] Figure 3.13b shows the data and the regression of the number of leaves per plant.

Diameter (D) measurements were available for the stalks from SMAPVEX12. In Figure 3.12a the radius(r) is plotted versus VWC (kg/m^2) by treating corn stalks as circular cylinders (r=D/2). Notice that the radius reaches its maximum around 1.1 cm for VWC larger than 2 kg/m^2. Based on the estimated radius, we can then apply geometrical formula (3.27) to compute the corresponding length. There are about 6 corn plants within 1 squared meter. The measurement data also shows the row spacing is around 70 cm, which means there are 3 corn plants in one row, totally 2 rows, within 1 squared meter. The volumetric moisture content of stalks and leaves are set to 44%, about 70% of gravimetric moisture content.[38] The moisture content for stalks is the same as in that in the previous example while the moisture content of leaves is chosen larger(the same as stalk) to fit the estimation of equivalent radius[41]. The length of the stalk, L_{stalk}, is computed and is shown in Figure 3.12b along with ground measurement data. The computed length falls nicely within the measurement data range.

In order to consider both stalks and leaves using the multiple scattering model, it is necessary to first compute the phase matrices. This also provides extinction coefficients for both components. Following this the phase matrices as well as the extinction coefficients are summed to account for the contribution from both stalks and leaves simultaneously. Next this result is combined with the given soil roughness and dielectric constant to compute the backscattering up to 2nd order. For a given VWC range, 0 to 5 kg/m^2, surface rms height range, 0.1 to 4 cm, and soil dielectric constant

rage, 3 to 30, the lookup table was established for corn fields. The lookup table is interpolated at finer resolutions of VWC, rms height, and soil dielectric constant and is subsequently validated with SMAPVEX12 measurement data for 9 fields. Figure 3.14 is the co-polarization time series comparison. Two fields are selected in Figure 3.14. The corresponding soil parameters can be found in Table 3.8. Both fields show significant increase of backscatters in early July while VWC increasing fast. From that point on multiple scattering contributes significantly, as shown in Figure 3.10b. The phenomenon is seen among all corn fields in SMAPVEX12.

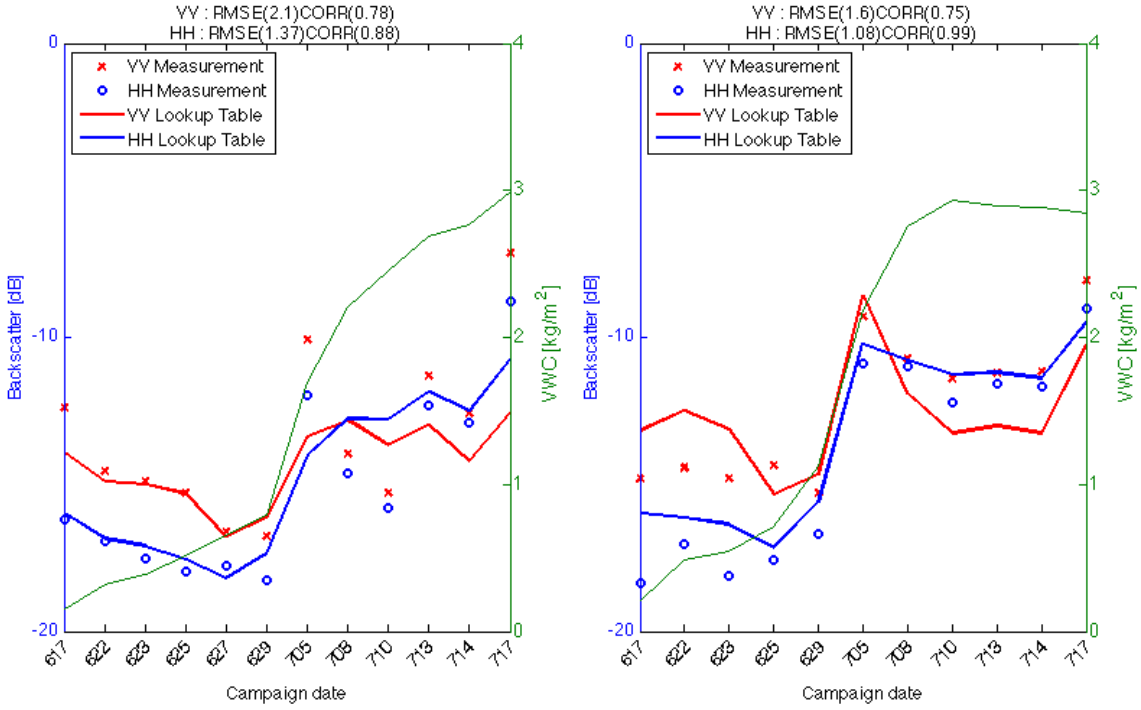

(a) Field 24 (b) Field 62

Figure 3.14 Field by field forward Model validation of co-polarization backscatters, VV & HH, with SMAPVEX12 measurement data using pre-computed lookup table

3.6.2 Soil moisture and vegetation water content retrieval

The lookup table is applied to time-series soil moisture retrieval using HH and VV time-series input (see [33] paper for the details of the retrieval approach)[44]. For each field, the time-series

soil moisture were retrieved after retrieving a static rms height. The retrieval results are shown in Figure 3.15. Both fields show good agreement with the measurement data. The root mean square error is 0.02 cm^3/cm^3 for both fields. Figure 3.16 shows the validation of co-polarizations and soil moisture retrieval over all 9 corn fields of the SMAPVEX12. In Figure 3.16a both VV and HH have a root mean square error within 2dB. Also, the mean bias is small. In Figure 3.16b, root mean square error of soil moisture is 0.06 cm^3/cm^3 with almost no bias. Since the multiple scattering is important especially when VWC is large, accurate VWC retrieval is essential. Figure 3.17 shows the time-series VWC retrieval and the scatter plots from all the retrieval results. Figure 3.17 shows the time series retrieved VWC agrees very well with the data. Also, the overall root mean square error is only 0.44 kg/m^2 with the bias of 0.057 kg/m^2.

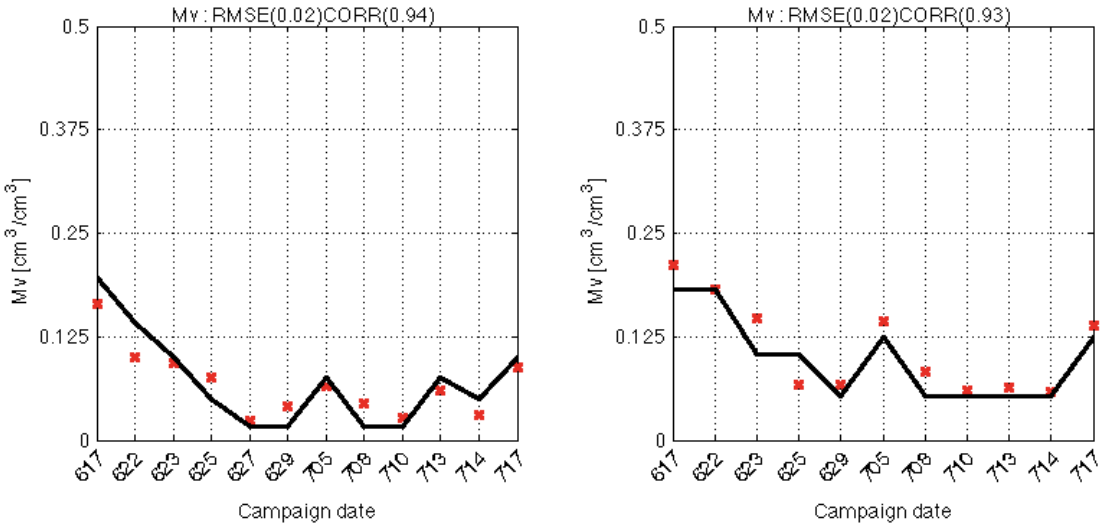

(a) Field 24 (b) Field 62

Figure 3.15 Field by field time-series soil moisture retrieval with SMAPVEX12 measurement data using pre-computed lookup table

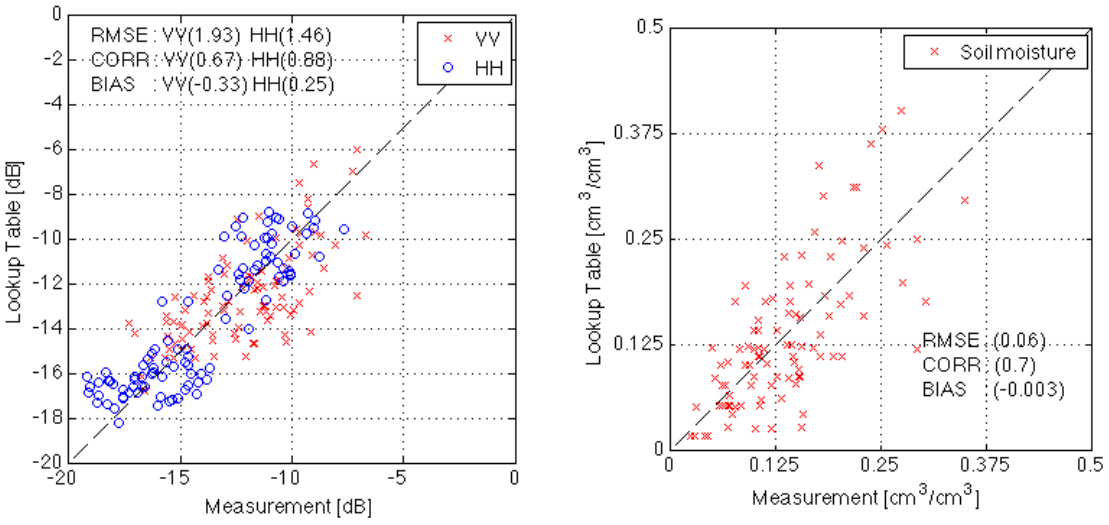

(a) (b)

Figure 3.16 Using pre-computed lookup table to do (a) Forward model validation and (b) Time-series soil moisture retrieval with 98 corn data from SMAPVEX12

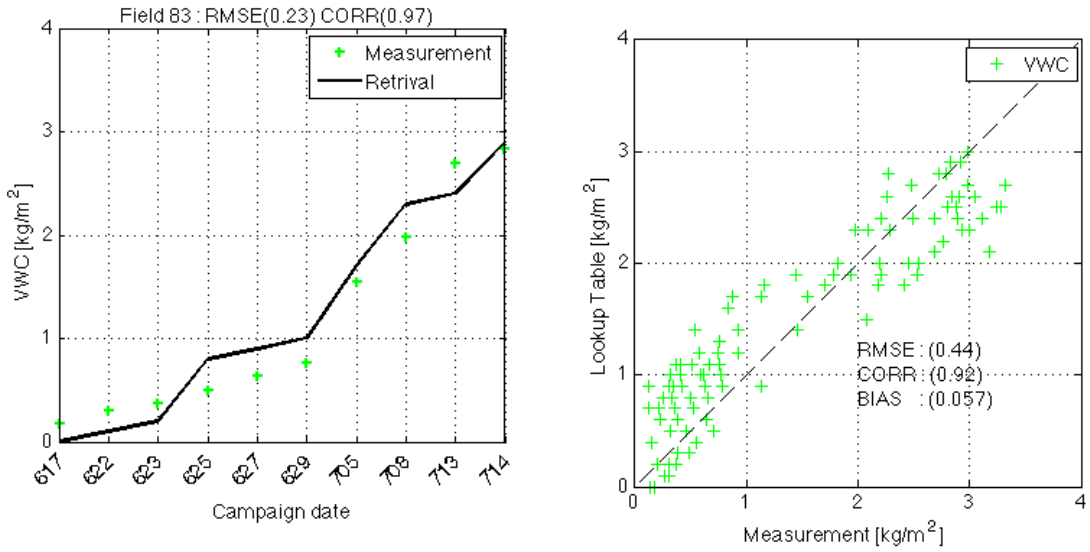

(a) (b)

Figure 3.17 (a) Time-series vegetation water content (VWC) retrieval using pre-computed lookup table for field 83 from SMAPVEX12 (b) Time-series VWC retrieval using pre-computed lookup table with 98 corn data from SMAPVEX12.

In summary, from the co-polarization validation, it was observed that multiple scattering provides a more accurate and larger backscatter than 1st order. Without multiple scattering, the backscatter is underestimated by considering only larger attenuation when VWC is large. This leads to correct

retrieval for soil moisture when VWC is large as well.

3.7 Summary

In this chapter, the multiple scattering and backscattering enhancement effects on volume scattering with the existence of one bottom reflective boundary are considered by applying the iterative numerical approach to solve the vector radiative transfer equation. The optical thickness dependence, frequency dependence and angular dependence of backscattering are considered in the analyses.

Multiple scattering effects are important when the optical thickness and the scattering albedo are large. When both the albedo and the optical thickness exceed 0.4, higher orders start to contribute significantly as shown in Figure 3.6a and Table 3.5. For L-band, the deviation between 1st order and multiple scattering for VV backscattering is larger than that of HH and could be 6.5 dB when VWC is 3 kg/m^2. Dominant scattering orders and mechanisms are identified. From C-band as shown in Figure 3.6a, multiple scattering effects contribute significantly to both VV and HH polarizations rather than VV for L-band. This would be essential for C-, X-, and Ku-bands since the underestimated backscatters caused by the attenuation could be corrected by multiple scattering.

The cyclical correction resulting from backscattering enhancement effects makes a RT approach agree with the wave approach in the backscattering direction, and become essential when both backscattering and brightness temperature are examined at the same time. Extensive validation of multiple scattering model using an a priori lookup table of corn fields with SMAPVEX12 measurement data was performed. Good agreement for both the forward co-polarization comparison and time series soil moisture retrieval are achieved. Multiple scattering model is also applied to time series soil moisture retrieval in recently launched NASA Soil Moisture Active Passive (SMAP) mission.

Chapter 4

Polarimetry in radar backscattering from soil and vegetated surfaces

4.1 SAR Polarimetry from Natural Terrain

SAR Polarimetry has become increasingly used for remote sensing of earth surfaces for monitoring water resources, forests, agriculture and natural disasters. Physical microwave scattering models are used to simulate the SAR polarimetric signatures and to study the microwave interactions with soil surfaces, vegetation and forests. In the past, the physical models and SAR simulators are based on simple analytical models and on assumed stochastic distributions of the signals. In this chapter, we use numerical solutions of Maxwell equations to model and simulate polarimetric SAR signatures to study speckle statistics at L and C band for rough soil surfaces

Electromagnetic scattering from soil surfaces has stochastic fluctuations known as speckle because of the stochastic nature of rough surface heights. In simulating SAR signatures, random rough surface is stochastically generated and then has been solved by Maxwell equations numerically for each sample. Numerical methods of 3D solutions of Maxwell equations (NMM3D) is applied as described in chapter 2. After solving Maxwell equations, the scattering matrices are computed accordingly (S_{VV},S_{HH},S_{VH},S_{HV}). Coherency matrix is studied using scattering matrices and as well as polarimetric SAR descriptors.

Coherency matrix and Interferometric Coherence of Vegetated Surfaces are introduced later by applying NMM3D with distorted Born approximation. Three kinds of scattering mechanisms are in this model including, volume scattering, double bounce scattering, surface scattering. Each scattering process has a distinct coherency matrix. The coherency matrix includes the correlation of the scattered fields from different combinations of polarizations. The interferometric coherence is the correlation as weighted by the product of vertical structure function and the interferometric phase. In chapter 2 and 3, the focus is more on the backscatters from physical model, however

from now on the scattered field correlation is more important to study the relation with the biomass from vegetated surface.

4.2 Scattering Matrix and Coherency Matrix from NMM3D for bare soil

Polarimetric synthetic aperture radar (PolSAR) images have been widely studied to retrieve target information in microwave remote sensing.[45] With the rapid increasing of interests on PolSAR for past decade, satellite missions such as L-band Advanced Land Observing Satellite-2 (ALOS2), C-band Radarsat2, X-band TerraSAR-X, TanDEM-X were designated for PolSAR application. In the future there will also be L-band missions such as NI-SAR and TanDEM-L. For bare soils, backscattering comes from rough surface. For vegetated surface, rough soil surface underneath the canopy can provide either direct backscattering or strong reflection from vegetation (double bounce). In the past, simple scattering models were used to simulate polarimetric radar speckle. Recently Numerical Maxwell Solutions in 3D (NMM3D) [46], also in chapter 2, is applied as polarimetric SAR simulators at L-band by directly calculating the scattering matrix for each realization. We will talk about the detail as follows.

4.2.1 Methodology

In chapter 2, NMM 3D gives the scattered electric field at backscattering direction for each realization, however this contains both coherent and incoherent scattering. To decompose them, first the coherent scattered field $\langle \overline{E}_s(\theta_s, \phi_s) \rangle$ is calculated by averaging over realizations

$$\langle \overline{E}_s(\theta_s, \phi_s) \rangle = \frac{1}{N} \sum_{n=1}^{N} \overline{E}_{s,n}(\theta_s, \phi_s) \tag{4.2.1}$$

where $\overline{E}_{s,n}$ is the scattered field for the realization n, and angular brackets represent the averag over realizations. The incoherent scattered field for the realization n is found by the subtraction of coherent field from total field.

$$\overline{E}_{s,n}^{incoh}(\theta_s, \phi_s) = \overline{E}_{s,n}(\theta_s, \phi_s) - \langle \overline{E}_s(\theta_s, \phi_s) \rangle \tag{4.2.2}$$

For a surface with infinite size, the coherent field exists only in the specular direction and will not contribute to radar backscattering. Thus for a very large surface, only the incoherent field contributes to the backscattering direction. However, for numerical simulations, the surface is not that large and the coherent wave has an angular spread which is of the order of the wavelength divided by L. Since the field at the backscattering direction is small, the subtraction is essential to get correct incoherent field.

The incoherent bistatic coefficients and backscattering coefficients are normalized by the incident power.

$$\gamma_{\beta\alpha}^{incoh}(\theta_s, \phi_s; \theta_i, \phi_i) = \frac{1}{N}\frac{1}{2\eta P_\alpha^{inc}}\sum_{n=1}^{N}\left|E_{\beta\alpha,n}^{incoh}(\theta_s, \phi_s; \theta_i, \phi_i)\right|^2 \tag{4.2.3}$$

The backscattering coefficients are

$$\sigma_{\beta\alpha}(\theta_s = \theta_i, \phi_s = \phi_i + \pi; \theta_i, \phi_i) = \cos\theta_i\, \gamma_{\beta\alpha}^{incoh}(\theta_i, \phi_i + \pi; \theta_i, \phi_i) \tag{4.2.4}$$

For polarimetric studies, we calculate the normalized scattering matrix for each nth realization by

$$S_{\beta\alpha,n} = \sqrt{\frac{1}{2\eta P_\alpha^{inc}}cos\theta_i}E_{\beta\alpha,n}^{incoh} \tag{4.2.5}$$

Using the above normalization, the average absolute square of the scattering matrix elements will give the backscattering coefficients. A sign change has also be used for polarimetry applications because the definitions of directions of polarizations in the NMM3D simulations are based on the incident and scattered wave vectors which are opposite in backscattering as $\hat{k}_s = -\hat{k}_i$ [34]. $\hat{k}_s$ and $\hat{k}_i$ can also be found in eq. (2.6 -2.7). Please note that the definition in (4.2.5) is unit-less on length since the normalization includes surface size.

4.2.2 Simulation for L- and C-bands

Polarimetric SAR simulation results from the rough surface are presented with emphasis on polarimetric properties. To ensure the data quality of the simulated coherency matrix, we examine the polarimetric speckle properties, including amplitude ratio and phase difference between two

polarized channels, of a supposed fully developed speckle scene such as randomly rough surface considered. Before proceeding, the simulation parameters are given. For L-band(1.26GHz), a total of 5 cases are considered by varying the surface roughness (*rms* height s and correlation length ℓ), surface dielectric constant. Detail is in Table 4.1. For C-band(5.4GHz), a total of 4 cases are considered as shown in Table 4.2. The incident angle is fixed at 40 degrees. Exponential correlation function is chosen since from most studies it represents best the natural surfaces such as soil surface. For L-band, the elements of the scattering matrix are calculated with 32 by 32 squared wavelengths rough surface, each is ensemble averaged from 958 realizations to ensure sufficient statistics. For C-band, the elements of the scattering matrix are calculated with 16 by 16 squared wavelengths rough surface, each is ensemble averaged from 250 realizations to ensure sufficient statistics. The computation time is dependent on the surface roughness and thus the sampling density. For L-band, the computation was using 16 processors on USA NSF TeraGrid's Steele cluster with 2.33 GHZ Dell 1950 CPUs for each processor. For L-band cases, it took about 1.5 min for each realization for the size of 16 squared wavelength, and roughly 8 min for the size of 32 squared wavelength. For C-band, the preconditioned NMM3D were performed with 256 CPU cores on NSF XSEDE Stampede (2.7GHz Xeon E5-2680 CPU) clusters. Detail of facility of NSF XSEDE is in appendix.

Table 4.1

Simulation parameters for the coherency matrix calculations (L-band)

	Radar Frequency	Surface Roughness	θ(deg)	Dielectric	Correlation Function
Case1	1.26GHz	s= 4cm (ks=1.055) λ=40cm(kλ=10.55)	40	8.35+j 1.99	Exponential
Case2	1.26GHz	s= 4cm (ks=1.055) λ=60cm (kλ=15.82)	40	9+j 2.5	Exponential
Case3	1.26GHz	s= 3cm (ks=0.791) λ=45cm (kλ=11.87)	40	9+j 2.5	Exponential
Case4	1.26GHz	s= 2cm (ks=0.527) λ=30cm (kλ=7.912)	40	9+j 2.5	Exponential
Case5	1.26GHz	s= 1cm (ks=0.263) λ=15cm (kλ=3.956)	40	9+j 2.5	Exponential

Table 4.2

Simulation parameters of rough surface using exponential correlation function (C-band) (250 realizations for each case)

	$\boldsymbol{\theta}$	Frequency	RMS Height	Correlation Length	Dielectric Constant
Case 1	$\mathbf{40^o}$	5.4 GHz	1 cm	15 cm	9+2.5i
Case 2	$\mathbf{40^o}$	5.4 GHz	2 cm	30 cm	9+2.5i
Case 3	$\mathbf{40^o}$	5.4 GHz	3 cm	45 cm	9+2.5i
Case 4	$\mathbf{40^o}$	5.4 GHz	4 cm	60 cm	9+2.5i

4.2.3 Polarimetric Speckle statistics

With the scattering matrix, results from different realization is actually results from different surface profile with the same statistical property, saying rms height and correlation length. Next, results are examined with the theoretical distribution from various aspects of amplitude and phase.

For amplitude from each polarized channel, S_{VV}, S_{HH}, S_{VH}, S_{HV}, it is known that for a single look data from a homogeneous area such as rough surface, the fully developed speckle follows the Rayleigh distribution [45]. Figure 4.1 shows 1-look comparison with Rayleigh distribution for L-band. Figure 4.2

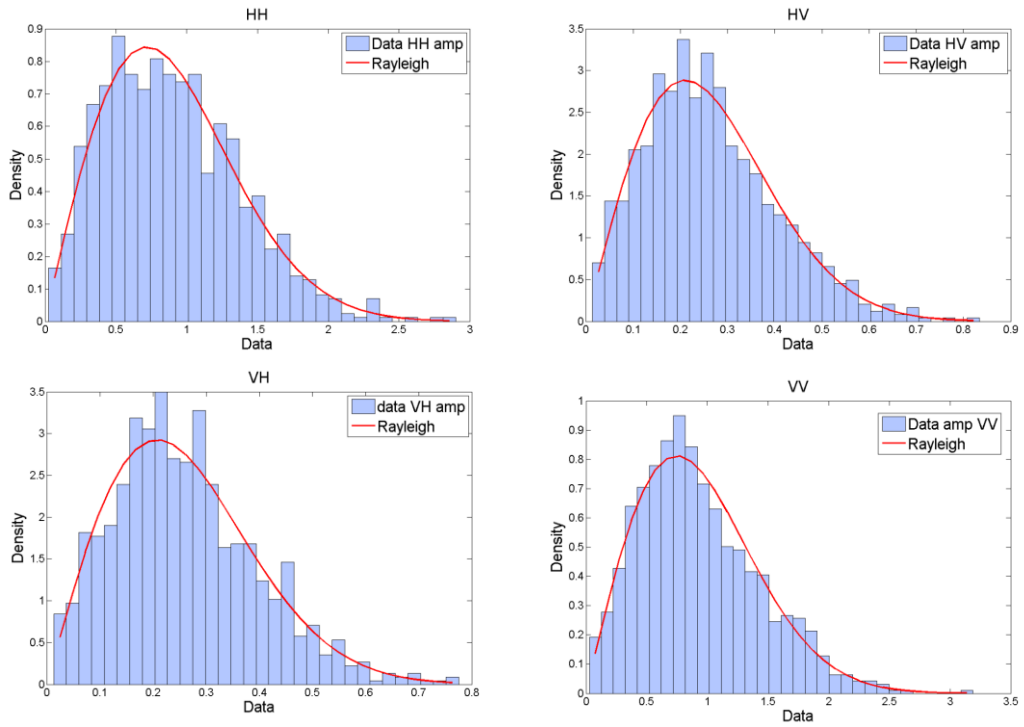

Figure 4.1 Comparison of amplitude distributions between simulated data– four polarized channels HH, VV, HV, and VH , and Rayleigh distribution. (L-band)

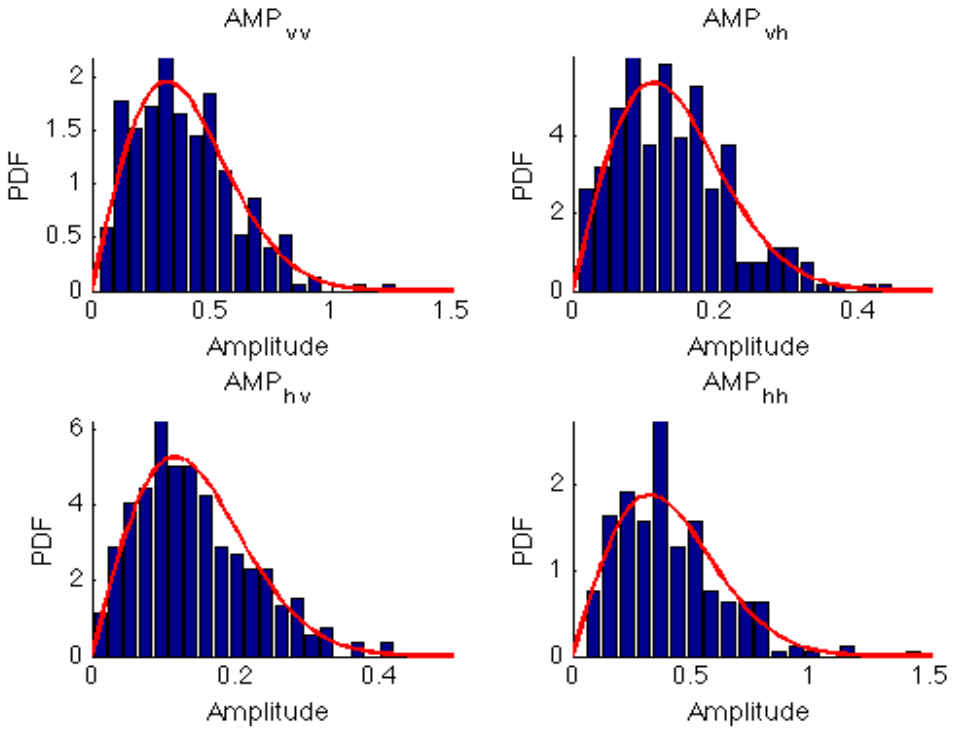

Figure 4.2 Amplitude Distribution compared with Rayleigh distribution for rms=4cm (C-band)

Lee and Pottier derived n-look (n realizations in simulation) distribution for phase difference as (4.2.6). In Fig.2-3, we show 1-look distribution comparison for phase difference of S_{HH} and S_{VV} and phase difference of S_{VH} and S_{HV}.

$$p^{(n)}(\psi) = \frac{(1-|\rho_c|^2)^n}{(1-\beta)^{2n}} \frac{2^{2(n-1)}}{\pi\left(n+\frac{1}{2}\right)} {}_2F_1\left(2n, n-\frac{1}{2}; n+\frac{3}{2}; -\frac{1-\beta}{1+\beta}\right) \quad -\pi < \psi < \pi \quad (4.2.6)$$

with

$$\beta = |\rho_c| \cos(\psi - \theta) \quad (4.2.7)$$

$$\rho_c = \frac{E\left[S_i S_j\right]}{\sqrt{E\left[|S_i|^2\right] E\left[\left|S_j\right|^2\right]}} = |\rho_c| e^{j\theta} \quad (4.2.8)$$

S_i and S_j are two components of the scattering matrix. ρ_c is according complex correlation coefficients. ${}_2F_1\left(2n, n-\frac{1}{2}; n+\frac{3}{2}; -\frac{1-\beta}{1+\beta}\right)$ is a Gauss hypergemetric function. n stands for number

of looks.

Simulation results show good agreement with statistical distribution for both L-band(Figure 4.3) and C-band(Figure 4.4 & Figure 4.5). Particularly for phase difference of cross-polarization. The NMM3D simulation results obey reciprocity very well for cross-polarization.

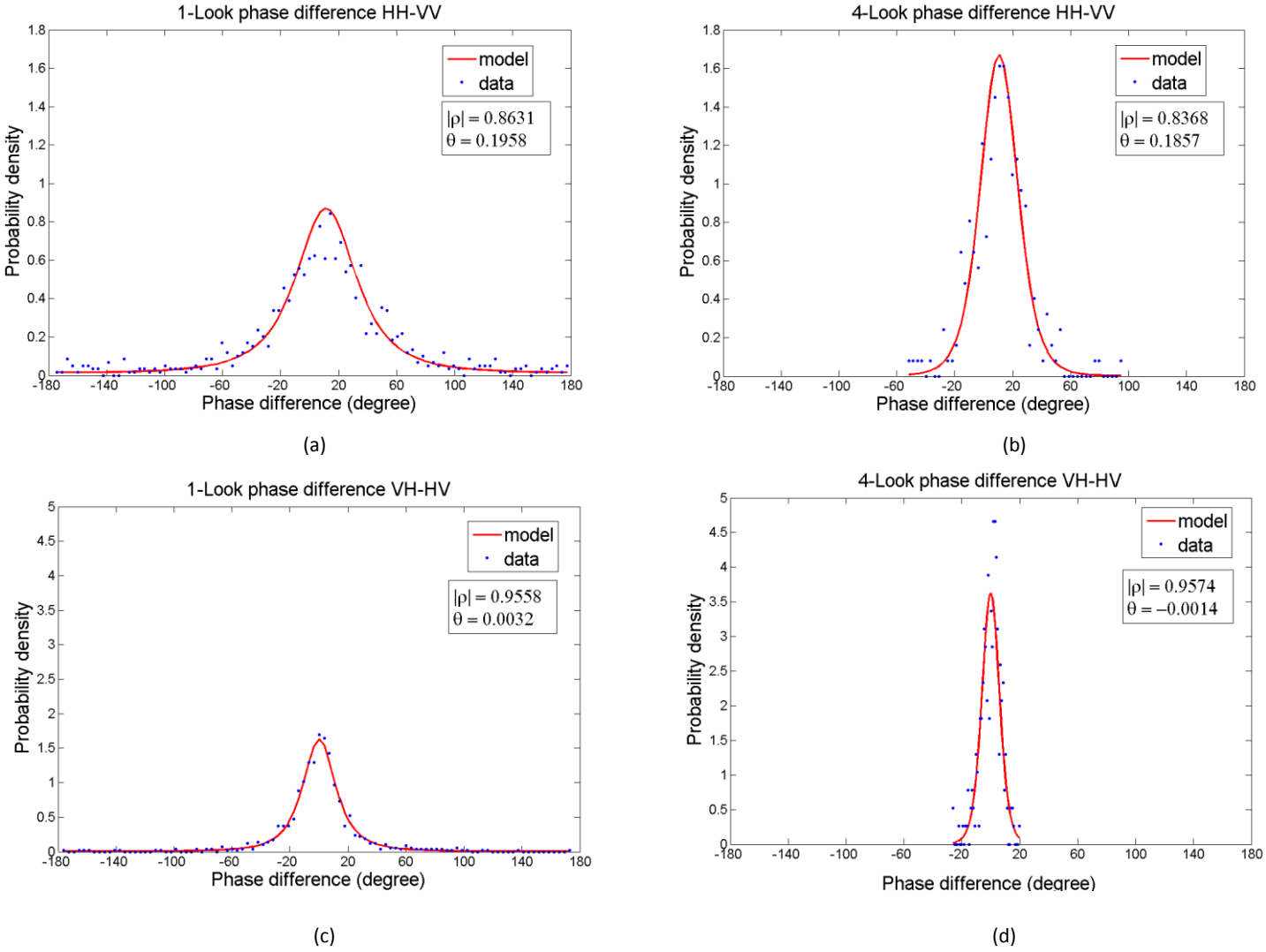

Figure 4.3 L-band comparison of statistical distribution of phase difference (a) S_{HH} to S_{VV} for 1 look (b) S_{HH} to S_{VV} for 4 look (c) S_{VH} to S_{HV} for 1 look (d) S_{VH} to S_{HV} for 4 look

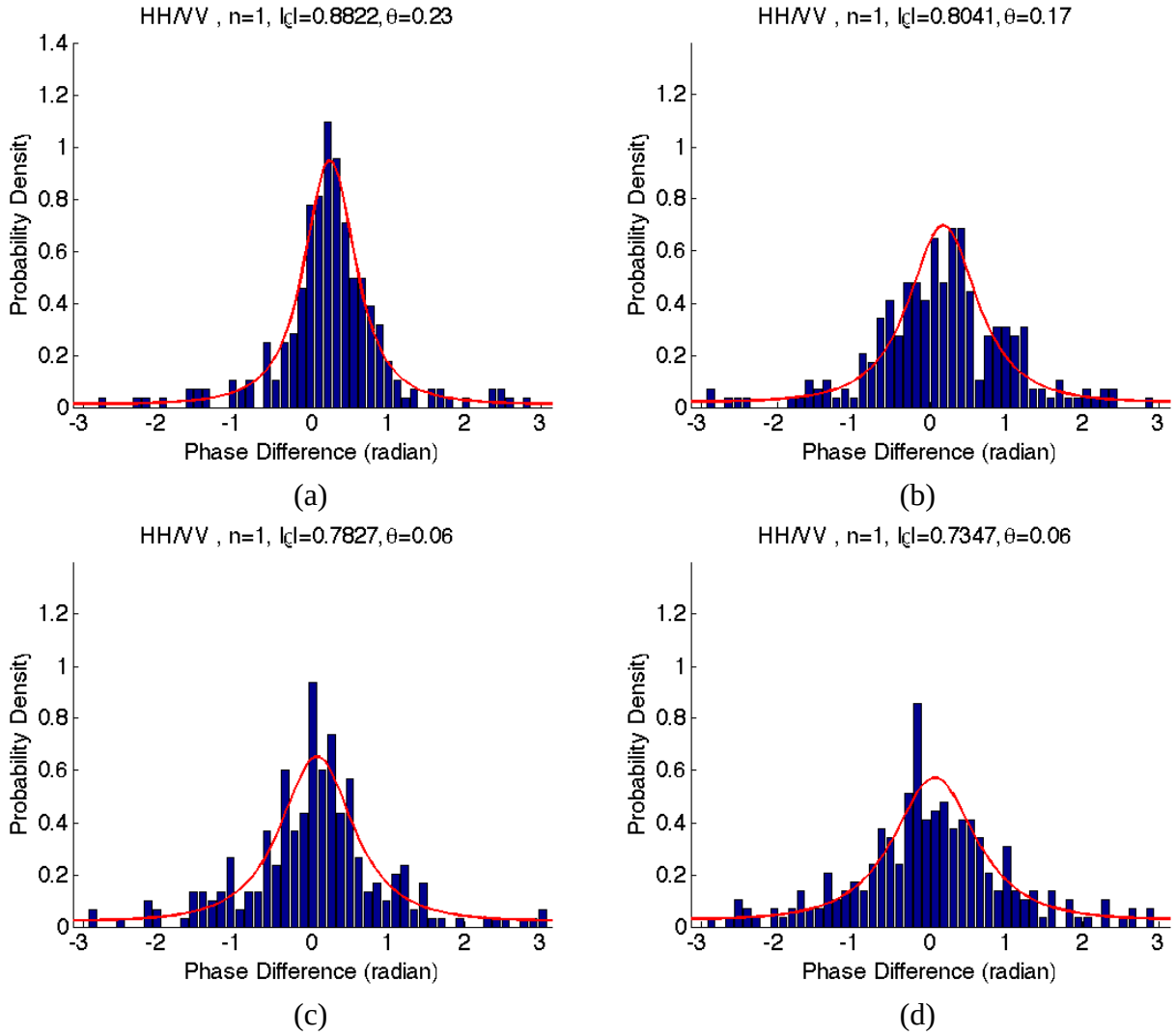

Figure 4.4 C-band phase difference of S_{HH} and S_{VV} compared with statistical distribution for 1-look (a) rms=1cm (b) rms=2cm (c) rms=3cm (d) rms=4cm

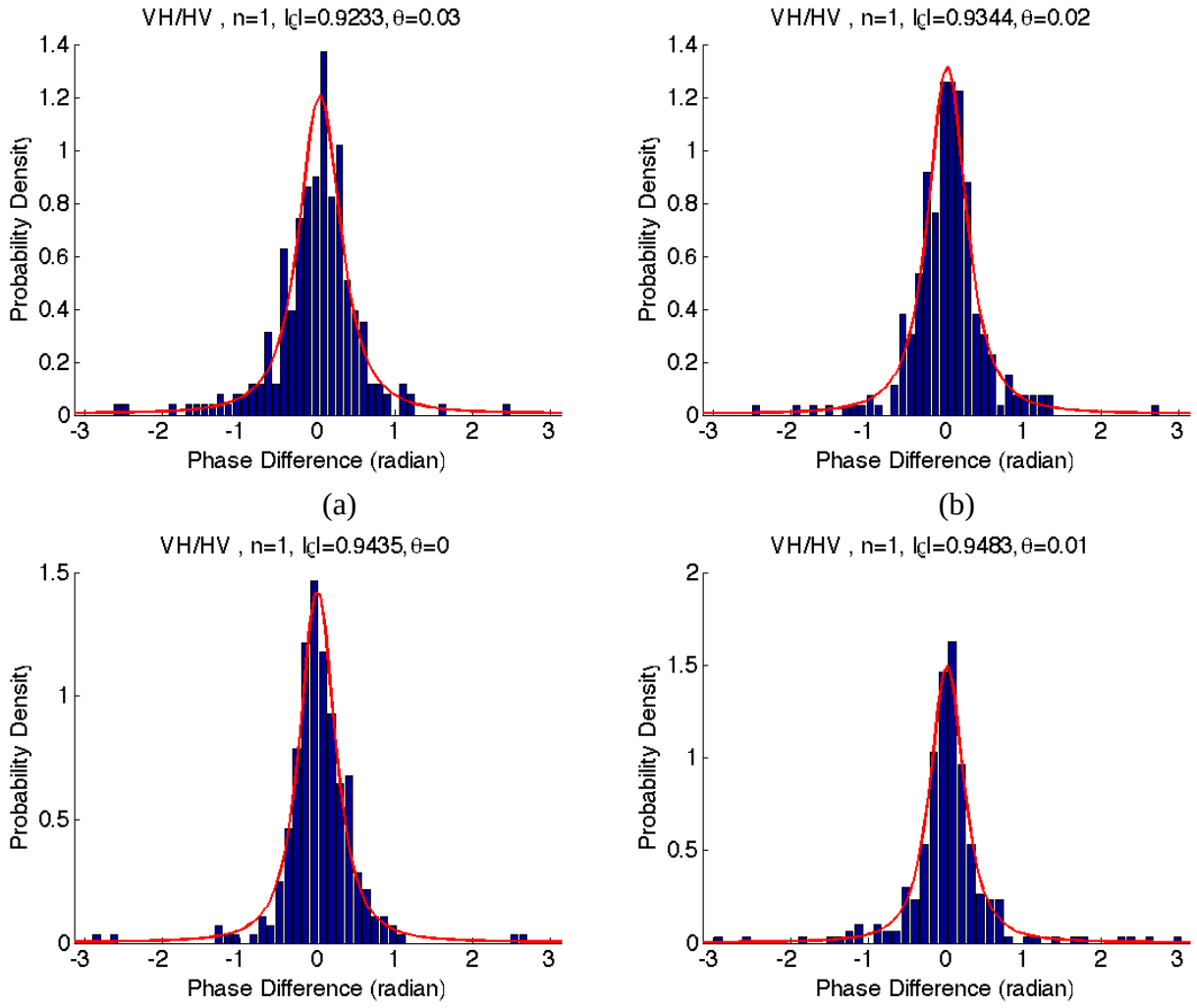

Figure 4.5 C-band phase difference of S_{VH} and S_{HV} compared with statistical distribution for 1-look (a) rms=1cm (b) rms=2cm (c) rms=3cm (d) rms=4cm

Besides the phase difference, there is also statistical distribution for amplitude raito for n-look as shown in (9).[47] z stands for the amplitude ratio for theorectical distribution between two scattering matrix elements. C_{ii} stands for the ensemble average of the intensity. τ is the ratio of two ensembled intensity considered.

$$p^{(n)}(z) = \frac{2\tau^n \Gamma(2n)(1-|\rho_c|^2)^n(\tau+z^2)z^{2n-1}}{\Gamma(n)\Gamma(n)[(\tau+z^2)^2 - 4\tau|\rho_c|^2 z^2]^{(2n+1)/2}} \tag{4.2.9}$$

$$\tau = \frac{C_{11}}{C_{22}} \tag{4.2.10}$$

$$C_{ii} = E[|S_i|^2] \tag{4.2.11}$$

In Figure 4.6, 1-look and 4-look distribution comparison for amplitude ratio of S_{HH} and S_{VV} and amplitude ratio of S_{VH} and S_{HV} are shown for L-band. In Figure 4.7 and Figure 4.8, results are shown for C-band for 1-look. All the results show good agreement with the theoretical distribution.

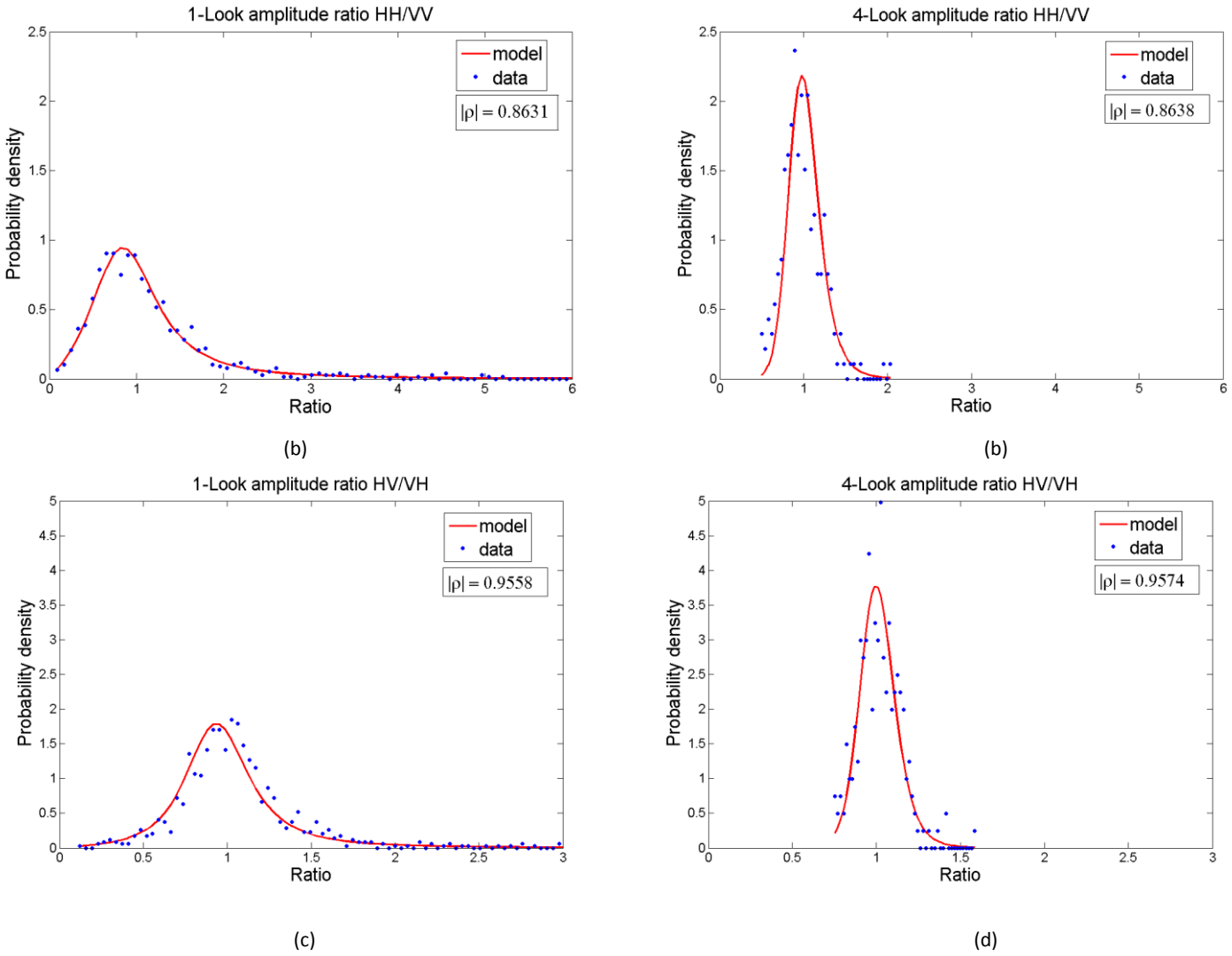

Figure 4.6 L-band comparison of statistical distribution of amplitude ratio (a) S_{HH} to S_{VV} for 1 look (b) S_{HH} to S_{VV} for 4 look (c) S_{HV} to S_{VH} for 1 look (d) S_{HV} to S_{VH} for 4 look

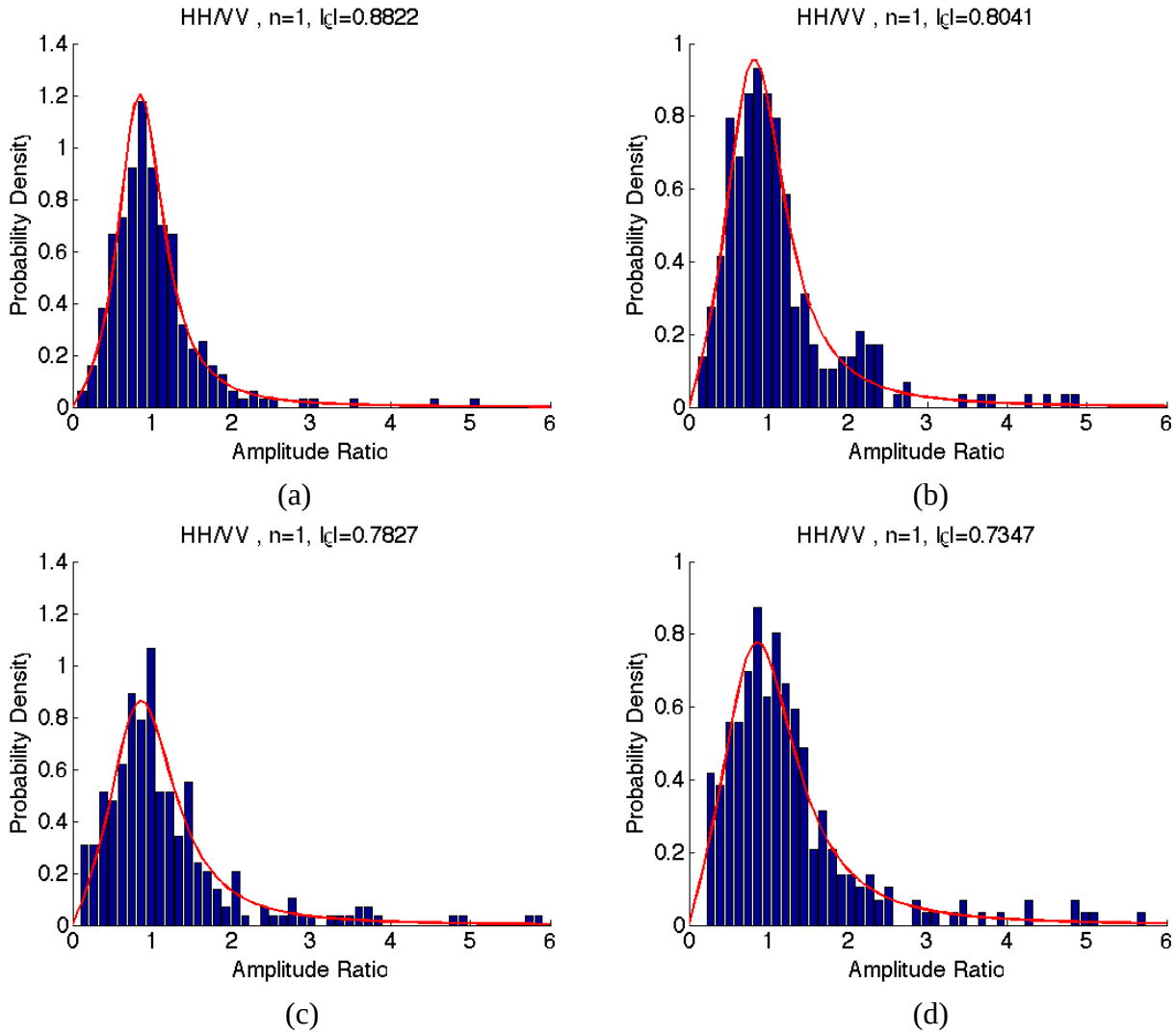

Figure 4.7 C-band amplitude ratio of S_{HH} and S_{VV} compared with statistical distribution for 1-look (a) rms=1cm (b) rms=2cm (c) rms=3cm (d) rms=4cm

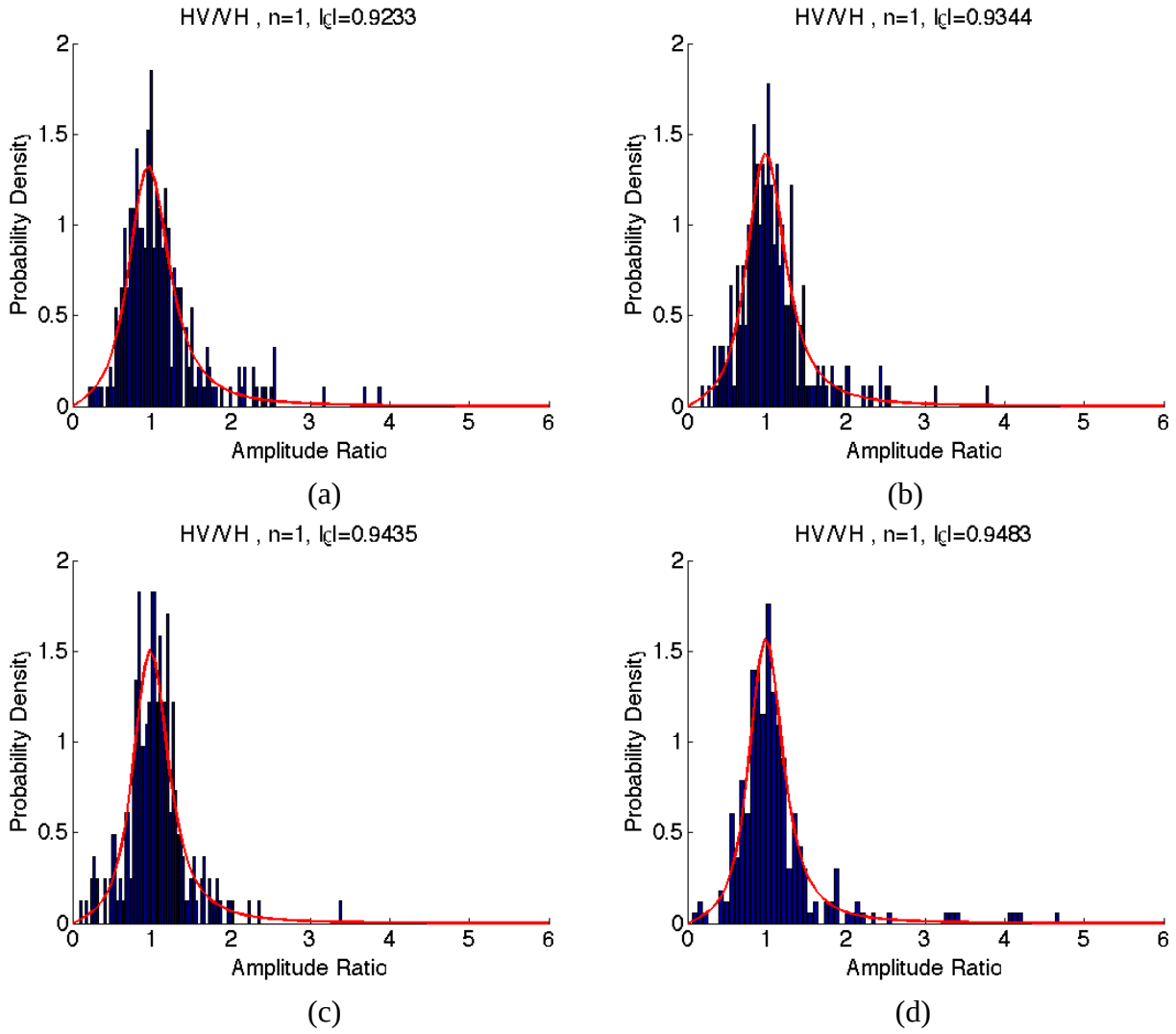

Figure 4.8 C-band Amplitude ratio of S_{HV} and S_{VH} compared with statistical distribution for 1-look (a) rms=1cm (b) rms=2cm (c) rms=3cm (d) rms=4cm

4.2.4 Polarimetric descriptor

In the backscattering direction, with the reciprocity of cross-polarized scattering matrix elements the coherency matrix is calculated by.

$$\bar{k} = [k_1 \quad k_2 \quad k_3]^T = \frac{1}{\sqrt{2}}[S_{vv} + S_{hh} \quad S_{vv} - S_{hh} \quad 2S_{vh}]^T \tag{4.2.12}$$

$$\bar{\bar{T}}_3 = \langle \bar{k}\bar{k}^{\dagger} \rangle = \begin{bmatrix} \langle k_1 k_1^* \rangle & \langle k_1 k_2^* \rangle & \langle k_1 k_3^* \rangle \\ \langle k_2 k_1^* \rangle & \langle k_2 k_2^* \rangle & \langle k_2 k_3^* \rangle \\ \langle k_3 k_1^* \rangle & \langle k_3 k_2^* \rangle & \langle k_3 k_3^* \rangle \end{bmatrix} \tag{4.2.7}$$

It follows that eigen-values and eigen-vectors from ensembled coherency matrix. Using the coherency matrix one can compute polarimetric descriptors, including entropy (H), anisotropy (A), and alpha angle (α) are calculated by (4.2.8)-(4.2.11). p_i denotes the eigen-value fraction and $\lambda_1 > \lambda_2 > \lambda_3$. α_i is extracted from unitary eigen vectors of coherency matrix.

$$p_i = \frac{\lambda_i}{\sum_{i=1}^{3} \lambda_i} \tag{4.2.8}$$

$$H = -\sum_{i=1}^{3} p_i \log_3 p_i \tag{4.2.9}$$

$$A = \frac{p_2 - p_3}{p_2 + p_3} \tag{4.2.10}$$

$$\alpha = \sum_{i=1}^{3} p_i \alpha_i \tag{4.2.11}$$

It has been presented that three polarimetric descriptors, entropy H, anisotropy A, and alpha angle α are highly related to surface dielectric constant and roughness scale [48]. Based on this hypothesis, various methods were developed to infer the surface soil moisture from polarimetric SAR imagery data [49-51]. Here we compute these polarimetric descriptors from results of NMM3D.

Figure 4.9 plots H, A, α versus roughness scale, *ks* from L-band simulations. Results are also listed in Table 4.3.It readily indicates that a clear increasing trend for H as *ks* increases, while A displays a non-linear effect versus *ks* - it increases for small values of *ks*, and turns to decrease when *ks* further increases. From Figure 4.9, we also observe that the alpha angle is not so sensitive to *ks*. At 40 degrees of incidence, it only spans from about 12 to 19 degrees.

Figure 4.10 shows ks dependence of entropy(H) and anisotropy(A). Results are also listed in Table 4.4. Entropy's dependence on ks is clear. The increase of entropy with ks is close to linear. In L-band plot, Figure 4.9, we also observe similar dependence. For anisotropy (A), there is no dependence on ks and it stays close to constant. Overall, entropy increases and anisotropy decreases at C-band compared to L-band. For alpha angle, it increases with ks. Here we see stronger dependence and larger alpha angle compared those at L-band.

Figure 4.11 depicts the simulated values in entropy/alpha plane for L-band. The loci is plotted

according to [52]. When the roughness changes, alpha angle only slightly shifts. The entropy can be as large as 0.5 meaning more depolarization occurs. Result agrees with the fact that exponentially correlated surface causes stronger depolarization. Figure 4.12 shows simulated values in entropy/alpha plane for C-band. As we see the relative rms height to wavelength increases and causes even larger depolarization as the entropy gets larger.

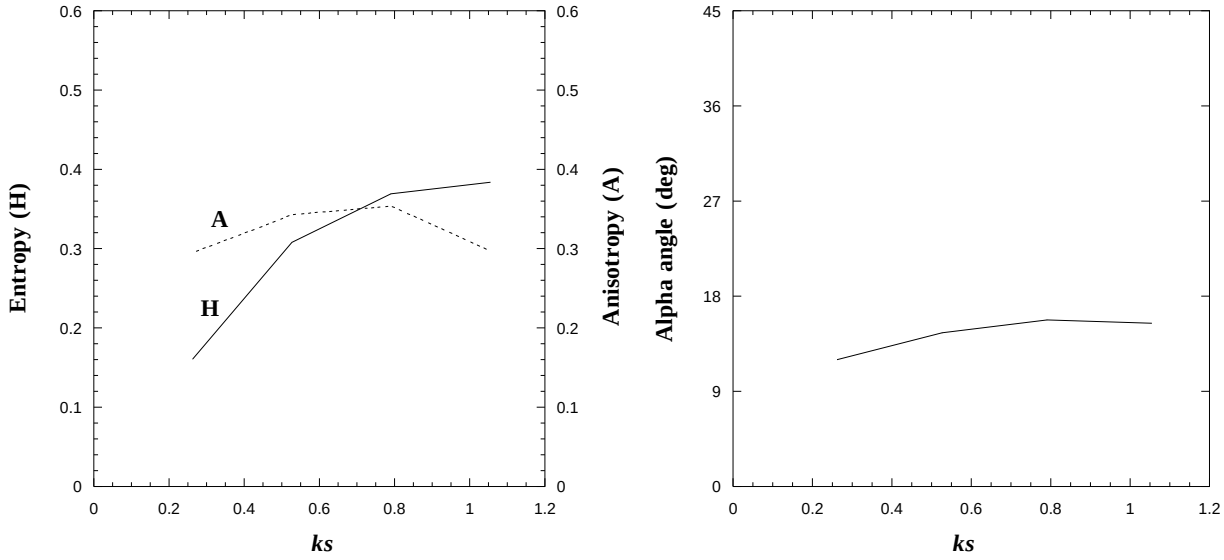

(a) (b)

Figure 4.9 L-band Polarimetric descriptors, H, A, and α versus surface roughness *ks*.

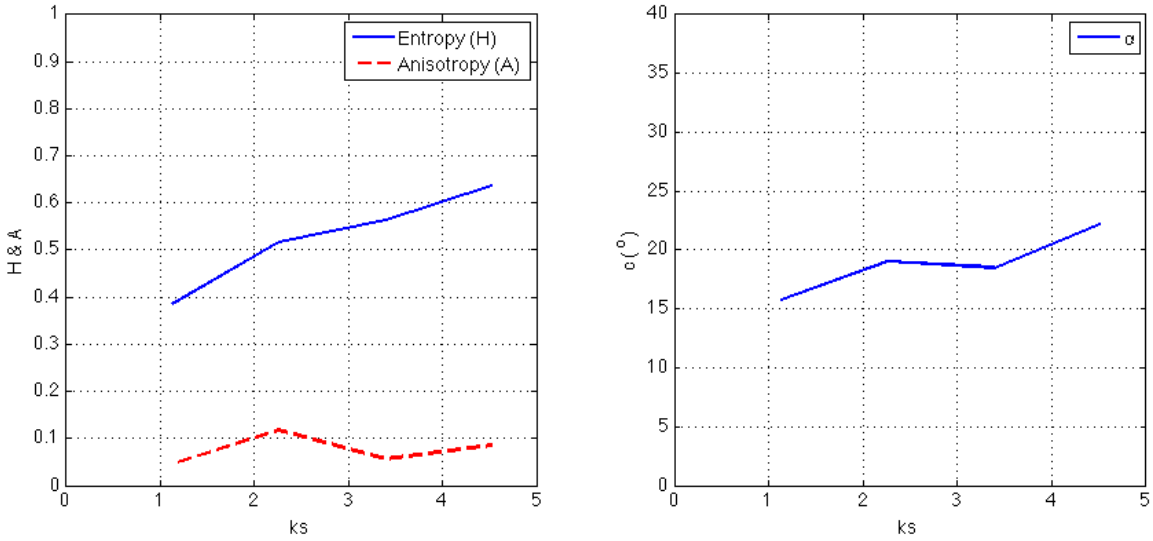

Figure 4.10 ks dependence of polarimetric descriptor, H, A, α at 5.4GHz (C-band)

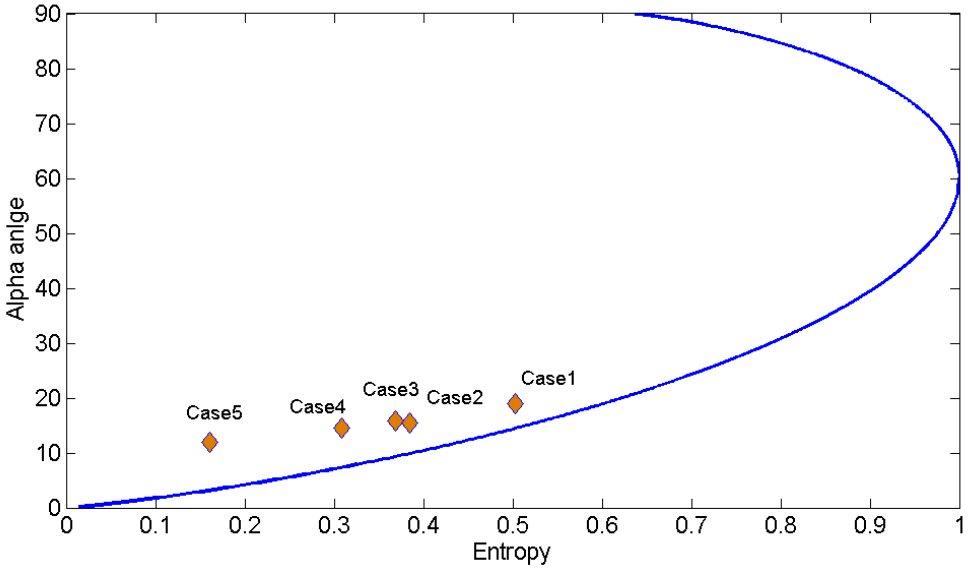

Figure 4.11 Geometrical distribution of simulated polarimetric descriptors values in H/A space. (L-band)

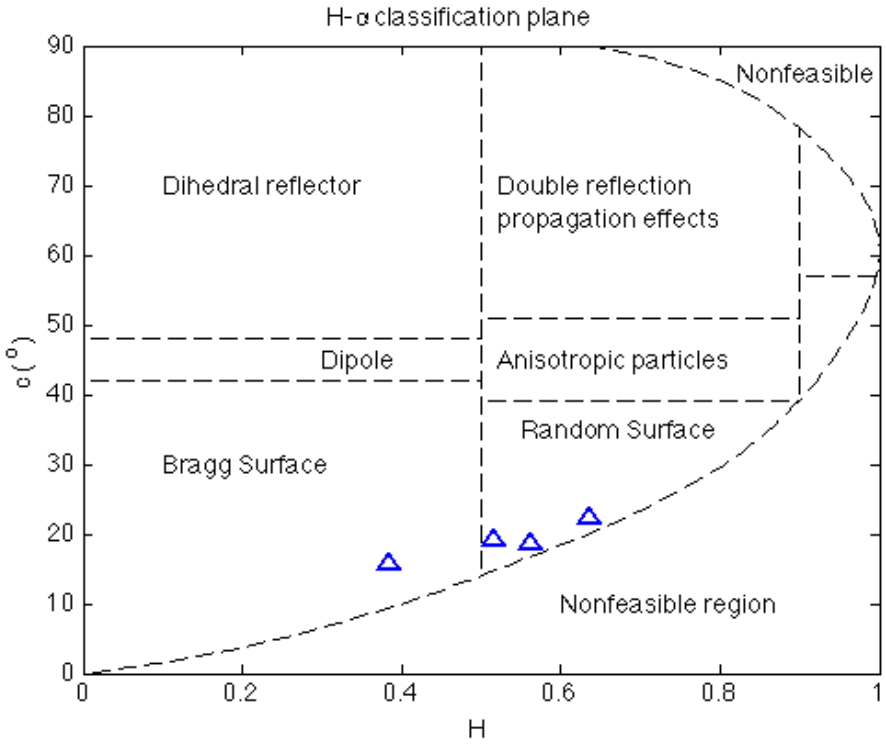

Figure 4.12 C-band Random scattering mechanisms classification

Table 4.3

Summary of H, A, and α values for cases considered (L-band)

	Surface Roughness	Dielectric Constant	Entropy (H)	Anisotropy (A)	Alpha angle (α)
Case1	s= 4cm (ks=1.055) λ=40cm(kλ=10.55)	8.35+j 1.99	0.503	0.0947	18.93
Case2	s= 4cm (ks=1.055) λ=60cm (kλ=15.82)	9+j 2.5	0.3841	0.297	15.45
Case3	s= 3cm (ks=0.791) λ=45cm (kλ=11.87)	9+j 2.5	0.3693	0.354	15.76
Case4	s= 2cm (ks=0.527) λ=30cm (kλ=7.912)	9+j 2.5	0.308	0.3428	14.55
Case5	s= 1cm (ks=0.263) λ=15cm (kλ=3.956)	9+j 2.5	0.161	0.2952	11.99

Table 4.4

Summary of H, A, and α from 4 cases (C-band)

	Entropy (H)	Anisotropy (A)	Alpha angle ($\boldsymbol{\alpha}$)
Case 1	0.3847	0.0455	$\mathbf{15.78^o}$
Case 2	0.5169	0.1177	$\mathbf{19.02^o}$
Case 3	0.5630	0.0569	$\mathbf{18.49^o}$
Case 4	0.6360	0.0853	$\mathbf{22.26^o}$

4.3 Coherency matrix from distorted Born approximation combined with NMM3D for vegetated surface

In this section, we derive the complete polarimetry for land surface using numerical Maxwell's equation 3D and Distorted Born approximation. Volume scattering, double bounce scattering, and surface scattering of coherency matrix are included. In distorted Born approximation, effective medium is considered inside the vegetation layer which has slight different propagation constant. These slight difference is important because they contribute to the attenuation of the scattering as well as causing significant difference of phase shift as the wave propagates inside the layer. The correlation between polarizations at the backscattering direction are the final outcome and can be applied to coherency matrix. Later the derivation will separate into 3 scattering mechanisms. Each of them will give out the coherency matrix, respectively.

From the book of Tsang etal[34], page 272, (4.3.1) and (4.3.2) show the coupled equation for coherent waves, E_v and E_h, along the propagation direction (θ, ϕ).

$$\frac{dE_v}{ds} = (ik + M_{vv})E_v + M_{vh}E_h \tag{4.3.1}$$

$$\frac{dE_h}{ds} = M_{hv}E_v + (ik + M_{hh})E_h \tag{4.3.2}$$

$$M_{pq} = \frac{i2\pi n_0}{k}\langle f_{pq}(\theta, \phi; \theta, \phi)\rangle, \;\; p, q = v, h \tag{4.3.3}$$

The attenuation rates solved from (4.3.1) and (4.2.2) are listed in (4.3.3). The angular bracket

denotes the average over orientation and size distribution of the particles. The effective propagation constants can be solved from the corresponding extinction matrix as in (4.3.4) and (4.3.5).

$$K_1 = k - \frac{i}{2}(M_{vv} + M_{hh} + r) \tag{4.3.4}$$

$$K_2 = k - \frac{i}{2}(M_{vv} + M_{hh} - r) \tag{4.3.5}$$

$$r = [(M_{vv} - M_{hh})^2 + 4M_{hv}M_{vh}]^{1/2} \tag{4.3.6}$$

Consider the case $M_{hv} = M_{vh} = 0$, K_1 and K_2 reduce to vertically and horizontally polarized waves, K_v and K_h, respectively.

$$k_v = k + \frac{2\pi n_0}{k}\langle f_{vv}(\theta, \phi; \theta, \phi)\rangle \tag{4.3.7}$$

$$k_h = k + \frac{2\pi n_0}{k}\langle f_{hh}(\theta, \phi; \theta, \phi)\rangle \tag{4.3.8}$$

Note that $f_{pp}(\theta, \phi; \theta, \phi)$ depends on the angle. Then for p-polarized incident wave with incident angle, θ_0, the effective propagation constant is in (4.3.9).

$$k_{pz} = \sqrt{k_p^2 - k_\rho^2} = \sqrt{k_p^2 - (k^2 - (k\cos\theta_0)^2)}$$

$$= \sqrt{\left(k + \frac{2\pi n_0}{k}\langle f_{pp}(\theta, \phi; \theta, \phi)\rangle\right)^2 - k^2 + k^2\cos^2\theta_0}$$

$$= \sqrt{4\pi n_0\langle f_{pp}(\theta, \phi; \theta, \phi)\rangle + \left(\frac{2\pi n_0}{k}\langle f_{pp}(\theta, \phi; \theta, \phi)\rangle\right)^2 + k^2\cos^2\theta_0}$$

$$= k\cos\theta_0\sqrt{1 + \frac{4\pi n_0\langle f_{pp}(\theta, \phi; \theta, \phi)\rangle + \left(\frac{2\pi n_0}{k}\langle f_{pp}(\theta, \phi; \theta, \phi)\rangle\right)^2}{k^2\cos^2\theta_0}} \tag{4.3.9}$$

Notice that $\left(\frac{2\pi n_0}{k}\langle f_{pp}(\theta, \phi; \theta, \phi)\rangle\right)^2 \ll 4\pi n_0\langle f_{pp}(\theta, \phi; \theta, \phi)\rangle \ll k^2\cos^2\theta_0$, one can approximate $(1 + x)^{1/2}$ by $1 + \frac{1}{2}x$.

$$k_{pz} = k\cos\theta_0\left(1 + \frac{1}{2}\frac{4\pi n_0\langle f_{pp}(\theta,\phi;\theta,\phi)\rangle}{k^2\cos^2\theta_0}\right) \tag{4.3.10}$$

Separate k_{pz} to real and imaginary parts, k'_{pz} and k''_{pz}.

$$k'_{pz} = k\cos\theta_0 + Re(\frac{2\pi n_0\langle f_{pp}(\theta,\phi;\theta,\phi)\rangle}{k\cos\theta_0}) \tag{4.3.11}$$

$$k''_{pz} = Im(\frac{2\pi n_0\langle f_{pp}(\theta,\phi;\theta,\phi)\rangle}{k\cos\theta_0}) \tag{4.3.12}$$

For vertical polarization

$$k_{vz} = k\cos\theta_0 + Re\left(\frac{2\pi n_0\langle f_{vv}(\theta,\phi;\theta,\phi)\rangle}{k\cos\theta_0}\right) + iIm\left(\frac{2\pi n_0\langle f_{vv}(\theta,\phi;\theta,\phi)\rangle}{k\cos\theta_0}\right)$$

$$= k\cos\theta_0 + \frac{2\pi n_0\langle f_{vv}(\theta,\phi;\theta,\phi)\rangle}{k\cos\theta_0} = \sqrt{\left(k + \frac{2\pi n_0}{k}\langle f_{vv}(\theta,\phi;\theta,\phi)\rangle\right)^2 - k^2\sin^2\theta_0} \tag{4.3.13}$$

$$k_v = k + \frac{2\pi n_0}{k}\langle f_{vv}(\theta,\phi;\theta,\phi)\rangle \tag{4.3.14}$$

Similar for horizontal polarization

$$k_{hz} = k\cos\theta_0 + Re\left(\frac{2\pi n_0\langle f_{hh}(\theta,\phi;\theta,\phi)\rangle}{k\cos\theta_0}\right) + iIm\left(\frac{2\pi n_0\langle f_{hh}(\theta,\phi;\theta,\phi)\rangle}{k\cos\theta_0}\right)$$

$$= k\cos\theta_0 + \frac{2\pi n_0\langle f_{hh}(\theta,\phi;\theta,\phi)\rangle}{k\cos\theta_0} = \sqrt{\left(k + \frac{2\pi n_0}{k}\langle f_{hh}(\theta,\phi;\theta,\phi)\rangle\right)^2 - k^2\sin^2\theta_0} \tag{4.3.15}$$

$$k_h = k + \frac{2\pi n_0}{k}\langle f_{hh}(\theta,\phi;\theta,\phi)\rangle \tag{4.3.16}$$

Note the difference from free space are the exponential phase and attenuation factors. Free space dyadic Green's function is then applied to calculate the volume scattering. For the scatterer at the origin and we ignore the singularity at the origin for free space.

$$\bar{\bar{G}}_P(\bar{r}) =$$

$$\begin{cases} \dfrac{i}{8\pi^2}\displaystyle\int_{-\infty}^{\infty}dk_x\int_{-\infty}^{\infty}dk_y\left[\hat{e}(k_z)\hat{e}(k_z) + \hat{h}(k_z)\hat{h}(k_z)\right]\dfrac{e^{ik_x x + ik_y y + ik_z z}}{k_z} & for\ z > 0 \\ \dfrac{i}{8\pi^2}\displaystyle\int_{-\infty}^{\infty}dk_x\int_{-\infty}^{\infty}dk_y\left[\hat{e}(-k_z)\hat{e}(-k_z) + \hat{h}(-k_z)\hat{h}(-k_z)\right]\dfrac{e^{ik_x x + ik_y y + ik_z z}}{k_z} & for\ z < 0 \end{cases} \tag{4.3.17}$$

For dyadic green's function used in effective medium, the effective propagation constants will have more effects on the phase while the effects on the amplitudes are small. Thus

$$\bar{\bar{G}}_P(\bar{r}) =$$

$$\begin{cases} \dfrac{i}{8\pi^2}\displaystyle\int_{-\infty}^{\infty} dk_x \int_{-\infty}^{\infty} dk_y \left[\hat{e}(k_z)\hat{e}(k_z)e^{ik_{hz}z} + \hat{h}(k_z)\hat{h}(k_z)e^{ik_{vz}z}\right]\dfrac{e^{ik_x x + ik_y y}}{k_z} & for\ z > 0 \\ \dfrac{i}{8\pi^2}\displaystyle\int_{-\infty}^{\infty} dk_x \int_{-\infty}^{\infty} dk_y \left[\hat{e}(-k_z)\hat{e}(-k_z)e^{-ik_{hz}z} + \hat{h}(-k_z)\hat{h}(-k_z)e^{-ik_{vz}z}\right]\dfrac{e^{ik_x x + ik_y}}{k_z} & for\ z < 0 \end{cases} \tag{4.3.18}$$

$$k_{vz} = \sqrt{k_v^2 - k_x^2 - k_y^2} \tag{4.3.19}$$

$$k_{hz} = \sqrt{k_h^2 - k_x^2 - k_y^2} \tag{4.3.20}$$

Note that we have not changed the amplitude vector, $\hat{e}(k_z)$ and $\hat{h}(k_z)$. A more exact expression can be

$$\bar{\bar{G}}_P(\bar{r}) =$$

$$\begin{cases} \dfrac{i}{8\pi^2}\displaystyle\int_{-\infty}^{\infty} dk_x \int_{-\infty}^{\infty} dk_y \left[\dfrac{\hat{e}(k_{hz})\hat{e}(k_{hz})e^{ik_{hz}z}}{k_{hz}} + \dfrac{\hat{h}(k_{vz})\hat{h}(k_{vz})e^{ik_{vz}z}}{k_{vz}}\right] e^{ik_x x + ik_y y} & for\ z > 0 \\ \dfrac{i}{8\pi^2}\displaystyle\int_{-\infty}^{\infty} dk_x \int_{-\infty}^{\infty} dk_y \left[\dfrac{\hat{e}(-k_{hz})\hat{e}(-k_{hz})e^{-ik_{hz}z}}{k_{hz}} + \dfrac{\hat{h}(-k_{vz})\hat{h}(-k_{vz})e^{-ik_{vz}z}}{k_{vz}}\right] e^{ik_x x + ik_y} & for\ z < 0 \end{cases} \tag{4.3.21}$$

However, we will take the simpler approximation as (4.3.18), that we use k_z for the amplitude polarization factor while we use k_{vz} and k_{hz} for the exponent.

Thus we consider a two layer medium, medium 0, medium 1, and medium 2. E.g. for vegetated surface, medium 0 is air, medium 1 is vegetation layer, and medium 2 is soil.

Since the scattering is in medium 1, we have the following.

$$TE\ polarization: \hat{e}(k_z) = \frac{\hat{k} \times \hat{z}}{\left|\hat{k} \times \hat{z}\right|} = \frac{1}{k_\rho}\left(\hat{x}k_y - \hat{y}k_x\right) \tag{4.3.22}$$

$$TM\ polarization: \hat{h}(k_z) = \hat{e} \times \hat{k} = -\frac{k_z}{kk_\rho}\left(\hat{x}k_x + \hat{y}k_y\right) + \frac{k_\rho}{k}\hat{z} \tag{4.3.23}$$

For amplitude factor, we use k_z

$$k_z = \sqrt{k^2 - k_x^2 - k_y^2} \tag{4.3.24}$$

Then we use lower case for upward going wave and capital case for downward going wave.

$$\bar{k}_v = k_x\hat{x} + k_y\hat{y} + k_{vz}\hat{z} \tag{4.3.25}$$

$$\bar{K}_v = k_x\hat{x} + k_y\hat{y} - k_{vz}\hat{z} \tag{4.3.26}$$

$$\bar{k}_h = k_x\hat{x} + k_y\hat{y} + k_{hz}\hat{z} \tag{4.3.27}$$

$$\bar{K}_h = k_x\hat{x} + k_y\hat{y} - k_{hz}\hat{z} \tag{4.3.28}$$

If the boundary is at $z = 0$, then the Green's function of reflected wave in effective medium(medium 1) is

$\bar{\bar{G}}_R(\bar{r}, \bar{r}') =$

$$\frac{i}{8\pi^2}\int d\bar{k}_\perp \frac{1}{k_z}\left[R^{TE}\hat{e}(k_z)e^{i\bar{k}_h\cdot\bar{r}}\hat{e}(-k_z)e^{-i\bar{K}_h\cdot\bar{r}'} + R^{TM}\hat{h}(k_z)e^{i\bar{k}_v\cdot\bar{r}}\hat{h}(-k_z)e^{-i\bar{K}_v\cdot\bar{r}'}\right] \tag{4.3.29}$$

However, in our case we consider the boundary at $z = -d$. Then we shift both z and z'.

$\bar{\bar{G}}_R(\bar{r}, \bar{r}') =$

$$\frac{i}{8\pi^2}\int d\bar{k}_\perp \frac{1}{k_z}\left[R^{TE}\hat{e}(k_z)e^{i\bar{k}_h\cdot\bar{r}+2ik_{hz}d}\hat{e}(-k_z)e^{-i\bar{K}_h\cdot\bar{r}'} + R^{TM}\hat{h}(k_z)e^{i\bar{k}_v\cdot\bar{r}+2ik_{vz}d}\hat{h}(-k_z)e^{-i\bar{K}_v\cdot\bar{r}'}\right]$$

$$= \frac{i}{8\pi^2}\int d\bar{k}_\perp \left[R^{TE}\hat{e}(k_z)e^{ik_{hz}z+2ik_{hz}d}\hat{e}(-k_z)e^{ik_{hz}z'}\right.$$

$$\left. + R^{TM}\hat{h}(k_z)e^{ik_{vz}z+2ik_{vz}d}\hat{h}(-k_z)e^{ik_{vz}z'}\right]\frac{e^{ik_x(x-x')+ik_y(y-y')}}{k_z} \tag{4.3.30}$$

Thus the half space Green's function in medium is

$$\bar{\bar{G}}_{11}(\bar{r}, \bar{r}') = \bar{\bar{G}}_P(\bar{r}, \bar{r}') + \bar{\bar{G}}_R(\bar{r}, \bar{r}') \tag{4.3.31}$$

$\bar{\bar{G}}_P(\bar{r}) =$

$$\begin{cases} \frac{i}{8\pi^2}\int_{-\infty}^{\infty} dk_x \int_{-\infty}^{\infty} dk_y \left[\hat{e}(k_z)\hat{e}(k_z)e^{ik_{hz}(z-z')} + \hat{h}(k_z)\hat{h}(k_z)e^{ik_{vz}(z-z')}\right]\frac{e^{ik_x(x-x')+ik_y(y-y')}}{k_z} & ; z > z' \\ \frac{i}{8\pi^2}\int_{-\infty}^{\infty} dk_x \int_{-\infty}^{\infty} dk_y \left[\hat{e}(-k_z)\hat{e}(-k_z)e^{-ik_{hz}(z-z')} + \hat{h}(-k_z)\hat{h}(-k_z)e^{-ik_{vz}(z-z')}\right]\frac{e^{ik_x(x-x')+ik_y(y-y')}}{k_z} & ; z < z' \end{cases} \tag{4.3.32}$$

Then for $z > z'$

$$\bar{\bar{G}}_{11}(\bar{r},\bar{r}') = \bar{\bar{G}}_P(\bar{r},\bar{r}')_{z>z'} + \bar{\bar{G}}_R(\bar{r},\bar{r}')$$

$$= \frac{i}{8\pi^2}\int_{-\infty}^{\infty} dk_x \int_{-\infty}^{\infty} dk_y \left[\hat{e}(k_z)\hat{e}(k_z)e^{ik_{hz}(z-z')} + \hat{h}(k_z)\hat{h}(k_z)e^{ik_{vz}(z-z')}\right]\frac{e^{ik_x(x-x')+ik_y(y-y')}}{k_z}$$

$$+ \frac{i}{8\pi^2}\int d\bar{k}_\perp \left[R^{TE}\hat{e}(k_z)e^{ik_{hz}z+2ik_{hz}d}\hat{e}(-k_z)e^{ik_{hz}z'}\right.$$

$$\left. + R^{TM}\hat{h}(k_z)e^{ik_{vz}z+2ik_{vz}d}\hat{h}(-k_z)e^{ik_{vz}z'}\right]\frac{e^{ik_x(x-x')+ik_y(y-y')}}{k_z} \qquad (4.3.33)$$

for $z < z'$

$$\bar{\bar{G}}_{11}(\bar{r},\bar{r}') = \bar{\bar{G}}_P(\bar{r},\bar{r}')_{z<z'} + \bar{\bar{G}}_R(\bar{r},\bar{r}')$$

$$= \frac{i}{8\pi^2}\int_{-\infty}^{\infty} dk_x \int_{-\infty}^{\infty} dk_y \left[\hat{e}(-k_z)\hat{e}(-k_z)e^{-ik_{hz}(z-z')}\right.$$

$$\left. + \hat{h}(-k_z)\hat{h}(-k_z)e^{-ik_{vz}(z-z')}\right]\frac{e^{ik_x(x-x')+ik_y(y-y')}}{k_z}$$

$$+ \frac{i}{8\pi^2}\int d\bar{k}_\perp \left[R^{TE}\hat{e}(k_z)e^{ik_{hz}z+2ik_{hz}d}\hat{e}(-k_z)e^{ik_{hz}z'}\right.$$

$$\left. + R^{TM}\hat{h}(k_z)e^{ik_{vz}z+2ik_{vz}d}\hat{h}(-k_z)e^{ik_{vz}z'}\right]\frac{e^{ik_x(x-x')+ik_y(y-y')}}{k_z} \qquad (4.3.34)$$

To continue $\bar{\bar{G}}_{11}$ into medium 0, let $z = 0$ in $z > z'$

$$\bar{\bar{G}}_{11}(\bar{r}|_{z=0},\bar{r}')_{z>z'}$$

$$= \frac{i}{8\pi^2}\int_{-\infty}^{\infty} dk_x \int_{-\infty}^{\infty} dk_y \left[\hat{e}(k_z)\hat{e}(k_z)e^{-ik_{hz}z'} + \hat{h}(k_z)\hat{h}(k_z)e^{-ik_{vz}z'}\right]\frac{e^{ik_x(x-x')+ik_y(y-y')}}{k_z}$$

$$+ \frac{i}{8\pi^2}\int d\bar{k}_\perp \left[R^{TE}\hat{e}(k_z)e^{2ik_{hz}d}\hat{e}(-k_z)e^{ik_{hz}z'}\right.$$

$$\left. + R^{TM}\hat{h}(k_z)e^{2ik_{vz}d}\hat{h}(-k_z)e^{ik_{vz}z'}\right]\frac{e^{ik_x(x-x')+ik_y(y-y')}}{k_z} \qquad (4.3.35)$$

Then separate $\hat{e}(k_z)$ and $\hat{h}(k_z)$

$$\bar{\bar{G}}_{11}(\bar{r}|_{z=0},\bar{r}')_{z>z'}$$

$$= \frac{i}{8\pi^2}\int_{-\infty}^{\infty} dk_x \int_{-\infty}^{\infty} dk_y\, \hat{e}(k_z)\left[\hat{e}(k_z)e^{-ik_{hz}z'} + R^{TE}e^{2ik_{hz}d}\hat{e}(-k_z)e^{ik_{hz}z'}\right]\frac{e^{ik_x(x-x')+ik_y(y-y')}}{k_z}$$

$$+\frac{i}{8\pi^2}\int d\bar{k}_\perp\,\hat{h}(k_z)\big[\hat{h}(k_z)e^{-ik_{vz}z'}$$

$$+R^{TM}e^{2ik_{vz}d}\hat{h}(-k_z)e^{ik_{vz}z'}\big]\frac{e^{ik_x(x-x')+ik_y(y-y')}}{k_z} \tag{4.3.36}$$

For $z>0$, we consider $\bar{\bar{G}}_{01}$. Since there is no physical reflection at $z=0$, we just continue $\bar{\bar{G}}_{11}(\bar{r}|_{z=0},\bar{r}')_{z>z'}$ with $e^{ik_z z}$.

$$\bar{\bar{G}}_{01}(\bar{r},\bar{r}')=$$

$$=\frac{i}{8\pi^2}\int_{-\infty}^{\infty}dk_x\int_{-\infty}^{\infty}dk_y\,\hat{e}(k_z)\big[\hat{e}(k_z)e^{-ik_{hz}z'}$$

$$+R^{TE}e^{2ik_{hz}d}\hat{e}(-k_z)e^{ik_{hz}z'}\big]\frac{e^{ik_x(x-x')+ik_y(y-y')}}{k_z}e^{ik_z z}$$

$$+\frac{i}{8\pi^2}\int d\bar{k}_\perp\,\hat{h}(k_z)\big[\hat{h}(k_z)e^{-ik_{vz}z'}+R^{TM}e^{2ik_{vz}d}\hat{h}(-k_z)e^{ik_{vz}z'}\big]\frac{e^{ik_x(x-x')+ik_y(y-y')}}{k_z}e^{ik_z z}$$

$$=\frac{i}{8\pi^2}\int_{-\infty}^{\infty}dk_x\int_{-\infty}^{\infty}dk_y\frac{e^{i\bar{k}\cdot\bar{r}}}{k_z}\,\hat{e}(k_z)\big[\hat{e}(k_z)e^{-ik_{hz}z'}+R^{TE}e^{2ik_{hz}d}\hat{e}(-k_z)e^{ik_{hz}z'}\big]e^{-ik_x x'-ik_y y'}$$

$$+\frac{i}{8\pi^2}\int d\bar{k}_\perp\frac{e^{i\bar{k}\cdot\bar{r}}}{k_z}\hat{h}(k_z)\big[\hat{h}(k_z)e^{-ik_{vz}z'}+R^{TM}e^{2ik_{vz}d}\hat{h}(-k_z)e^{ik_{vz}z'}\big]e^{-ik_x x'-ik_y y'} \tag{4.3.37}$$

In the far field, using stationary phase method, we have

$$\frac{i}{8\pi^2}\int_{-\infty}^{\infty}dk_x\int_{-\infty}^{\infty}dk_y\frac{e^{i\bar{k}\cdot\bar{r}}}{k_z}\quad\rightarrow\quad\frac{e^{ikr}}{4\pi r} \tag{4.3.38}$$

$$\begin{aligned}k_x&=k\sin\theta_s\cos\phi_s\\k_y&=k\sin\theta_s\sin\phi_s\\k_z&=k\cos\theta_s\end{aligned} \tag{4.3.39}$$

$$TE\ polarization:\ \hat{e}(k_z)=\frac{\hat{k}\times\hat{z}}{|\hat{k}\times\hat{z}|}=\frac{1}{k_\rho}\left(\hat{x}k_y-\hat{y}k_x\right)$$

$$=\frac{1}{k\sin\theta_s}\left(\hat{x}k\sin\theta_s\sin\phi_s-\hat{y}k\sin\theta_s\cos\phi_s\right)$$

$$=\hat{x}\sin\phi_s-\hat{y}\cos\phi_s=-\hat{h}(\theta_s,\phi_s)=-\hat{h}(\pi-\theta_s,\phi_s) \tag{4.3.40}$$

$$\hat{e}(-k_z)=\hat{x}\sin\phi_s-\hat{y}\cos\phi_s=-\hat{h}(\theta_s,\phi_s)=-\hat{h}(\pi-\theta_s,\phi_s) \tag{4.3.41}$$

$$TM\ polarization: \hat{h}(k_z) = \hat{e} \times \hat{k} = -\frac{k_z}{kk_\rho}\left(\hat{x}k_x + \hat{y}k_y\right) + \frac{k_\rho}{k}\hat{z}$$

$$= -\frac{k\cos\theta_s}{kk\sin\theta_s}\left(\hat{x}k\sin\theta_s\cos\phi_s + \hat{y}k\sin\theta_s\sin\phi_s\right) + \frac{k\sin\theta_s}{k}\hat{z}$$

$$= -\cos\theta_s\left(\hat{x}\cos\phi_s + \hat{y}\sin\phi_s\right) + \sin\theta_s\,\hat{z} = -\hat{v}(\theta_s, \phi_s) \tag{4.3.42}$$

$$\hat{h}(-k_z) = \cos\theta_s\left(\hat{x}\cos\phi_s + \hat{y}\sin\phi_s\right) + \sin\theta_s\,\hat{z} = -\hat{v}(\pi - \theta_s, \phi_s) \tag{4.3.43}$$

Also for remote sensing convention, $R^{TM} = R_v$ and $R^{TE} = R_h$

$$\bar{\bar{G}}_{01}(\bar{r}, \bar{r}') = \frac{e^{ikr}}{4\pi r}\,\hat{e}(k_z)\left[\hat{e}(k_z)e^{-ik_{hz}z'} + R^{TE}e^{2ik_{hz}d}\hat{e}(-k_z)e^{ik_{hz}z'}\right]e^{-ik_x x' - ik_y y'}$$

$$+\frac{e^{ikr}}{4\pi r}\hat{h}(k_z)\left[\hat{h}(k_z)e^{-ik_{vz}z'} + R^{TM}e^{2ik_{vz}d}\hat{h}(-k_z)e^{ik_{vz}z'}\right]e^{-ik_x x' - ik_y y'} \tag{4.3.44}$$

Then we separate $\bar{\bar{G}}_{01}(\bar{r}, \bar{r}')$ into two terms

$$\bar{\bar{G}}_{01}(\bar{r}, \bar{r}') = \bar{\bar{G}}_{01}^{(0)}(\bar{r}, \bar{r}') + \bar{\bar{G}}_{01}^{(R)}(\bar{r}, \bar{r}') \tag{4.3.45}$$

$$\bar{\bar{G}}_{01}^{(0)}(\bar{r}, \bar{r}') = \frac{e^{ikr}}{4\pi r}\,\hat{e}(k_z)\left[\hat{e}(k_z)e^{-ik_{hz}z'}\right]e^{-ik_x x' - ik_y y'} + \frac{e^{ikr}}{4\pi r}\hat{h}(k_z)\left[\hat{h}(k_z)e^{-ik_{vz}z'}\right]e^{-ik_x x' - ik_y y'}$$

$$= \frac{e^{ikr}}{4\pi r}\left[\hat{e}(k_z)\hat{e}(k_z)e^{-ik_{hz}z'} + \hat{h}(k_z)\hat{h}(k_z)e^{-ik_{vz}z'}\right]e^{-ik_x x' - ik_y y'} \tag{4.3.46}$$

$$\bar{\bar{G}}_{01}^{(R)}(\bar{r}, \bar{r}')$$

$$= \frac{e^{ikr}}{4\pi r}\,\hat{e}(k_z)\left[R^{TE}e^{2ik_{hz}d}\hat{e}(-k_z)e^{ik_{hz}z'}\right]e^{-ik_x x' - ik_y y'}$$

$$+\frac{e^{ikr}}{4\pi r}\hat{h}(k_z)\left[R^{TM}e^{2ik_{vz}d}\hat{h}(-k_z)e^{ik_{vz}z'}\right]e^{-ik_x x' - ik_y y'}$$

$$= \frac{e^{ikr}}{4\pi r}\left[\hat{e}(k_z)R^{TE}e^{2ik_{hz}d}\hat{e}(-k_z)e^{ik_{hz}z'}\right.$$

$$\left.+\,\hat{h}(k_z)R^{TM}e^{2ik_{vz}d}\hat{h}(-k_z)e^{ik_{vz}z'}\right]e^{-ik_x x' - ik_y y'} \tag{4.3.47}$$

Next calculate the scattering from foldy lax equation. Consider the plane wave incidence.

$$\bar{E}_{inc} = \hat{e}_i e^{i\bar{K}_i\cdot\bar{r}} \tag{4.3.48}$$

For vertical polarized incident waves in medium 1,

$$\bar{E}_{inc} = \hat{h}(-k_{iz})e^{ik_{ix}x+ik_{iy}y-ik_{izv}z} \tag{4.3.48}$$

$$\bar{E}_{ref} = R_{vi}\hat{h}(k_{iz})e^{ik_{ix}x+ik_{iy}y+ik_{izv}z} \tag{4.3.49}$$

For horizontal polarized incident waves in medium 1,

$$\bar{E}_{inc} = \hat{e}(-k_{iz})e^{ik_{ix}x+ik_{iy}y-ik_{izv}z} \tag{4.3.50}$$

$$\bar{E}_{ref} = R_{hi}\hat{e}(k_{iz})e^{ik_{ix}x+ik_{iy}y+ik_{izv}z} \tag{4.3.51}$$

Then

$$\bar{E}_{inc}(\bar{r}) = E_{vi}\hat{v}(\pi-\theta_i,\phi_i)e^{i\bar{K}_{iv}\cdot\bar{r}} + E_{hi}\hat{h}(\pi-\theta_i,\phi_i)e^{i\bar{K}_{ih}\cdot\bar{r}} \tag{4.3.52}$$

For reflected wave, we take into account the phase shift considering surface at $z = -d$.

$$\bar{E}_{ref}(\bar{r}) = E_{vi}R_{vi}e^{2ik_{izv}d}\hat{v}(\theta_i,\phi_i)e^{i\bar{k}_{iv}\cdot\bar{r}} + E_{hi}R_{hi}e^{2ik_{izh}d}\hat{h}(\theta_i,\phi_i)e^{i\bar{k}_{ih}\cdot\bar{r}} \tag{4.3.53}$$

We write the field in foldy lax equation in medium 1.

$$\bar{E} = \bar{E}_{inc} + \bar{E}_{ref} + \sum_{j=1}^{N} \bar{\bar{G}}_{11}\bar{\bar{T}}_j\bar{E}_j^{ex} \tag{4.3.54}$$

Subscript j denotes the index for the scatterer. Then for the first iteration

$$\bar{E} = \bar{E}_{inc} + \bar{E}_{ref} + \sum_{j=1}^{N} \bar{\bar{G}}_{11}\bar{\bar{T}}_j(\bar{E}_{inc} + \bar{E}_{ref}) \tag{4.3.55}$$

In medium 0, the scattered field is

$$\bar{E}_s = \sum_{j=1}^{N} \bar{\bar{G}}_{01}\bar{\bar{T}}_j(\bar{E}_{inc} + \bar{E}_{ref}) \tag{4.3.56}$$

Using (45)

$$\bar{E}_s = \sum_{j=1}^{N} (\bar{\bar{G}}_{01}^{(0)} + \bar{\bar{G}}_{01}^{(R)})\bar{\bar{T}}_j(\bar{E}_{inc} + \bar{E}_{ref}) \tag{4.3.57}$$

$$\bar{E}_s = \sum_{j=1}^{N} \bar{E}_{sj} \tag{4.3.58}$$

Then scattered field from scatterer j is

$$\bar{\bar{E}}_{sj} = \left(\bar{\bar{G}}_{01}^{(0)} + \bar{\bar{G}}_{01}^{(R)}\right)\bar{\bar{T}}_j\left(\bar{\bar{E}}_{inc} + \bar{\bar{E}}_{ref}\right) \tag{4.3.59}$$

Then we expand it

$$\bar{\bar{E}}_{sj} = \bar{\bar{G}}_{01}^{(0)}\bar{\bar{T}}_j\bar{\bar{E}}_{inc} + \bar{\bar{G}}_{01}^{(R)}\bar{\bar{T}}_j\bar{\bar{E}}_{inc} + \bar{\bar{G}}_{01}^{(0)}\bar{\bar{T}}_j\bar{\bar{E}}_{ref} + \bar{\bar{G}}_{01}^{(R)}\bar{\bar{T}}_j\bar{\bar{E}}_{ref} \tag{4.3.60}$$

We only keep first three which are relevant to distorted born approximation.

$$\bar{\bar{E}}_{sj} = \bar{\bar{G}}_{01}^{(0)}\bar{\bar{T}}_j\bar{\bar{E}}_{inc} + \bar{\bar{G}}_{01}^{(R)}\bar{\bar{T}}_j\bar{\bar{E}}_{inc} + \bar{\bar{G}}_{01}^{(0)}\bar{\bar{T}}_j\bar{\bar{E}}_{ref} \tag{4.3.61}$$

The first one is volume scattering. The second and third ones are the double bounce scattering. Then we examine each term and derive the corresponding scattering matrix.

4.3.1 Volume scattering [vol]

$$\bar{\bar{E}}_{sj}^{(vol)} = \bar{\bar{G}}_{01}^{(0)}\bar{\bar{T}}_j\bar{\bar{E}}_{inc} \tag{4.3.62}$$

Apply Dirac notation, $\bar{\bar{T}}_j(\bar{r}', \bar{r}'') = \langle \bar{r}' | \bar{\bar{T}}_j | \bar{r}'' \rangle$ and $\bar{E}_{inc}(\bar{r}'') = \langle \bar{r}'' | \bar{E}_{inc} \rangle$.

$$\bar{\bar{E}}_{sj}^{(vol)}(\bar{r}) = \int d\bar{r}'\, \bar{\bar{G}}_{01}^{(0)}(\bar{r}, \bar{r}') \int d\bar{r}''\, \langle \bar{r}' | \bar{\bar{T}}_j | \bar{r}'' \rangle \langle \bar{r}'' | \bar{E}_{inc} \rangle \tag{4.3.63}$$

where

$$\bar{\bar{G}}_{01}^{(0)}(\bar{r}, \bar{r}') = \frac{e^{ikr}}{4\pi r}\left[\hat{e}(k_z)\hat{e}(k_z)e^{-ik_{hz}z'} + \hat{h}(k_z)\hat{h}(k_z)e^{-ik_{vz}z'}\right]e^{-ik_x x' - ik_y y'} \tag{4.3.64}$$

$$\bar{\bar{E}}_{sj}^{(vol)}(\bar{r}) = \frac{e^{ikr}}{4\pi r}\int d\bar{r}'\, \left[\hat{e}(k_z)\hat{e}(k_z)e^{-ik_{hz}z'} + \hat{h}(k_z)\hat{h}(k_z)e^{-ik_{vz}z'}\right]e^{-ik_x x' - ik_y y'} \int d\bar{r}''\, \langle \bar{r}' | \bar{\bar{T}}_j | \bar{r}'' \rangle \langle \bar{r}'' | \bar{E}_{inc} \rangle$$

$$= \frac{e^{ikr}}{4\pi r}\int d\bar{r}'\, \left[\hat{e}(k_z)\hat{e}(k_z)e^{-i\bar{k}_h\cdot\bar{r}'} + \hat{h}(k_z)\hat{h}(k_z)e^{-i\bar{k}_v\cdot\bar{r}'}\right] \int d\bar{r}''\, \langle \bar{r}' | \bar{\bar{T}}_j | \bar{r}'' \rangle \langle \bar{r}'' | \bar{\bar{E}}_{inc} \rangle \tag{4.3.65}$$

Then we substitute the incident field

$$\bar{\bar{E}}_{sj}^{(vol)}(\bar{r}) = \frac{e^{ikr}}{4\pi r}\int d\bar{r}'\, \left[\hat{e}(k_z)\hat{e}(k_z)e^{-i\bar{k}_h\cdot\bar{r}'} + \hat{h}(k_z)\hat{h}(k_z)e^{-i\bar{k}_v\cdot\bar{r}'}\right] \int d\bar{r}''\, \langle \bar{r}' | \bar{\bar{T}}_j | \bar{r}'' \rangle$$

$$\left[E_{vi}\hat{v}(\pi - \theta_i, \phi_i)e^{i\bar{K}_{iv}\cdot\bar{r}''} + E_{hi}\hat{h}(\pi - \theta_i, \phi_i)e^{i\bar{K}_{ih}\cdot\bar{r}''}\right] \tag{4.3.66}$$

By the translational theorem of operators, $\bar{\bar{T}}_j$ is related to $\bar{\bar{T}}$ centered at the origin by the operator equation.

$$\bar{\bar{T}}_j = e^{-i\bar{p}_{op}\cdot\bar{r}_j}\bar{\bar{T}}e^{i\bar{p}_{op}\cdot\bar{r}_j} \tag{4.3.67}$$

The momentum representation of $\bar{\bar{T}}$ is

$$\langle\bar{p}|\bar{\bar{T}}|\bar{p}'\rangle = \int d\bar{r}' \int d\bar{r}'' \langle\bar{p}|\bar{r}'\rangle\langle\bar{r}'|\bar{\bar{T}}|\bar{r}''\rangle\langle\bar{r}''|\bar{p}'\rangle = \int d\bar{r}' \int d\bar{r}'' e^{-i\bar{p}\cdot\bar{r}'}\langle\bar{r}'|\bar{\bar{T}}|\bar{r}''\rangle e^{i\bar{p}'\cdot\bar{r}''} \tag{4.3.68}$$

Where $\langle\bar{p}|\bar{r}'\rangle = e^{-i\bar{p}\cdot\bar{r}'}$ and $\langle\bar{r}''|\bar{p}'\rangle = e^{i\bar{p}'\cdot\bar{r}''}$ come from momentum representation with the inner product. Then

$$\langle\bar{p}|\bar{\bar{T}}_j|\bar{p}'\rangle = \langle\bar{p}|e^{-i\bar{p}_{op}\cdot\bar{r}_j}\bar{\bar{T}}e^{i\bar{p}_{op}\cdot\bar{r}_j}|\bar{p}'\rangle = e^{-i\bar{p}\cdot\bar{r}_j}\langle\bar{p}|\bar{\bar{T}}|\bar{p}'\rangle e^{i\bar{p}'\cdot\bar{r}_j} = e^{-i(\bar{p}-\bar{p}')\cdot\bar{r}_j}\langle\bar{p}|\bar{\bar{T}}|\bar{p}'\rangle \tag{4.3.69}$$

$$\begin{aligned}\langle\bar{r}'|\bar{\bar{T}}_j|\bar{r}''\rangle &= \int \frac{d\bar{p}}{(2\pi)^3}\int \frac{d\bar{p}'}{(2\pi)^3}\langle\bar{r}'|\bar{p}\rangle\langle\bar{p}|\bar{\bar{T}}_j|\bar{p}'\rangle\langle\bar{p}'|\bar{r}''\rangle \\ &= \int \frac{d\bar{p}}{(2\pi)^3}\int \frac{d\bar{p}'}{(2\pi)^3} e^{i\bar{p}\cdot\bar{r}'}e^{-i(\bar{p}-\bar{p}')\cdot\bar{r}_j}\langle\bar{p}|\bar{\bar{T}}|\bar{p}'\rangle\, e^{-i\bar{p}'\cdot\bar{r}''} \\ &= \int \frac{d\bar{p}}{(2\pi)^3}\int \frac{d\bar{p}'}{(2\pi)^3} e^{i\bar{p}\cdot\bar{r}'-i\bar{p}'\cdot\bar{r}''}e^{-i(\bar{p}-\bar{p}')\cdot\bar{r}_j}\langle\bar{p}|\bar{\bar{T}}|\bar{p}'\rangle\end{aligned} \tag{4.3.70}$$

Let $\bar{\bar{T}}_p(\bar{p},\bar{p}') = \langle\bar{p}|\bar{\bar{T}}|\bar{p}'\rangle$

$$\begin{aligned}\bar{E}_{sj}^{(vol)}(\bar{r}) = \frac{e^{ikr}}{4\pi r}\int d\bar{r}'\ &\left[\hat{e}(k_z)\hat{e}(k_z)e^{-i\bar{k}_h\cdot\bar{r}'} + \hat{h}(k_z)\hat{h}(k_z)e^{-i\bar{k}_v\cdot\bar{r}'}\right]\int d\bar{r}'' \\ &\int \frac{d\bar{p}}{(2\pi)^3}\int \frac{d\bar{p}'}{(2\pi)^3} e^{i\bar{p}\cdot\bar{r}'-i\bar{p}'\cdot\bar{r}''}e^{-i(\bar{p}-\bar{p}')\cdot\bar{r}_j}\bar{\bar{T}}_p(\bar{p},\bar{p}')\left[E_{vi}\hat{v}(\pi-\theta_i,\phi_i)e^{i\bar{K}_{iv}\cdot\bar{r}''}\right. \\ &\left. + E_{hi}\hat{h}(\pi-\theta_i,\phi_i)e^{i\bar{K}_{ih}\cdot\bar{r}''}\right]\end{aligned}$$

$$\begin{aligned}= \frac{e^{ikr}}{4\pi r}\int d\bar{r}'\int d\bar{r}''\int \frac{d\bar{p}}{(2\pi)^3}\int \frac{d\bar{p}'}{(2\pi)^3}\ &\left[\hat{e}(k_z)\hat{e}(k_z)e^{-i\bar{k}_h\cdot\bar{r}'} + \hat{h}(k_z)\hat{h}(k_z)e^{-i\bar{k}_v\cdot\bar{r}'}\right] \\ e^{i\bar{p}\cdot\bar{r}'-i\bar{p}'\cdot\bar{r}''}e^{-i(\bar{p}-\bar{p}')\cdot\bar{r}_j}&\bar{\bar{T}}_p(\bar{p},\bar{p}')\left[E_{vi}\hat{v}(\pi-\theta_i,\phi_i)e^{i\bar{K}_{iv}\cdot\bar{r}''} + E_{hi}\hat{h}(\pi-\theta_i,\phi_i)e^{i\bar{K}_{ih}\cdot\bar{r}''}\right]\end{aligned} \tag{4.3.71}$$

Then the orthogonality relation for momentum state is

$$\langle\bar{p}|\bar{p}'\rangle = \int d\bar{r}'\langle\bar{p}|\bar{r}'\rangle\langle\bar{r}'|\bar{p}'\rangle = \int d\bar{r}' e^{-i\bar{p}\cdot\bar{r}'}e^{i\bar{p}'\cdot\bar{r}'} = (2\pi)^3\delta(\bar{p}-\bar{p}') \tag{4.3.72}$$

We apply orthogonality relation over $\bar{r}'$.

$$\bar{E}_{sj}^{(vol)}(\bar{r}) = \frac{e^{ikr}}{4\pi r}\int d\bar{r}'' \int \frac{d\bar{p}}{(2\pi)^3}\int \frac{d\bar{p}'}{(2\pi)^3}\big[\hat{e}(k_z)\hat{e}(k_z)(2\pi)^3\delta(\bar{k}_h - \bar{p})$$
$$+ \hat{h}(k_z)\hat{h}(k_z)(2\pi)^3\delta(\bar{k}_v - \bar{p})\big]$$
$$e^{-i\bar{p}'\cdot\bar{r}''}e^{-i(\bar{p}-\bar{p}')\cdot\bar{r}_j}\bar{\bar{T}}_p(\bar{p},\bar{p}')\big[E_{vi}\hat{v}(\pi-\theta_i,\phi_i)e^{i\bar{K}_{iv}\cdot\bar{r}''} + E_{hi}\hat{h}(\pi-\theta_i,\phi_i)e^{i\bar{K}_{ih}\cdot\bar{r}''}\big]$$
$$= \frac{e^{ikr}}{4\pi r}\int d\bar{r}'' \int \frac{d\bar{p}'}{(2\pi)^3}e^{-i\bar{p}'\cdot\bar{r}''}\Big[\hat{e}(k_z)\hat{e}(k_z)e^{-i(\bar{k}_h-\bar{p}')\cdot\bar{r}_j}\bar{\bar{T}}_p(\bar{k}_h,\bar{p}')$$
$$+ \hat{h}(k_z)\hat{h}(k_z)e^{-i(\bar{k}_v-\bar{p}')\cdot\bar{r}_j}\bar{\bar{T}}_p(\bar{k}_v,\bar{p}')\Big]$$
$$\big[E_{vi}\hat{v}(\pi-\theta_i,\phi_i)e^{i\bar{K}_{iv}\cdot\bar{r}''} + E_{hi}\hat{h}(\pi-\theta_i,\phi_i)e^{i\bar{K}_{ih}\cdot\bar{r}''}\big] \qquad (4.3.73)$$

We then apply orthogonality relation over $\bar{r}''$.

$$\bar{E}_{sj}^{(vol)}(\bar{r}) = \frac{e^{ikr}}{4\pi r}\int \frac{d\bar{p}'}{(2\pi)^3}\Big[\hat{e}(k_z)\hat{e}(k_z)e^{-i(\bar{k}_h-\bar{p}')\cdot\bar{r}_j}\bar{\bar{T}}_p(\bar{k}_h,\bar{p}')$$
$$+ \hat{h}(k_z)\hat{h}(k_z)e^{-i(\bar{k}_v-\bar{p}')\cdot\bar{r}_j}\bar{\bar{T}}_p(\bar{k}_v,\bar{p}')\Big]$$
$$\big[E_{vi}\hat{v}(\pi-\theta_i,\phi_i)(2\pi)^3\delta(\bar{p}'-\bar{K}_{iv}) + E_{hi}\hat{h}(\pi-\theta_i,\phi_i)(2\pi)^3\delta(\bar{p}'-\bar{K}_{ih})\big]$$
$$= \frac{e^{ikr}}{4\pi r}\big[\hat{e}(k_z)\hat{e}(k_z)e^{-i(\bar{k}_h-\bar{K}_{iv})\cdot\bar{r}_j}\cdot\bar{\bar{T}}_p(\bar{k}_h,\bar{K}_{iv})\big][E_{vi}\hat{v}(\pi-\theta_i,\phi_i)]$$
$$+\frac{e^{ikr}}{4\pi r}\big[\hat{h}(k_z)\hat{h}(k_z)e^{-i(\bar{k}_v-\bar{K}_{iv})\cdot\bar{r}_j}\bar{\bar{T}}_p(\bar{k}_v,\bar{K}_{iv})\big][E_{vi}\hat{v}(\pi-\theta_i,\phi_i)]$$
$$+\frac{e^{ikr}}{4\pi r}\big[\hat{e}(k_z)\hat{e}(k_z)e^{-i(\bar{k}_h-\bar{K}_{ih})\cdot\bar{r}_j}\bar{\bar{T}}_p(\bar{k}_h,\bar{K}_{ih})\big]\big[E_{hi}\hat{h}(\pi-\theta_i,\phi_i)\big]$$
$$+\frac{e^{ikr}}{4\pi r}\big[\hat{h}(k_z)\hat{h}(k_z)e^{-i(\bar{k}_v-\bar{K}_{ih})\cdot\bar{r}_j}\bar{\bar{T}}_p(\bar{k}_v,\bar{K}_{ih})\big]\big[E_{hi}\hat{h}(\pi-\theta_i,\phi_i)\big] \qquad (4.3.74)$$

The relation between T matrix and scattering amplitude is

$$\bar{\bar{F}}(\hat{k}_s,\hat{k}_i)\cdot\hat{e}_i = \frac{1}{4\pi}\big[\hat{v}_s\hat{v}_s + \hat{h}_s\hat{h}_s\big]\cdot\bar{\bar{T}}_p(k\hat{k}_s,k\hat{k}_i)\cdot\hat{e}_i \qquad (4.3.75)$$

In terms of incident and scattering angles

$$\bar{\bar{F}}(\theta_s,\phi_s;\theta_i,\phi_i)\cdot\hat{e}_i$$
$$= \frac{1}{4\pi}\big[\hat{v}_s(\theta_s,\phi_s)\hat{v}_s(\theta_s,\phi_s) + \hat{h}_s(\theta_s,\phi_s)\hat{h}_s(\theta_s,\phi_s)\big]\cdot\bar{\bar{T}}_p\left(k\hat{k}_s(\theta_s,\phi_s),k\hat{k}_i(\theta_i,\phi_i)\right)\cdot\hat{e}_i \quad (4.3.76)$$

Which means

$$f_{vv}(\theta_s,\phi_s;\theta_i,\phi_i) = \hat{v}_s \cdot \bar{\bar{F}}(\theta_s,\phi_s;\theta_i,\phi_i) \cdot \hat{v}_i$$
$$= \frac{1}{4\pi}\hat{v}_s \cdot \bar{\bar{T}}_p\left(k\hat{k}_s(\theta_s,\phi_s), k\hat{k}_i(\theta_i,\phi_i)\right) \cdot \hat{v}_i \quad (4.3.77)$$

$$f_{hv}(\theta_s,\phi_s;\theta_i,\phi_i) = \hat{h}_s \cdot \bar{\bar{F}}(\theta_s,\phi_s;\theta_i,\phi_i) \cdot \hat{v}_i$$
$$= \frac{1}{4\pi}\hat{h}_s \cdot \bar{\bar{T}}_p\left(k\hat{k}_s(\theta_s,\phi_s), k\hat{k}_i(\theta_i,\phi_i)\right) \cdot \hat{v}_i \quad (4.3.78)$$

$$f_{hh}(\theta_s,\phi_s;\theta_i,\phi_i) = \hat{h}_s \cdot \bar{\bar{F}}(\theta_s,\phi_s;\theta_i,\phi_i) \cdot \hat{h}_i$$
$$= \frac{1}{4\pi}\hat{h}_s \cdot \bar{\bar{T}}_p\left(k\hat{k}_s(\theta_s,\phi_s), k\hat{k}_i(\theta_i,\phi_i)\right) \cdot \hat{h}_i \quad (4.3.79)$$

$$f_{vh}(\theta_s,\phi_s;\theta_i,\phi_i) = \hat{v}_s \cdot \bar{\bar{F}}(\theta_s,\phi_s;\theta_i,\phi_i) \cdot \hat{h}_i$$
$$= \frac{1}{4\pi}\hat{v}_s \cdot \bar{\bar{T}}_p\left(k\hat{k}_s(\theta_s,\phi_s), k\hat{k}_i(\theta_i,\phi_i)\right) \cdot \hat{h}_i \quad (4.3.80)$$

The correlation between different notations of scattering polarization vectors are.

$$\hat{e}(k_z) = \hat{x}\sin\phi_s - \hat{y}\cos\phi_s = -\hat{h}(\theta_s,\phi_s) = -\hat{h}(\pi-\theta_s,\phi_s) \quad (4.3.81)$$

$$\hat{e}(-k_z) = \hat{x}\sin\phi_s - \hat{y}\cos\phi_s = -\hat{h}(\theta_s,\phi_s) = -\hat{h}(\pi-\theta_s,\phi_s) \quad (4.3.82)$$

$$\hat{h}(k_z) = -\cos\theta_s\,(\hat{x}\cos\phi_s + \hat{y}\sin\phi_s) + \sin\theta_s\,\hat{z} = -\hat{v}(\theta_s,\phi_s) \quad (4.3.83)$$

$$\hat{h}(-k_z) = \cos\theta_s\,(\hat{x}\cos\phi_s + \hat{y}\sin\phi_s) + \sin\theta_s\,\hat{z} = -\hat{v}(\pi-\theta_s,\phi_s) \quad (4.3.84)$$

Also for incident scattering polarization vectors

$$\hat{e}(k_{iz}) = -\hat{h}(\pi-\theta_i,\phi_i) \quad (4.3.85)$$

$$\hat{e}(-k_{iz}) = -\hat{h}(\pi-\theta_i,\phi_i) \quad (4.3.86)$$

$$\hat{h}(k_{iz}) = -\hat{v}(\theta_i,\phi_i) \quad (4.3.87)$$

$$\hat{h}(-k_{iz}) = -\hat{v}(\pi-\theta_i,\phi_i) \quad (4.3.88)$$

Then replace the representation of polarization vectors for $\bar{E}_{sj}^{(vol)}(\bar{r})$

$$\bar{E}_{sj}^{(vol)}(\bar{r}) = \frac{e^{ikr}}{4\pi r}\left[\hat{h}(\theta_s,\phi_s)e^{-i(\bar{k}_h-\bar{K}_{iv})\cdot\bar{r}_j}\right][E_{vi}]$$

$$+\frac{e^{ikr}}{4\pi r}\left[\hat{v}(\theta_s,\phi_s)\hat{v}(\theta_s,\phi_s)e^{-i(\bar{k}_v-\bar{K}_{iv})\cdot\bar{r}_j}\bar{\bar{T}}_p\left(\bar{k}_v,\bar{K}_{iv}\right)\right][E_{vi}\hat{v}(\pi-\theta_i,\phi_i)]$$

$$+\frac{e^{ikr}}{4\pi r}\left[\hat{h}(\theta_s,\phi_s)\hat{h}(\theta_s,\phi_s)e^{-i(\bar{k}_h-\bar{K}_{ih})\cdot\bar{r}_j}\bar{\bar{T}}_p\left(\bar{k}_h,\bar{K}_{ih}\right)\right]\left[E_{hi}\hat{h}(\pi-\theta_i,\phi_i)\right]$$

$$+\frac{e^{ikr}}{4\pi r}\left[\hat{v}(\theta_s,\phi_s)\hat{v}(\theta_s,\phi_s)e^{-i(\bar{k}_v-\bar{K}_{ih})\cdot\bar{r}_j}\bar{\bar{T}}_p\left(\bar{k}_v,\bar{K}_{ih}\right)\right]\left[E_{hi}\hat{h}(\pi-\theta_i,\phi_i)\right] \qquad (4.3.89)$$

Next, replace the T matrix with scattering amplitude

$$\bar{E}_{sj}^{(vol)}(\bar{r})=\frac{e^{ikr}}{r}\hat{h}(\theta_s,\phi_s)e^{-i(\bar{k}_h-\bar{K}_{iv})\cdot\bar{r}_j}f_{hv}(\theta_s,\phi_s;\pi-\theta_i,\phi_i)E_{vi}$$

$$+\frac{e^{ikr}}{r}\hat{v}(\theta_s,\phi_s)e^{-i(\bar{k}_v-\bar{K}_{iv})\cdot\bar{r}_j}f_{vv}(\theta_s,\phi_s;\pi-\theta_i,\phi_i)E_{vi}$$

$$+\frac{e^{ikr}}{r}\hat{h}(\theta_s,\phi_s)e^{-i(\bar{k}_h-\bar{K}_{ih})\cdot\bar{r}_j}f_{hh}(\theta_s,\phi_s;\pi-\theta_i,\phi_i)E_{hi}$$

$$+\frac{e^{ikr}}{r}\hat{v}(\theta_s,\phi_s)e^{-i(\bar{k}_v-\bar{K}_{ih})\cdot\bar{r}_j}f_{vh}(\theta_s,\phi_s;\pi-\theta_i,\phi_i)E_{hi} \qquad (4.3.90)$$

Thus we sum up scattering from all scatterers

$$\bar{E}_{s}^{(vol)}(\bar{r})=\sum_{j=1}^{N}\frac{e^{ikr}}{r}\hat{h}(\theta_s,\phi_s)e^{-i(\bar{k}_h-\bar{K}_{iv})\cdot\bar{r}_j}f_{hv}(\theta_s,\phi_s;\pi-\theta_i,\phi_i)E_{vi}$$

$$+\sum_{j=1}^{N}\frac{e^{ikr}}{r}\hat{v}(\theta_s,\phi_s)e^{-i(\bar{k}_v-\bar{K}_{iv})\cdot\bar{r}_j}f_{vv}(\theta_s,\phi_s;\pi-\theta_i,\phi_i)E_{vi}$$

$$+\sum_{j=1}^{N}\frac{e^{ikr}}{r}\hat{h}(\theta_s,\phi_s)e^{-i(\bar{k}_h-\bar{K}_{ih})\cdot\bar{r}_j}f_{hh}(\theta_s,\phi_s;\pi-\theta_i,\phi_i)E_{hi}$$

$$+\sum_{j=1}^{N}\frac{e^{ikr}}{r}\hat{v}(\theta_s,\phi_s)e^{-i(\bar{k}_v-\bar{K}_{ih})\cdot\bar{r}_j}f_{vh}(\theta_s,\phi_s;\pi-\theta_i,\phi_i)E_{hi} \qquad (4.3.91)$$

We can also write it in terms of scattering matrix elements

$$\bar{E}_{s}^{(vol)}(\bar{r})=\frac{e^{ikr}}{r}\hat{h}(\theta_s,\phi_s)S_{hv}^{(vol)}E_{vi}+\frac{e^{ikr}}{r}\hat{v}(\theta_s,\phi_s)S_{vv}^{(vol)}E_{vi}+\frac{e^{ikr}}{r}\hat{h}(\theta_s,\phi_s)S_{hh}^{(vol)}E_{hi}$$

$$+\frac{e^{ikr}}{r}\hat{v}(\theta_s,\phi_s)S_{vh}^{(vol)}E_{hi} \tag{4.3.92}$$

Then

$$S_{hv}^{(vol)}=\sum_{j=1}^{N}e^{-i(\bar{k}_h-\bar{K}_{iv})\cdot\bar{r}_j}f_{hv}(\theta_s,\phi_s;\pi-\theta_i,\phi_i) \tag{4.3.93}$$

$$S_{vv}^{(vol)}=\sum_{j=1}^{N}e^{-i(\bar{k}_v-\bar{K}_{iv})\cdot\bar{r}_j}f_{vv}(\theta_s,\phi_s;\pi-\theta_i,\phi_i) \tag{4.3.94}$$

$$S_{hh}^{(vol)}=\sum_{j=1}^{N}e^{-i(\bar{k}_h-\bar{K}_{ih})\cdot\bar{r}_j}f_{hh}(\theta_s,\phi_s;\pi-\theta_i,\phi_i) \tag{4.3.95}$$

$$S_{vh}^{(vol)}=\sum_{j=1}^{N}e^{-i(\bar{k}_v-\bar{K}_{ih})\cdot\bar{r}_j}f_{vh}(\theta_s,\phi_s;\pi-\theta_i,\phi_i) \tag{4.3.96}$$

Based on the scattering matrix, Coherency matrix can then be computed. The following shows the summary of the polarization vector's definition used here.

$$\hat{h}_s=\hat{h}(\theta_s,\phi_s)=-\hat{x}\sin\phi_s+\hat{y}\cos\phi_s \tag{4.3.97}$$

$$\hat{v}_s=\hat{v}(\theta_s,\phi_s)=\cos\theta_s\,(\hat{x}\cos\phi_s+\hat{y}\sin\phi_s)-\sin\theta_s\,\hat{z} \tag{4.3.98}$$

For the incident wave, the wave is coming down

$$\hat{h}_i=\hat{h}(\pi-\theta_i,\phi_i)=-\hat{x}\sin\phi_i+\hat{y}\cos\phi_i \tag{4.3.99}$$

$$\hat{v}_i=\hat{v}(\pi-\theta_i,\phi_i)=-\cos\theta_i\,(\hat{x}\cos\phi_i+\hat{y}\sin\phi_i)-\sin\theta_i\,\hat{z} \tag{4.3.100}$$

In the backscattering direction, the wave is going up

$$\begin{aligned}\hat{h}_{back}=\hat{h}(\theta_i,\pi+\phi_i)&=\hat{x}\sin\phi_i-\hat{y}\cos\phi_i\\&=-\hat{h}(\pi-\theta_i,\phi_i)=-\hat{h}_i\end{aligned} \tag{4.3.101}$$

$$\begin{aligned}\hat{v}_{back}=\hat{v}(\theta_i,\pi+\phi_i)&=-\cos\theta_i\,(\hat{x}\cos\phi_i+\hat{y}\sin\phi_i)-\sin\theta_i\,\hat{z}\\&=\hat{v}(\pi-\theta_i,\phi_i)=\hat{v}_i\end{aligned} \tag{4.3.102}$$

$$f_{vv}(\theta_i,\pi+\phi_i;\pi-\theta_i,\phi_i)=\frac{1}{4\pi}\hat{v}_i\cdot\bar{\bar{T}}_p\left(-\bar{k}_i,\bar{k}_i\right)\cdot\hat{v}_i \tag{4.3.103}$$

$$f_{hv}(\theta_i, \pi+\phi_i; \pi-\theta_i, \phi_i) = \frac{-1}{4\pi}\hat{h}_i \cdot \bar{\bar{T}}_p(-\bar{k}_i, \bar{k}_i) \cdot \hat{v}_i \tag{4.3.104}$$

$$f_{hh}(\theta_i, \pi+\phi_i; \pi-\theta_i, \phi_i) = \frac{-1}{4\pi}\hat{h}_i \cdot \bar{\bar{T}}_p(-\bar{k}_i, \bar{k}_i) \cdot \hat{h}_i \tag{4.3.105}$$

$$f_{vh}(\theta_i, \pi+\phi_i; \pi-\theta_i, \phi_i) = \frac{1}{4\pi}\hat{v}_i \cdot \bar{\bar{T}}_p(-\bar{k}_i, \bar{k}_i) \cdot \hat{h}_i \tag{4.3.106}$$

Note that the reciprocity here is

$$f_{hv}(\theta_i, \pi+\phi_i; \pi-\theta_i, \phi_i) = -f_{vh}(\theta_i, \pi+\phi_i; \pi-\theta_i, \phi_i) \tag{4.3.107}$$

The scattering matrix elements at backscattering direction are

$$S_{hv,back}^{(vol)} = \sum_{j=1}^{N} e^{-i(\bar{k}_{h,back} - \bar{K}_{iv})\cdot\bar{r}_j} \frac{-1}{4\pi}\hat{h}_i \cdot \bar{\bar{T}}_p(-\bar{k}_i, \bar{k}_i) \cdot \hat{v}_i \tag{4.3.108}$$

$$S_{vv,back}^{(vol)} = \sum_{j=1}^{N} e^{-i(\bar{k}_{v,back} - \bar{K}_{iv})\cdot\bar{r}_j} \frac{1}{4\pi}\hat{v}_i \cdot \bar{\bar{T}}_p(-\bar{k}_i, \bar{k}_i) \cdot \hat{v}_i \tag{4.3.109}$$

$$S_{hh,back}^{(vol)} = \sum_{j=1}^{N} e^{-i(\bar{k}_{h,back} - \bar{K}_{ih})\cdot\bar{r}_j} \frac{-1}{4\pi}\hat{h}_i \cdot \bar{\bar{T}}_p(-\bar{k}_i, \bar{k}_i) \cdot \hat{h}_i \tag{4.3.110}$$

$$S_{vh,back}^{(vol)} = \sum_{j=1}^{N} e^{-i(\bar{k}_{v,back} - \bar{K}_{ih})\cdot\bar{r}_j} \frac{1}{4\pi}\hat{v}_i \cdot \bar{\bar{T}}_p(-\bar{k}_i, \bar{k}_i) \cdot \hat{h}_i \tag{4.3.111}$$

$$\bar{K}_{iv} = k\sin\theta_i\cos\phi_i\,\hat{x} + k\sin\theta_i\sin\phi_i\,\hat{y} - \sqrt{k_v^2 - k^2\sin^2\theta_i}\,\hat{z} \tag{4.3.112}$$

$$\bar{K}_{ih} = k\sin\theta_i\cos\phi_i\,\hat{x} + k\sin\theta_i\sin\phi_i\,\hat{y} - \sqrt{k_h^2 - k^2\sin^2\theta_i}\,\hat{z} \tag{4.3.113}$$

$$\bar{k}_{v,back} = -k\sin\theta_i\cos\phi_i\,\hat{x} - k\sin\theta_i\sin\phi_i\,\hat{y} + \sqrt{k_v^2 - k^2\sin^2\theta_i}\,\hat{z} \tag{4.3.114}$$

$$\bar{k}_{h,back} = -k\sin\theta_i\cos\phi_i\,\hat{x} - k\sin\theta_i\sin\phi_i\,\hat{y} + \sqrt{k_h^2 - k^2\sin^2\theta_i}\,\hat{z} \tag{4.3.115}$$

Then

$$\bar{k}_{h,back} - \bar{K}_{iv} =$$

$$-2k\sin\theta_i\cos\phi_i\,\hat{x} - 2k\sin\theta_i\sin\phi_i\,\hat{y} + \left(\sqrt{k_h^2 - k^2\sin^2\theta_i} + \sqrt{k_v^2 - k^2\sin^2\theta_i}\right)\hat{z} \tag{4.3.116}$$

$$\bar{k}_{v,back} - \bar{K}_{ih} =$$

$$-2k\sin\theta_i\cos\phi_i\,\hat{x} - 2k\sin\theta_i\sin\phi_i\,\hat{y} + \left(\sqrt{k_v^2 - k^2\sin^2\theta_i} + \sqrt{k_h^2 - k^2\sin^2\theta_i}\right)\hat{z} \quad (4.3.117)$$

$$\bar{k}_{h,back} - \bar{K}_{iv} = \bar{k}_{v,back} - \bar{K}_{ih} \quad (4.3.118)$$

Then the reciprocal relation is

$$S_{hv,back}^{(vol)} = -S_{vh,back}^{(vol)} \quad (4.3.119)$$

Compared with the definition in Lee's book [45] for horizontal polarization changes the sign while vertical polarization stays the same.

$$\hat{h}_{back}^{Lee} = \hat{h}_i = -\hat{h}_{back} \quad (4.3.120)$$

$$\hat{v}_{back}^{Lee} = \hat{v}_i = \hat{v}_{back} \quad (4.3.121)$$

Thus in the backscattering direction

$$S_{hv,back}^{(vol),Lee} = -S_{hv,back}^{(vol)} \quad (4.3.122)$$

$$S_{vv,back}^{(vol),Lee} = S_{vv,back}^{(vol)} \quad (4.3.123)$$

$$S_{hh,back}^{(vol),Lee} = -S_{hh,back}^{(vol)} \quad (4.3.124)$$

$$S_{vh,back}^{(vol),Lee} = S_{vh,back}^{(vol)} \quad (4.3.125)$$

Then

$$S_{hv,back}^{(vol),Lee} = S_{vh,back}^{(vol),Lee} \quad (4.3.126)$$

To proceed to the coherency matrix for volume scattering, we first identify those important correlations for scattering matrix elements.

The target vector is

$$\bar{k} = [k_1 \quad k_2 \quad k_3]^T = \frac{1}{\sqrt{2}}[S_{vv} + S_{hh} \quad S_{vv} - S_{hh} \quad 2S_{vh}]^T \quad (4.3.127)$$

The coherency matrix

$$\bar{\bar{T}}_3 = \langle \bar{k}\bar{k}^\dagger \rangle = \begin{bmatrix} \langle k_1 k_1^* \rangle & \langle k_1 k_2^* \rangle & \langle k_1 k_3^* \rangle \\ \langle k_2 k_1^* \rangle & \langle k_2 k_2^* \rangle & \langle k_2 k_3^* \rangle \\ \langle k_3 k_1^* \rangle & \langle k_3 k_2^* \rangle & \langle k_3 k_3^* \rangle \end{bmatrix} \quad (4.3.128)$$

$$\langle k_1 k_1^* \rangle = \langle \frac{1}{2}(S_{vv} + S_{hh})(S_{vv} + S_{hh})^* \rangle = \frac{1}{2}(\langle S_{vv}S_{vv}^* \rangle + \langle S_{hh}S_{hh}^* \rangle + \langle S_{vv}S_{hh}^* \rangle + \langle S_{hh}S_{vv}^* \rangle)$$

$$= \frac{1}{2}(\langle S_{vv}S_{vv}^* \rangle + \langle S_{hh}S_{hh}^* \rangle + 2Re(\langle S_{vv}S_{hh}^* \rangle)) \quad (4.3.129)$$

$$\langle k_1 k_2^* \rangle = \langle \frac{1}{2}(S_{vv} + S_{hh})(S_{vv} - S_{hh})^* \rangle = \frac{1}{2}(\langle S_{vv}S_{vv}^* \rangle - \langle S_{hh}S_{hh}^* \rangle - \langle S_{vv}S_{hh}^* \rangle + \langle S_{hh}S_{vv}^* \rangle)$$

$$= \frac{1}{2}(\langle S_{vv}S_{vv}^* \rangle - \langle S_{hh}S_{hh}^* \rangle - 2iIm(\langle S_{vv}S_{hh}^* \rangle)) \quad (4.3.130)$$

$$\langle k_1 k_3^* \rangle = \langle \frac{1}{2}(S_{vv} + S_{hh})(2S_{vh})^* \rangle = \langle S_{vv}S_{vh}^* \rangle + \langle S_{hh}S_{vh}^* \rangle \quad (4.3.131)$$

$$\langle k_2 k_1^* \rangle = \langle \frac{1}{2}(S_{vv} - S_{hh})(S_{vv} + S_{hh})^* \rangle = \frac{1}{2}(\langle S_{vv}S_{vv}^* \rangle - \langle S_{hh}S_{hh}^* \rangle + \langle S_{vv}S_{hh}^* \rangle - \langle S_{hh}S_{vv}^* \rangle) =$$

$$= \frac{1}{2}(\langle S_{vv}S_{vv}^* \rangle - \langle S_{hh}S_{hh}^* \rangle + 2iIm(\langle S_{vv}S_{hh}^* \rangle)) \quad (4.3.132)$$

$$\langle k_2 k_2^* \rangle = \langle \frac{1}{2}(S_{vv} - S_{hh})(S_{vv} - S_{hh})^* \rangle = \frac{1}{2}(\langle S_{vv}S_{vv}^* \rangle + \langle S_{hh}S_{hh}^* \rangle - \langle S_{vv}S_{hh}^* \rangle - \langle S_{hh}S_{vv}^* \rangle) =$$

$$= \frac{1}{2}(\langle S_{vv}S_{vv}^* \rangle + \langle S_{hh}S_{hh}^* \rangle - 2Re(\langle S_{vv}S_{hh}^* \rangle)) \quad (4.3.133)$$

$$\langle k_2 k_3^* \rangle = \langle \frac{1}{2}(S_{vv} - S_{hh})(2S_{vh})^* \rangle = \langle S_{vv}S_{vh}^* \rangle - \langle S_{hh}S_{vh}^* \rangle \quad (4.3.134)$$

$$\langle k_3 k_1^* \rangle = \langle \frac{1}{2}(2S_{vh})(S_{vv} + S_{hh})^* \rangle = \langle S_{vh}S_{vv}^* \rangle + \langle S_{vh}S_{hh}^* \rangle = \langle S_{vv}S_{vh}^* \rangle^* + \langle S_{hh}S_{vh}^* \rangle^* \quad (4.3.135)$$

$$\langle k_3 k_2^* \rangle = \langle \frac{1}{2}(2S_{vh})(S_{vv} - S_{hh})^* \rangle = \langle S_{vh}S_{vv}^* \rangle - \langle S_{vh}S_{hh}^* \rangle = \langle S_{vv}S_{vh}^* \rangle^* - \langle S_{hh}S_{vh}^* \rangle^* \quad (4.3.136)$$

$$\langle k_3 k_3^* \rangle = \langle \frac{1}{2}(2S_{vh})(2S_{vh})^* \rangle = 2\langle S_{vh}S_{vh}^* \rangle \quad (4.3.137)$$

Consider 6 essential correlations$\langle S_{vv}S_{hh}^* \rangle, \langle S_{vv}S_{vv}^* \rangle, \langle S_{hh}S_{hh}^* \rangle, \langle S_{vv}S_{vh}^* \rangle, \langle S_{hh}S_{vh}^* \rangle, \langle S_{vh}S_{vh}^* \rangle$ when the reciprocity is applied. For the volume scattering, note that we can have correlation between scatterers and the propagation vector is complex because the z component is complex. We first derive $\langle S_{vv,back}^{(vol)} S_{hh,back}^{(vol)*} \rangle$

$\langle S_{vv}^{(vol)} S_{hh}^{(vol)*} \rangle$

$$= \langle \sum_{j=1}^{N} e^{-i(\bar{k}_v - \bar{K}_{iv})\cdot \bar{r}_j} f_{vv,j}(\theta_s, \phi_s; \pi - \theta_i, \phi_i) \sum_{p=1}^{N} e^{i(\bar{k}_h^* - \bar{K}_{ih}^*)\cdot \bar{r}_p} f_{hh,p}^*(\theta_s, \phi_s; \pi - \theta_i, \phi_i) \rangle \quad (4.3.138)$$

For coherent model, one can introduce the joint probability between scatterers. However, at this moment we ignore correlation and assume independent scattering.

$$\langle S_{vv}^{(vol)} S_{hh}^{(vol)*} \rangle$$

$$= \sum_{j=1}^{N} \langle e^{-i(\bar{k}_v - \bar{K}_{iv})\cdot \bar{r}_j} e^{i(\bar{k}_h^* - \bar{K}_{ih}^*)\cdot \bar{r}_j} \rangle \langle f_{vv,j}(\theta_s, \phi_s; \pi - \theta_i, \phi_i) f_{hh,j}^*(\theta_s, \phi_s; \pi - \theta_i, \phi_i) \rangle \quad (4.3.139)$$

The ensemble average is considered with the particle distribution, $p(\bar{r}_j)$, which is assumed uniformly distributed over the volume, V.

$$\langle e^{-i(\bar{k}_v - \bar{K}_{iv})\cdot \bar{r}_j} e^{i(\bar{k}_h^* - \bar{K}_{ih}^*)\cdot \bar{r}_j} \rangle = \int d\bar{r}_j \, e^{-i(\bar{k}_v - \bar{K}_{iv})\cdot \bar{r}_j} e^{i(\bar{k}_h^* - \bar{K}_{ih}^*)\cdot \bar{r}_j} p(\bar{r}_j)$$

$$= \frac{1}{V} \int d\bar{r}_j \, e^{-i(\bar{k}_v - \bar{K}_{iv})\cdot \bar{r}_j} e^{i(\bar{k}_h^* - \bar{K}_{ih}^*)\cdot \bar{r}_j} \quad (4.3.140)$$

Then

$$\langle S_{vv}^{(vol)} S_{hh}^{(vol)*} \rangle$$

$$= \sum_{j=1}^{N} \frac{1}{V} \int d\bar{r}_j \, e^{-i(\bar{k}_v - \bar{K}_{iv})\cdot \bar{r}_j} e^{i(\bar{k}_h^* - \bar{K}_{ih}^*)\cdot \bar{r}_j} \langle f_{vv,j}(\theta_s, \phi_s; \pi - \theta_i, \phi_i) f_{hh,j}^*(\theta_s, \phi_s; \pi - \theta_i, \phi_i) \rangle$$

$$= \frac{N}{V} \int d\bar{r}' \, e^{-i(\bar{k}_v - \bar{K}_{iv})\cdot \bar{r}'} e^{i(\bar{k}_h^* - \bar{K}_{ih}^*)\cdot \bar{r}'} \langle f_{vv}(\theta_s, \phi_s; \pi - \theta_i, \phi_i) f_{hh}^*(\theta_s, \phi_s; \pi - \theta_i, \phi_i) \rangle$$

$$= n_0 \langle f_{vv}(\theta_s, \phi_s; \pi - \theta_i, \phi_i) f_{hh}^*(\theta_s, \phi_s; \pi - \theta_i, \phi_i) \rangle \int d\bar{r}' \, e^{-i[(\bar{k}_v - \bar{K}_{iv}) - (\bar{k}_h^* - \bar{K}_{ih}^*)]\cdot \bar{r}'} \quad (4.3.141)$$

n_0 is volume density for particles within thickness, d, and area, A.

To consider the phase shifts, we reexamine all involved propagation vectors.

$$\bar{k}_v = k \sin\theta_s \cos\phi_s \, \hat{x} + k \sin\theta_s \sin\phi_s \, \hat{y} + \sqrt{k_v^2 - k^2 \sin^2\theta_s} \, \hat{z}$$

$$= k \sin\theta_s \cos\phi_s \, \hat{x} + k \sin\theta_s \sin\phi_s \, \hat{y} + (Re(k_{vz}) + iIm(k_{vz}))\hat{z} \quad (4.3.142)$$

$$\bar{k}_h = k \sin\theta_s \cos\phi_s \, \hat{x} + k \sin\theta_s \sin\phi_s \, \hat{y} + (Re(k_{hz}) + iIm(k_{hz}))\hat{z} \quad (4.3.143)$$

$$\bar{K}_{iv} = k \sin\theta_i \cos\phi_i \, \hat{x} + k \sin\theta_i \sin\phi_i \, \hat{y} - (Re(k_{ivz}) + iIm(k_{ivz}))\hat{z} \quad (4.3.144)$$

$$\bar{K}_{ih} = k\sin\theta_i\cos\phi_i\,\hat{x} + k\sin\theta_i\sin\phi_i\,\hat{y} - ((Re(k_{ihz}) + iIm(k_{ihz})))\hat{z} \quad (4.3.145)$$

where $k_{ivz} = \sqrt{k_v^2 - k^2\sin^2\theta_i}$ and $k_{ihz} = \sqrt{k_h^2 - k^2\sin^2\theta_i}$ are complex square roots.

Then in the backscattering direction, let $\theta_s = \theta_i$, $\phi_i = 0$, and $\phi_s = \pi$.

$$\bar{k}_{v,back} = -k\sin\theta_i\,\hat{x} + \sqrt{k_v^2 - k^2\sin^2\theta_i}\,\hat{z}$$

$$= -k\sin\theta_i\,\hat{x} + (Re(k_{ivz}) + iIm(k_{ivz}))\hat{z} \quad (4.3.146)$$

$$\bar{k}_{h,back} = -k\sin\theta_i\,\hat{x} + (Re(k_{ihz}) + iIm(k_{ihz}))\hat{z} \quad (4.3.147)$$

$$\bar{K}_{iv} = k\sin\theta_i\,\hat{x} - (Re(k_{ivz}) + iIm(k_{ivz}))\hat{z} \quad (4.3.148)$$

$$\bar{K}_{ih} = k\sin\theta_i\,\hat{x} - (Re(k_{ihz}) + iIm(k_{ihz}))\hat{z} \quad (4.3.149)$$

Then

$$\bar{k}_{v,back} - \bar{K}_{iv} = -2k\sin\theta_i\,\hat{x} + 2\big(Re(k_{ivz}) + iIm(k_{ivz})\big)\hat{z} \quad (4.3.150)$$

$$\bar{k}_{h,back} - \bar{K}_{ih} = -2k\sin\theta_i\,\hat{x} + 2(Re(k_{ihz}) + iIm(k_{ihz}))\hat{z} \quad (4.3.151)$$

$$\bar{k}^*_{h,back} - \bar{K}^*_{ih} = -2k\sin\theta_i\,\hat{x} + 2(Re(k_{ihz}) - iIm(k_{ihz}))\hat{z} \quad (4.3.152)$$

Then in the backscattering direction

$$\big(\bar{k}_{v,back} - \bar{K}_{iv}\big) - \big(\bar{k}^*_{h,back} - \bar{K}^*_{ih}\big)$$

$$= 2(Re(k_{ivz}) - Re(k_{ihz}) + i(Im(k_{ivz}) + Im(k_{ihz})))\hat{z} \quad (4.3.153)$$

Then

$$\langle S^{(vol)}_{vv,back} S^{(vol)*}_{hh,back}\rangle$$

$$= n_0\langle f_{vv}(\theta_i,\pi;\pi-\theta_i,0) f^*_{hh}(\theta_i,\pi;\pi-\theta_i,0)\rangle \int d\bar{r}' e^{-i2\left(Re(k_{ivz}) - Re(k_{ihz}) + i\left(Im(k_{ivz}) + Im(k_{ihz})\right)\right)z'}$$

$$= n_0\langle f_{vv}(\theta_i,\pi;\pi-\theta_i,0) f^*_{hh}(\theta_i,\pi;\pi-\theta_i,0)\rangle$$

$$A\int_{-d}^{0} dz' e^{-i2\left(Re(k_{ivz}) - Re(k_{ihz}) + i\left(Im(k_{ivz}) + Im(k_{ihz})\right)\right)z'}$$

$$= n_0\langle f_{vv}(\theta_i,\pi;\pi-\theta_i,0) f^*_{hh}(\theta_i,\pi;\pi-\theta_i,0)\rangle A \left.\frac{e^{-i2\left(Re(k_{ivz}) - Re(k_{ihz}) + i\left(Im(k_{ivz}) + Im(k_{ihz})\right)\right)z'}}{-i2\left(Re(k_{ivz}) - Re(k_{ihz}) + i\left(Im(k_{ivz}) + Im(k_{ihz})\right)\right)}\right|_{z'=-d}^{z'=0}$$

$$= n_0 A \frac{1-e^{i2d\left(Re(k_{ivz})-Re(k_{ihz})+i\left(Im(k_{ivz})+Im(k_{ihz})\right)\right)}}{-2i\left(Re(k_{ivz})-Re(k_{ihz})+i\left(Im(k_{ivz})+Im(k_{ihz})\right)\right)} \langle f_{vv}(\theta_i, \pi; \pi-\theta_i, 0) f_{hh}^*(\theta_i, \pi; \pi-\theta_i, 0)\rangle$$

$$= n_0 A \frac{1-e^{i2d\left(Re(k_{ivz})-Re(k_{ihz})+i\left(Im(k_{ivz})+Im(k_{ihz})\right)\right)}}{-2i\left(Re(k_{ivz})-Re(k_{ihz})+i\left(Im(k_{ivz})+Im(k_{ihz})\right)\right)}$$

$$\langle f_{vv}(\theta_i, \pi; \pi-\theta_i, 0) f_{hh}^*(\theta_i, \pi; \pi-\theta_i, 0)\rangle \qquad (4.3.154)$$

Note there is no dependence on x' and y' for the phase terms during the integration.

The alternative expression for k_{vz} and k_{hz} are

$$k_{vz} = Re(k_{vz}) + iIm(k_{vz}) = \sqrt{k_v^2 - k^2 \sin^2\theta_s} = \sqrt{\left(Re(k_v) + iIm(k_v)\right)^2 - k^2 \sin^2\theta_s}$$

$$\cong \sqrt{\left(Re(k_v)\right)^2 + 2iRe(k_v)Im(k_v) - k^2 \sin^2\theta_s}$$

$$= \sqrt{\left(\left(Re(k_v)\right)^2 - k^2 \sin^2\theta_s\right)\left[1 + \frac{2iRe(k_v)Im(k_v)}{\left(Re(k_v)\right)^2 - k^2 \sin^2\theta_s}\right]}$$

$$\cong \sqrt{\left(\left(Re(k_v)\right)^2 - k^2 \sin^2\theta_s\right)}\left[1 + \frac{iRe(k_v)Im(k_v)}{\left(Re(k_v)\right)^2 - k^2 \sin^2\theta_s}\right]$$

$$= Re(k_{vz}) + i\frac{Re(k_v)Im(k_v)}{Re(k_{vz})} \qquad (4.3.155)$$

$$k_{hz} \cong Re(k_{hz}) + i\frac{Re(k_h)Im(k_h)}{Re(k_{hz})} \qquad (4.3.156)$$

Some useful combinations

$$\bar{k}_{v,back}^* - \bar{K}_{iv}^* = -2k \sin\theta_i\, \hat{x} + 2\left(Re(k_{ivz}) - iIm(k_{ivz})\right)\hat{z} \qquad (4.3.157)$$

$$\bar{k}_{v,back} - \bar{K}_{ih} = -2k \sin\theta_i\, \hat{x} + \left(Re(k_{ivz}) + Re(k_{ihz}) + i\left(Im(k_{ivz}) + Im(k_{ihz})\right)\right)\hat{z} \qquad (4.3.158)$$

$$\bar{k}_{v,back}^* - \bar{K}_{ih}^* = -2k \sin\theta_i\, \hat{x} + \left(Re(k_{ivz}) + Re(k_{ihz}) - i\left(Im(k_{ivz}) + Im(k_{ihz})\right)\right)\hat{z} \qquad (4.3.159)$$

Then the similar derivation can be applied for other correlations at the backscattering direction.

$$\langle S_{vv,back}^{(vol)} S_{vv,back}^{(vol)*}\rangle$$

$$= n_0 \langle f_{vv}(\theta_i, \pi; \pi-\theta_i, 0) f_{vv}^*(\theta_i, \pi; \pi-\theta_i, 0)\rangle \int d\bar{r}'\, e^{-i\left[\left(\bar{k}_{v,back}-\bar{K}_{iv}\right)-\left(\bar{k}_{v,back}^*-\bar{K}_{iv}^*\right)\right]\cdot\bar{r}'}$$

$$= n_0\langle f_{vv}(\theta_i,\pi;\pi-\theta_i,0)f_{vv}^*(\theta_i,\pi;\pi-\theta_i,0)\rangle \int d\bar{r}'\, e^{-i[4iIm(k_{ivz})]z'}$$

$$= n_0\langle f_{vv}(\theta_i,\pi;\pi-\theta_i,0)f_{vv}^*(\theta_i,\pi;\pi-\theta_i,0)\rangle A\int_{-d}^{0} dz' e^{4Im(k_{ivz})z'}$$

$$= n_0 A\frac{1-e^{-4dIm(k_{ivz})}}{4Im(k_{ivz})}\langle f_{vv}(\theta_i,\pi;\pi-\theta_i,0)f_{vv}^*(\theta_i,\pi;\pi-\theta_i,0)\rangle \qquad (4.3.160)$$

$\langle S_{hh,back}^{(vol)} S_{hh,back}^{(vol)*}\rangle$

$$= n_0\langle f_{hh}(\theta_i,\pi;\pi-\theta_i,0)f_{hh}^*(\theta_i,\pi;\pi-\theta_i,0)\rangle \int d\bar{r}'\, e^{-i[(\bar{k}_{h,back}-\bar{K}_{ih})-(\bar{k}_{h,back}^*-\bar{K}_{ih}^*)]\cdot\bar{r}'}$$

$$= n_0\langle f_{hh}(\theta_i,\pi;\pi-\theta_i,0)f_{hh}^*(\theta_i,\pi;\pi-\theta_i,0)\rangle \int d\bar{r}'\, e^{-i[4iIm(k_{ihz})]z'}$$

$$= n_0\langle f_{hh}(\theta_i,\pi;\pi-\theta_i,0)f_{hh}^*(\theta_i,\pi;\pi-\theta_i,0)\rangle A\int_{-d}^{0} dz' e^{4Im(k_{ihz})z'}$$

$$= n_0 A\frac{1-e^{-4dIm(k_{ihz})}}{4Im(k_{ihz})}\langle f_{hh}(\theta_i,\pi;\pi-\theta_i,0)f_{hh}^*(\theta_i,\pi;\pi-\theta_i,0)\rangle \qquad (4.3.161)$$

$\langle S_{vv,back}^{(vol)} S_{vh,back}^{(vol)*}\rangle$

$$= n_0\langle f_{vv}(\theta_i,\pi;\pi-\theta_i,0)f_{vh}^*(\theta_i,\pi;\pi-\theta_i,0)\rangle \int d\bar{r}'\, e^{-i[(\bar{k}_{v,back}-\bar{K}_{iv})-(\bar{k}_{v,back}^*-\bar{K}_{ih}^*)]\cdot\bar{r}'}$$

$$= n_0\langle f_{vv}(\theta_i,\pi;\pi-\theta_i,0)f_{vh}^*(\theta_i,\pi;\pi-\theta_i,0)\rangle \int d\bar{r}'\, e^{-i\left[Re(k_{ivz})-Re(k_{ihz})+i\left(3Im(k_{ivz})+Im(k_{ihz})\right)\right]z'}$$

$$= n_0\langle f_{vv}(\theta_i,\pi;\pi-\theta_i,0)f_{vh}^*(\theta_i,\pi;\pi$$

$$-\theta_i,0)\rangle A\int_{-d}^{0} dz' e^{-i\left[Re(k_{ivz})-Re(k_{ihz})+i\left(3Im(k_{ivz})+Im(k_{ihz})\right)\right]z'}$$

$$= n_0 A\frac{1-e^{i\left[Re(k_{ivz})-Re(k_{ihz})+i\left(3Im(k_{ivz})+Im(k_{ihz})\right)\right]d}}{-i\left[Re(k_{ivz})-Re(k_{ihz})+i\left(3Im(k_{ivz})+Im(k_{ihz})\right)\right]}$$

$$\langle f_{vv}(\theta_i,\pi;\pi-\theta_i,0)f_{vh}^*(\theta_i,\pi;\pi-\theta_i,0)\rangle \qquad (4.3.162)$$

$$\langle S_{hh,back}^{(vol)} S_{vh,back}^{(vol)*} \rangle$$

$$= n_0 \langle f_{hh}(\theta_i, \pi; \pi - \theta_i, 0) f_{vh}^*(\theta_i, \pi; \pi - \theta_i, 0) \rangle \int d\bar{r}' \, e^{-i[(\bar{k}_{h,back} - \bar{K}_{ih}) - (\bar{k}_{v,back}^* - \bar{K}_{ih}^*)] \cdot \bar{r}'}$$

$$= n_0 \langle f_{hh}(\theta_i, \pi; \pi - \theta_i, 0) f_{vh}^*(\theta_i, \pi; \pi - \theta_i, 0) \rangle \int d\bar{r}' \, e^{-i\left[-Re(k_{ivz}) + Re(k_{ihz}) + i\left(Im(k_{ivz}) + 3Im(k_{ihz})\right)\right] z'}$$

$$= n_0 \langle f_{hh}(\theta_i, \pi; \pi - \theta_i, 0) f_{vh}^*(\theta_i, \pi; \pi - \theta_i, 0) \rangle A \int_{-d}^{0} dz' e^{-i\left[-Re(k_{ivz}) + Re(k_{ihz}) + i\left(Im(k_{ivz}) + 3Im(k_{ihz})\right)\right] z'}$$

$$= n_0 A \frac{1 - e^{i\left[-Re(k_{ivz}) + Re(k_{ihz}) + i\left(Im(k_{ivz}) + 3Im(k_{ihz})\right)\right] d}}{-i\left[-Re(k_{ivz}) + Re(k_{ihz}) + i\left(Im(k_{ivz}) + 3Im(k_{ihz})\right)\right]} \langle f_{hh}(\theta_i, \pi; \pi - \theta_i, 0) f_{vh}^*(\theta_i, \pi; \pi - \theta_i, 0) \rangle \quad (4.3.163)$$

$$\langle S_{vh,back}^{(vol)} S_{vh,back}^{(vol)*} \rangle$$

$$= n_0 \langle f_{vh}(\theta_i, \pi; \pi - \theta_i, 0) f_{vh}^*(\theta_i, \pi; \pi - \theta_i, 0) \rangle \int d\bar{r}' \, e^{-i[(\bar{k}_{v,back} - \bar{K}_{ih}) - (\bar{k}_{v,back}^* - \bar{K}_{ih}^*)] \cdot \bar{r}'}$$

$$= n_0 \langle f_{vh}(\theta_i, \pi; \pi - \theta_i, 0) f_{vh}^*(\theta_i, \pi; \pi - \theta_i, 0) \rangle \int d\bar{r}' \, e^{-i\left[2i\left(Im(k_{ivz}) + Im(k_{ihz})\right)\right] z'}$$

$$= n_0 \langle f_{vh}(\theta_i, \pi; \pi - \theta_i, 0) f_{vh}^*(\theta_i, \pi; \pi - \theta_i, 0) \rangle A \int_{-d}^{0} dz' e^{-i\left[2i\left(Im(k_{ivz}) + Im(k_{ihz})\right)\right] z'}$$

$$= n_0 A \frac{1 - e^{-2\left(Im(k_{ivz}) + Im(k_{ihz})\right) d}}{2\left(Im(k_{ivz}) + Im(k_{ihz})\right)} \langle f_{vh}(\theta_i, \pi; \pi - \theta_i, 0) f_{vh}^*(\theta_i, \pi; \pi - \theta_i, 0) \rangle \quad (4.3164)$$

4.3.2 Volume scattering followed by reflection : Double Bounce 1st kind [DB1]

Next, the scattered field from volume scattering followed by surface reflection is considered.

$$\bar{E}_{sj}^{(DB1)}(\bar{r}) = \int d\bar{r}' \, \bar{\bar{G}}_{01}^{(R)}(\bar{r}, \bar{r}') \int d\bar{r}'' \left\langle \bar{r}' \middle| \bar{\bar{T}}_j \middle| \bar{r}'' \right\rangle \langle \bar{r}'' | \bar{E}_{inc} \rangle \quad (4.3.165)$$

From (4.2.45)

$\bar{\bar{G}}_{01}^{(R)}(\bar{r},\bar{r}')$

$$= \frac{e^{ikr}}{4\pi r}\left[\hat{e}(k_z)R^{TE}e^{2ik_{hz}d}\hat{e}(-k_z)e^{ik_{hz}z'} + \hat{h}(k_z)R^{TM}e^{2ik_{vz}d}\hat{h}(-k_z)e^{ik_{vz}z'}\right]e^{-ik_x x'-ik_y y'}$$

$$= \frac{e^{ikr}}{4\pi r}\left[\hat{e}(k_z)R^{TE}e^{2ik_{hz}d}\hat{e}(-k_z)e^{-i\bar{K}_h\cdot\bar{r}'} + \hat{h}(k_z)R^{TM}e^{2ik_{vz}d}\hat{h}(-k_z)e^{-i\bar{K}_v\cdot\bar{r}'}\right] \qquad (4.3.166)$$

Then

$\bar{E}_{sj}^{(DB1)}(\bar{r})$

$$= \frac{e^{ikr}}{4\pi r}\int d\bar{r}'\left[\hat{e}(k_z)R^{TE}e^{2ik_{hz}d}\hat{e}(-k_z)e^{-i\bar{K}_h\cdot\bar{r}'} + \hat{h}(k_z)R^{TM}e^{2ik_{vz}d}\hat{h}(-k_z)e^{-i\bar{K}_v\cdot\bar{r}'}\right]$$

$$\int d\bar{r}''\left\langle\bar{r}'\middle|\bar{\bar{T}}_j\middle|\bar{r}''\right\rangle\langle\bar{r}''|\bar{E}_{inc}\rangle \qquad (4.3.167)$$

$$\langle\bar{r}''|\bar{E}_{inc}\rangle = \bar{E}_{inc}(\bar{r}'') = E_{vi}\hat{v}(\pi-\theta_i,\phi_i)e^{i\bar{K}_{iv}\cdot\bar{r}''} + E_{hi}\hat{h}(\pi-\theta_i,\phi_i)e^{i\bar{K}_{ih}\cdot\bar{r}''} \qquad (4.3.168)$$

$$\left\langle\bar{r}'\middle|\bar{\bar{T}}_j\middle|\bar{r}''\right\rangle = \int\frac{d\bar{p}}{(2\pi)^3}\int\frac{d\bar{p}'}{(2\pi)^3}e^{i\bar{p}\cdot\bar{r}'-i\bar{p}'\cdot\bar{r}''}e^{-i(\bar{p}-\bar{p}')\cdot\bar{r}_j}\bar{\bar{T}}_p(\bar{p},\bar{p}') \qquad (4.3.169)$$

$\bar{E}_{sj}^{(DB1)}(\bar{r})$

$$= \frac{e^{ikr}}{4\pi r}\int d\bar{r}'\left[\hat{e}(k_z)R^{TE}e^{2ik_{hz}d}\hat{e}(-k_z)e^{-i\bar{K}_h\cdot\bar{r}'} + \hat{h}(k_z)R^{TM}e^{2ik_{vz}d}\hat{h}(-k_z)e^{-i\bar{K}_v\cdot\bar{r}'}\right]\cdot$$

$$\int d\bar{r}''\int\frac{d\bar{p}}{(2\pi)^3}\int\frac{d\bar{p}'}{(2\pi)^3}e^{i\bar{p}\cdot\bar{r}'-i\bar{p}'\cdot\bar{r}''}e^{-i(\bar{p}-\bar{p}')\cdot\bar{r}_j}\bar{\bar{T}}_p(\bar{p},\bar{p}')$$

$$\cdot\left[E_{vi}\hat{v}(\pi-\theta_i,\phi_i)e^{i\bar{K}_{iv}\cdot\bar{r}''} + E_{hi}\hat{h}(\pi-\theta_i,\phi_i)e^{i\bar{K}_{ih}\cdot\bar{r}''}\right] \qquad (4.3.170)$$

$$\int d\bar{r}'\,e^{i\bar{p}\cdot\bar{r}'}e^{-i\bar{K}_h\cdot\bar{r}'} = (2\pi)^3\delta(\bar{K}_h-\bar{p}) \qquad (4.3.171)$$

$$\int d\bar{r}'\,e^{i\bar{p}\cdot\bar{r}'}e^{-i\bar{K}_v\cdot\bar{r}'} = (2\pi)^3\delta(\bar{K}_v-\bar{p}) \qquad (4.3.172)$$

$$\int d\bar{r}''\,e^{-i\bar{p}'\cdot\bar{r}''}e^{i\bar{K}_{iv}\cdot\bar{r}''} = (2\pi)^3\delta(\bar{p}'-\bar{K}_{iv}) \qquad (4.3.173)$$

$$\int d\bar{r}''\,e^{-i\bar{p}'\cdot\bar{r}''}e^{i\bar{K}_{ih}\cdot\bar{r}''} = (2\pi)^3\delta(\bar{p}'-\bar{K}_{ih}) \qquad (4.3.174)$$

Then

$$\bar{E}_{sj}^{(DB1)}(\bar{r})$$

$$= \frac{e^{ikr}}{4\pi r} \int d\bar{p} \left[\hat{e}(k_z) R^{TE} e^{2ik_{hz}d} \hat{e}(-k_z) \delta(\bar{K}_h - \bar{p}) + \hat{h}(k_z) R^{TM} e^{2ik_{vz}d} \hat{h}(-k_z) \delta(\bar{K}_v - \bar{p}) \right] \cdot$$

$$\int d\bar{p}' \, e^{-i(\bar{p}-\bar{p}')\cdot\bar{r}_j} \bar{\bar{T}}_p(\bar{p}, \bar{p}') \cdot \left[E_{vi} \hat{v}(\pi - \theta_i, \phi_i) \delta(\bar{p}' - \bar{K}_{iv}) + E_{hi} \hat{h}(\pi - \theta_i, \phi_i) \delta(\bar{p}' - \bar{K}_{ih}) \right]$$

$$= \frac{e^{ikr}}{4\pi r} \hat{e}(k_z) R^{TE} e^{2ik_{hz}d} \hat{e}(-k_z) e^{-i(\bar{K}_h - \bar{K}_{iv})\cdot\bar{r}_j} \cdot \bar{\bar{T}}_p(\bar{K}_h, \bar{K}_{iv}') \cdot E_{vi} \hat{v}(\pi - \theta_i, \phi_i)$$

$$+ \frac{e^{ikr}}{4\pi r} \hat{e}(k_z) R^{TE} e^{2ik_{hz}d} \hat{e}(-k_z) e^{-i(\bar{K}_h - \bar{K}_{ih})\cdot\bar{r}_j} \cdot \bar{\bar{T}}_p(\bar{K}_h, \bar{K}_{ih}) \cdot E_{hi} \hat{h}(\pi - \theta_i, \phi_i)$$

$$+ \frac{e^{ikr}}{4\pi r} \hat{h}(k_z) R^{TM} e^{2ik_{vz}d} \hat{h}(-k_z) e^{-i(\bar{K}_v - \bar{K}_{iv})\cdot\bar{r}_j} \cdot \bar{\bar{T}}_p(\bar{K}_v, \bar{K}_{iv}) \cdot E_{vi} \hat{v}(\pi - \theta_i, \phi_i)$$

$$+ \frac{e^{ikr}}{4\pi r} \hat{h}(k_z) R^{TM} e^{2ik_{vz}d} \hat{h}(-k_z) e^{-i(\bar{K}_v - \bar{K}_{ih})\cdot\bar{r}_j} \cdot \bar{\bar{T}}_p(\bar{K}_v, \bar{K}_{ih}) \cdot E_{hi} \hat{h}(\pi - \theta_i, \phi_i) \quad (4.3.175)$$

For the polarization vectors

$$\hat{e}(k_z) = \hat{x} \sin\phi_s - \hat{y} \cos\phi_s = -\hat{h}(\theta_s, \phi_s) = -\hat{h}(\pi - \theta_s, \phi_s) \quad (4.3.176)$$

$$\hat{e}(-k_z) = \hat{x} \sin\phi_s - \hat{y} \cos\phi_s = -\hat{h}(\theta_s, \phi_s) = -\hat{h}(\pi - \theta_s, \phi_s) \quad (4.3.177)$$

$$\hat{h}(k_z) = -\cos\theta_s \, (\hat{x} \cos\phi_s + \hat{y} \sin\phi_s) + \sin\theta_s \, \hat{z} = -\hat{v}(\theta_s, \phi_s) \quad (4.3.178)$$

$$\hat{h}(-k_z) = \cos\theta_s \, (\hat{x} \cos\phi_s + \hat{y} \sin\phi_s) + \sin\theta_s \, \hat{z} = -\hat{v}(\pi - \theta_s, \phi_s) \quad (4.3.179)$$

Then

$$\hat{v}(\theta_s, \phi_s) = \cos\theta_s \, (\hat{x} \cos\phi_s + \hat{y} \sin\phi_s) - \sin\theta_s \, \hat{z} \quad (4.3.180)$$

$$\hat{h}(\theta_s, \phi_s) = -\hat{x} \sin\phi_s + \hat{y} \cos\phi_s \quad (4.3.181)$$

$$\bar{E}_{sj}^{(DB1)}(\bar{r})$$

$$= \frac{e^{ikr}}{4\pi r} \hat{h}(\theta_s, \phi_s) R^{TE} e^{2ik_{hz}d} \hat{h}(\pi - \theta_s, \phi_s) e^{-i(\bar{K}_h - \bar{K}_{iv})\cdot\bar{r}_j} \cdot \bar{\bar{T}}_p(\bar{K}_h, \bar{K}_{iv}') \cdot E_{vi} \hat{v}(\pi - \theta_i, \phi_i)$$

$$+ \frac{e^{ikr}}{4\pi r} \hat{h}(\theta_s, \phi_s) R^{TE} e^{2ik_{hz}d} \hat{h}(\pi - \theta_s, \phi_s) e^{-i(\bar{K}_h - \bar{K}_{ih})\cdot\bar{r}_j} \cdot \bar{\bar{T}}_p(\bar{K}_h, \bar{K}_{ih}) \cdot E_{hi} \hat{h}(\pi - \theta_i, \phi_i)$$

$$+ \frac{e^{ikr}}{4\pi r} \hat{v}(\theta_s, \phi_s) \, R^{TM} e^{2ik_{vz}d} \hat{v}(\pi - \theta_s, \phi_s) e^{-i(\bar{K}_v - \bar{K}_{iv})\cdot\bar{r}_j} \cdot \bar{\bar{T}}_p(\bar{K}_v, \bar{K}_{iv}) \cdot E_{vi} \hat{v}(\pi - \theta_i, \phi_i)$$

$$+\frac{e^{ikr}}{4\pi r}\hat{v}(\theta_s,\phi_s)\,R^{TM}e^{2ik_{vz}d}\hat{v}(\pi-\theta_s,\phi_s)e^{-i(\bar{K}_v-\bar{K}_{ih})\cdot\bar{r}_j}\cdot\bar{\bar{T}}_p(\bar{K}_v,\bar{K}_{ih})\cdot E_{hi}\hat{h}(\pi-\theta_i,\phi_i) \quad (4.3.182)$$

Then we transform T matrix to scattering amplitude for both incident and scattering wave going downwards.

$$f_{vv}(\pi-\theta_s,\phi_s;\pi-\theta_i,\phi_i)$$

$$=\frac{1}{4\pi}\hat{v}(\pi-\theta_s,\phi_s)\cdot\bar{\bar{T}}_p\left(k\hat{k}_s(\pi-\theta_s,\phi_s),k\hat{k}_i(\pi-\theta_i,\phi_i)\right)\cdot\hat{v}(\pi-\theta_i,\phi_i) \quad (4.3.183)$$

$$f_{hv}(\pi-\theta_s,\phi_s;\pi-\theta_i,\phi_i)$$

$$=\frac{1}{4\pi}\hat{h}(\pi-\theta_s,\phi_s)\cdot\bar{\bar{T}}_p\left(k\hat{k}_s(\pi-\theta_s,\phi_s),k\hat{k}_i(\pi-\theta_i,\phi_i)\right)\cdot\hat{v}(\pi-\theta_i,\phi_i) \quad (4.3.184)$$

$$f_{hh}(\pi-\theta_s,\phi_s;\pi-\theta_i,\phi_i)$$

$$=\frac{1}{4\pi}\hat{h}(\pi-\theta_s,\phi_s)\cdot\bar{\bar{T}}_p\left(k\hat{k}_s(\pi-\theta_s,\phi_s),k\hat{k}_i(\pi-\theta_i,\phi_i)\right)\cdot\hat{h}(\pi-\theta_i,\phi_i) \quad (4.3.185)$$

$$f_{vh}(\pi-\theta_s,\phi_s;\pi-\theta_i,\phi_i)$$

$$=\frac{1}{4\pi}\hat{v}(\pi-\theta_s,\phi_s)\cdot\bar{\bar{T}}_p\left(k\hat{k}_s(\pi-\theta_s,\phi_s),k\hat{k}_i(\pi-\theta_i,\phi_i)\right)\cdot\hat{h}(\pi-\theta_i,\phi_i) \quad (4.3.186)$$

Then

$$\bar{E}_{sj}^{(DB1)}(\bar{r})$$

$$=\frac{e^{ikr}}{r}\,\hat{h}(\theta_s,\phi_s)R^{TE}e^{2ik_{hz}d}e^{-i(\bar{K}_h-\bar{K}_{iv})\cdot\bar{r}_j}f_{hv}(\pi-\theta_s,\phi_s;\pi-\theta_i,\phi_i)E_{vi}$$

$$+\frac{e^{ikr}}{r}\hat{h}(\theta_s,\phi_s)R^{TE}e^{2ik_{hz}d}e^{-i(\bar{K}_h-\bar{K}_{ih})\cdot\bar{r}_j}f_{hh}(\pi-\theta_s,\phi_s;\pi-\theta_i,\phi_i)E_{hi}$$

$$+\frac{e^{ikr}}{r}\hat{v}(\theta_s,\phi_s)\,R^{TM}e^{2ik_{vz}d}e^{-i(\bar{K}_v-\bar{K}_{iv})\cdot\bar{r}_j}f_{vv}(\pi-\theta_s,\phi_s;\pi-\theta_i,\phi_i)E_{vi}$$

$$+\frac{e^{ikr}}{r}\hat{v}(\theta_s,\phi_s)\,R^{TM}e^{2ik_{vz}d}e^{-i(\bar{K}_v-\bar{K}_{ih})\cdot\bar{r}_j}f_{vh}(\pi-\theta_s,\phi_s;\pi-\theta_i,\phi_i)E_{hi} \quad (4.3.187)$$

The scattered field from all scatterers is

$$\bar{E}_s^{(DB1)}(\bar{r})$$

$$= \sum_{j=1}^{N} \frac{e^{ikr}}{r}\, \hat{h}(\theta_s, \phi_s) R^{TE} e^{2ik_{hz}d} e^{-i(\bar{K}_h - \bar{K}_{iv})\cdot \bar{r}_j} f_{hv}(\pi - \theta_s, \phi_s; \pi - \theta_i, \phi_i) E_{vi}$$

$$+ \sum_{j=1}^{N} \frac{e^{ikr}}{r} \hat{h}(\theta_s, \phi_s) R^{TE} e^{2ik_{hz}d} e^{-i(\bar{K}_h - \bar{K}_{ih})\cdot \bar{r}_j} f_{hh}(\pi - \theta_s, \phi_s; \pi - \theta_i, \phi_i) E_{hi}$$

$$+ \sum_{j=1}^{N} \frac{e^{ikr}}{r} \hat{v}(\theta_s, \phi_s)\, R^{TM} e^{2ik_{vz}d} e^{-i(\bar{K}_v - \bar{K}_{iv})\cdot \bar{r}_j} f_{vv}(\pi - \theta_s, \phi_s; \pi - \theta_i, \phi_i) E_{vi}$$

$$+ \sum_{j=1}^{N} \frac{e^{ikr}}{r} \hat{v}(\theta_s, \phi_s)\, R^{TM} e^{2ik_{vz}d} e^{-i(\bar{K}_v - \bar{K}_{ih})\cdot \bar{r}_j} f_{vh}(\pi - \theta_s, \phi_s; \pi - \theta_i, \phi_i) E_{hi} \qquad (4.3.188)$$

Write it in terms of scattering matrix elements.

$$\bar{E}_s^{(DB1)}(\bar{r}) = \frac{e^{ikr}}{r}\, \hat{h}(\theta_s, \phi_s) S_{hv}^{(DB1)} E_{vi} + \frac{e^{ikr}}{r} \hat{h}(\theta_s, \phi_s) S_{hh}^{(DB1)} E_{hi} + \frac{e^{ikr}}{r} \hat{v}(\theta_s, \phi_s) S_{vv}^{(DB1)} E_{vi}$$

$$+ \frac{e^{ikr}}{r} \hat{v}(\theta_s, \phi_s) S_{vh}^{(DB1)} E_{hi} \qquad (4.3.189)$$

$$S_{vv}^{(DB1)} = \sum_{j=1}^{N} R^{TM} e^{2ik_{vz}d} e^{-i(\bar{K}_v - \bar{K}_{iv})\cdot \bar{r}_j} f_{vv}(\pi - \theta_s, \phi_s; \pi - \theta_i, \phi_i) \qquad (4.3.190)$$

$$S_{hv}^{(DB1)} = \sum_{j=1}^{N} R^{TE} e^{2ik_{hz}d} e^{-i(\bar{K}_h - \bar{K}_{iv})\cdot \bar{r}_j} f_{hv}(\pi - \theta_s, \phi_s; \pi - \theta_i, \phi_i) \qquad (4.3.191)$$

$$S_{hh}^{(DB1)} = \sum_{j=1}^{N} R^{TE} e^{2ik_{hz}d} e^{-i(\bar{K}_h - \bar{K}_{ih})\cdot \bar{r}_j} f_{hh}(\pi - \theta_s, \phi_s; \pi - \theta_i, \phi_i) \qquad (4.3.192)$$

$$S_{vh}^{(DB1)} = \sum_{j=1}^{N} R^{TM} e^{2ik_{vz}d} e^{-i(\bar{K}_v - \bar{K}_{ih})\cdot \bar{r}_j} f_{vh}(\pi - \theta_s, \phi_s; \pi - \theta_i, \phi_i) \qquad (4.3.193)$$

Note that $S_{hv}^{(DB1)} \neq S_{vh}^{(DB1)}$. This is different from volume scattering, however the reciprocity relation will be addressed later while considering both volume-surface and surface-volume interactions. Next consider the correlation. Again the correlation between scatterers is ignored and it assumes independent scattering

$$S_{vv}^{(DB1)}S_{hh}^{(DB1)*} = \sum_{j=1}^{N} R^{TM}e^{2ik_{vz}d}e^{-i(\bar{K}_v-\bar{K}_{iv})\cdot\bar{r}_j}f_{vv,j}(\pi-\theta_s,\phi_s;\pi-\theta_i,\phi_i)$$

$$\sum_{p=1}^{N} R^{TE^*}e^{-2ik_{hz}^*d}e^{i(\bar{K}_h^*-\bar{K}_{ih}^*)\cdot\bar{r}_p}f_{hh,p}^*(\pi-\theta_s,\phi_s;\pi-\theta_i,\phi_i)$$

$$= \sum_{j=1}^{N} R^{TM}e^{2ik_{vz}d}e^{-i(\bar{K}_v-\bar{K}_{iv})\cdot\bar{r}_j}f_{vv,j}(\pi-\theta_s,\phi_s;\pi-\theta_i,\phi_i)$$

$$R^{TE^*}e^{-2ik_{hz}^*d}e^{i(\bar{K}_h^*-\bar{K}_{ih}^*)\cdot\bar{r}_j}f_{hh,j}^*(\pi-\theta_s,\phi_s;\pi-\theta_i,\phi_i) \quad (4.3.194)$$

Similar to volume scattering, we take ensemble average.

$$\langle S_{vv}^{(DB1)}S_{hh}^{(DB1)*}\rangle = \sum_{j=1}^{N} R^{TM}e^{2ik_{vz}d}R^{TE^*}e^{-2ik_{hz}^*d}\langle e^{-i(\bar{K}_v-\bar{K}_{iv})\cdot\bar{r}_j}e^{i(\bar{K}_h^*-\bar{K}_{ih}^*)\cdot\bar{r}_j}\rangle$$

$$\langle f_{vv,j}(\pi-\theta_s,\phi_s;\pi-\theta_i,\phi_i)f_{hh,j}^*(\pi-\theta_s,\phi_s;\pi-\theta_i,\phi_i)\rangle$$

$$= n_0R^{TM}e^{2ik_{vz}d}R^{TE^*}e^{-2ik_{hz}^*d}\int d\bar{r}'e^{-i[(\bar{K}_v-\bar{K}_{iv})-(\bar{K}_h^*-\bar{K}_{ih}^*)]\cdot\bar{r}'}$$

$$\langle f_{vv}(\pi-\theta_s,\phi_s;\pi-\theta_i,\phi_i)f_{hh}^*(\pi-\theta_s,\phi_s;\pi-\theta_i,\phi_i)\rangle \quad (4.3.195)$$

n_0 is volume density. The involved propagation vectors are

$$\bar{K}_v = k\sin\theta_s\cos\phi_s\,\hat{x} + k\sin\theta_s\sin\phi_s\,\hat{y} - \sqrt{k_v^2 - k^2\sin^2\theta_s}\,\hat{z}$$

$$= k\sin\theta_s\cos\phi_s\,\hat{x} + k\sin\theta_s\sin\phi_s\,\hat{y} - (Re(k_{vz}) + iIm(k_{vz}))\hat{z} \quad (4.3.196)$$

$$\bar{K}_h = k\sin\theta_s\cos\phi_s\,\hat{x} + k\sin\theta_s\sin\phi_s\,\hat{y} - (Re(k_{hz}) + iIm(k_{hz}))\hat{z} \quad (4.3.197)$$

$$\bar{K}_{iv} = k\sin\theta_i\cos\phi_i\,\hat{x} + k\sin\theta_i\sin\phi_i\,\hat{y} - (Re(k_{ivz}) + iIm(k_{ivz}))\hat{z} \quad (4.3.198)$$

$$\bar{K}_{ih} = k\sin\theta_i\cos\phi_i\,\hat{x} + k\sin\theta_i\sin\phi_i\,\hat{y} - (Re(k_{ihz}) + iIm(k_{ihz}))\hat{z} \quad (4.3.199)$$

Consider propagation vectors in the backscattering direction. $\theta_s = \theta_i$, $\phi_i = 0$, and $\phi_s = \pi$

$$\bar{K}_v = -k\sin\theta_i\,\hat{x} - (Re(k_{ivz}) + iIm(k_{ivz}))\hat{z} \quad (4.3.200)$$

$$\bar{K}_h = -k\sin\theta_i\,\hat{x} - (Re(k_{ihz}) + iIm(k_{ihz}))\hat{z} \quad (4.3.201)$$

$$\bar{K}_{iv} = k\sin\theta_i\,\hat{x} - (Re(k_{ivz}) + iIm(k_{ivz}))\hat{z} \quad (4.3.202)$$

$$\bar{K}_{ih} = k\sin\theta_i\,\hat{x} - (Re(k_{ihz}) + iIm(k_{ihz}))\hat{z} \quad (4.3.203)$$

Those combinations will be used in deriving correlation for the coherence matrix are

$$\overline{K}_v - \overline{K}_{iv} = -2k \sin\theta_i \, \hat{x} \tag{4.3.204}$$

$$\overline{K}_h - \overline{K}_{ih} = -2k \sin\theta_i \, \hat{x} \tag{4.3.205}$$

$$\overline{K}_v - \overline{K}_{ih} = -2k \sin\theta_i \, \hat{x} - (Re(k_{ivz}) - Re(k_{ihz}) + i(Im(k_{ivz}) - Im(k_{ihz})))\hat{z} \tag{4.3.206}$$

$$\overline{K}_h - \overline{K}_{iv} = -2k \sin\theta_i \, \hat{x} - \left(Re(k_{ihz}) - Re(k_{ivz}) + i(Im(k_{ihz}) - Im(k_{ivz}))\right)\hat{z} \tag{4.3.207}$$

$$\overline{K}_h^* - \overline{K}_{iv}^* = -2k \sin\theta_i \, \hat{x} - \left(Re(k_{ihz}) - Re(k_{ivz}) - i(Im(k_{ihz}) - Im(k_{ivz}))\right)\hat{z} \tag{4.3.208}$$

Then the essential subtractions are

$$(\overline{K}_v - \overline{K}_{iv}) - (\overline{K}_h^* - \overline{K}_{ih}^*) = (-2k \sin\theta_i \, \hat{x}) - (-2k \sin\theta_i \, \hat{x}) = \overline{0} \tag{4.3.209}$$

$$(\overline{K}_v - \overline{K}_{iv}) - (\overline{K}_v^* - \overline{K}_{iv}^*) = (-2k \sin\theta_i \, \hat{x}) - (-2k \sin\theta_i \, \hat{x}) = \overline{0} \tag{4.3.210}$$

$$(\overline{K}_h - \overline{K}_{ih}) - (\overline{K}_h^* - \overline{K}_{ih}^*) = (-2k \sin\theta_i \, \hat{x}) - (-2k \sin\theta_i \, \hat{x}) = \overline{0} \tag{4.3.211}$$

$$\begin{aligned}(\overline{K}_v - \overline{K}_{iv}) - (\overline{K}_v^* - \overline{K}_{ih}^*) \\ = (-2k \sin\theta_i \, \hat{x}) - \left(-2k \sin\theta_i \, \hat{x} - \left(Re(k_{ivz}) - Re(k_{ihz}) - i\left(Im(k_{ivz}) - Im(k_{ihz})\right)\right)\hat{z}\right) \\ = \left(Re(k_{ivz}) - Re(k_{ihz}) - i\left(Im(k_{ivz}) - Im(k_{ihz})\right)\right)\hat{z}\end{aligned} \tag{4.3.212}$$

$$\begin{aligned}(\overline{K}_v - \overline{K}_{iv}) - (\overline{K}_h^* - \overline{K}_{iv}^*) \\ = -2k \sin\theta_i \, \hat{x} - (-2k \sin\theta_i \, \hat{x} - \left(Re(k_{ihz}) - Re(k_{ivz}) - i(Im(k_{ihz}) - Im(k_{ivz}))\right)\hat{z}) \\ = \left(Re(k_{ihz}) - Re(k_{ivz}) - i(Im(k_{ihz}) - Im(k_{ivz}))\right)\hat{z}\end{aligned} \tag{4.3.213}$$

$$\begin{aligned}(\overline{K}_h - \overline{K}_{ih}) - (\overline{K}_h^* - \overline{K}_{iv}^*) \\ = -2k \sin\theta_i \, \hat{x} - (-2k \sin\theta_i \, \hat{x} - \left(Re(k_{ihz}) - Re(k_{ivz}) - i(Im(k_{ihz}) - Im(k_{ivz}))\right)\hat{z}) \\ = \left(Re(k_{ihz}) - Re(k_{ivz}) - i(Im(k_{ihz}) - Im(k_{ivz}))\right)\hat{z}\end{aligned} \tag{4.3.214}$$

$$\begin{aligned}(\overline{K}_h - \overline{K}_{ih}) - (\overline{K}_v^* - \overline{K}_{ih}^*) \\ = (-2k \sin\theta_i \, \hat{x}) - \left(-2k \sin\theta_i \, \hat{x} - \left(Re(k_{ivz}) - Re(k_{ihz}) - i\left(Im(k_{ivz}) - Im(k_{ihz})\right)\right)\hat{z}\right) \\ = \left(Re(k_{ivz}) - Re(k_{ihz}) - i\left(Im(k_{ivz}) - Im(k_{ihz})\right)\right)\hat{z}\end{aligned} \tag{4.3.215}$$

$$(\overline{K}_v - \overline{K}_{ih}) - (\overline{K}_v^* - \overline{K}_{ih}^*)$$

$$= \left(-2k\sin\theta_i\,\hat{x} - \left(Re(k_{ivz}) - Re(k_{ihz}) + i\left(Im(k_{ivz}) - Im(k_{ihz})\right)\right)\hat{z}\right)$$
$$- \left(-2k\sin\theta_i\,\hat{x} - \left(Re(k_{ivz}) - Re(k_{ihz}) - i\left(Im(k_{ivz}) - Im(k_{ihz})\right)\right)\hat{z}\right)$$
$$= -2i\left(Im(k_{ivz}) - Im(k_{ihz})\right)\hat{z} \quad (4.3.216)$$

$$(\bar{K}_v - \bar{K}_{ih}) - (\bar{K}_h^* - \bar{K}_{iv}^*)$$
$$= -2k\sin\theta_i\,\hat{x} - \left(Re(k_{ivz}) - Re(k_{ihz}) + i\left(Im(k_{ivz}) - Im(k_{ihz})\right)\right)\hat{z} - (-2k\sin\theta_i\,\hat{x}$$
$$- \left(Re(k_{ihz}) - Re(k_{ivz}) - i(Im(k_{ihz}) - Im(k_{ivz}))\right)\hat{z})$$
$$= 2\left(Re(k_{ihz}) - Re(k_{ivz})\right)\hat{z} \quad (4.3.217)$$

$$(\bar{K}_h - \bar{K}_{iv}) - (\bar{K}_h^* - \bar{K}_{iv}^*)$$
$$= -2k\sin\theta_i\,\hat{x} - \left(Re(k_{ihz}) - Re(k_{ivz}) + i\left(Im(k_{ihz}) - Im(k_{ivz})\right)\right)\hat{z} - (-2k\sin\theta_i\,\hat{x}$$
$$- \left(Re(k_{ihz}) - Re(k_{ivz}) - i(Im(k_{ihz}) - Im(k_{ivz}))\right)\hat{z})$$
$$= -2i\left(Im(k_{ihz}) - Im(k_{ivz})\right)\hat{z} \quad (4.3.218)$$

$$(\bar{K}_h - \bar{K}_{iv}) - (\bar{K}_v^* - \bar{K}_{ih}^*)$$
$$= -2k\sin\theta_i\,\hat{x} - \left(Re(k_{ihz}) - Re(k_{ivz}) + i\left(Im(k_{ihz}) - Im(k_{ivz})\right)\right)\hat{z}$$
$$- \left(-2k\sin\theta_i\,\hat{x} - \left(Re(k_{ivz}) - Re(k_{ihz}) - i\left(Im(k_{ivz}) - Im(k_{ihz})\right)\right)\hat{z}\right)$$
$$= -2\left(Re(k_{ihz}) - Re(k_{ivz})\right)\hat{z} \quad (4.3.219)$$

In the backscattering direction.

$$\bar{k}_v = -k\sin\theta_i\,\hat{x} + \sqrt{k_v^2 - k^2\sin^2\theta_i}\,\hat{z}$$
$$= -k\sin\theta_i\,\hat{x} + (Re(k_{ivz}) + iIm(k_{ivz}))\hat{z} \quad (4.3.220)$$

$$\bar{k}_h = -k\sin\theta_i\,\hat{x} + (Re(k_{ihz}) + iIm(k_{ihz}))\hat{z} \quad (4.3.221)$$

For the essential terms to compute the coherence matrix. Note that here more terms are included for the later analysis in the reciprocity section.

$$\langle S_{vv,back}^{(DB1)} S_{hh,back}^{(DB1)*}\rangle = n_0 R_{vi} e^{2ik_{ivz}d} {R_{hi}}^* e^{-2ik_{ihz}^* d} \int d\bar{r}' e^{-i[(\bar{K}_v - \bar{K}_{iv}) - (\bar{K}_h^* - \bar{K}_{ih}^*)]\cdot\bar{r}'}$$
$$\langle f_{vv}(\pi - \theta_i, \pi; \pi - \theta_i, 0) f_{hh}^*(\pi - \theta_i, \pi; \pi - \theta_i, 0)\rangle$$

$$= n_0 R_{vi} e^{2ik_{ivz}d} {R_{hi}}^* e^{-2ik^*_{ihz}d} \int d\bar{r}' \langle f_{vv}(\pi-\theta_i,\pi;\pi-\theta_i,0) f^*_{hh}(\pi-\theta_i,\pi;\pi-\theta_i,0)\rangle$$

$$= n_0 A d R_{vi} e^{2ik_{ivz}d} {R_{hi}}^* e^{-2ik^*_{ihz}d} \langle f_{vv}(\pi-\theta_i,\pi;\pi-\theta_i,0) f^*_{hh}(\pi-\theta_i,\pi;\pi-\theta_i,0)\rangle \quad (4.3.222)$$

$$\langle S^{(DB1)}_{vv,back} S^{(DB1)*}_{vv,back}\rangle = n_0 R_{vi} e^{2ik_{ivz}d} {R_{vi}}^* e^{-2ik^*_{ivz}d} \int d\bar{r}' e^{-i[(\bar{K}_v-\bar{K}_{iv})-(\bar{K}^*_v-\bar{K}^*_{iv})]\cdot\bar{r}'}$$

$$\langle f_{vv}(\pi-\theta_i,\pi;\pi-\theta_i,0) f^*_{vv}(\pi-\theta_i,\pi;\pi-\theta_i,0)\rangle$$

$$= n_0 R_{vi} e^{2ik_{ivz}d} {R_{vi}}^* e^{-2ik^*_{ivz}d} \int d\bar{r}' \langle f_{vv}(\pi-\theta_i,\pi;\pi-\theta_i,0) f^*_{vv}(\pi-\theta_i,\pi;\pi-\theta_i,0)\rangle$$

$$= n_0 A d R_{vi} e^{2ik_{ivz}d} {R_{vi}}^* e^{-2ik^*_{ivz}d} \langle f_{vv}(\pi-\theta_i,\pi;\pi-\theta_i,0) f^*_{vv}(\pi-\theta_i,\pi;\pi-\theta_i,0)\rangle \quad (4.3.223)$$

$$\langle S^{(DB1)}_{hh,back} S^{(DB1)*}_{hh,back}\rangle = n_0 R_{hi} e^{2ik_{ihz}d} {R_{hi}}^* e^{-2ik^*_{ihz}d} \int d\bar{r}' e^{-i[(\bar{K}_h-\bar{K}_{ih})-(\bar{K}^*_h-\bar{K}^*_{ih})]\cdot\bar{r}'}$$

$$\langle f_{hh}(\pi-\theta_i,\pi;\pi-\theta_i,0) f^*_{hh}(\pi-\theta_i,\pi;\pi-\theta_i,0)\rangle$$

$$= n_0 R_{hi} e^{2ik_{ihz}d} {R_{hi}}^* e^{-2ik^*_{ihz}d} \int d\bar{r}' \langle f_{hh}(\pi-\theta_i,\pi;\pi-\theta_i,0) f^*_{hh}(\pi-\theta_i,\pi;\pi-\theta_i,0)\rangle$$

$$= n_0 A d R_{hi} e^{2ik_{ihz}d} {R_{hi}}^* e^{-2ik^*_{ihz}d} \langle f_{hh}(\pi-\theta_i,\pi;\pi-\theta_i,0) f^*_{hh}(\pi-\theta_i,\pi;\pi-\theta_i,0)\rangle \quad (4.3.224)$$

$$\langle S^{(DB1)}_{vv,back} S^{(DB1)*}_{vh,back}\rangle = n_0 R_{vi} e^{2ik_{ivz}d} {R_{vi}}^* e^{-2ik^*_{ivz}d} \int d\bar{r}' e^{-i[(\bar{K}_v-\bar{K}_{iv})-(\bar{K}^*_v-\bar{K}^*_{ih})]\cdot\bar{r}'}$$

$$\langle f_{vv}(\pi-\theta_i,\pi;\pi-\theta_i,0) f^*_{vh}(\pi-\theta_i,\pi;\pi-\theta_i,0)\rangle$$

$$= n_0 R_{vi} e^{2ik_{ivz}d} {R_{vi}}^* e^{-2ik^*_{ivz}d} A \int_{-d}^{0} dz' e^{-i\left[Re(k_{ivz})-Re(k_{ihz})-i\left(Im(k_{ivz})-Im(k_{ihz})\right)\right]z'}$$

$$\langle f_{vv}(\pi-\theta_i,\pi;\pi-\theta_i,0) f^*_{vh}(\pi-\theta_i,\pi;\pi-\theta_i,0)\rangle$$

$$= n_0 A \frac{1-e^{i\left[Re(k_{ivz})-Re(k_{ihz})-i\left(Im(k_{ivz})-Im(k_{ihz})\right)\right]d}}{-i\left[Re(k_{ivz})-Re(k_{ihz})-i\left(Im(k_{ivz})-Im(k_{ihz})\right)\right]} R_{vi} e^{2ik_{ivz}d} {R_{vi}}^* e^{-2ik^*_{ivz}d}$$

$$\langle f_{vv}(\pi-\theta_i,\pi;\pi-\theta_i,0) f^*_{vh}(\pi-\theta_i,\pi;\pi-\theta_i,0)\rangle \quad (4.3.225)$$

$$\langle S_{hh,back}^{(DB1)} S_{vh,back}^{(DB1)*} \rangle = n_0 R_{hi} e^{2ik_{ihz}d} {R_{vi}}^* e^{-2ik_{ivz}^* d} \int d\bar{r}' e^{-i[(\bar{K}_h - \bar{K}_{ih}) - (\bar{K}_v^* - \bar{K}_{ih}^*)]\cdot \bar{r}'}$$

$$\langle f_{hh}(\pi - \theta_i, \pi; \pi - \theta_i, 0) f_{vh}^*(\pi - \theta_i, \pi; \pi - \theta_i, 0) \rangle$$

$$= n_0 R_{hi} e^{2ik_{ihz}d} {R_{vi}}^* e^{-2ik_{ivz}^* d} A \int_{-d}^{0} dz' e^{-i[Re(k_{ivz}) - Re(k_{ihz}) - i\left(Im(k_{ivz}) - Im(k_{ihz})\right)]z'}$$

$$\langle f_{hh}(\pi - \theta_i, \pi; \pi - \theta_i, 0) f_{vh}^*(\pi - \theta_i, \pi; \pi - \theta_i, 0) \rangle$$

$$= n_0 A \frac{1 - e^{i[Re(k_{ivz}) - Re(k_{ihz}) - i\left(Im(k_{ivz}) - Im(k_{ihz})\right)]d}}{-i[Re(k_{ivz}) - Re(k_{ihz}) - i\left(Im(k_{ivz}) - Im(k_{ihz})\right)]} R_{hi} e^{2ik_{ihz}d} {R_{vi}}^* e^{-2ik_{ivz}^* d}$$

$$\langle f_{hh}(\pi - \theta_i, \pi; \pi - \theta_i, 0) f_{vh}^*(\pi - \theta_i, \pi; \pi - \theta_i, 0) \rangle \quad (4.3.226)$$

$$\langle S_{vh,back}^{(DB1)} S_{vh,back}^{(DB1)*} \rangle = n_0 R_{vi} e^{2ik_{ivz}d} {R_{vi}}^* e^{-2ik_{ivz}^* d} \int d\bar{r}' e^{-i[(\bar{K}_v - \bar{K}_{ih}) - (\bar{K}_v^* - \bar{K}_{ih}^*)]\cdot \bar{r}'}$$

$$\langle f_{vh}(\pi - \theta_i, \pi; \pi - \theta_i, 0) f_{vh}^*(\pi - \theta_i, \pi; \pi - \theta_i, 0) \rangle$$

$$= n_0 R_{vi} e^{2ik_{ivz}d} {R_{vi}}^* e^{-2ik_{ivz}^* d} A \int_{-d}^{0} dz' e^{-2\left(Im(k_{ivz}) - Im(k_{ihz})\right)z'}$$

$$\langle f_{vh}(\pi - \theta_i, \pi; \pi - \theta_i, 0) f_{vh}^*(\pi - \theta_i, \pi; \pi - \theta_i, 0) \rangle$$

$$= n_0 A \frac{1 - e^{2\left(Im(k_{ivz}) - Im(k_{ihz})\right)d}}{-2\left(Im(k_{ivz}) - Im(k_{ihz})\right)} R_{vi} e^{2ik_{ivz}d} {R_{vi}}^* e^{-2ik_{ivz}^* d}$$

$$\langle f_{vh}(\pi - \theta_i, \pi; \pi - \theta_i, 0) f_{vh}^*(\pi - \theta_i, \pi; \pi - \theta_i, 0) \rangle \quad (4.3.227)$$

$$\langle S_{vv,back}^{(DB1)} S_{hv,back}^{(DB1)*} \rangle = n_0 R_{vi} e^{2ik_{ivz}d} R_{hi}^* e^{-2ik_{ihz}^* d} \int d\bar{r}' e^{-i\left[(\bar{K}_v - \bar{K}_{iv}) - (\bar{K}_h^* - \bar{K}_{iv}^*)\right]\cdot \bar{r}'}$$

$$\langle f_{vv}(\pi - \theta_i, \pi; \pi - \theta_i, 0) f_{hv}^*(\pi - \theta_i, \pi; \pi - \theta_i, 0) \rangle$$

$$= n_0 R_{vi} e^{2ik_{ivz}d} R_{hi}^* e^{-2ik_{ihz}^* d} A \int_{-d}^{0} dz' e^{-i[Re(k_{ihz}) - Re(k_{ivz}) - i(Im(k_{ihz}) - Im(k_{ivz}))]z'}$$

$$\langle f_{vv}(\pi - \theta_i, \pi; \pi - \theta_i, 0) f_{hv}^*(\pi - \theta_i, \pi; \pi - \theta_i, 0) \rangle$$

$$= n_0 A R_{vi} e^{2ik_{ivz}d} R_{hi}^* e^{-2ik_{ihz}^* d} \frac{1 - e^{i[Re(k_{ihz}) - Re(k_{ivz}) - i(Im(k_{ihz}) - Im(k_{ivz}))]d}}{-i[Re(k_{ihz}) - Re(k_{ivz}) - i(Im(k_{ihz}) - Im(k_{ivz}))]}$$

$$\langle f_{vv}(\pi-\theta_i,\pi;\pi-\theta_i,0)f_{hv}^*(\pi-\theta_i,\pi;\pi-\theta_i,0)\rangle \quad (4.3.228)$$

$$\langle S_{hh,back}^{(DB1)} S_{hv,back}^{(DB1)*}\rangle = n_0 R_{hi} e^{2ik_{ihz}d} R_{hi}^* e^{-2ik_{ihz}^* d} \int d\bar{r}' e^{-i[(\bar{K}_h-\bar{K}_{ih})-(\bar{K}_h^*-\bar{K}_{iv}^*)]\cdot\bar{r}'}$$

$$\langle f_{hh}(\pi-\theta_i,\pi;\pi-\theta_i,0)f_{hv}^*(\pi-\theta_i,\pi;\pi-\theta_i,0)\rangle$$

$$= n_0 R_{hi} e^{2ik_{ihz}d} R_{hi}^* e^{-2ik_{ihz}^* d} A \int_{-d}^{0} dz' e^{-i[Re(k_{ihz})-Re(k_{ivz})-i(Im(k_{ihz})-Im(k_{ivz}))]z'}$$

$$\langle f_{hh}(\pi-\theta_i,\pi;\pi-\theta_i,0)f_{hv}^*(\pi-\theta_i,\pi;\pi-\theta_i,0)\rangle$$

$$= n_0 A R_{hi} e^{2ik_{ihz}d} R_{hi}^* e^{-2ik_{ihz}^* d} \frac{1-e^{i[Re(k_{ihz})-Re(k_{ivz})-i(Im(k_{ihz})-Im(k_{ivz}))]d}}{-i[Re(k_{ihz})-Re(k_{ivz})-i(Im(k_{ihz})-Im(k_{ivz}))]}$$

$$\langle f_{hh}(\pi-\theta_i,\pi;\pi-\theta_i,0)f_{hv}^*(\pi-\theta_i,\pi;\pi-\theta_i,0)\rangle \quad (4.3.229)$$

$$\langle S_{vh,back}^{(DB1)} S_{hv,back}^{(DB1)*}\rangle = n_0 R_{vi} e^{2ik_{ivz}d} R_{hi}^* e^{-2ik_{ihz}^* d} \int d\bar{r}' e^{-i[(\bar{K}_v-\bar{K}_{ih})-(\bar{K}_h^*-\bar{K}_{iv}^*)]\cdot\bar{r}'}$$

$$\langle f_{vh}(\pi-\theta_i,\pi;\pi-\theta_i,0)f_{hv}^*(\pi-\theta_i,\pi;\pi-\theta_i,0)\rangle$$

$$= n_0 R_{vi} e^{2ik_{ivz}d} R_{hi}^* e^{-2ik_{ihz}^* d} A \int_{-d}^{0} dz' e^{-i\left[2\left(Re(k_{ihz})-Re(k_{ivz})\right)\right]z'}$$

$$\langle f_{vh}(\pi-\theta_i,\pi;\pi-\theta_i,0)f_{hv}^*(\pi-\theta_i,\pi;\pi-\theta_i,0)\rangle$$

$$= n_0 A R_{vi} e^{2ik_{ivz}d} R_{hi}^* e^{-2ik_{ihz}^* d} \frac{1-e^{i\left[2\left(Re(k_{ihz})-Re(k_{ivz})\right)\right]d}}{-i\left[2\left(Re(k_{ihz})-Re(k_{ivz})\right)\right]}$$

$$\langle f_{vh}(\pi-\theta_i,\pi;\pi-\theta_i,0)f_{hv}^*(\pi-\theta_i,\pi;\pi-\theta_i,0)\rangle \quad (4.3.230)$$

$$\langle S_{hv,back}^{(DB1)} S_{hv,back}^{(DB1)*}\rangle = n_0 R_{hi} e^{2ik_{ihz}d} R_{hi}^* e^{-2ik_{ihz}^* d} \int d\bar{r}' e^{-i[(\bar{K}_h-\bar{K}_{iv})-(\bar{K}_h^*-\bar{K}_{iv}^*)]\cdot\bar{r}'}$$

$$\langle f_{hv}(\pi-\theta_i,\pi;\pi-\theta_i,0)f_{hv}^*(\pi-\theta_i,\pi;\pi-\theta_i,0)\rangle$$

$$= n_0 R_{hi} e^{2ik_{ihz}d} R_{hi}^* e^{-2ik_{ihz}^* d} A \int_{-d}^{0} dz' e^{-i\left[-2i\left(Im(k_{ihz})-Im(k_{ivz})\right)\right]z'}$$

$$\langle f_{hv}(\pi-\theta_i,\pi;\pi-\theta_i,0)f_{hv}^*(\pi-\theta_i,\pi;\pi-\theta_i,0)\rangle$$

$$= n_0 A R_{hi} e^{2ik_{ihz}d} R_{hi}^* e^{-2ik_{ihz}^* d} \frac{1 - e^{[2(Im(k_{ihz}) - Im(k_{ivz}))]d}}{-[2(Im(k_{ihz}) - Im(k_{ivz}))]}$$

$$\langle f_{hv}(\pi - \theta_i, \pi; \pi - \theta_i, 0) f_{hv}^*(\pi - \theta_i, \pi; \pi - \theta_i, 0) \rangle \quad (4.3.231)$$

4.3.3 Reflection before volume scattering : Double Bounce 2nd kind [DB2]

Similar derivation is performed here, but considering reflection before volume scattering.

$$\bar{E}_{sj}^{(DB2)}(\bar{r}) = \int d\bar{r}' \, \bar{\bar{G}}_{01}^{(0)}(\bar{r}, \bar{r}') \int d\bar{r}'' \, \langle \bar{r}' | \bar{\bar{T}}_j | \bar{r}'' \rangle \langle \bar{r}'' | \bar{E}_{ref} \rangle$$

$$= \frac{e^{ikr}}{4\pi r} \int d\bar{r}' \, \left[\hat{e}(k_z) \hat{e}(k_z) e^{-i\bar{k}_h \cdot \bar{r}'} + \hat{h}(k_z) \hat{h}(k_z) e^{-i\bar{k}_v \cdot \bar{r}'} \right]$$

$$\int d\bar{r}'' \, \langle \bar{r}' | \bar{\bar{T}}_j | \bar{r}'' \rangle \langle \bar{r}'' | \bar{E}_{ref} \rangle \quad (4.3.232)$$

$$\langle \bar{r}'' | \bar{E}_{ref} \rangle = \bar{E}_{ref}(\bar{r}'')$$

$$= E_{vi} R_{vi} e^{2ik_{izv}d} \hat{v}(\theta_i, \phi_i) e^{i\bar{k}_{iv} \cdot \bar{r}''} + E_{hi} R_{hi} e^{2ik_{izh}d} \hat{h}(\theta_i, \phi_i) e^{i\bar{k}_{ih} \cdot \bar{r}''} \quad (4.3.233)$$

$$\langle \bar{r}' | \bar{\bar{T}}_j | \bar{r}'' \rangle = \int \frac{d\bar{p}}{(2\pi)^3} \int \frac{d\bar{p}'}{(2\pi)^3} e^{i\bar{p} \cdot \bar{r}' - i\bar{p}' \cdot \bar{r}''} e^{-i(\bar{p} - \bar{p}') \cdot \bar{r}_j} \bar{\bar{T}}_p(\bar{p}, \bar{p}') \quad (4.3.234)$$

Then

$$\bar{E}_{sj}^{(DB2)}(\bar{r}) = \frac{e^{ikr}}{4\pi r} \int d\bar{r}' \, \left[\hat{e}(k_z) \hat{e}(k_z) e^{-i\bar{k}_h \cdot \bar{r}'} + \hat{h}(k_z) \hat{h}(k_z) e^{-i\bar{k}_v \cdot \bar{r}'} \right] \cdot$$

$$\int d\bar{r}'' \int \frac{d\bar{p}}{(2\pi)^3} \int \frac{d\bar{p}'}{(2\pi)^3} e^{i\bar{p} \cdot \bar{r}' - i\bar{p}' \cdot \bar{r}''} e^{-i(\bar{p} - \bar{p}') \cdot \bar{r}_j} \bar{\bar{T}}_p(\bar{p}, \bar{p}') \cdot$$

$$\left[E_{vi} R_{vi} e^{2ik_{izv}d} \hat{v}(\theta_i, \phi_i) e^{i\bar{k}_{iv} \cdot \bar{r}''} + E_{hi} R_{hi} e^{2ik_{izh}d} \hat{h}(\theta_i, \phi_i) e^{i\bar{k}_{ih} \cdot \bar{r}''} \right] \quad (4.3.235)$$

$$\int d\bar{r}' \, e^{i\bar{p} \cdot \bar{r}'} e^{-i\bar{k}_h \cdot \bar{r}'} = (2\pi)^3 \delta(\bar{k}_h - \bar{p}) \quad (4.3.236)$$

$$\int d\bar{r}' \, e^{i\bar{p} \cdot \bar{r}'} e^{-i\bar{k}_v \cdot \bar{r}'} = (2\pi)^3 \delta(\bar{k}_v - \bar{p}) \quad (4.3.237)$$

$$\int d\bar{r}'' \, e^{-i\bar{p}' \cdot \bar{r}''} e^{i\bar{k}_{iv} \cdot \bar{r}''} = (2\pi)^3 \delta(\bar{p}' - \bar{k}_{iv}) \quad (4.3.238)$$

$$\int d\bar{r}'' \, e^{-i\bar{p}'\cdot\bar{r}''} e^{i\bar{k}_{ih}\cdot\bar{r}''} = (2\pi)^3 \delta\left(\bar{p}' - \bar{k}_{ih}\right) \tag{4.3.239}$$

$$\bar{E}_{sj}^{(DB2)}(\bar{r}) = \frac{e^{ikr}}{4\pi r} \int \frac{d\bar{p}}{(2\pi)^3}$$

$$\int \frac{d\bar{p}'}{(2\pi)^3} \left[\hat{e}(k_z)\hat{e}(k_z)(2\pi)^3\delta\left(\bar{k}_h - \bar{p}\right) + \hat{h}(k_z)\hat{h}(k_z)(2\pi)^3\delta\left(\bar{k}_v - \bar{p}\right)\right] \cdot e^{-i\left(\bar{p}-\bar{p}'\right)\cdot\bar{r}_j} \bar{\bar{T}}_p(\bar{p},\bar{p}') \cdot$$

$$\left[E_{vi}R_{vi}e^{2ik_{izv}d}\hat{v}(\theta_i,\phi_i)(2\pi)^3\delta\left(\bar{p}' - \bar{k}_{iv}\right) + E_{hi}R_{hi}e^{2ik_{izh}d}\hat{h}(\theta_i,\phi_i)(2\pi)^3\delta\left(\bar{p}' - \bar{k}_{ih}\right)\right]$$

$$= \frac{e^{ikr}}{4\pi r} \int d\bar{p} \int d\bar{p}' \left[\hat{e}(k_z)\hat{e}(k_z)\delta\left(\bar{k}_h - \bar{p}\right) + \hat{h}(k_z)\hat{h}(k_z)\delta\left(\bar{k}_v - \bar{p}\right)\right] \cdot e^{-i\left(\bar{p}-\bar{p}'\right)\cdot\bar{r}_j} \bar{\bar{T}}_p(\bar{p},\bar{p}') \cdot$$

$$\left[E_{vi}R_{vi}e^{2ik_{izv}d}\hat{v}(\theta_i,\phi_i)\delta\left(\bar{p}' - \bar{k}_{iv}\right) + E_{hi}R_{hi}e^{2ik_{izh}d}\hat{h}(\theta_i,\phi_i)\delta\left(\bar{p}' - \bar{k}_{ih}\right)\right]$$

$$= \frac{e^{ikr}}{4\pi r}\, \hat{e}(k_z)\hat{e}(k_z)e^{-i\left(\bar{k}_h - \bar{k}_{iv}\right)\cdot\bar{r}_j} \cdot \bar{\bar{T}}_p\left(\bar{k}_h, \bar{k}_{iv}\right) \cdot E_{vi}R_{vi}e^{2ik_{izv}d}\hat{v}(\theta_i,\phi_i)$$

$$+ \frac{e^{ikr}}{4\pi r}\hat{e}(k_z)\hat{e}(k_z)e^{-i\left(\bar{k}_h - \bar{k}_{ih}\right)\cdot\bar{r}_j} \cdot \bar{\bar{T}}_p\left(\bar{k}_h, \bar{k}_{ih}\right) \cdot E_{hi}R_{hi}e^{2ik_{izh}d}\hat{h}(\theta_i,\phi_i)$$

$$+ \frac{e^{ikr}}{4\pi r}\hat{h}(k_z)\hat{h}(k_z)e^{-i\left(\bar{k}_v - \bar{k}_{iv}\right)\cdot\bar{r}_j} \cdot \bar{\bar{T}}_p\left(\bar{k}_v, \bar{k}_{iv}\right) \cdot E_{vi}R_{vi}e^{2ik_{izv}d}\hat{v}(\theta_i,\phi_i)$$

$$+ \frac{e^{ikr}}{4\pi r}\hat{h}(k_z)\hat{h}(k_z)e^{-i\left(\bar{k}_v - \bar{k}_{ih}\right)\cdot\bar{r}_j} \cdot \bar{\bar{T}}_p\left(\bar{k}_v, \bar{k}_{ih}\right) \cdot E_{hi}R_{hi}e^{2ik_{izh}d}\hat{h}(\theta_i,\phi_i) \tag{4.3.240}$$

Then

$$\hat{e}(k_z) = \hat{x}\sin\phi_s - \hat{y}\cos\phi_s = -\hat{h}(\theta_s,\phi_s) \tag{4.3.241}$$

$$\hat{h}(k_z) = -\cos\theta_s\left(\hat{x}\cos\phi_s + \hat{y}\sin\phi_s\right) + \sin\theta_s\,\hat{z} = -\hat{v}(\theta_s,\phi_s) \tag{4.3.242}$$

$\bar{E}_{sj}^{(DB2)}(\bar{r})$

$$= \frac{e^{ikr}}{4\pi r}\, \hat{h}(\theta_s,\phi_s)\hat{h}(\theta_s,\phi_s)e^{-i\left(\bar{k}_h - \bar{k}_{iv}\right)\cdot\bar{r}_j} \cdot \bar{\bar{T}}_p\left(\bar{k}_h, \bar{k}_{iv}\right) \cdot E_{vi}R_{vi}e^{2ik_{izv}d}\hat{v}(\theta_i,\phi_i)$$

$$+ \frac{e^{ikr}}{4\pi r}\hat{h}(\theta_s,\phi_s)\hat{h}(\theta_s,\phi_s)e^{-i\left(\bar{k}_h - \bar{k}_{ih}\right)\cdot\bar{r}_j} \cdot \bar{\bar{T}}_p\left(\bar{k}_h, \bar{k}_{ih}\right) \cdot E_{hi}R_{hi}e^{2ik_{izh}d}\hat{h}(\theta_i,\phi_i)$$

$$+ \frac{e^{ikr}}{4\pi r}\hat{v}(\theta_s,\phi_s)\hat{v}(\theta_s,\phi_s)e^{-i\left(\bar{k}_v - \bar{k}_{iv}\right)\cdot\bar{r}_j} \cdot \bar{\bar{T}}_p\left(\bar{k}_v, \bar{k}_{iv}\right) \cdot E_{vi}R_{vi}e^{2ik_{izv}d}\hat{v}(\theta_i,\phi_i)$$

$$+\frac{e^{ikr}}{4\pi r}\hat{v}(\theta_s,\phi_s)\hat{v}(\theta_s,\phi_s)e^{-i(\bar{k}_v-\bar{k}_{ih})\cdot\bar{r}_j}\cdot\bar{\bar{T}}_p\left(\bar{k}_v,\bar{k}_{ih}\right)\cdot E_{hi}R_{hi}e^{2ik_{izh}d}\hat{h}(\theta_i,\phi_i)$$

$$=\frac{e^{ikr}}{4\pi r}\hat{h}(\theta_s,\phi_s)\hat{h}(\theta_s,\phi_s)e^{-i(\bar{k}_h-\bar{k}_{iv})\cdot\bar{r}_j}\cdot\bar{\bar{T}}_p\left(k\hat{k}_s(\theta_s,\phi_s),k\hat{k}_i(\theta_i,\phi_i)\right)$$
$$\cdot E_{vi}R_{vi}e^{2ik_{izv}d}\hat{v}(\theta_i,\phi_i)$$
$$+\frac{e^{ikr}}{4\pi r}\hat{h}(\theta_s,\phi_s)\hat{h}(\theta_s,\phi_s)e^{-i(\bar{k}_h-\bar{k}_{ih})\cdot\bar{r}_j}\cdot\bar{\bar{T}}_p\left(k\hat{k}_s(\theta_s,\phi_s),k\hat{k}_i(\theta_i,\phi_i)\right)$$
$$\cdot E_{hi}R_{hi}e^{2ik_{izh}d}\hat{h}(\theta_i,\phi_i)$$
$$+\frac{e^{ikr}}{4\pi r}\hat{v}(\theta_s,\phi_s)\hat{v}(\theta_s,\phi_s)e^{-i(\bar{k}_v-\bar{k}_{iv})\cdot\bar{r}_j}\cdot\bar{\bar{T}}_p\left(k\hat{k}_s(\theta_s,\phi_s),k\hat{k}_i(\theta_i,\phi_i)\right)$$
$$\cdot E_{vi}R_{vi}e^{2ik_{izv}d}\hat{v}(\theta_i,\phi_i)$$
$$+\frac{e^{ikr}}{4\pi r}\hat{v}(\theta_s,\phi_s)\hat{v}(\theta_s,\phi_s)$$
$$e^{-i(\bar{k}_v-\bar{k}_{ih})\cdot\bar{r}_j}\cdot\bar{\bar{T}}_p\left(k\hat{k}_s(\theta_s,\phi_s),k\hat{k}_i(\theta_i,\phi_i)\right)\cdot E_{hi}R_{hi}e^{2ik_{izh}d}\hat{h}(\theta_i,\phi_i) \quad (4.3.243)$$

Then transfrom T matrix to scattering amplitude for both incident and scattering wave going upwards.

$$f_{vv}(\theta_s,\phi_s;\theta_i,\phi_i)=\frac{1}{4\pi}\hat{v}(\theta_s,\phi_s)\cdot\bar{\bar{T}}_p\left(k\hat{k}_s(\theta_s,\phi_s),k\hat{k}_i(\theta_i,\phi_i)\right)\cdot\hat{v}(\theta_i,\phi_i) \quad (4.3.244)$$

$$f_{hv}(\theta_s,\phi_s;\theta_i,\phi_i)=\frac{1}{4\pi}\hat{h}(\theta_s,\phi_s)\cdot\bar{\bar{T}}_p\left(k\hat{k}_s(\theta_s,\phi_s),k\hat{k}_i(\theta_i,\phi_i)\right)\cdot\hat{v}(\theta_i,\phi_i) \quad (4.3.245)$$

$$f_{hh}(\theta_s,\phi_s;\theta_i,\phi_i)=\frac{1}{4\pi}\hat{h}(\theta_s,\phi_s)\cdot\bar{\bar{T}}_p\left(k\hat{k}_s(\theta_s,\phi_s),k\hat{k}_i(\theta_i,\phi_i)\right)\cdot\hat{h}(\theta_i,\phi_i) \quad (4.3.246)$$

$$f_{vh}(\theta_s,\phi_s;\theta_i,\phi_i)=\frac{1}{4\pi}\hat{v}(\theta_s,\phi_s)\cdot\bar{\bar{T}}_p\left(k\hat{k}_s(\theta_s,\phi_s),k\hat{k}_i(\theta_i,\phi_i)\right)\cdot\hat{h}(\theta_i,\phi_i) \quad (4.3.247)$$

$$\bar{E}_{sj}^{(DB2)}(\bar{r})=\frac{e^{ikr}}{r}\hat{h}(\theta_s,\phi_s)e^{-i(\bar{k}_h-\bar{k}_{iv})\cdot\bar{r}_j}f_{hv}(\theta_s,\phi_s;\theta_i,\phi_i)E_{vi}R_{vi}e^{2ik_{izv}d}$$
$$+\frac{e^{ikr}}{r}\hat{h}(\theta_s,\phi_s)e^{-i(\bar{k}_h-\bar{k}_{ih})\cdot\bar{r}_j}f_{hh}(\theta_s,\phi_s;\theta_i,\phi_i)E_{hi}R_{hi}e^{2ik_{izh}d}$$
$$+\frac{e^{ikr}}{r}\hat{v}(\theta_s,\phi_s)e^{-i(\bar{k}_v-\bar{k}_{iv})\cdot\bar{r}_j}f_{vv}(\theta_s,\phi_s;\theta_i,\phi_i)E_{vi}R_{vi}e^{2ik_{izv}d}$$

$$+\frac{e^{ikr}}{r}\hat{v}(\theta_s,\phi_s)e^{-i(\bar{k}_v-\bar{k}_{ih})\cdot\bar{r}_j}f_{vh}(\theta_s,\phi_s;\theta_i,\phi_i)E_{hi}R_{hi}e^{2ik_{izh}d} \tag{4.3.248}$$

The scattered field from all scatterers is

$$\begin{aligned}\bar{E}_s^{(DB2)}(\bar{r}) = &\sum_{j=1}^{N}\frac{e^{ikr}}{r}\,\hat{h}(\theta_s,\phi_s)e^{-i(\bar{k}_h-\bar{k}_{iv})\cdot\bar{r}_j}f_{hv}(\theta_s,\phi_s;\theta_i,\phi_i)E_{vi}R_{vi}e^{2ik_{izv}d}\\ &+\sum_{j=1}^{N}\frac{e^{ikr}}{r}\hat{h}(\theta_s,\phi_s)e^{-i(\bar{k}_h-\bar{k}_{ih})\cdot\bar{r}_j}f_{hh}(\theta_s,\phi_s;\theta_i,\phi_i)E_{hi}R_{hi}e^{2ik_{izh}d}\\ &+\sum_{j=1}^{N}\frac{e^{ikr}}{r}\hat{v}(\theta_s,\phi_s)e^{-i(\bar{k}_v-\bar{k}_{iv})\cdot\bar{r}_j}f_{vv}(\theta_s,\phi_s;\theta_i,\phi_i)E_{vi}R_{vi}e^{2ik_{izv}d}\\ &+\sum_{j=1}^{N}\frac{e^{ikr}}{r}\hat{v}(\theta_s,\phi_s)e^{-i(\bar{k}_v-\bar{k}_{ih})\cdot\bar{r}_j}f_{vh}(\theta_s,\phi_s;\theta_i,\phi_i)E_{hi}R_{hi}e^{2ik_{izh}d}\end{aligned} \tag{4.3.249}$$

Write it in terms of scattering matrix elements.

$$\begin{aligned}\bar{E}_s^{(DB2)}(\bar{r}) = &\frac{e^{ikr}}{r}\,\hat{h}(\theta_s,\phi_s)S_{hv}^{(DB2)}E_{vi}+\frac{e^{ikr}}{r}\hat{h}(\theta_s,\phi_s)S_{hh}^{(DB2)}E_{hi}+\frac{e^{ikr}}{r}\hat{v}(\theta_s,\phi_s)S_{vv}^{(DB2)}E_{vi}\\ &+\frac{e^{ikr}}{r}\hat{v}(\theta_s,\phi_s)S_{vh}^{(DB2)}E_{hi}\end{aligned} \tag{4.3.250}$$

$$S_{vv}^{(DB2)} = \sum_{j=1}^{N} e^{-i(\bar{k}_v-\bar{k}_{iv})\cdot\bar{r}_j}f_{vv}(\theta_s,\phi_s;\theta_i,\phi_i)R_{vi}e^{2ik_{izv}d} \tag{4.3.251}$$

$$S_{hv}^{(DB2)} = \sum_{j=1}^{N} e^{-i(\bar{k}_h-\bar{k}_{iv})\cdot\bar{r}_j}f_{hv}(\theta_s,\phi_s;\theta_i,\phi_i)R_{vi}e^{2ik_{izv}d} \tag{4.3.252}$$

$$S_{hh}^{(DB2)} = \sum_{j=1}^{N} e^{-i(\bar{k}_h-\bar{k}_{ih})\cdot\bar{r}_j}f_{hh}(\theta_s,\phi_s;\theta_i,\phi_i)R_{hi}e^{2ik_{izh}d} \tag{4.3.253}$$

$$S_{vh}^{(DB2)} = \sum_{j=1}^{N} e^{-i(\bar{k}_v-\bar{k}_{ih})\cdot\bar{r}_j}f_{vh}(\theta_s,\phi_s;\theta_i,\phi_i)R_{hi}e^{2ik_{izh}d} \tag{4.3.254}$$

Similar to volume-surface interaction, note that $S_{hv}^{(DB2)} \neq S_{vh}^{(DB2)}$. Next consider the correlation. Correlation between scatterers is ignored and assume independent scattering

$$S_{vv}^{(DB2)} S_{hh}^{(DB2)*}$$

$$= \sum_{j=1}^{N} e^{-i(\bar{k}_v - \bar{k}_{iv})\cdot \bar{r}_j} f_{vv,j}(\theta_s, \phi_s; \theta_i, \phi_i) R_{vi} e^{2ik_{izv}d} \sum_{p=1}^{N} e^{i(\bar{k}_h^* - \bar{k}_{ih}^*)\cdot \bar{r}_p} f_{hh,p}^*(\theta_s, \phi_s; \theta_i, \phi_i) R_{hi}^* e^{-2ik_{izh}^* d}$$

$$= \sum_{j=1}^{N} e^{-i(\bar{k}_v - \bar{k}_{iv})\cdot \bar{r}_j} f_{vv}(\theta_s, \phi_s; \theta_i, \phi_i) R_{vi} e^{2ik_{izv}d}\, e^{i(\bar{k}_h^* - \bar{k}_{ih}^*)\cdot \bar{r}_j} f_{hh}^*(\theta_s, \phi_s; \theta_i, \phi_i) R_{hi}^* e^{-2ik_{izh}^* d} \quad (4.3.255)$$

Take the ensemble average.

$$\langle S_{vv}^{(DB2)} S_{hh}^{(DB2)*} \rangle$$

$$= \sum_{j=1}^{N} R_{vi} e^{2ik_{izv}d}\, R_{hi}^* e^{-2ik_{izh}^* d} \langle e^{-i[(\bar{k}_v - \bar{k}_{iv}) - (\bar{k}_h^* - \bar{k}_{ih}^*)]\cdot \bar{r}_j} \rangle \langle f_{vv}(\theta_s, \phi_s; \theta_i, \phi_i) f_{hh}^*(\theta_s, \phi_s; \theta_i, \phi_i) \rangle$$

$$= n_0 R_{vi} e^{2ik_{izv}d} R_{hi}^* e^{-2ik_{izh}^* d} \int d\bar{r}_j e^{-i[(\bar{k}_v - \bar{k}_{iv}) - (\bar{k}_h^* - \bar{k}_{ih}^*)]\cdot \bar{r}_j} \langle f_{vv}(\theta_s, \phi_s; \theta_i, \phi_i) f_{hh}^*(\theta_s, \phi_s; \theta_i, \phi_i) \rangle \quad (4.3.256)$$

n_0 is volume density. The involved propagation vectors are

$$\bar{k}_v = k \sin\theta_s \cos\phi_s\, \hat{x} + k \sin\theta_s \sin\phi_s\, \hat{y} + \sqrt{k_v^2 - k^2 \sin^2\theta_s}\, \hat{z}$$

$$= k \sin\theta_s \cos\phi_s\, \hat{x} + k \sin\theta_s \sin\phi_s\, \hat{y} + (Re(k_{vz}) + iIm(k_{vz}))\hat{z} \quad (4.3.257)$$

$$\bar{k}_h = k \sin\theta_s \cos\phi_s\, \hat{x} + k \sin\theta_s \sin\phi_s\, \hat{y} + (Re(k_{hz}) + iIm(k_{hz}))\hat{z} \quad (4.3.258)$$

$$\bar{k}_{iv} = k \sin\theta_i \cos\phi_i\, \hat{x} + k \sin\theta_i \sin\phi_i\, \hat{y} + (Re(k_{ivz}) + iIm(k_{ivz}))\hat{z} \quad (4.3.259)$$

$$\bar{k}_{ih} = k \sin\theta_i \cos\phi_i\, \hat{x} + k \sin\theta_i \sin\phi_i\, \hat{y} + (Re(k_{ihz}) + iIm(k_{ihz}))\hat{z} \quad (4.3.260)$$

Consider propagation vectors in the backscattering direction. $\theta_s = \theta_i$, $\phi_i = 0$, and $\phi_s = \pi$

$$\bar{k}_v = -k \sin\theta_i\, \hat{x} + (Re(k_{ivz}) + iIm(k_{ivz}))\hat{z} \quad (4.3.261)$$

$$\bar{k}_h = -k \sin\theta_i\, \hat{x} + (Re(k_{ihz}) + iIm(k_{ihz}))\hat{z} \quad (4.3.262)$$

$$\bar{k}_{iv} = k \sin\theta_i\, \hat{x} + (Re(k_{ivz}) + iIm(k_{ivz}))\hat{z} \quad (4.3.263)$$

$$\bar{k}_{ih} = k \sin\theta_i\, \hat{x} + (Re(k_{ihz}) + iIm(k_{ihz}))\hat{z} \quad (4.3.264)$$

Find the difference between propagation constants

$$\bar{k}_v - \bar{k}_{iv} = -2k \sin\theta_i\, \hat{x} \quad (4.3.265)$$

$$\bar{k}_h - \bar{k}_{ih} = -2k \sin\theta_i\, \hat{x} \quad (4.3.266)$$

$$\bar{k}_v - \bar{k}_{ih} = -2k\sin\theta_i\,\hat{x} + (Re(k_{ivz}) - Re(k_{ihz}) + i(Im(k_{ivz}) - Im(k_{ihz})))\hat{z} \quad (4.3.267)$$

$$\left(\bar{k}_v - \bar{k}_{iv}\right) - \left(\bar{k}_h^* - \bar{k}_{ih}^*\right) = (-2k\sin\theta_i\,\hat{x}) - (-2k\sin\theta_i\,\hat{x}) = \bar{0} \quad (4.3.268)$$

$$\left(\bar{k}_v - \bar{k}_{iv}\right) - \left(\bar{k}_v^* - \bar{k}_{iv}^*\right) = (-2k\sin\theta_i\,\hat{x}) - (-2k\sin\theta_i\,\hat{x}) = \bar{0} \quad (4.3.269)$$

$$\left(\bar{k}_h - \bar{k}_{ih}\right) - \left(\bar{k}_h^* - \bar{k}_{ih}^*\right) = (-2k\sin\theta_i\,\hat{x}) - (-2k\sin\theta_i\,\hat{x}) = \bar{0} \quad (4.3.270)$$

$$\begin{aligned}&\left(\bar{k}_v - \bar{k}_{iv}\right) - \left(\bar{k}_v^* - \bar{k}_{ih}^*\right)\\ &= (-2k\sin\theta_i\,\hat{x}) - (-2k\sin\theta_i\,\hat{x} + (Re(k_{ivz}) - Re(k_{ihz}) - i(Im(k_{ivz}) - Im(k_{ihz})))\hat{z})\\ &= -\left(Re(k_{ivz}) - Re(k_{ihz}) - i\left(Im(k_{ivz}) - Im(k_{ihz})\right)\right)\hat{z}\end{aligned} \quad (4.3.271)$$

$$\begin{aligned}&\left(\bar{k}_h - \bar{k}_{ih}\right) - \left(\bar{k}_v^* - \bar{k}_{ih}^*\right)\\ &= (-2k\sin\theta_i\,\hat{x}) - (-2k\sin\theta_i\,\hat{x} + (Re(k_{ivz}) - Re(k_{ihz}) - i(Im(k_{ivz}) - Im(k_{ihz})))\hat{z})\\ &= -\left(Re(k_{ivz}) - Re(k_{ihz}) - i\left(Im(k_{ivz}) - Im(k_{ihz})\right)\right)\hat{z}\end{aligned} \quad (4.3.272)$$

$$\begin{aligned}&\left(\bar{k}_v - \bar{k}_{ih}\right) - \left(\bar{k}_v^* - \bar{k}_{ih}^*\right)\\ &= (-2k\sin\theta_i\,\hat{x} + (Re(k_{ivz}) - Re(k_{ihz}) + i(Im(k_{ivz}) - Im(k_{ihz})))\hat{z})\\ &\qquad - \left(-2k\sin\theta_i\,\hat{x} + \left(Re(k_{ivz}) - Re(k_{ihz}) - i\left(Im(k_{ivz}) - Im(k_{ihz})\right)\right)\hat{z}\right)\\ &= 2i\left(Im(k_{ivz}) - Im(k_{ihz})\right)\hat{z}\end{aligned} \quad (4.3.273)$$

For the essential terms to compute the coherence matrix. Consider propagation vectors in the backscattering direction. $\theta_s = \theta_i$, $\phi_i = 0$, and $\phi_s = \pi$. Since the reciprocity is going to apply to reduce the terms for correlations, here only I only show one calculation of the correlation.

$$\begin{aligned}&\langle S_{vv,back}^{(DB2)} S_{hh,back}^{(DB2)*}\rangle\\ &= n_0 R_{vi} e^{2ik_{izv}d} R_{hi}^* e^{-2ik_{izh}^* d} \int d\bar{r}' e^{-i[(\bar{k}_v - \bar{k}_{iv}) - (\bar{k}_h^* - \bar{k}_{ih}^*)]\cdot\bar{r}'} \langle f_{vv}(\theta_i, \pi; \theta_i, 0) f_{hh}^*(\theta_i, \pi; \theta_i, 0)\rangle\\ &= n_0 R_{vi} e^{2ik_{izv}d} R_{hi}^* e^{-2ik_{izh}^* d} \int d\bar{r}' \langle f_{vv}(\theta_i, \pi; \theta_i, 0) f_{hh}^*(\theta_i, \pi; \theta_i, 0)\rangle\\ &= n_0 A d R_{vi} e^{2ik_{izv}d} R_{hi}^* e^{-2ik_{izh}^* d} \langle f_{vv}(\theta_i, \pi; \theta_i, 0) f_{hh}^*(\theta_i, \pi; \theta_i, 0)\rangle\end{aligned} \quad (4.3.274)$$

4.3.4 Reciprocity between 1st and 2nd kind of double bounce

Here we examine the reciprocity relation for double bounce scattering. Let DB to denote the double bounce scattering including both 1st and 2nd kinds.

$$\bar{E}_s^{(DB)}(\bar{r}) = \bar{E}_s^{(DB1)}(\bar{r}) + \bar{E}_s^{(B2)}(\bar{r})$$

$$= \frac{e^{ikr}}{r}\,\hat{h}(\theta_s,\phi_s)\left[S_{hv}^{(DB1)} + S_{hv}^{(DB2)}\right]E_{vi} + \frac{e^{ikr}}{r}\hat{h}(\theta_s,\phi_s)\left[S_{hh}^{(DB1)} + S_{hh}^{(DB2)}\right]E_{hi}$$

$$+\frac{e^{ikr}}{r}\hat{v}(\theta_s,\phi_s)\left[S_{vv}^{(DB1)} + S_{vv}^{(DB2)}\right]E_{vi} + \frac{e^{ikr}}{r}\hat{v}(\theta_s,\phi_s)\left[S_{vh}^{(DB1)} + S_{vh}^{(DB2)}\right]E_{hi}$$

$$= \frac{e^{ikr}}{r}\,\hat{h}(\theta_s,\phi_s)S_{hv}^{(DB)}E_{vi} + \frac{e^{ikr}}{r}\hat{h}(\theta_s,\phi_s)S_{hh}^{(DB)}E_{hi} + \frac{e^{ikr}}{r}\hat{v}(\theta_s,\phi_s)S_{vv}^{(DB)}E_{vi}$$

$$+\frac{e^{ikr}}{r}\hat{v}(\theta_s,\phi_s)S_{vh}^{(DB)}E_{hi} \tag{4.3.275}$$

$$S_{vv}^{(DB)} = S_{vv}^{(DB1)} + S_{vv}^{(DB2)}$$

$$= \sum_{j=1}^{N} R^{TM}e^{2ik_{vz}d}e^{-i(\bar{K}_v-\bar{K}_{iv})\cdot\bar{r}_j}f_{vv}(\pi-\theta_s,\phi_s;\pi-\theta_i,\phi_i)$$

$$+e^{-i(\bar{k}_v-\bar{k}_{iv})\cdot\bar{r}_j}f_{vv}(\theta_s,\phi_s;\theta_i,\phi_i)R_{vi}e^{2ik_{izv}d} \tag{4.3.276}$$

$$S_{hv}^{(DB)} = S_{hv}^{(DB1)} + S_{hv}^{(DB2)}$$

$$= \sum_{j=1}^{N} R^{TE}e^{2ik_{hz}d}e^{-i(\bar{K}_h-\bar{K}_{iv})\cdot\bar{r}_j}f_{hv}(\pi-\theta_s,\phi_s;\pi-\theta_i,\phi_i)$$

$$+e^{-i(\bar{k}_h-\bar{k}_{iv})\cdot\bar{r}_j}f_{hv}(\theta_s,\phi_s;\theta_i,\phi_i)R_{vi}e^{2ik_{izv}d} \tag{4.3.277}$$

$$S_{hh}^{(DB)} = S_{hh}^{(DB1)} + S_{hh}^{(DB2)}$$

$$= \sum_{j=1}^{N} R^{TE}e^{2ik_{hz}d}e^{-i(\bar{K}_h-\bar{K}_{ih})\cdot\bar{r}_j}f_{hh}(\pi-\theta_s,\phi_s;\pi-\theta_i,\phi_i)$$

$$+e^{-i(\bar{k}_h-\bar{k}_{ih})\cdot\bar{r}_j}f_{hh}(\theta_s,\phi_s;\theta_i,\phi_i)R_{hi}e^{2ik_{izh}d} \tag{4.3.278}$$

$$S_{vh}^{(DB)} = S_{vh}^{(DB1)} + S_{vh}^{(DB2)}$$

$$= \sum_{j=1}^{N} R^{TM} e^{2ik_{vz}d} e^{-i(\bar{K}_v - \bar{K}_{ih})\cdot\bar{r}_j} f_{vh}(\pi - \theta_s, \phi_s; \pi - \theta_i, \phi_i)$$

$$+ e^{-i(\bar{k}_v - \bar{k}_{ih})\cdot\bar{r}_j} f_{vh}(\theta_s, \phi_s; \theta_i, \phi_i) R_{hi} e^{2ik_{izh}d} \quad (4.3.279)$$

Assume the reciprocity is held for the scatterer

$$f_{vv}(\theta_s, \phi_s; \theta_i, \phi_i) = f_{vv}(\pi - \theta_i, \pi + \phi_i; \pi - \theta_s, \pi + \phi_s) \quad (4.3.280)$$

$$f_{hh}(\theta_s, \phi_s; \theta_i, \phi_i) = f_{hh}(\pi - \theta_i, \pi + \phi_i; \pi - \theta_s, \pi + \phi_s) \quad (4.3.281)$$

$$f_{vh}(\theta_s, \phi_s; \theta_i, \phi_i) = -f_{hv}(\pi - \theta_i, \pi + \phi_i; \pi - \theta_s, \pi + \phi_s) \quad (4.3.282)$$

$$f_{hv}(\theta_s, \phi_s; \theta_i, \phi_i) = -f_{vh}(\pi - \theta_i, \pi + \phi_i; \pi - \theta_s, \pi + \phi_s) \quad (4.3.283)$$

Then in the backscattering, $\theta_s = \theta_i$, $\phi_i = 0$, and $\phi_s = \pi$

$$S_{vv,back}^{(DB1)} = \sum_{j=1}^{N} R^{TM} e^{2ik_{vz}d} e^{-i(\bar{K}_v - \bar{K}_{iv})\cdot\bar{r}_j} f_{vv}(\pi - \theta_s, \phi_s; \pi - \theta_i, \phi_i)$$

$$= \sum_{j=1}^{N} R_{vi} e^{2ik_{ivz}d} e^{-i(-2k\sin\theta_i \hat{x})\cdot\bar{r}_j} f_{vv}(\pi - \theta_i, \pi; \pi - \theta_i, 0) \quad (4.3.284)$$

$$S_{vv,back}^{(DB2)} = \sum_{j=1}^{N} e^{-i(\bar{k}_v - \bar{k}_{iv})\cdot\bar{r}_j} f_{vv}(\theta_s, \phi_s; \theta_i, \phi_i) R_{vi} e^{2ik_{izv}d}$$

$$= \sum_{j=1}^{N} e^{-i(-2k\sin\theta_i \hat{x})\cdot\bar{r}_j} f_{vv}(\theta_i, \pi; \theta_i, 0) R_{vi} e^{2ik_{izv}d} \quad (4.3.285)$$

By reciprocity

$$f_{vv}(\theta_i, \pi; \theta_i, 0) = f_{vv}(\pi - \theta_i, \pi; \pi - \theta_i, 0) \quad (4.3.286)$$

We have

$$S_{vv,back}^{(DB1)} = S_{vv,back}^{(DB2)} \quad (4.3.287)$$

Similarly

$$S_{hh,back}^{(DB1)} = \sum_{j=1}^{N} R^{TE} e^{2ik_{hz}d} e^{-i(\bar{K}_h - \bar{K}_{ih})\cdot\bar{r}_j} f_{hh}(\pi - \theta_s, \phi_s; \pi - \theta_i, \phi_i)$$

$$= \sum_{j=1}^{N} R_{hi} e^{2ik_{ihz}d} e^{-i(-2k\sin\theta_i \hat{x})\cdot\bar{r}_j} f_{hh}(\pi-\theta_i, \pi; \pi-\theta_i, 0) \tag{4.3.288}$$

$$S_{hh,back}^{(DB2)} = \sum_{j=1}^{N} e^{-i(\bar{k}_h - \bar{k}_{ih})\cdot\bar{r}_j} f_{hh}(\theta_s, \phi_s; \theta_i, \phi_i) R_{hi} e^{2ik_{izh}d}$$

$$= \sum_{j=1}^{N} e^{-i(-2k\sin\theta_i \hat{x})\cdot\bar{r}_j} f_{hh}(\theta_i, \pi; \theta_i, 0) R_{hi} e^{2ik_{izh}d} \tag{4.3.289}$$

By reciprocity

$$f_{hh}(\theta_i, \pi; \theta_i, 0) = f_{hh}(\pi-\theta_i, \pi; \pi-\theta_i, 0) \tag{4.3.290}$$

We have

$$S_{hh,back}^{(DB1)} = S_{hh,back}^{(DB2)} \tag{4.3.291}$$

For cross polarization

$$S_{hv,back}^{(DB1)} = \sum_{j=1}^{N} R^{TE} e^{2ik_{hz}d} e^{-i(\bar{K}_h - \bar{K}_{iv})\cdot\bar{r}_j} f_{hv}(\pi-\theta_s, \phi_s; \pi-\theta_i, \phi_i)$$

$$= \sum_{j=1}^{N} R_{hi} e^{2ik_{ihz}d} e^{-i(-2k\sin\theta_i \hat{x} + (k_{ivz} - k_{ihz})\hat{z})\cdot\bar{r}_j} f_{hv}(\pi-\theta_i, \pi; \pi-\theta_i, 0) \tag{4.3.292}$$

$$S_{hv,back}^{(DB2)} = \sum_{j=1}^{N} e^{-i(\bar{k}_h - \bar{k}_{iv})\cdot\bar{r}_j} f_{hv}(\theta_s, \phi_s; \theta_i, \phi_i) R_{vi} e^{2ik_{izv}d}$$

$$= \sum_{j=1}^{N} e^{-i(-2k\sin\theta_i \hat{x} - (k_{ivz} - k_{ihz})\hat{z})\cdot\bar{r}_j} f_{hv}(\theta_i, \pi; \theta_i, 0) R_{vi} e^{2ik_{izv}d} \tag{4.3.293}$$

Apparently

$$S_{hv,back}^{(DB1)} \neq S_{hv,back}^{(DB2)} \tag{4.3.294}$$

$$S_{vh,back}^{(DB1)} = \sum_{j=1}^{N} R^{TM} e^{2ik_{vz}d} e^{-i(\bar{K}_v - \bar{K}_{ih})\cdot\bar{r}_j} f_{vh}(\pi-\theta_s, \phi_s; \pi-\theta_i, \phi_i)$$

$$= \sum_{j=1}^{N} R_{vi} e^{2ik_{ivz}d} e^{-i(-2k\sin\theta_i \hat{x} - (k_{ivz} - k_{ihz})\hat{z})\cdot \bar{r}_j} f_{vh}(\pi - \theta_i, \pi; \pi - \theta_i, 0) \quad (4.3.295)$$

$$S_{vh,back}^{(DB2)} = \sum_{j=1}^{N} e^{-i(\bar{k}_v - \bar{k}_{ih})\cdot \bar{r}_j} f_{vh}(\theta_s, \phi_s; \theta_i, \phi_i) R_{hi} e^{2ik_{izh}d}$$

$$= \sum_{j=1}^{N} e^{-i(-2k\sin\theta_i \hat{x} + (k_{ivz} - k_{ihz})\hat{z})\cdot \bar{r}_j} f_{vh}(\theta_i, \pi; \theta_i, 0) R_{hi} e^{2ik_{izh}d} \quad (4.3.296)$$

Also

$$S_{vh,back}^{(DB1)} \neq S_{vh,back}^{(DB2)} \quad (4.3.297)$$

However, when we cross compare vh-polarization and hv-polarization, we notice that

By reciprocity

$$f_{vh}(\theta_i, \pi; \theta_i, 0) = -f_{hv}(\pi - \theta_i, \pi; \pi - \theta_i, 0) \quad (4.3.298)$$

$$f_{hv}(\theta_i, \pi; \theta_i, 0) = -f_{vh}(\pi - \theta_i, \pi; \pi - \theta_i, 0) \quad (4.3.299)$$

Then

$$S_{vh,back}^{(DB1)} = -S_{hv,back}^{(DB2)} \quad (4.3.300)$$

$$S_{hv,back}^{(DB1)} = -S_{vh,back}^{(DB2)} \quad (4.3.301)$$

Then

$$S_{vv,back}^{(DB)} = S_{vv,back}^{(DB1)} + S_{vv,back}^{(DB2)} = 2S_{vv,back}^{(DB1)} \quad (4.3.302)$$

$$S_{hh,back}^{(DB)} = S_{hh,back}^{(DB1)} + S_{hh,back}^{(DB2)} = 2S_{hh,back}^{(DB1)} \quad (4.3.303)$$

$$S_{hv,back}^{(DB)} = S_{hv,back}^{(DB1)} + S_{hv,back}^{(DB2)} = S_{vh,back}^{(DB2)} + S_{vh,back}^{(DB1)} = S_{vh,back}^{(DB)} \quad (4.3.304)$$

Consider correlations for the coherency matrix and represent them using only 1st kind of double bounce scattering.

$$\langle S_{vv,back}^{(DB)} S_{hh,back}^{(DB)*} \rangle = \langle 2S_{vv,back}^{(DB1)} 2S_{hh,back}^{(DB1)*} \rangle = 4\langle S_{vv,back}^{(DB1)} S_{hh,back}^{(DB1)*} \rangle \quad (4.3.305)$$

$$\langle S_{vv,back}^{(DB)} S_{vv,back}^{(DB)*} \rangle = \langle 2S_{vv,back}^{(DB1)} 2S_{vv,back}^{(DB1)*} \rangle = 4\langle S_{vv,back}^{(DB1)} S_{vv,back}^{(DB1)*} \rangle \quad (4.3.306)$$

$$\langle S_{hh,back}^{(DB)} S_{hh,back}^{(DB)*} \rangle = \langle 2S_{hh,back}^{(DB1)} 2S_{hh,back}^{(DB1)*} \rangle = 4\langle S_{hh,back}^{(DB1)} S_{hh,back}^{(DB1)*} \rangle \quad (4.3.307)$$

$$\langle S_{vv,back}^{(DB)} S_{vh,back}^{(DB)*} \rangle = \langle 2S_{vv,back}^{(DB1)} \left(S_{vh,back}^{(DB1)} + S_{vh,back}^{(DB2)} \right)^* \rangle = \langle 2S_{vv,back}^{(DB1)} \left(S_{vh,back}^{(DB1)} - S_{hv,back}^{(DB1)} \right)^* \rangle$$
$$= 2\langle S_{vv,back}^{(DB1)} S_{vh,back}^{(DB1)*} \rangle - 2\langle S_{vv,back}^{(DB1)} S_{hv,back}^{(DB1)*} \rangle \quad (4.3.308)$$

$$\langle S_{hh,back}^{(DB)} S_{vh,back}^{(DB)*} \rangle = \langle 2S_{hh,back}^{(DB1)} \left(S_{vh,back}^{(DB1)} + S_{vh,back}^{(DB2)} \right)^* \rangle = \langle 2S_{hh,back}^{(DB1)} \left(S_{vh,back}^{(DB1)} - S_{hv,back}^{(DB1)} \right)^* \rangle$$
$$= 2\langle S_{hh,back}^{(DB1)} S_{vh,back}^{(DB1)*} \rangle - 2\langle S_{hh,back}^{(DB1)} S_{hv,back}^{(DB1)*} \rangle \quad (4.3.309)$$

$$\langle S_{vh,back}^{(DB)} S_{vh,back}^{(DB)*} \rangle = \langle \left(S_{vh,back}^{(DB1)} + S_{vh,back}^{(DB2)} \right) \left(S_{vh,back}^{(DB1)} + S_{vh,back}^{(DB2)} \right)^* \rangle$$
$$= \langle \left(S_{vh,back}^{(DB1)} - S_{hv,back}^{(DB1)} \right) \left(S_{vh,back}^{(DB1)} - S_{hv,back}^{(DB1)} \right)^* \rangle$$
$$= \langle S_{vh,back}^{(DB1)} S_{vh,back}^{(DB1)*} \rangle - 2Re\left(\langle S_{vh,back}^{(DB1)} S_{hv,back}^{(DB1)*} \rangle \right) + \langle S_{hv,back}^{(DB1)} S_{hv,back}^{(DB1)*} \rangle \quad (4.3.310)$$

Then the complete expression for correlations in the coherency matrix for double bounce are

$$\langle S_{vv,back}^{(DB)} S_{hh,back}^{(DB)*} \rangle$$
$$= 4n_0 A d R_{vi} e^{2ik_{ivz}d} {R_{hi}}^* e^{-2ik_{ihz}^* d} \langle f_{vv}(\pi - \theta_i, \pi; \pi - \theta_i, 0) f_{hh}^*(\pi - \theta_i, \pi; \pi - \theta_i, 0) \rangle \quad (4.3.311)$$

$$\langle S_{vv,back}^{(DB)} S_{vv,back}^{(DB)*} \rangle$$
$$= 4n_0 A d R_{vi} e^{2ik_{ivz}d} {R_{vi}}^* e^{-2ik_{ivz}^* d} \langle f_{vv}(\pi - \theta_i, \pi; \pi - \theta_i, 0) f_{vv}^*(\pi - \theta_i, \pi; \pi - \theta_i, 0) \rangle \quad (4.3.312)$$

$$\langle S_{hh,back}^{(DB)} S_{hh,back}^{(DB)*} \rangle$$
$$= 4n_0 A d R_{hi} e^{2ik_{ihz}d} {R_{hi}}^* e^{-2ik_{ihz}^* d} \langle f_{hh}(\pi - \theta_i, \pi; \pi - \theta_i, 0) f_{hh}^*(\pi - \theta_i, \pi; \pi - \theta_i, 0) \rangle \quad (4.3.313)$$

$$\langle S_{vv,back}^{(DB)} S_{vh,back}^{(DB)*} \rangle$$

$$= 2n_0 A \frac{1 - e^{i\left[Re(k_{ivz}) - Re(k_{ihz}) - i\left(Im(k_{ivz}) - Im(k_{ihz})\right)\right]d}}{-i\left[Re(k_{ivz}) - Re(k_{ihz}) - i\left(Im(k_{ivz}) - Im(k_{ihz})\right)\right]} R_{vi} e^{2ik_{ivz}d} {R_{vi}}^* e^{-2ik_{ivz}^* d}$$

$$\langle f_{vv}(\pi - \theta_i, \pi; \pi - \theta_i, 0) f_{vh}^*(\pi - \theta_i, \pi; \pi - \theta_i, 0) \rangle$$

$$-2n_0 A R_{vi} e^{2ik_{ivz}d} R_{hi}^* e^{-2ik_{ihz}^* d} \frac{1 - e^{i\left[Re(k_{ihz}) - Re(k_{ivz}) - i\left(Im(k_{ihz}) - Im(k_{ivz})\right)\right]d}}{-i\left[Re(k_{ihz}) - Re(k_{ivz}) - i\left(Im(k_{ihz}) - Im(k_{ivz})\right)\right]}$$

$$\langle f_{vv}(\pi - \theta_i, \pi; \pi - \theta_i, 0) f_{hv}^*(\pi - \theta_i, \pi; \pi - \theta_i, 0) \rangle \qquad (4.3.314)$$

$$\langle S_{hh,back}^{(DB)} S_{vh,back}^{(DB)*} \rangle$$

$$= 2n_0 A \frac{1 - e^{i[Re(k_{ivz}) - Re(k_{ihz}) - i\left(Im(k_{ivz}) - Im(k_{ihz})\right)]d}}{-i[Re(k_{ivz}) - Re(k_{ihz}) - i\left(Im(k_{ivz}) - Im(k_{ihz})\right)]} R_{hi} e^{2ik_{ihz}d} {R_{vi}}^* e^{-2ik_{ivz}^* d}$$

$$\langle f_{hh}(\pi - \theta_i, \pi; \pi - \theta_i, 0) f_{vh}^*(\pi - \theta_i, \pi; \pi - \theta_i, 0) \rangle$$

$$-2n_0 A R_{hi} e^{2ik_{ihz}d} R_{hi}^* e^{-2ik_{ihz}^* d} \frac{1 - e^{i\left[Re(k_{ihz}) - Re(k_{ivz}) - i\left(Im(k_{ihz}) - Im(k_{ivz})\right)\right]d}}{-i\left[Re(k_{ihz}) - Re(k_{ivz}) - i\left(Im(k_{ihz}) - Im(k_{ivz})\right)\right]}$$

$$\langle f_{hh}(\pi - \theta_i, \pi; \pi - \theta_i, 0) f_{hv}^*(\pi - \theta_i, \pi; \pi - \theta_i, 0) \rangle \qquad (4.3.315)$$

$$\langle S_{vh,back}^{(DB)} S_{vh,back}^{(DB)*} \rangle$$

$$= n_0 A \frac{1 - e^{2\left(Im(k_{ivz}) - Im(k_{ihz})\right)d}}{-2\left(Im(k_{ivz}) - Im(k_{ihz})\right)} R_{vi} e^{2ik_{ivz}d} {R_{vi}}^* e^{-2ik_{ivz}^* d}$$

$$\langle f_{vh}(\pi - \theta_i, \pi; \pi - \theta_i, 0) f_{vh}^*(\pi - \theta_i, \pi; \pi - \theta_i, 0) \rangle$$

$$-2n_0 A Re\{R_{vi} e^{2ik_{ivz}d} R_{hi}^* e^{-2ik_{ihz}^* d} \frac{1 - e^{i\left[2\left(Re(k_{ihz}) - Re(k_{ivz})\right)\right]d}}{-i\left[2\left(Re(k_{ihz}) - Re(k_{ivz})\right)\right]}$$

$$\langle f_{vh}(\pi - \theta_i, \pi; \pi - \theta_i, 0) f_{hv}^*(\pi - \theta_i, \pi; \pi - \theta_i, 0) \rangle\}$$

$$+n_0 A R_{hi} e^{2ik_{ihz}d} R_{hi}^* e^{-2ik_{ihz}^* d} \frac{1 - e^{\left[2\left(Im(k_{ihz}) - Im(k_{ivz})\right)\right]d}}{-\left[2\left(Im(k_{ihz}) - Im(k_{ivz})\right)\right]}$$

$$\langle f_{hv}(\pi-\theta_i,\pi;\pi-\theta_i,0)f_{hv}^{*}(\pi-\theta_i,\pi;\pi-\theta_i,0)\rangle \tag{4.3.316}$$

4.3.5 Surface Scattering [Surf]

For rough surface scattering, this term comes from 3D Numerical Solutions of Maxwell Equation. We also use T-matrix to represent the scattered wave. Firs we consider the scattered wave in free space.

$$\bar{E}_s^{(R)} = \bar{\bar{G}}_0 \bar{\bar{T}}^{(R)} \bar{E}_{inc} \tag{4.3.317}$$

$\bar{\bar{T}}^{(R)}$ is the rough surface scattering T-matrix. For free space propagation

$$\bar{\bar{G}}_0(\bar{r},\bar{r}') = \begin{cases} \dfrac{i}{8\pi^2}\displaystyle\int_{-\infty}^{\infty} dk_x \int_{-\infty}^{\infty} dk_y \left[\hat{e}(k_z)\hat{e}(k_z)e^{ik_{hz}(z-z')} + \hat{h}(k_z)\hat{h}(k_z)e^{ik_{vz}(z-z')}\right] \dfrac{e^{ik_x(x-x')+ik_y(y-y')}}{k_z} & for\ z > z' \\ \dfrac{i}{8\pi^2}\displaystyle\int_{-\infty}^{\infty} dk_x \int_{-\infty}^{\infty} dk_y \left[\hat{e}(-k_z)\hat{e}(-k_z)e^{-ik_{hz}(z-z')} + \hat{h}(-k_z)\hat{h}(-k_z)e^{-ik_{vz}(z-z')}\right] \dfrac{e^{ik_x(x-x')+ik_y(y-y')}}{k_z} & for\ z < z' \end{cases} \tag{4.3.318}$$

Let the rough surface be treated as a scatterer at the origin, then $\bar{r}'$ and $\bar{r}''$ are points on the rough surface.

$$\bar{E}_s^{(R)}(\bar{r}) = \int d\bar{r}'\, \bar{\bar{G}}_0(\bar{r},\bar{r}') \int d\bar{r}''\, \langle \bar{r}' | \bar{\bar{T}}^R | \bar{r}'' \rangle \langle \bar{r}'' | \bar{E}_{inc} \rangle \tag{4.3.319}$$

$$\bar{\bar{G}}_0(\bar{r},\bar{r}') = \left(\bar{\bar{I}} + \frac{\nabla\nabla}{k^2}\right) \frac{e^{ik|\bar{r}-\bar{r}'|}}{4\pi|\bar{r}-\bar{r}'|} = \left(\bar{\bar{I}} - \hat{k}\hat{k}\right) \frac{e^{ikr}}{4\pi r} e^{-ik\hat{k}\cdot\bar{r}'} \tag{4.3.320}$$

Then

$$\bar{E}_s^{(R)}(\bar{r}) = \left(\bar{\bar{I}} - \hat{k}\hat{k}\right) \frac{e^{ikr}}{4\pi r} \int d\bar{r}'\, e^{-ik\hat{k}\cdot\bar{r}'} \int d\bar{r}''\, \langle \bar{r}' | \bar{\bar{T}}^R | \bar{r}'' \rangle \langle \bar{r}'' | \bar{E}_{inc} \rangle$$

$$= \left(\hat{v}_s\hat{v}_s + \hat{h}_s\hat{h}_s\right) \frac{e^{ikr}}{4\pi r} \int d\bar{r}'\, e^{-ik\hat{k}\cdot\bar{r}'} \int d\bar{r}''\, \langle \bar{r}' | \bar{\bar{T}}^R | \bar{r}'' \rangle \langle \bar{r}'' | \bar{E}_{inc} \rangle \tag{4.3.321}$$

$$\langle \bar{r}'' | \bar{E}_{inc} \rangle = E_{vi}\hat{v}(\pi-\theta_i,\phi_i) e^{ik\hat{k}(\pi-\theta_i,\phi_i)\cdot\bar{r}''} + E_{hi}\hat{h}(\pi-\theta_i,\phi_i) e^{ik\hat{k}(\pi-\theta_i,\phi_i)\cdot\bar{r}''} \tag{4.3.322}$$

$$\bar{E}_s^{(R)}(\bar{r}) = \left(\bar{\bar{I}} - \hat{k}\hat{k}\right)\frac{e^{ikr}}{4\pi r}\int d\bar{r}'\, e^{-ik\hat{k}\cdot\bar{r}'}\int d\bar{r}''\, \langle \bar{r}'|\bar{\bar{T}}^R|\bar{r}''\rangle\langle \bar{r}''|\bar{E}_{inc}\rangle$$

$$= \left(\hat{v}(\theta_s,\phi_s)\hat{v}(\theta_s,\phi_s) + \hat{h}(\theta_s,\phi_s)\hat{h}(\theta_s,\phi_s)\right)\frac{e^{ikr}}{4\pi r}\int d\bar{r}'\, e^{-ik\hat{k}\cdot\bar{r}'}\int d\bar{r}''\, \langle \bar{r}'|\bar{\bar{T}}^R|\bar{r}''\rangle$$

$$\left[E_{vi}\hat{v}(\pi-\theta_i,\phi_i)e^{ik\hat{k}(\pi-\theta_i,\phi_i)\cdot\bar{r}''} + E_{hi}\hat{h}(\pi-\theta_i,\phi_i)e^{ik\hat{k}(\pi-\theta_i,\phi_i)\cdot\bar{r}''}\right] \qquad (4.3.323)$$

$$\langle \bar{r}'|\bar{\bar{T}}^R|\bar{r}''\rangle = \int\frac{d\bar{p}}{(2\pi)^3}\int\frac{d\bar{p}'}{(2\pi)^3}e^{i\bar{p}\cdot\bar{r}'-i\bar{p}'\cdot\bar{r}''}\bar{\bar{T}}_p^R(\bar{p},\bar{p}') \qquad (4.3.324)$$

$$\bar{E}_s^{(R)}(\bar{r}) = \frac{e^{ikr}}{4\pi r}\left(\hat{v}(\theta_s,\phi_s)\hat{v}(\theta_s,\phi_s) + \hat{h}(\theta_s,\phi_s)\hat{h}(\theta_s,\phi_s)\right)$$

$$\int d\bar{r}'\, e^{-ik\hat{k}\cdot\bar{r}'}\int d\bar{r}''\int\frac{d\bar{p}}{(2\pi)^3}\int\frac{d\bar{p}'}{(2\pi)^3}e^{i\bar{p}\cdot\bar{r}'-i\bar{p}'\cdot\bar{r}''}\cdot\bar{\bar{T}}_p^R(\bar{p},\bar{p}')\cdot$$

$$\left[E_{vi}\hat{v}(\pi-\theta_i,\phi_i)e^{ik\hat{k}(\pi-\theta_i,\phi_i)\cdot\bar{r}''} + E_{hi}\hat{h}(\pi-\theta_i,\phi_i)e^{ik\hat{k}(\pi-\theta_i,\phi_i)\cdot\bar{r}''}\right] \qquad (4.3.325)$$

$$\int d\bar{r}'\, e^{-ik\hat{k}\cdot\bar{r}'}e^{i\bar{p}\cdot\bar{r}'} = (2\pi)^3\delta\left(k\hat{k}-\bar{p}\right) \qquad (4.3.326)$$

$$\int d\bar{r}''\, e^{-i\bar{p}'\cdot\bar{r}''}e^{ik\hat{k}(\pi-\theta_i,\phi_i)\cdot\bar{r}''} = (2\pi)^3\delta\left(\bar{p}'-k\hat{k}(\pi-\theta_i,\phi_i)\right) \qquad (4.3.327)$$

$$\bar{E}_s^{(R)}(\bar{r}) = \frac{e^{ikr}}{4\pi r}\left(\hat{v}(\theta_s,\phi_s)\hat{v}(\theta_s,\phi_s) + \hat{h}(\theta_s,\phi_s)\hat{h}(\theta_s,\phi_s)\right)$$

$$\int\frac{d\bar{p}}{(2\pi)^3}\int\frac{d\bar{p}'}{(2\pi)^3}(2\pi)^3\delta\left(k\hat{k}-\bar{p}\right)(2\pi)^3\delta\left(\bar{p}'-k\hat{k}(\pi-\theta_i,\phi_i)\right)\cdot\bar{\bar{T}}_p^R(\bar{p},\bar{p}')\cdot$$

$$\left[E_{vi}\hat{v}(\pi-\theta_i,\phi_i) + E_{hi}\hat{h}(\pi-\theta_i,\phi_i)\right]$$

$$= \frac{e^{ikr}}{4\pi r}\left(\hat{v}(\theta_s,\phi_s)\hat{v}(\theta_s,\phi_s) + \hat{h}(\theta_s,\phi_s)\hat{h}(\theta_s,\phi_s)\right)\cdot\bar{\bar{T}}_p^R\left(k\hat{k},k\hat{k}(\pi-\theta_i,\phi_i)\right)\cdot$$

$$\left[E_{vi}\hat{v}(\pi-\theta_i,\phi_i) + E_{hi}\hat{h}(\pi-\theta_i,\phi_i)\right]$$

$$= \frac{e^{ikr}}{4\pi r}\hat{v}(\theta_s,\phi_s)\hat{v}(\theta_s,\phi_s)\cdot\bar{\bar{T}}_p^R\left(k\hat{k},k\hat{k}(\pi-\theta_i,\phi_i)\right)\cdot E_{vi}\hat{v}(\pi-\theta_i,\phi_i)$$

$$+\frac{e^{ikr}}{4\pi r}\hat{v}(\theta_s,\phi_s)\hat{v}(\theta_s,\phi_s)\cdot\bar{\bar{T}}_p^R\left(k\hat{k},k\hat{k}(\pi-\theta_i,\phi_i)\right)\cdot E_{hi}\hat{h}(\pi-\theta_i,\phi_i)$$

$$+\frac{e^{ikr}}{4\pi r}\hat{h}(\theta_s,\phi_s)\hat{h}(\theta_s,\phi_s)\cdot\bar{\bar{T}}_p^R\left(k\hat{k},k\hat{k}(\pi-\theta_i,\phi_i)\right)\cdot E_{vi}\hat{v}(\pi-\theta_i,\phi_i)$$

$$+\frac{e^{ikr}}{4\pi r}\hat{h}(\theta_s,\phi_s)\hat{h}(\theta_s,\phi_s)\cdot\bar{\bar{T}}_p^R\left(k\hat{k},k\hat{k}(\pi-\theta_i,\phi_i)\right)\cdot E_{hi}\hat{h}(\pi-\theta_i,\phi_i)$$

$$= \frac{e^{ikr}}{r}\hat{v}(\theta_s,\phi_s)S_{vv}^R E_{vi} + \frac{e^{ikr}}{r}\hat{v}(\theta_s,\phi_s)S_{vh}^R E_{hi} + \frac{e^{ikr}}{r}\hat{h}(\theta_s,\phi_s)S_{hv}^R E_{vi}$$

$$+\frac{e^{ikr}}{r}\hat{h}(\theta_s,\phi_s)S_{hh}^R E_{hi} \qquad (4.3.328)$$

Then

$$S_{vv}^R = \frac{1}{4\pi}\hat{v}(\theta_s,\phi_s)\cdot\bar{\bar{T}}_p^R\left(k\hat{k},k\hat{k}(\pi-\theta_i,\phi_i)\right)\cdot\hat{v}(\pi-\theta_i,\phi_i) \qquad (4.3.329)$$

$$S_{vh}^R = \frac{1}{4\pi}\hat{v}(\theta_s,\phi_s)\cdot\bar{\bar{T}}_p^R\left(k\hat{k},k\hat{k}(\pi-\theta_i,\phi_i)\right)\cdot\hat{h}(\pi-\theta_i,\phi_i) \qquad (4.3.330)$$

$$S_{hv}^R = \frac{1}{4\pi}\hat{h}(\theta_s,\phi_s)\cdot\bar{\bar{T}}_p^R\left(k\hat{k},k\hat{k}(\pi-\theta_i,\phi_i)\right)\cdot\hat{v}(\pi-\theta_i,\phi_i) \qquad (4.3.331)$$

$$S_{hh}^R = \frac{1}{4\pi}\hat{h}(\theta_s,\phi_s)\cdot\bar{\bar{T}}_p^R\left(k\hat{k},k\hat{k}(\pi-\theta_i,\phi_i)\right)\cdot\hat{h}(\pi-\theta_i,\phi_i) \qquad (4.3.332)$$

In the backscattering direction. Let $\theta_s = \theta_i$ and $\phi_s = \phi_i + \pi$

$$S_{vv,back}^R = \frac{1}{4\pi}\hat{v}(\theta_i,\phi_i+\pi)\cdot\bar{\bar{T}}_p^R\left(-k\hat{k}_i,k\hat{k}_i\right)\cdot\hat{v}(\pi-\theta_i,\phi_i)$$

$$= \frac{1}{4\pi}\hat{v}_i\cdot\bar{\bar{T}}_p^R\left(-k\hat{k}_i,k\hat{k}_i\right)\cdot\hat{v}_i \qquad (4.3.333)$$

$$S_{vh,back}^R = \frac{1}{4\pi}\hat{v}(\theta_i,\phi_i+\pi)\cdot\bar{\bar{T}}_p^R\left(-k\hat{k}_i,k\hat{k}_i\right)\cdot\hat{h}(\pi-\theta_i,\phi_i)$$

$$= \frac{1}{4\pi}\hat{v}_i\cdot\bar{\bar{T}}_p^R\left(-k\hat{k}_i,k\hat{k}_i\right)\cdot\hat{h}_i \qquad (4.3.334)$$

$$S_{hv,back}^R = \frac{1}{4\pi}\hat{h}(\theta_i,\phi_i+\pi)\cdot\bar{\bar{T}}_p^R\left(-k\hat{k}_i,k\hat{k}_i\right)\cdot\hat{v}(\pi-\theta_i,\phi_i)$$

$$= \frac{1}{4\pi}\left(-\hat{h}_i\right) \cdot \bar{\bar{T}}_p^R\left(-k\hat{k}_i, k\hat{k}_i\right) \cdot \hat{v}_i \tag{4.3.335}$$

$$S_{hh,back}^R = \frac{1}{4\pi}\widehat{hs}(\theta_i, \phi_i + \pi) \cdot \bar{\bar{T}}_p^R\left(-k\hat{k}_i, k\hat{k}_i\right) \cdot \hat{v}(\pi - \theta_i, \phi_i)$$

$$= \frac{1}{4\pi}\left(-\hat{h}_i\right) \cdot \bar{\bar{T}}_p^R\left(-k\hat{k}_i, k\hat{k}_i\right) \cdot \hat{h}_i \tag{4.3.336}$$

Note that

$$S_{vh,back}^R = -S_{hv,back}^R \tag{4.3.337}$$

Next consider layer of vegetation above the rough surface. Rough surface is located at $z = -d$. Replace the free space green's function with $\bar{\bar{G}}_{01}^{(0)}(\bar{r}, \bar{r}')$.

$$\bar{E}_s^{(RV)}(\bar{r}) = \int d\bar{r}'\, \bar{\bar{G}}_{01}^{(0)}(\bar{r}, \bar{r}') \int d\bar{r}''\, \left\langle \bar{r}' \middle| \bar{\bar{T}}_d^R \middle| \bar{r}'' \right\rangle \langle \bar{r}'' | \bar{E}_{inc} \rangle \tag{4.3.338}$$

RV stands for rough surface below vegetation. $\bar{\bar{T}}_d^R$ is $\bar{\bar{T}}^R$ shifted down by d.

$$\bar{\bar{T}}_d^R = e^{-i\bar{p}_{op}\cdot\bar{r}_j}\bar{\bar{T}}^R e^{i\bar{p}_{op}\cdot\bar{r}_j} \tag{4.3.339}$$

$$\bar{r}_j = (0,0,-d) \tag{4.3.340}$$

$$\bar{\bar{T}}_d^R = e^{ip_{op,z}d}\bar{\bar{T}}^R e^{-ip_{op,z}d} \tag{4.3.341}$$

$$\left\langle \bar{r}' \middle| \bar{\bar{T}}_d^R \middle| \bar{r}'' \right\rangle = \int \frac{d\bar{p}}{(2\pi)^3} \int \frac{d\bar{p}'}{(2\pi)^3} \langle \bar{r}' | \bar{p} \rangle \left\langle \bar{p} \middle| \bar{\bar{T}}_d^R \middle| \bar{p}' \right\rangle \langle \bar{p}' | \bar{r}'' \rangle$$

$$= \int \frac{d\bar{p}}{(2\pi)^3} \int \frac{d\bar{p}'}{(2\pi)^3} \langle \bar{r}' | \bar{p} \rangle \left\langle \bar{p} \middle| e^{ip_{op,z}d}\bar{\bar{T}}^R e^{-ip_{op,z}d} \middle| \bar{p}' \right\rangle \langle \bar{p}' | \bar{r}'' \rangle$$

$$= \int \frac{d\bar{p}}{(2\pi)^3} \int \frac{d\bar{p}'}{(2\pi)^3} \langle \bar{r}' | \bar{p} \rangle e^{ip_z d} \left\langle \bar{p} \middle| \bar{\bar{T}}^R \middle| \bar{p}' \right\rangle e^{-ip'_z d} \langle \bar{p}' | \bar{r}'' \rangle$$

$$= \int \frac{d\bar{p}}{(2\pi)^3} \int \frac{d\bar{p}'}{(2\pi)^3} e^{i\bar{p}\cdot\bar{r}' - i\bar{p}'\cdot\bar{r}''} e^{ip_z d} \left\langle \bar{p} \middle| \bar{\bar{T}}^R \middle| \bar{p}' \right\rangle e^{-ip'_z d} \tag{4.3.342}$$

$$\bar{E}_s^{(RV)}(\bar{r}) = \int d\bar{r}'\, \bar{\bar{G}}_{01}^{(0)}(\bar{r}, \bar{r}') \int d\bar{r}'' \int \frac{d\bar{p}}{(2\pi)^3} \int \frac{d\bar{p}'}{(2\pi)^3} e^{i\bar{p}\cdot\bar{r}' - i\bar{p}'\cdot\bar{r}''} e^{ip_z d} \left\langle \bar{p} \middle| \bar{\bar{T}}^R \middle| \bar{p}' \right\rangle e^{-ip'_z d}$$

$$\left[E_{vi}\hat{v}(\pi - \theta_i, \phi_i) e^{i\bar{K}_{iv}\cdot\bar{r}''} + E_{hi}\hat{h}(\pi - \theta_i, \phi_i) e^{i\bar{K}_{ih}\cdot\bar{r}''}\right] \tag{4.3.343}$$

$$\bar{\bar{G}}_{01}^{(0)}(\bar{r},\bar{r}') = \frac{e^{ikr}}{4\pi r}\left[\hat{e}(k_z)\hat{e}(k_z)e^{-i\bar{k}_h\cdot\bar{r}'} + \hat{h}(k_z)\hat{h}(k_z)e^{-i\bar{k}_v\cdot\bar{r}'}\right] \tag{4.3.344}$$

$$\bar{E}_s^{(RV)}(\bar{r}) = \frac{e^{ikr}}{4\pi r}\int d\bar{r}'\left[\hat{e}(k_z)\hat{e}(k_z)e^{-i\bar{k}_h\cdot\bar{r}'} + \hat{h}(k_z)\hat{h}(k_z)e^{-i\bar{k}_v\cdot\bar{r}'}\right]$$

$$\int d\bar{r}'' \int \frac{d\bar{p}}{(2\pi)^3}\int \frac{d\bar{p}'}{(2\pi)^3} e^{i\bar{p}\cdot\bar{r}'-i\bar{p}'\cdot\bar{r}''}e^{ip_z d}\left\langle\bar{p}\middle|\bar{\bar{T}}^R\middle|\bar{p}'\right\rangle e^{-ip'_z d}$$

$$\left[E_{vi}\hat{v}(\pi-\theta_i,\phi_i)e^{i\bar{K}_{iv}\cdot\bar{r}''} + E_{hi}\hat{h}(\pi-\theta_i,\phi_i)e^{i\bar{K}_{ih}\cdot\bar{r}''}\right] \tag{4.3.345}$$

$$\int d\bar{r}'\, e^{-i\bar{k}_h\cdot\bar{r}'}e^{i\bar{p}\cdot\bar{r}'} = (2\pi)^3\delta\left(\bar{k}_h-\bar{p}\right) \tag{4.3.346}$$

$$\int d\bar{r}'\, e^{-i\bar{k}_v\cdot\bar{r}'}e^{i\bar{p}\cdot\bar{r}'} = (2\pi)^3\delta\left(\bar{k}_v-\bar{p}\right) \tag{4.3.347}$$

$$\int d\bar{r}''\, e^{-i\bar{p}'\cdot\bar{r}''}e^{i\bar{K}_{iv}\cdot\bar{r}''} = (2\pi)^3\delta(\bar{p}'-\bar{K}_{iv}) \tag{4.3.348}$$

$$\int d\bar{r}''\, e^{-i\bar{p}'\cdot\bar{r}''}e^{i\bar{K}_{ih}\cdot\bar{r}''} = (2\pi)^3\delta(\bar{p}'-\bar{K}_{ih}) \tag{4.3.349}$$

$$\bar{E}_s^{(RV)}(\bar{r}) = \frac{e^{ikr}}{4\pi r}\int \frac{d\bar{p}}{(2\pi)^3}\int \frac{d\bar{p}'}{(2\pi)^3}$$

$$\left[\hat{e}(k_z)\hat{e}(k_z)(2\pi)^3\delta\left(\bar{k}_h-\bar{p}\right) + \hat{h}(k_z)\hat{h}(k_z)(2\pi)^3\delta\left(\bar{k}_v-\bar{p}\right)\right]e^{ip_z d}\left\langle\bar{p}\middle|\bar{\bar{T}}^R\middle|\bar{p}'\right\rangle e^{-ip'_z d}$$

$$\left[E_{vi}\hat{v}(\pi-\theta_i,\phi_i)(2\pi)^3\delta(\bar{p}'-\bar{K}_{iv}) + E_{hi}\hat{h}(\pi-\theta_i,\phi_i)(2\pi)^3\delta(\bar{p}'-\bar{K}_{ih})\right] \tag{4.3.350}$$

For $\bar{p} = \bar{k}_h$

$$\left(p_x,p_y,p_z\right) = \left(k_x,k_y,k_{hz}\right) \tag{4.3.351}$$

For $\bar{p} = \bar{k}_v$

$$\left(p_x,p_y,p_z\right) = \left(k_x,k_y,k_{vz}\right) \tag{4.3.352}$$

For $\bar{p}' = \bar{K}_{ih}$

$$\left(p'_x,p'_y,p'_z\right) = \left(k_{ix},k_{iy},-k_{ihz}\right) \tag{4.3.353}$$

For $\bar{p}' = \bar{K}_{iv}$

$$\left(p'_x,p'_y,p'_z\right) = \left(k_{ix},k_{iy},-k_{ivz}\right) \tag{4.3.354}$$

$$\bar{E}_s^{(RV)}(\bar{r}) = \frac{e^{ikr}}{4\pi r}\hat{e}(k_z)\hat{e}(k_z)e^{ik_{hz}d}\langle \bar{k}_h|\bar{\bar{T}}^R|\bar{K}_{iv}\rangle e^{ik_{ivz}d}E_{vi}\hat{v}(\pi-\theta_i,\phi_i)$$
$$+\frac{e^{ikr}}{4\pi r}\hat{e}(k_z)\hat{e}(k_z)e^{ik_{hz}d}\langle \bar{k}_h|\bar{\bar{T}}^R|\bar{K}_{ih}\rangle e^{ik_{izh}d}E_{hi}\hat{h}(\pi-\theta_i,\phi_i)$$
$$+\frac{e^{ikr}}{4\pi r}\hat{h}(k_z)\hat{h}(k_z)e^{ik_{vz}d}\langle \bar{k}_v|\bar{\bar{T}}^R|\bar{K}_{iv}\rangle e^{ik_{ivz}d}E_{vi}\hat{v}(\pi-\theta_i,\phi_i)$$
$$+\frac{e^{ikr}}{4\pi r}\hat{h}(k_z)\hat{h}(k_z)e^{ik_{vz}d}\langle \bar{k}_v|\bar{\bar{T}}^R|\bar{K}_{ih}\rangle e^{ik_{ihz}d}E_{hi}\hat{h}(\pi-\theta_i,\phi_i) \quad (4.3.355)$$

$$\hat{e}(k_z) = \hat{x}\sin\phi_s - \hat{y}\cos\phi_s = -\hat{h}(\theta_s,\phi_s) \quad (4.3.356)$$

$$\hat{h}(k_z) = -\cos\theta_s(\hat{x}\cos\phi_s + \hat{y}\sin\phi_s) + \sin\theta_s\,\hat{z} = -\hat{v}(\theta_s,\phi_s) \quad (4.3.357)$$

$$\bar{E}_s^{(RV)}(\bar{r}) = \frac{e^{ikr}}{4\pi r}\hat{h}(\theta_s,\phi_s)\hat{h}(\theta_s,\phi_s)e^{ik_{hz}d}\langle \bar{k}_h|\bar{\bar{T}}^R|\bar{K}_{iv}\rangle e^{ik_{ivz}d}E_{vi}\hat{v}(\pi-\theta_i,\phi_i)$$
$$+\frac{e^{ikr}}{4\pi r}\hat{h}(\theta_s,\phi_s)\hat{h}(\theta_s,\phi_s)e^{ik_{hz}d}\langle \bar{k}_h|\bar{\bar{T}}^R|\bar{K}_{ih}\rangle e^{ik_{izh}d}E_{hi}\hat{h}(\pi-\theta_i,\phi_i)$$
$$+\frac{e^{ikr}}{4\pi r}\hat{v}(\theta_s,\phi_s)\hat{v}(\theta_s,\phi_s)e^{ik_{vz}d}\langle \bar{k}_v|\bar{\bar{T}}^R|\bar{K}_{iv}\rangle e^{ik_{ivz}d}E_{vi}\hat{v}(\pi-\theta_i,\phi_i)$$
$$+\frac{e^{ikr}}{4\pi r}\hat{v}(\theta_s,\phi_s)\hat{v}(\theta_s,\phi_s)e^{ik_{vz}d}\langle \bar{k}_v|\bar{\bar{T}}^R|\bar{K}_{ih}\rangle e^{ik_{ihz}d}E_{hi}\hat{h}(\pi-\theta_i,\phi_i) \quad (4.3.358)$$

From previous derivation, (4.2.333)~(4.2.336)

$$S_{vv}^R = \frac{1}{4\pi}\hat{v}(\theta_s,\phi_s)\cdot\bar{\bar{T}}_p^R\left(k\hat{k},k\hat{k}(\pi-\theta_i,\phi_i)\right)\cdot\hat{v}(\pi-\theta_i,\phi_i) \quad (4.3.359)$$

$$S_{vh}^R = \frac{1}{4\pi}\hat{v}(\theta_s,\phi_s)\cdot\bar{\bar{T}}_p^R\left(k\hat{k},k\hat{k}(\pi-\theta_i,\phi_i)\right)\cdot\hat{h}(\pi-\theta_i,\phi_i) \quad (4.3.360)$$

$$S_{hv}^R = \frac{1}{4\pi}\hat{h}(\theta_s,\phi_s)\cdot\bar{\bar{T}}_p^R\left(k\hat{k},k\hat{k}(\pi-\theta_i,\phi_i)\right)\cdot\hat{v}(\pi-\theta_i,\phi_i) \quad (4.3.361)$$

$$S_{hh}^R = \frac{1}{4\pi}\hat{h}(\theta_s,\phi_s)\cdot\bar{\bar{T}}_p^R\left(k\hat{k},k\hat{k}(\pi-\theta_i,\phi_i)\right)\cdot\hat{h}(\pi-\theta_i,\phi_i) \quad (4.3.362)$$

Then

$$\bar{E}_s^{(RV)}(\bar{r}) = \frac{e^{ikr}}{r}\hat{h}(\theta_s,\phi_s)e^{ik_{hz}d}S_{hv}^R e^{ik_{ivz}d}E_{vi} + \frac{e^{ikr}}{r}\hat{h}(\theta_s,\phi_s)e^{ik_{hz}d}S_{hh}^R e^{ik_{izh}d}E_{hi}$$
$$+\frac{e^{ikr}}{r}\hat{v}(\theta_s,\phi_s)e^{ik_{vz}d}S_{vv}^R e^{ik_{ivz}d}E_{vi} + \frac{e^{ikr}}{r}\hat{v}(\theta_s,\phi_s)e^{ik_{vz}d}S_{vh}^R e^{ik_{ihz}d}E_{hi}$$
$$= \frac{e^{ikr}}{r}\hat{h}(\theta_s,\phi_s)S_{hv}^{RV}E_{vi} + \frac{e^{ikr}}{r}\hat{h}(\theta_s,\phi_s)S_{hh}^{RV}E_{hi} + \frac{e^{ikr}}{r}\hat{v}(\theta_s,\phi_s)S_{vv}^{RV}E_{vi}$$
$$+\frac{e^{ikr}}{r}\hat{v}(\theta_s,\phi_s)S_{vh}^{RV}E_{hi} \qquad (4.3.363)$$

Then

$$S_{hv}^{RV} = e^{ik_{hz}d}e^{ik_{ivz}d}S_{hv}^R \qquad (4.3.364)$$
$$S_{hh}^{RV} = e^{ik_{hz}d}e^{ik_{ihz}d}S_{hh}^R \qquad (4.3.365)$$
$$S_{vv}^{RV} = e^{ik_{vz}d}e^{ik_{ivz}d}S_{vv}^R \qquad (4.3.366)$$
$$S_{vh}^{RV} = e^{ik_{vz}d}e^{ik_{ihz}d}S_{vh}^R \qquad (4.3.367)$$

In the backscattering direction

$$S_{hv,back}^{RV} = e^{ik_{ihz}d}e^{ik_{ivz}d}S_{hv,back}^R \qquad (4.3.368)$$
$$S_{hh,back}^{RV} = e^{ik_{ihz}d}e^{ik_{ihz}d}S_{hh,back}^R \qquad (4.3.369)$$
$$S_{vv,back}^{RV} = e^{ik_{ivz}d}e^{ik_{ivz}d}S_{vv,back}^R \qquad (4.3.370)$$
$$S_{vh,back}^{RV} = e^{ik_{ivz}d}e^{ik_{ihz}d}S_{vh,back}^R \qquad (4.3.371)$$

Note that

$$S_{vh,back}^{RV} = -S_{hv,back}^{RV} \qquad (4.3.372)$$

Then we consider the correlations for the coherency matrix.

$$\langle S_{vv,back}^{RV}S_{hh,back}^{RV*}\rangle = \langle e^{ik_{ivz}d}e^{ik_{ivz}d}S_{vv,back}^R e^{-ik_{ihz}^*d}e^{-ik_{ihz}^*d}S_{hh,back}^{R*}\rangle$$
$$= e^{2i[Re(k_{ivz})-Re(k_{ihz})+iIm(k_{ivz})+iIm(k_{ihz})]d}\langle S_{vv,back}^R S_{hh,back}^{R*}\rangle \qquad (4.3.373)$$

$$\langle S_{vv,back}^{RV}S_{vv,back}^{RV*}\rangle = \langle e^{ik_{ivz}d}e^{ik_{ivz}d}S_{vv,back}^R e^{-ik_{ivz}^*d}e^{-ik_{ivz}^*d}S_{vv,back}^{R*}\rangle$$
$$= e^{2ik_{ivz}d-2ik_{ivz}^*d}\langle S_{vv,back}^R S_{vv,back}^{R*}\rangle = e^{-4Im(k_{ivz})d}\langle S_{vv,back}^R S_{vv,back}^{R*}\rangle \qquad (4.3.374)$$

$$\langle S_{hh,back}^{RV} S_{hh,back}^{RV*} \rangle = \langle e^{ik_{ihz}d} e^{ik_{ihz}d} S_{hh,back}^{R} e^{-ik_{ihz}^{*}d} e^{-ik_{ihz}^{*}d} S_{hh,back}^{R*} \rangle$$
$$= e^{2ik_{ihz}d - 2ik_{ihz}^{*}d} \langle S_{hh,back}^{R} S_{hh,back}^{R*} \rangle = e^{-4Im(k_{ihz})d} \langle S_{hh,back}^{R} S_{hh,back}^{R*} \rangle \quad (4.3.375)$$

$$\langle S_{vv,back}^{RV} S_{vh,back}^{RV*} \rangle = \langle e^{ik_{ivz}d} e^{ik_{ivz}d} S_{vv,back}^{R} e^{-ik_{ivz}^{*}d} e^{-ik_{ihz}^{*}d} S_{vh,back}^{R*} \rangle$$
$$= e^{i[2k_{ivz} - k_{ivz}^{*} - k_{ihz}^{*}]d} \langle S_{vv,back}^{R} S_{vh,back}^{R*} \rangle$$
$$= e^{i[Re(k_{ivz}) - Re(k_{ihz}) + 3iIm(k_{ivz}) + iIm(k_{ihz})]d} \langle S_{vv,back}^{R} S_{vh,back}^{R*} \rangle \quad (4.3.376)$$

$$\langle S_{hh,back}^{RV} S_{vh,back}^{RV*} \rangle = \langle e^{ik_{ihz}d} e^{ik_{ihz}d} S_{hh,back}^{R} e^{-ik_{ivz}^{*}d} e^{-ik_{ihz}^{*}d} S_{vh,back}^{R*} \rangle$$
$$= e^{i[2k_{ihz} - k_{ivz}^{*} - k_{ihz}^{*}]d} \langle S_{hh,back}^{R} S_{vh,back}^{R*} \rangle$$
$$= e^{i[Re(k_{ihz}) - Re(k_{ivz}) + 3iIm(k_{ihz}) + iIm(k_{ivz})]d} \langle S_{hh,back}^{R} S_{vh,back}^{R*} \rangle \quad (4.3.377)$$

$$\langle S_{vh,back}^{RV} S_{vh,back}^{RV*} \rangle = \langle e^{ik_{ivz}d} e^{ik_{ihz}d} S_{vh,back}^{R} e^{-ik_{ivz}^{*}d} e^{-ik_{ihz}^{*}d} S_{vh,back}^{R*} \rangle$$
$$= e^{i[k_{ivz} - k_{ivz}^{*} + k_{ihz} - k_{ihz}^{*}]d} \langle S_{vh,back}^{R} S_{vh,back}^{R*} \rangle$$
$$= e^{-2[Im(k_{ivz}) + Im(k_{ihz})]d} \langle S_{vh,back}^{R} S_{vh,back}^{R*} \rangle \quad (4.3.378)$$

4.3.6 Summary

Notice that in the above derivation of elements of the coherency matrices, the dimension is squared length, similar to scattering cross-section. Here we normalize these elements with area A to become dimensionless similar to scattering coefficient. Also we summarize all terms from

For volume scattering

$$\frac{\langle S_{vv,back}^{(vol)} S_{hh,back}^{(vol)*} \rangle}{A} = n_0 \frac{1 - e^{i2d\left(Re(k_{ivz}) - Re(k_{ihz}) + i\left(Im(k_{ivz}) + Im(k_{ihz})\right)\right)}}{-2i\left(Re(k_{ivz}) - Re(k_{ihz}) + i\left(Im(k_{ivz}) + Im(k_{ihz})\right)\right)}$$
$$\langle f_{vv}(\theta_i, \pi; \pi - \theta_i, 0) f_{hh}^{*}(\theta_i, \pi; \pi - \theta_i, 0) \rangle \quad (4.3.379)$$

$$\frac{\langle S_{vv,back}^{(vol)} S_{vv,back}^{(vol)*} \rangle}{A} = n_0 \frac{1 - e^{-4dIm(k_{ivz})}}{4Im(k_{ivz})} \langle f_{vv}(\theta_i, \pi; \pi - \theta_i, 0) f_{vv}^*(\theta_i, \pi; \pi - \theta_i, 0) \rangle \quad (4.3.380)$$

$$\frac{\langle S_{hh,back}^{(vol)} S_{hh,back}^{(vol)*} \rangle}{A} = n_0 \frac{1 - e^{-4dIm(k_{ihz})}}{4Im(k_{ihz})} \langle f_{hh}(\theta_i, \pi; \pi - \theta_i, 0) f_{hh}^*(\theta_i, \pi; \pi - \theta_i, 0) \rangle \quad (4.3.381)$$

$$\frac{\langle S_{vv,back}^{(vol)} S_{vh,back}^{(vol)*} \rangle}{A} = n_0 \frac{1 - e^{i\left[Re(k_{ivz}) - Re(k_{ihz}) + i\left(3Im(k_{ivz}) + Im(k_{ihz})\right)\right]d}}{-i\left[Re(k_{ivz}) - Re(k_{ihz}) + i\left(3Im(k_{ivz}) + Im(k_{ihz})\right)\right]} \langle f_{vv}(\theta_i, \pi; \pi - \theta_i, 0) f_{vh}^*(\theta_i, \pi; \pi - \theta_i, 0) \rangle \quad (4.3.382)$$

$$\frac{\langle S_{hh,back}^{(vol)} S_{vh,back}^{(vol)*} \rangle}{A} = n_0 \frac{1 - e^{i\left[-Re(k_{ivz}) + Re(k_{ihz}) + i\left(Im(k_{ivz}) + 3Im(k_{ihz})\right)\right]d}}{-i\left[-Re(k_{ivz}) + Re(k_{ihz}) + i\left(Im(k_{ivz}) + 3Im(k_{ihz})\right)\right]} \langle f_{hh}(\theta_i, \pi; \pi - \theta_i, 0) f_{vh}^*(\theta_i, \pi; \pi - \theta_i, 0) \rangle \quad (4.3.383)$$

$$\frac{\langle S_{vh,back}^{(vol)} S_{vh,back}^{(vol)*} \rangle}{A} = n_0 \frac{1 - e^{-2\left(Im(k_{ivz}) + Im(k_{ihz})\right)d}}{2\left(Im(k_{ivz}) + Im(k_{ihz})\right)} \langle f_{vh}(\theta_i, \pi; \pi - \theta_i, 0) f_{vh}^*(\theta_i, \pi; \pi - \theta_i, 0) \rangle \quad (4.3.384)$$

For Double Bounce

$$\frac{\langle S_{vv,back}^{(DB)} S_{hh,back}^{(DB)*} \rangle}{A} = 4n_0 dR_{vi} e^{2ik_{ivz}d} R_{hi}{}^* e^{-2ik_{ihz}^* d} \langle f_{vv}(\pi - \theta_i, \pi; \pi - \theta_i, 0) f_{hh}^*(\pi - \theta_i, \pi; \pi - \theta_i, 0) \rangle \quad (4.3.385)$$

$$\frac{\langle S_{vv,back}^{(DB)} S_{vv,back}^{(DB)*} \rangle}{A}$$

$$= 4n_0 dR_{vi} e^{2ik_{ivz}d} {R_{vi}}^* e^{-2ik^*_{ivz}d} \langle f_{vv}(\pi-\theta_i,\pi;\pi-\theta_i,0) f^*_{vv}(\pi-\theta_i,\pi;\pi-\theta_i,0)\rangle \quad (4.3.386)$$

$$\frac{\langle S^{(DB)}_{hh,back} S^{(DB)*}_{hh,back}\rangle}{A}$$

$$= 4n_0 dR_{hi} e^{2ik_{ihz}d} {R_{hi}}^* e^{-2ik^*_{ihz}d} \langle f_{hh}(\pi-\theta_i,\pi;\pi-\theta_i,0) f^*_{hh}(\pi-\theta_i,\pi;\pi-\theta_i,0)\rangle \quad (4.3.387)$$

$$\frac{\langle S^{(DB)}_{vv,back} S^{(DB)*}_{vh,back}\rangle}{A}$$

$$= 2n_0 \frac{1-e^{i\left[Re(k_{ivz})-Re(k_{ihz})-i\left(Im(k_{ivz})-Im(k_{ihz})\right)\right]d}}{-i\left[Re(k_{ivz})-Re(k_{ihz})-i\left(Im(k_{ivz})-Im(k_{ihz})\right)\right]} R_{vi} e^{2ik_{ivz}d} {R_{vi}}^* e^{-2ik^*_{ivz}d}$$

$$\langle f_{vv}(\pi-\theta_i,\pi;\pi-\theta_i,0) f^*_{vh}(\pi-\theta_i,\pi;\pi-\theta_i,0)\rangle$$

$$-2n_0 R_{vi} e^{2ik_{ivz}d} R^*_{hi} e^{-2ik^*_{ihz}d} \frac{1-e^{i\left[Re(k_{ihz})-Re(k_{ivz})-i\left(Im(k_{ihz})-Im(k_{ivz})\right)\right]d}}{-i\left[Re(k_{ihz})-Re(k_{ivz})-i\left(Im(k_{ihz})-Im(k_{ivz})\right)\right]}$$

$$\langle f_{vv}(\pi-\theta_i,\pi;\pi-\theta_i,0) f^*_{hv}(\pi-\theta_i,\pi;\pi-\theta_i,0)\rangle \quad (4.3.388)$$

$$\frac{\langle S^{(DB)}_{hh,back} S^{(DB)*}_{vh,back}\rangle}{A}$$

$$= 2n_0 \frac{1-e^{i[Re(k_{ivz})-Re(k_{ihz})-i\left(Im(k_{ivz})-Im(k_{ihz})\right)]d}}{-i[Re(k_{ivz})-Re(k_{ihz})-i\left(Im(k_{ivz})-Im(k_{ihz})\right)]} R_{hi} e^{2ik_{ihz}d} {R_{vi}}^* e^{-2ik^*_{ivz}d}$$

$$\langle f_{hh}(\pi-\theta_i,\pi;\pi-\theta_i,0) f^*_{vh}(\pi-\theta_i,\pi;\pi-\theta_i,0)\rangle$$

$$-2n_0 R_{hi} e^{2ik_{ihz}d} R^*_{hi} e^{-2ik^*_{ihz}d} \frac{1-e^{i\left[Re(k_{ihz})-Re(k_{ivz})-i\left(Im(k_{ihz})-Im(k_{ivz})\right)\right]d}}{-i\left[Re(k_{ihz})-Re(k_{ivz})-i\left(Im(k_{ihz})-Im(k_{ivz})\right)\right]}$$

$$\langle f_{hh}(\pi-\theta_i,\pi;\pi-\theta_i,0) f^*_{hv}(\pi-\theta_i,\pi;\pi-\theta_i,0)\rangle \quad (4.3.389)$$

$$\frac{\langle S_{vh,back}^{(DB)} S_{vh,back}^{(DB)*} \rangle}{A} = n_0 \frac{1 - e^{2(Im(k_{ivz}) - Im(k_{ihz}))d}}{-2\left(Im(k_{ivz}) - Im(k_{ihz})\right)} R_{vi} e^{2ik_{ivz}d} {R_{vi}}^* e^{-2ik_{ivz}^* d}$$

$$\langle f_{vh}(\pi - \theta_i, \pi; \pi - \theta_i, 0) f_{vh}^*(\pi - \theta_i, \pi; \pi - \theta_i, 0) \rangle$$

$$-2n_0 Re\{R_{vi} e^{2ik_{ivz}d} R_{hi}^* e^{-2ik_{ihz}^* d} \frac{1 - e^{i[2(Re(k_{ihz}) - Re(k_{ivz}))]d}}{-i\left[2\left(Re(k_{ihz}) - Re(k_{ivz})\right)\right]}$$

$$\langle f_{vh}(\pi - \theta_i, \pi; \pi - \theta_i, 0) f_{hv}^*(\pi - \theta_i, \pi; \pi - \theta_i, 0) \rangle\}$$

$$+n_0 R_{hi} e^{2ik_{ihz}d} R_{hi}^* e^{-2ik_{ihz}^* d} \frac{1 - e^{2(Im(k_{ihz}) - Im(k_{ivz}))d}}{-2\left(Im(k_{ihz}) - Im(k_{ivz})\right)}$$

$$\langle f_{hv}(\pi - \theta_i, \pi; \pi - \theta_i, 0) f_{hv}^*(\pi - \theta_i, \pi; \pi - \theta_i, 0) \rangle \quad (4.3.390)$$

For surface scattering

$$\frac{\langle S_{vv,back}^{RV} S_{hh,back}^{RV*} \rangle}{A} = e^{2i[Re(k_{ivz}) - Re(k_{ihz}) + iIm(k_{ivz}) + iIm(k_{ihz})]d} \frac{\langle S_{vv,back}^{R} S_{hh,back}^{R*} \rangle}{A} \quad (4.3.391)$$

$$\frac{\langle S_{vv,back}^{RV} S_{vv,back}^{RV*} \rangle}{A} = e^{-4Im(k_{ivz})d} \frac{\langle S_{vv,back}^{R} S_{vv,back}^{R*} \rangle}{A} \quad (4.3.392)$$

$$\frac{\langle S_{hh,back}^{RV} S_{hh,back}^{RV*} \rangle}{A} = e^{-4Im(k_{ihz})d} \frac{\langle S_{hh,back}^{R} S_{hh,back}^{R*} \rangle}{A} \quad (4.3.393)$$

$$\frac{\langle S_{vv,back}^{RV} S_{vh,back}^{RV*} \rangle}{A} = e^{i[Re(k_{ivz}) - Re(k_{ihz}) + 3iIm(k_{ivz}) + iIm(k_{ihz})]d} \frac{\langle S_{vv,back}^{R} S_{vh,back}^{R*} \rangle}{A} \quad (4.3.394)$$

$$\frac{\langle S_{hh,back}^{RV} S_{vh,back}^{RV*} \rangle}{A} = e^{i[Re(k_{ihz}) - Re(k_{ivz}) + 3iIm(k_{ihz}) + iIm(k_{ivz})]d} \frac{\langle S_{hh,back}^{R} S_{vh,back}^{R*} \rangle}{A} \quad (4.3.395)$$

$$\frac{\langle S_{vh,back}^{RV} S_{vh,back}^{RV*} \rangle}{A} = e^{-2[Im(k_{ivz}) + Im(k_{ihz})]d} \frac{\langle S_{vh,back}^{R} S_{vh,back}^{R*} \rangle}{A} \quad (4.3.396)$$

Notice that rough surface scattering computed by NMM3D is already normalized to the surface area for all realizations. [46]

$$\frac{S_{vh,back}^{R}}{A^{1/2}} = \frac{1}{N}\sum_{n=1}^{N} S_{\beta\alpha,n,back}^{NMM3D} = \frac{1}{N}\sum_{n=1}^{N}\sqrt{\frac{1}{2\eta P_{\alpha}^{inc}}cos\theta_i}E_{\beta\alpha,n}^{incoh,NMM3D} \tag{4.3.397}$$

Where

$$S_{\beta\alpha,n,back}^{NMM3D} = \sqrt{\frac{1}{2\eta P_{\alpha}^{inc}}cos\theta_i}E_{\beta\alpha,n}^{incoh,NMM3D} \tag{4.3.398}$$

Then

$$\frac{\langle S_{vv,back}^{RV} S_{hh,back}^{RV*}\rangle}{A}$$

$$= e^{2i[Re(k_{ivz})-Re(k_{ihz})+iIm(k_{ivz})+iIm(k_{ihz})]d}\frac{1}{N}\sum_{n=1}^{N} S_{vv,n,back}^{NMM3D} S_{hh,n,back}^{NMM3D\ *} \tag{4.3.399}$$

$$\frac{\langle S_{vv,back}^{RV} S_{vv,back}^{RV*}\rangle}{A} = e^{-4Im(k_{ivz})d}\frac{1}{N}\sum_{n=1}^{N} S_{vv,n,back}^{NMM3D} S_{vv,n,back}^{NMM3D\ *} \tag{4.3.400}$$

$$\frac{\langle S_{hh,back}^{RV} S_{hh,back}^{RV*}\rangle}{A} = e^{-4Im(k_{ihz})d}\frac{1}{N}\sum_{n=1}^{N} S_{hh,n,back}^{NMM3D} S_{hh,n,back}^{NMM3D\ *} \tag{4.3.401}$$

$$\frac{\langle S_{vv,back}^{RV} S_{vh,back}^{RV*}\rangle}{A} = e^{i[Re(k_{ivz})-Re(k_{ihz})+3iIm(k_{ivz})+iIm(k_{ihz})]d}\frac{1}{N}\sum_{n=1}^{N} S_{vv,n,back}^{NMM3D} S_{vh,n,back}^{NMM3D\ *} \tag{4.3.402}$$

$$\frac{\langle S_{hh,back}^{RV} S_{vh,back}^{RV*}\rangle}{A}$$

$$= e^{i[Re(k_{ihz})-Re(k_{ivz})+3iIm(k_{ihz})+iIm(k_{ivz})]d}\frac{1}{N}\sum_{n=1}^{N} S_{hh,n,back}^{NMM3D} S_{vh,n,back}^{NMM3D\ *} \tag{4.3.403}$$

$$\frac{\langle S_{vh,back}^{RV} S_{vh,back}^{RV*}\rangle}{A} = e^{-2[Im(k_{ivz})+Im(k_{ihz})]d}\frac{1}{N}\sum_{n=1}^{N} S_{vh,n,back}^{NMM3D} S_{vh,n,back}^{NMM3D\ *} \tag{4.3.404}$$

Next, let's correlate four coherency terms to the backscattering coefficients, σ_{pq}^0. The scattering cross section is determined by incident and scattered electric fields.

$$\gamma_{\beta\alpha}(\theta_s,\phi_s;\theta_i,\phi_i) = \lim_{r\to\infty}\frac{4\pi r^2\left|E_\beta^s\right|^2}{A\cos\theta_i\left|E_\alpha^i\right|^2} \tag{4.3.405}$$

$$\sigma_{pq}^0(\theta_i,\phi_i) = \cos\theta_i\,\gamma_{\beta\alpha}(\theta_i,\pi+\phi_i;\theta_i,\phi_i) \tag{4.3.406}$$

$$\sigma_{pq}^0(\theta_i,\phi_i) = \lim_{r\to\infty}\frac{4\pi r^2\left|E_\beta^s\right|^2}{A\left|E_\alpha^i\right|^2} \tag{4.3.407}$$

If we use the scattering matrix to represent, it is

$$\sigma_{pq}^0(\theta_i,\phi_i) = 4\pi\frac{\langle\left|S_{pq,back}\right|^2\rangle}{A} \tag{4.3.408}$$

Note both expressions are dimensionless. This expression is suitable for volume, double bounce, and surface scattering.

For the terms with angular brackets in volume scattering and double bounce scattering, we consider the ensemble average over the particle distributions. For the vegetation, scatterers are usually described by simple geometry such as cylinders and disks. Then to describe the dielectric cylinders and disks we need the following parameters.

Cylinder parameters	**Disk parameters**
Radius	Radius
Length	Thickness
Dielectric constant	Dielectric constant

Elevation angle, α	Elevation angle, α
Azimuthal angle, β	Azimuthal angle, β

For a given biomass described by vegetation water content (VWC), we can infer the geometrical parameters with specified geometry. Take wheat for example, we can use just cylinders to describe it. Once the radius, length, and dielectric constant are computed, we consider these cylinders distributed over certain orientation range described by elevation and azimuthal angles with respect to the axial direction of the cylinder. The angle distribution is $p(\alpha,\beta)$. Cylinders are distributed with α between 0 and 2π and β between β_1 and β_2. Then consider α and β are independent to each other. Also, the distribution is uniform in α and has a sinusoidal distribution in β.

$$p(\alpha,\beta) = p(\alpha)p(\beta) \qquad for\ 0 \le \alpha < 2\pi, \beta_1 \le \beta < \beta_2 \tag{4.3.409}$$

$$p(\alpha) = \frac{1}{2\pi} \qquad for\ 0 \le \alpha < 2\pi \tag{4.3.410}$$

$$p(\beta) = \frac{1}{C}\sin^{\zeta}\beta\cos^{\gamma}\beta \quad for\ \beta_1 \le \beta < \beta_2 \tag{4.3.411}$$

The normalization factor C_β is calculated numerically for the given ζ and γ.

$$C_\beta = \int_{\beta_1}^{\beta_2} \sin^{\zeta}\beta\cos^{\gamma}\beta\, d\beta \tag{4.3.412}$$

Note this is a special form compared to the uniform distribution over solid angle shown in [34 pp.313] with $\zeta = 1$ and $\gamma = 0$.

$$p(\alpha,\beta) = \frac{1}{C_\beta}\frac{\sin^{\zeta}\beta\cos^{\gamma}\beta}{2\pi} \qquad for\ 0 \le \alpha < 2\pi, \beta_1 \le \beta < \beta_2 \tag{4.3.413}$$

Then for the coherency matrix element, a general form of ensemble average we need to deal with is

$$\langle f_{pq} f^*_{p'q'}\rangle_{\alpha,\beta} = \int_{\beta_1}^{\beta_2} d\beta \int_0^{2\pi} d\alpha\, f_{pq}(\alpha,\beta) f^*_{p'q'}(\alpha,\beta) p(\alpha,\beta) \tag{4.3.414}$$

p, q, p', q'represent the polarizations, either v or h. f_{pq} and $f^*_{p'q'}$ come from the same geometrical parameters as well as dielectric constant, however they can come from different incident and

scattering angles. To further simplify

$$\langle f_{pq} f^*_{p'q'} \rangle_{\alpha,\beta} = \frac{1}{2\pi}\frac{1}{C_\beta}\int_{\beta_1}^{\beta_2} d\beta \sin^\zeta \beta \cos^\gamma \beta \int_0^{2\pi} d\alpha \, f_{pq}(\alpha,\beta) f^*_{p'q'}(\alpha,\beta) \qquad (4.3.415)$$

For the integration of α and β, we use Gauss-Legendre Quadrature. The general form of N-points Gauss-Lengendre Quadrature is

$$\int_{-1}^{1} dx \, f(x) = \sum_{i=1}^{N} w_i f(x_i) \qquad (4.3.416)$$

Consider the following general form of integration from a to b instead of -1 to 1.

$$\int_a^b dx \, f(x) \qquad (4.3.417)$$

Let

$$x = a + \frac{b-a}{2}(x'+1) = \frac{b-a}{2}x' + \frac{b+a}{2} \qquad (4.3.418)$$

Then

$$dx = \frac{b-a}{2}dx' \qquad (4.3.419)$$

$$\int_a^b dx \, f(x) = \frac{b-a}{2}\int_{-1}^{1} dx' \, f\left(\frac{b-a}{2}x' + \frac{b+a}{2}\right)$$

$$= \frac{b-a}{2}\sum_{i=1}^{N} w_i f\left(\frac{b-a}{2}x_i' + \frac{b+a}{2}\right) \quad ; \quad x_i' \in [-1,1] \qquad (4.3.420)$$

For 8-points Gauss-Lengendre Quadrature

x_i	w_i
± 0.183434642495650	0.362683783378362
± 0.525532409916329	0.313706645877887
± 0.796666477413627	0.222381034453375
± 0.960289856497536	0.101228536290376

For 16-points Gauss-Lengendre Quadrature

x_i	w_i
$\pm$0.095012509837637	0.189450610455068
$\pm$0.281603550779259	0.182603415044925
$\pm$0.458016777657227	0.169156519395003
$\pm$0.617876244402644	0.149595988816576
$\pm$0.755404408355003	0.124628971255534
$\pm$0.865631202387832	0.095158511682493
$\pm$0.944575023073233	0.062253523938647
$\pm$0.989400934991650	0.027152459411755

Depending on the smoothness of the scattering pattern over α and β, we can choose different number of points to do the numerical integration. Smoother pattern requires less points to get converged.

4.4 Interferometric SAR polarimetry for vegetated surface

Based on the derivation of coherency matrix of polarimetric SAR in 4.2 for volume scattering, double bounce scattering, and surface scattering, next we further derive the coherency matrix for interferometric SAR.

To calculate the coherency matrix element we consider two scattering elements from two slightly different incident angles.

4.4.1 Volume scattering

$S_{vv(1)}^{(vol)}$ comes from angle 1 ; $S_{hh(2)}^{(vol)}$ comes from angle 2. Two angles are close so that it makes no difference for scattering amplitude. The only difference is the phase. Recall from the scattering matrix element from (4.3.93)~(4.3.96) for volume scattering. We now assume the backscattering. $\theta_s = \theta_i$ and $\phi_s = \pi + \phi_i$

$$S_{hv}^{(vol)} = \sum_{j=1}^{N} e^{-i(\bar{k}_h - \bar{K}_{iv})\cdot\bar{r}_j} f_{hv}(\theta_i, \pi + \phi_i; \pi - \theta_i, \phi_i) \tag{4.4.1}$$

$$S_{vv}^{(vol)} = \sum_{j=1}^{N} e^{-i(\bar{k}_v - \bar{K}_{iv})\cdot\bar{r}_j} f_{vv}(\theta_i, \pi + \phi_i; \pi - \theta_i, \phi_i) \tag{4.4.2}$$

$$S_{hh}^{(vol)} = \sum_{j=1}^{N} e^{-i(\bar{k}_h - \bar{K}_{ih})\cdot\bar{r}_j} f_{hh}(\theta_i, \pi + \phi_i; \pi - \theta_i, \phi_i) \tag{4.4.3}$$

$$S_{vh}^{(vol)} = \sum_{j=1}^{N} e^{-i(\bar{k}_v - \bar{K}_{ih})\cdot\bar{r}_j} f_{vh}(\theta_i, \pi + \phi_i; \pi - \theta_i, \phi_i) \tag{4.4.4}$$

Then we consider correlation of scattering matrix elements from two slightly different angles.

$\langle S_{vv(1)}^{(vol)} S_{hh(2)}^{(vol)*} \rangle$

$$= \langle \sum_{j=1}^{N} e^{-i\left(\bar{k}_v(\theta_{1i}) - \bar{K}_{iv}(\theta_{1i})\right)\cdot\bar{r}_j} f_{vv,j}(\theta_i, \pi + \phi_i; \pi - \theta_i, \phi_i) \sum_{p=1}^{N} e^{i\left(\bar{k}_h^*(\theta_{2i}) - \bar{K}_{ih}^*(\theta_{2i})\right)\cdot\bar{r}_p} f_{hh,p}^*(\theta_i, \pi + \phi_i; \pi - \theta_i, \phi_i) \rangle \tag{4.4.5}$$

Note $\theta_i \sim \theta_{1i} \sim \theta_{2i}$

Here we ignore the correlation between scatterers and consider independent scattering.

$\langle S_{vv}^{(vol)} S_{hh}^{(vol)*} \rangle$

$$= \sum_{j=1}^{N} \langle e^{-i\left(\bar{k}_v(\theta_{1i}) - \bar{K}_{iv}(\theta_{1i})\right)\cdot\bar{r}_j} e^{i\left(\bar{k}_h^*(\theta_{2i}) - \bar{K}_{ih}^*(\theta_{2i})\right)\cdot\bar{r}_j} \rangle \langle f_{vv,j}(\theta_i, \pi + \phi_i; \pi - \theta_i, \phi_i) f_{hh,j}^*(\theta_i, \pi + \phi_i; \pi - \theta_i, \phi_i) \rangle$$

$$= \sum_{j=1}^{N} \frac{1}{V} \int d\bar{r}_j \, e^{-i\left(\bar{k}_v(\theta_{1i}) - \bar{K}_{iv}(\theta_{1i})\right)\cdot \bar{r}_j} e^{i\left(\bar{k}_h^*(\theta_{2i}) - \bar{K}_{ih}^*(\theta_{2i})\right)\cdot \bar{r}_j} \langle f_{vv,j}(\theta_i, \pi + \phi_i; \pi - \theta_i, \phi_i) f_{hh,j}^*(\theta_i, \pi + \phi_i; \pi - \theta_i, \phi_i) \rangle$$

$$= \frac{N}{V} \int d\bar{r}' \, e^{-i\left(\bar{k}_v(\theta_{1i}) - \bar{K}_{iv}(\theta_{1i})\right)\cdot \bar{r}'} e^{i\left(\bar{k}_h^*(\theta_{2i}) - \bar{K}_{ih}^*(\theta_{2i})\right)\cdot \bar{r}'} \langle f_{vv}(\theta_i, \pi + \phi_i; \pi - \theta_i, \phi_i) f_{hh}^*(\theta_i, \pi + \phi_i; \pi - \theta_i, \phi_i) \rangle$$

$$= n_0 \int d\bar{r}' \, e^{-i\left[\left(\bar{k}_v(\theta_{1i}) - \bar{K}_{iv}(\theta_{1i})\right) - \left(\bar{k}_h^*(\theta_{2i}) - \bar{K}_{ih}^*(\theta_{2i})\right)\right]\cdot \bar{r}'} \langle f_{vv}(\theta_i, \pi + \phi_i; \pi - \theta_i, \phi_i) f_{hh}^*(\theta_i, \pi + \phi_i; \pi - \theta_i, \phi_i) \rangle \quad (4.4.6)$$

In the backscattering direction, we consider $\theta_s = \theta_i; \phi_i = 0; \phi_s = \pi$

$$\bar{k}_v(\theta_{1i}) = -k \sin\theta_{1i}\, \hat{x} + k_{ivz}(\theta_{1i})\, \hat{z} = -k \sin\theta_{1i}\, \hat{x} + \left(Re(k_{ivz}) + i\, Im(k_{ivz})\right) \hat{z} \quad (4.4.7)$$

$$\bar{K}_{iv}(\theta_{1i}) = k \sin\theta_{1i}\, \hat{x} - k_{ivz}(\theta_{1i})\, \hat{z} = k \sin\theta_{1i}\, \hat{x} - \left(Re(k_{ivz}) + i\, Im(k_{ivz})\right) \hat{z} \quad (4.4.8)$$

$$\bar{k}_v(\theta_{1i}) - \bar{K}_{iv}(\theta_{1i}) = -2k \sin\theta_{1i}\, \hat{x} + 2k_{ivz}(\theta_{1i})\, \hat{z}$$

$$= -2k \sin\theta_{1i}\, \hat{x} + 2\left(Re(k_{ivz}) + i\, Im(k_{ivz})\right) \hat{z} \quad (4.4.9)$$

Note

$$k_{ivz}(\theta_{1i}) = \sqrt{k_v^2 - k^2 \sin^2\theta_{1i}} = Re(k_{ivz}) + i\, Im(k_{ivz}) \quad (4.4.10)$$

Also

$$\bar{k}_h(\theta_{2i}) = -k \sin\theta_{2i}\, \hat{x} + k_{ihz}(\theta_{2i})\, \hat{z} = -k \sin\theta_{2i}\, \hat{x} + \left(Re(k_{ihz}) + i\, Im(k_{ihz})\right) \hat{z} \quad (4.4.11)$$

$$\bar{K}_{ih}(\theta_{2i}) = k \sin\theta_{2i}\, \hat{x} - k_{ihz}(\theta_{2i})\, \hat{z} = k \sin\theta_{2i}\, \hat{x} - \left(Re(k_{ihz}) + i\, Im(k_{ihz})\right) \hat{z} \quad (4.4.12)$$

$$\bar{k}_h(\theta_{2i}) - \bar{K}_{ih}(\theta_{2i}) = -2k \sin\theta_{2i}\, \hat{x} + 2k_{ihz}(\theta_{2i})\, \hat{z}$$

$$= -2k \sin\theta_{2i}\, \hat{x} + 2\left(Re(k_{ihz}) + i\, Im(k_{ihz})\right) \hat{z} \quad (4.4.13)$$

Note

$$k_{ihz}(\theta_{2i}) = \sqrt{k_h^2 - k^2 \sin^2\theta_{2i}} = Re(k_{ihz}) + i\, Im(k_{ihz}) \quad (4.4.14)$$

$$\bar{k}_h^*(\theta_{2i}) - \bar{K}_{ih}^*(\theta_{2i}) = -2k \sin\theta_{2i}\, \hat{x} + 2\left(Re(k_{ihz}) - i\, Im(k_{ihz})\right) \hat{z} \quad (4.4.15)$$

Then

$$\left(\bar{k}_v(\theta_{1i}) - \bar{K}_{iv}(\theta_{1i})\right) - \left(\bar{k}_h^*(\theta_{2i}) - \bar{K}_{ih}^*(\theta_{2i})\right)$$

$$= -2k\sin\theta_{1i}\,\hat{x} + 2\left(Re(k_{ivz}) + i\,Im(k_{ivz})\right)\hat{z} + 2k\sin\theta_{2i}\,\hat{x} - 2\left(Re(k_{ihz}) - i\,Im(k_{ihz})\right)\hat{z}$$

$$= 2[-k\sin\theta_{1i} + k\sin\theta_{2i}]\hat{x} + 2\left(Re(k_{ivz}) + i\,Im(k_{ivz})\right)\hat{z}$$

$$-2\left(Re(k_{ihz}) - i\,Im(k_{ihz})\right)\hat{z} \qquad (4.4.16)$$

The key is the two scattering matrix elements also come with slightly different frequency to cancel the phase shift in the horizontal direction. This is also a range spectral filtering in the horizontal direction.

$$\left(\bar{k}_{v1}(\theta_{1i}) - \bar{K}_{iv1}(\theta_{1i})\right) - \left(\bar{k}_{h2}^*(\theta_{2i}) - \bar{K}_{ih2}^*(\theta_{2i})\right)$$

$$= 2[-k_1\sin\theta_{1i} + k_2\sin\theta_{2i}]\hat{x} + 2\left(Re(k_{ivz1}) + i\,Im(k_{ivz1})\right)\hat{z}$$

$$-2\left(Re(k_{ihz2}) - i\,Im(k_{ihz2})\right)\hat{z} \qquad (4.4.17)$$

Let the phase shift in the horizontal direction to be zero.

$$-k_1\sin\theta_{1i}\,\hat{x} + k_2\sin\theta_{2i} = 0$$

$$-\omega_1\sqrt{\mu\epsilon}\sin\theta_{1i} + \omega_2\sqrt{\mu\epsilon}\sin(\theta_{1i} + \Delta\theta) = 0$$

$$-\omega_1\sqrt{\mu\epsilon}\sin\theta_{1i} + \omega_2\sqrt{\mu\epsilon}\sin\theta_{1i}\cos\Delta\theta + \omega_2\sqrt{\mu\epsilon}\cos\theta_{1i}\sin\Delta\theta = 0$$

For small increment of $\Delta\theta$

$$\Delta\theta \sim \sin\Delta\theta$$

Then

$$-\omega_1\sqrt{\mu\epsilon}\sin\theta_{1i} + \omega_2\sqrt{\mu\epsilon}\sin\theta_{1i} + \Delta\theta\,\omega_2\sqrt{\mu\epsilon}\cos\theta_{1i} = 0$$

$$\frac{(\omega_1 - \omega_2)}{\omega_2} = \frac{\Delta\theta}{\tan\theta_{1i}} \qquad (4.4.18)$$

Let $\omega_1 - \omega_2 = \Delta\omega$, also $\theta_{1i} \sim \theta_{2i} \sim \theta_i$; $\omega_1 \sim \omega_2 \sim \omega$

$$\Delta\omega = \omega\frac{\Delta\theta}{\tan\theta_i} \qquad (4.4.19)$$

For the given difference in incident angle, we can find the corresponding frequency offset to cancel the horizontal phase shift. So far the difference in frequency and incident angle only affect

the phase. Now we have only phase shift in z direction

$$\left(\bar{k}_{v1}(\theta_{1i}) - \bar{K}_{iv1}(\theta_{1i})\right) - \left(\bar{k}^*_{h2}(\theta_{2i}) - \bar{K}^*_{ih2}(\theta_{2i})\right) = 2\left(k_{ivz1}(\theta_{1i}) - k^*_{ihz2}(\theta_{2i})\right)\hat{z}$$

$$= 2\left(Re\left(k_{ivz1}(\theta_{1i})\right) + i\, Im\left(k_{ivz1}(\theta_{1i})\right)\right)\hat{z} - 2\left(Re\left(k_{ihz2}(\theta_{2i})\right) - i\, Im\left(k_{ihz2}(\theta_{2i})\right)\right)\hat{z} \quad (4.4.20)$$

Then the real part gives the phase shift, $2\left(Re\left(k_{ivz1}(\theta_{1i})\right) - Re\left(k_{ihz2}(\theta_{2i})\right)\right)$

From the effective medium we have effective propagation constants for both vertical polarization and horizontal polarization.

$$k_{pz} = k\cos\theta_0 + Re\left(\frac{2\pi n_0\langle f_{pp}(\theta,\phi;\theta,\phi)\rangle}{k\cos\theta_0}\right) + iIm\left(\frac{2\pi n_0\langle f_{pp}(\theta,\phi;\theta,\phi)\rangle}{k\cos\theta_0}\right)$$

$$= k\cos\theta_0 + \frac{2\pi n_0\langle f_{pp}(\theta,\phi;\theta,\phi)\rangle}{k\cos\theta_0} \quad (4.4.20)$$

Then

$$Re\left(k_{pz}\right) = k\cos\theta_0 + Re\left(\frac{2\pi n_0\langle f_{pp}(\theta,\phi;\theta,\phi)\rangle}{k\cos\theta_0}\right) \quad (4.4.21)$$

Then

$$2\left(Re\left(k_{ivz1}(\theta_{1i})\right) - Re\left(k_{ihz2}(\theta_{2i})\right)\right)$$

$$= 2\left(k_1\cos\theta_{1i} + Re\left(\frac{2\pi n_0\langle f_{vv}(\pi-\theta_{1i},\phi_i;\pi-\theta_{1i},\phi_i)\rangle}{k_1\cos\theta_{1i}}\right) - k_2\cos\theta_{2i}\right.$$

$$\left. - Re\left(\frac{2\pi n_0\langle f_{hh}(\pi-\theta_{2i},\phi_i;\pi-\theta_{2i},\phi_i)\rangle}{k_2\cos\theta_{2i}}\right)\right)$$

$$= 2(k_1\cos\theta_{1i} - k_2\cos\theta_{2i})$$

$$+Re\left(\frac{4\pi n_0\langle f_{vv}(\pi-\theta_{1i},\phi_i;\pi-\theta_{1i},\phi_i)\rangle}{k_1\cos\theta_{1i}} - \frac{4\pi n_0\langle f_{hh}(\pi-\theta_{2i},\phi_i;\pi-\theta_{2i},\phi_i)\rangle}{k_2\cos\theta_{2i}}\right) \quad (4.4.22)$$

Note that for the free space, we have only the first term

$$2(k_1\cos\theta_{1i} - k_2\cos\theta_{2i})$$

$$= 2(k_1\cos\theta_{1i} - k_2\cos(\theta_{1i}+\Delta\theta))$$

$$= 2\left(\omega_1\sqrt{\mu\epsilon}\cos\theta_{1i} - (\omega_1-\Delta\omega)\sqrt{\mu\epsilon}\cos(\theta_{1i}+\Delta\theta)\right)$$

$$= 2\left(\omega_1\sqrt{\mu\epsilon}\cos\theta_{1i} - (\omega_1 - \Delta\omega)\sqrt{\mu\epsilon}(\cos\theta_{1i}\cos(\Delta\theta) - \sin\theta_{1i}\sin(\Delta\theta))\right)$$

$$\cong 2\left(\omega\sqrt{\mu\epsilon}\cos\theta_i - \left(\omega - \omega\frac{\Delta\theta}{\tan\theta_i}\right)\sqrt{\mu\epsilon}(\cos\theta_i - \Delta\theta\sin\theta_i)\right)$$

$$= 2\left(k\cos\theta_i - k\left(1 - \frac{\Delta\theta}{\tan\theta_i}\right)(\cos\theta_i - \Delta\theta\sin\theta_i)\right)$$

$$= 2\left(k\cos\theta_i - k\cos(\theta_i) + k\,\Delta\theta\sin\theta_i + k\frac{\Delta\theta}{\tan\theta_i}\cos\theta_i - k\frac{(\Delta\theta)^2}{\cos\theta_i}\right)$$

$$\cong 2\left(k\,\Delta\theta\sin\theta_i + k\frac{\Delta\theta}{\tan\theta_i}\cos\theta_i\right) = 2k\Delta\theta\left(\sin\theta_i + \frac{\cos^2\theta_i}{\sin\theta_i}\right) = \frac{2k\Delta\theta}{\sin\theta_i} \qquad (4.4.23)$$

This factor is also vertical sensitivity, β_z,of the interferometer in Cloude's book [52].

$$\beta_z = \frac{4\pi\Delta\theta}{\lambda\sin\theta_i} \qquad (4.4.24)$$

To consider effective medium

$$\beta_{z,eff} = \beta_z + Re\left(\frac{4\pi n_0\langle f_{vv}(\pi - \theta_{1i}, \phi_i; \pi - \theta_{1i}, \phi_i)\rangle}{k_1\cos\theta_{1i}} - \frac{4\pi n_0\langle f_{hh}(\pi - \theta_{2i}, \phi_i; \pi - \theta_{2i}, \phi_i)\rangle}{k_2\cos\theta_{2i}}\right)$$

$$\cong \beta_z + \frac{4\pi n_0}{k\cos\theta_i}Re(\langle f_{vv}(\pi - \theta_i, \phi_i; \pi - \theta_i, \phi_i)\rangle - \langle f_{hh}(\pi - \theta_i, \phi_i; \pi - \theta_i, \phi_i)\rangle) \quad (4.4.25)$$

Let

$$\beta_{zd} = \frac{4\pi n_0}{k\cos\theta_i}Re(\langle f_{vv}(\pi - \theta_i, \phi_i; \pi - \theta_i, \phi_i)\rangle - \langle f_{hh}(\pi - \theta_i, \phi_i; \pi - \theta_i, \phi_i)\rangle) \qquad (4.4.26)$$

$$\beta_{z,eff} = \beta_z + \beta_{zd} \qquad (4.4.27)$$

$$\left(\bar{k}_{v1}(\theta_{1i}) - \bar{K}_{iv1}(\theta_{1i})\right) - \left(\bar{k}^*_{h2}(\theta_{2i}) - \bar{K}^*_{ih2}(\theta_{2i})\right)$$

$$\cong \left[\beta_z + \beta_{zd} + 2i\left(\,Im(k_{ivz}) + \,Im(k_{ihz})\right)\right]\hat{z} \qquad (4.4.28)$$

Then in the backscattering direction

$$\langle S^{(vol)}_{vv,back}S^{(vol)*}_{hh,back}\rangle = n_0\int d\bar{r}'\, e^{-i[\beta_z+\beta_{zd}+2i(\,Im(k_{ivz1})+\,Im(k_{ihz2}))]\hat{z}\cdot\bar{r}'}$$

$$\langle f_{vv}(\theta_i, \pi + \phi_i; \pi - \theta_i, \phi_i)f^*_{hh}(\theta_i, \pi + \phi_i; \pi - \theta_i, \phi_i)\rangle \qquad (4.4.29)$$

$$= n_0 A \int_{-d}^{0} dz' e^{-i[\beta_z + \beta_{zd} + 2i(\, Im(k_{ivz1}) + Im(k_{ihz2}))]z'}$$

$$\langle f_{vv}(\theta_i, \pi + \phi_i; \pi - \theta_i, \phi_i) f_{hh}^{*}(\theta_i, \pi + \phi_i; \pi - \theta_i, \phi_i) \rangle \qquad (4.4.30)$$

Let $f_{vvhh}(z')$ to be the structure function

$$f_{vvhh}(z') = n_0 e^{2(\, Im(k_{ivz1}) + Im(k_{ihz2}))z'}$$

$$\langle f_{vv}(\theta_i, \pi + \phi_i; \pi - \theta_i, \phi_i) f_{hh}^{*}(\theta_i, \pi + \phi_i; \pi - \theta_i, \phi_i) \rangle \qquad (4.4.31)$$

Then

$$\langle S_{vv,back}^{(vol)} S_{hh,back}^{(vol)*} \rangle_{PolInSAR} = A \int_{-d}^{0} dz' e^{-i\beta_z z'} e^{-i\beta_{zd} z'} f_{vvhh}(z') \qquad (4.4.32)$$

Let's compare this with this with the similar correlation in polarimetric SAR derived in 4.2, (same angle with same frequency) [subscript, PolSAR, means the derivation from 4.2]

$$\langle S_{vv}^{(vol)} S_{hh}^{(vol)*} \rangle_{PolSAR} = n_0 \langle f_{vv}(\theta_i, \pi; \pi - \theta_i, 0) f_{hh}^{*}(\theta_i, \pi; \pi - \theta_i, 0) \rangle A$$

$$\int_{-d}^{0} dz' e^{-i2\left(Re(k_{ivz}) - Re(k_{ihz}) + i\left(Im(k_{ivz}) + Im(k_{ihz})\right)\right)z'}$$

$$= A \int_{-d}^{0} dz' e^{-i\beta_{zd} z'} f_{vvhh}(z') \qquad (4.4.33)$$

This clearly shows that in order to cancel the horizontal phase shift by using slightly different frequency and incident angle, we bring in the additional phase factor to the structure function, β_z.

Next one, we examine

$$\langle S_{vv,back}^{(vol)} S_{vv,back}^{(vol)*} \rangle_{PolSAR} = n_0 \langle f_{vv}(\theta_i, \pi; \pi - \theta_i, 0) f_{vv}^{*}(\theta_i, \pi; \pi - \theta_i, 0) \rangle A \int_{-d}^{0} dz' e^{4Im(k_{ivz})z'}$$

$$= A \int_{-d}^{0} dz' \, f_{vvvv}(z') \qquad (4.4.34)$$

The structure function for this correlation is

$$f_{vvvv}(z') = n_0 e^{4Im(k_{ivz})z'} \langle f_{vv}(\theta_i, \pi; \pi - \theta_i, 0) f_{vv}^{*}(\theta_i, \pi; \pi - \theta_i, 0) \rangle \qquad (4.4.35)$$

The only thing we need to do to get the correlation for interferometry is to add the phase shift term to the structure function.

$$\langle S_{vv,back}^{(vol)} S_{vv,back}^{(vol)*} \rangle_{PolSAR} = A \int_{-d}^{0} dz'\, e^{-i\beta_z z'} f_{vvvv}(z') \tag{4.4.36}$$

We can repeat the similar derivation for the other essential terms for volume scattering.

$$\langle S_{hh,back}^{(vol)} S_{hh,back}^{(vol)*} \rangle_{PolSAR} = n_0 \langle f_{hh}(\theta_i, \pi; \pi - \theta_i, 0) f_{hh}^*(\theta_i, \pi; \pi - \theta_i, 0) \rangle A \int_{-d}^{0} dz' e^{4Im(k_{ihz})z'}$$

$$= A \int_{-d}^{0} dz'\, f_{hhhh}(z') \tag{4.4.37}$$

where

$$f_{hhhh}(z') = n_0 \langle f_{hh}(\theta_i, \pi; \pi - \theta_i, 0) f_{hh}^*(\theta_i, \pi; \pi - \theta_i, 0) \rangle e^{4Im(k_{ihz})z'} \tag{4.4.38}$$

$$\langle S_{hh,back}^{(vol)} S_{hh,back}^{(vol)*} \rangle_{PolInSAR} = A \int_{-d}^{0} dz'\, e^{-i\beta_z z'} f_{hhhh}(z') \tag{4.4.39}$$

$$\langle S_{vv,back}^{(vol)} S_{vh,back}^{(vol)*} \rangle_{PolSAR} = n_0 \langle f_{vv}(\theta_i, \pi; \pi - \theta_i, 0) f_{vh}^*(\theta_i, \pi; \pi - \theta_i, 0) \rangle A$$

$$\int_{-d}^{0} dz' e^{-i\left[Re(k_{ivz}) - Re(k_{ihz}) + i\left(3Im(k_{ivz}) + Im(k_{ihz})\right)\right]z'}$$

$$= A \int_{-d}^{0} dz' e^{-i\beta_{zd} z'} f_{vvvh}(z') \tag{4.4.40}$$

where

$$f_{vvvh}(z') = n_0 \langle f_{vv}(\theta_i, \pi; \pi - \theta_i, 0) f_{vh}^*(\theta_i, \pi; \pi - \theta_i, 0) \rangle e^{\left(3Im(k_{ivz}) + Im(k_{ihz})\right)z'} \tag{4.4.41}$$

$$\langle S_{vv,back}^{(vol)} S_{vh,back}^{(vol)*} \rangle_{PolInSAR} = A \int_{-d}^{0} dz' e^{-i\beta_z z'} e^{-i\beta_{zd} z'} f_{vvvh}(z') \tag{4.4.42}$$

$$\langle S_{hh,back}^{(vol)} S_{vh,back}^{(vol)*} \rangle_{PolSAR} = n_0 \langle f_{hh}(\theta_i, \pi; \pi - \theta_i, 0) f_{vh}^*(\theta_i, \pi; \pi - \theta_i, 0) \rangle A$$

$$\int_{-d}^{0} dz' e^{-i\left[-Re(k_{ivz}) + Re(k_{ihz}) + i\left(Im(k_{ivz}) + 3Im(k_{ihz})\right)\right]z'}$$

$$= A \int_{-d}^{0} dz' e^{+i\beta_{zd} z'} f_{hhvh}(z') \quad (4.4.43)$$

Where

$$f_{hhvh}(z') = n_0 \langle f_{hh}(\theta_i, \pi; \pi - \theta_i, 0) f_{vh}^*(\theta_i, \pi; \pi - \theta_i, 0) \rangle e^{(Im(k_{ivz}) + 3Im(k_{ihz}))z'} \quad (4.4.44)$$

$$\langle S_{hh,back}^{(vol)} S_{vh,back}^{(vol)*} \rangle_{PolInSAR} = A \int_{-d}^{0} dz' e^{-i\beta_z z'} e^{+i\beta_{zd} z'} f_{hhvh}(z') \quad (4.4.45)$$

$$\langle S_{vh,back}^{(vol)} S_{vh,back}^{(vol)*} \rangle_{PolSAR} = n_0 \langle f_{vh}(\theta_i, \pi; \pi - \theta_i, 0) f_{vh}^*(\theta_i, \pi; \pi - \theta_i, 0) \rangle A \int_{-d}^{0} dz' e^{[2(Im(k_{ivz}) + Im(k_{ihz}))]z'}$$

$$= A \int_{-d}^{0} dz' f_{vhvh}(z') \quad (4.4.46)$$

Where

$$f_{vhvh}(z') = n_0 \langle f_{vh}(\theta_i, \pi; \pi - \theta_i, 0) f_{vh}^*(\theta_i, \pi; \pi - \theta_i, 0) \rangle e^{[2(Im(k_{ivz}) + Im(k_{ihz}))]z'} \quad (4.4.47)$$

$$\langle S_{vh,back}^{(vol)} S_{vh,back}^{(vol)*} \rangle_{PolInSAR} = A \int_{-d}^{0} dz' e^{-i\beta_z z'} f_{vhvh}(z') \quad (4.4.48)$$

4.4.2 Double Bounce Scattering

Consider we apply the reciprocity for volume-surface interaction and surface-volume interaction, here we only derive volume-surface interaction, 1st kind of double bounce (DB1). We examine the essential phase terms for correlations.

$$\left(\bar{K}_{v1}(\theta_{1i}) - \bar{K}_{iv1}(\theta_{1i})\right) - \left(\bar{K}_{h2}^*(\theta_{2i}) - \bar{K}_{ih2}^*(\theta_{2i})\right) = (-2k_1 \sin\theta_{1i}\, \hat{x}) - (-2k_2 \sin\theta_{2i}\, \hat{x}) = \bar{0} \quad (4.4.49)$$

$$\left(\bar{K}_{v1}(\theta_{1i}) - \bar{K}_{iv1}(\theta_{1i})\right) - \left(\bar{K}_{v2}^*(\theta_{2i}) - \bar{K}_{iv2}^*(\theta_{2i})\right) = (-2k_1 \sin\theta_{1i}\, \hat{x}) - (-2k_2 \sin\theta_{2i}\, \hat{x}) = \bar{0} \quad (4.4.50)$$

$$\left(\overline{K}_{h1}(\theta_{1i}) - \overline{K}_{ih1}(\theta_{1i})\right) - \left(\overline{K}^{*}_{h2}(\theta_{2i}) - \overline{K}^{*}_{ih2}(\theta_{2i})\right)$$

$$= (-2k_1 \sin\theta_{1i}\,\hat{x}) - (-2k_2 \sin\theta_{2i}\,\hat{x}) = \bar{0} \qquad (4.4.51)$$

$$\left(\overline{K}_{v1}(\theta_{1i}) - \overline{K}_{iv1}(\theta_{1i})\right) - \left(\overline{K}^{*}_{v2}(\theta_{2i}) - \overline{K}^{*}_{ih2}(\theta_{2i})\right)$$

$$= (-2k_1 \sin\theta_{1i}\,\hat{x}) + 2k_2 \sin\theta_{2i}\,\hat{x}$$

$$+ \left(Re\left(k_{ivz2}(\theta_{2i})\right) - Re\left(k_{ihz2}(\theta_{2i})\right) - i\left(Im\left(k_{ivz2}(\theta_{2i})\right) - Im\left(k_{ihz2}(\theta_{2i})\right)\right)\right)\hat{z}$$

$$\cong \left(\beta_{zd} - i\left(Im(k_{ivz}) - Im(k_{ihz})\right)\right)\hat{z} \qquad (4.4.52)$$

$$\left(\overline{K}_{v1}(\theta_{1i}) - \overline{K}_{iv1}(\theta_{1i})\right) - \left(\overline{K}^{*}_{h2}(\theta_{2i}) - \overline{K}^{*}_{iv2}(\theta_{2i})\right)$$

$$= \left(-\beta_{zd} - i(Im(k_{ihz}) - Im(k_{ivz}))\right)\hat{z} \qquad (4.4.53)$$

$$\left(\overline{K}_{h1}(\theta_{1i}) - \overline{K}_{ih1}(\theta_{1i})\right) - \left(\overline{K}^{*}_{v2}(\theta_{2i}) - \overline{K}^{*}_{ih2}(\theta_{2i})\right)$$

$$= \left(\beta_{zd} - i\left(Im(k_{ivz}) - Im(k_{ihz})\right)\right)\hat{z} \qquad (4.4.54)$$

$$\left(\overline{K}_{h1}(\theta_{1i}) - \overline{K}_{ih1}(\theta_{1i})\right) - \left(\overline{K}^{*}_{h2}(\theta_{2i}) - \overline{K}^{*}_{iv2}(\theta_{2i})\right)$$

$$= \left(-\beta_{zd} - i(Im(k_{ihz}) - Im(k_{ivz}))\right)\hat{z} \qquad (4.4.55)$$

$$\left(\overline{K}_{v1}(\theta_{1i}) - \overline{K}_{ih1}(\theta_{1i})\right) - \left(\overline{K}^{*}_{v2}(\theta_{2i}) - \overline{K}^{*}_{ih2}(\theta_{2i})\right) = -2i\left(Im(k_{ivz}) - Im(k_{ihz})\right)\hat{z} \qquad (4.4.56)$$

$$\left(\overline{K}_{v1}(\theta_{1i}) - \overline{K}_{ih1}(\theta_{1i})\right) - \left(\overline{K}^{*}_{h2}(\theta_{2i}) - \overline{K}^{*}_{iv2}(\theta_{2i})\right) = -2\beta_{zd}\hat{z} \qquad (4.4.57)$$

$$\left(\overline{K}_{h1}(\theta_{1i}) - \overline{K}_{iv1}(\theta_{1i})\right) - \left(\overline{K}^{*}_{h2}(\theta_{2i}) - \overline{K}^{*}_{iv2}(\theta_{2i})\right) = -2i\left(Im(k_{ihz}) - Im(k_{ivz})\right)\hat{z} \qquad (4.4.58)$$

$$\left(\overline{K}_{h1}(\theta_{1i}) - \overline{K}_{iv1}(\theta_{1i})\right) - \left(\overline{K}^{*}_{v2}(\theta_{2i}) - \overline{K}^{*}_{ih2}(\theta_{2i})\right) = 2\beta_{zd}\hat{z} \qquad (4.4.59)$$

Apparently, all the phase terms involved in the integration are the same as those in the derivation for polarimetry in 4.2. The other phase terms come from the round trip in the vegetation layer, those outside the integration.

$$k_{ivz1}(\theta_{1i}) - k^{*}_{ihz2}(\theta_{2i}) \cong \beta_z + \beta_{zd} + i\left(\, Im(k_{ivz}) + \, Im(k_{ihz})\right) \qquad (4.4.60)$$

$$k_{ivz1}(\theta_{1i}) - k^{*}_{ivz2}(\theta_{2i}) \cong \beta_z + 2iIm(k_{ivz}) \qquad (4.4.61)$$

$$k_{ihz1}(\theta_{1i}) - k^{*}_{ihz2}(\theta_{2i}) \cong \beta_z + 2iIm(k_{ihz}) \qquad (4.4.62)$$

$$k_{ihz1}(\theta_{1i}) - k^*_{ivz2}(\theta_{2i}) \cong \beta_z - \beta_{zd} + i\big(\, Im(k_{ihz}) + \, Im(k_{ivz})\big) \tag{4.4.63}$$

Then

$$\langle S^{(DB1)}_{vv,back} S^{(DB1)*}_{hh,back}\rangle_{PolSAR} = n_0 A d R_{vi} {R_{hi}}^* e^{2i\beta_{zd}d} e^{-2\left(\, Im(k_{ivz}) + Im(k_{ihz})\right)d}$$

$$\langle f_{vv}(\pi-\theta_i,\pi;\pi-\theta_i,0) f^*_{hh}(\pi-\theta_i,\pi;\pi-\theta_i,0)\rangle \tag{4.4.64}$$

$$\langle S^{(DB1)}_{vv,back} S^{(DB1)*}_{hh,back}\rangle_{PolInSAR} = e^{2i\beta_z d}\langle S^{(DB1)}_{vv,back} S^{(DB1)*}_{hh,back}\rangle_{PolSAR} \tag{4.4.65}$$

$$\langle S^{(DB1)}_{vv,back} S^{(DB1)*}_{vv,back}\rangle_{PolSAR}$$

$$= n_0 A d R_{vi} {R_{vi}}^* e^{-4Im(k_{ivz})d}\langle f_{vv}(\pi-\theta_i,\pi;\pi-\theta_i,0) f^*_{vv}(\pi-\theta_i,\pi;\pi-\theta_i,0)\rangle \tag{4.4.66}$$

$$\langle S^{(DB1)}_{vv,back} S^{(DB1)*}_{vv,back}\rangle_{PolInSAR} = e^{2i\beta_z d}\langle S^{(DB1)}_{vv,back} S^{(DB1)*}_{vv,back}\rangle_{PolSAR} \tag{4.4.67}$$

$$\langle S^{(DB1)}_{hh,back} S^{(DB1)*}_{hh,back}\rangle_{PolSAR}$$

$$= n_0 A d R_{hi} {R_{hi}}^* e^{-4Im(k_{ihz})d}\langle f_{hh}(\pi-\theta_i,\pi;\pi-\theta_i,0) f^*_{hh}(\pi-\theta_i,\pi;\pi-\theta_i,0)\rangle \tag{4.4.68}$$

$$\langle S^{(DB1)}_{hh,back} S^{(DB1)*}_{hh,back}\rangle_{PolInSAR} = e^{2i\beta_z d}\langle S^{(DB1)}_{hh,back} S^{(DB1)*}_{hh,back}\rangle_{PolSAR} \tag{4.4.69}$$

$$\langle S^{(DB1)}_{vv,back} S^{(DB1)*}_{vh,back}\rangle_{PolSAR} = A n_0 R_{vi} {R_{vi}}^* e^{-4Im(k_{ivz})d} \int_{-d}^{0} dz' e^{-i\beta_{zd}z'} e^{-\left(Im(k_{ivz}) - Im(k_{ihz})\right)z'}$$

$$\langle f_{vv}(\pi-\theta_i,\pi;\pi-\theta_i,0) f^*_{vh}(\pi-\theta_i,\pi;\pi-\theta_i,0)\rangle \tag{4.4.70}$$

$$\langle S^{(DB1)}_{vv,back} S^{(DB1)*}_{vh,back}\rangle_{PolInSAR} = e^{2i\beta_z d}\langle S^{(DB1)}_{vv,back} S^{(DB1)*}_{vh,back}\rangle_{PolSAR} \tag{4.4.71}$$

$$\langle S^{(DB1)}_{vv,back} S^{(DB1)*}_{hv,back}\rangle_{PolSAR}$$

$$= n_0 A R_{vi} R^*_{hi} e^{2i\beta_{zd}d} e^{-2\left(\, Im(k_{ivz}) + Im(k_{ihz})\right)d} \int_{-d}^{0} dz' e^{i\beta_{zd}z'} e^{-(Im(k_{ihz}) - Im(k_{ivz}))z'}$$

$$\langle f_{vv}(\pi-\theta_i,\pi;\pi-\theta_i,0) f^*_{hv}(\pi-\theta_i,\pi;\pi-\theta_i,0)\rangle \tag{4.4.72}$$

$$\langle S^{(DB1)}_{vv,back} S^{(DB1)*}_{hv,back}\rangle_{PolInSAR} = e^{2i\beta_z d}\langle S^{(DB1)}_{vv,back} S^{(DB1)*}_{hv,back}\rangle_{PolSAR} \tag{4.4.73}$$

$$\langle S_{hh,back}^{(DB1)} S_{vh,back}^{(DB1)*} \rangle_{PolSAR}$$

$$= n_0 A R_{hi} {R_{vi}}^* e^{-2i\beta_{zd} d} e^{-2(\, Im(k_{ihz}) + Im(k_{ivz}))d} \int_{-d}^{0} dz' e^{-2(Im(k_{ivz}) - Im(k_{ihz}))z'}$$

$$\langle f_{hh}(\pi - \theta_i, \pi; \pi - \theta_i, 0) f_{vh}^*(\pi - \theta_i, \pi; \pi - \theta_i, 0) \rangle \quad (4.4.74)$$

$$\langle S_{hh,back}^{(DB1)} S_{vh,back}^{(DB1)*} \rangle_{PolInSAR} = e^{2i\beta_z d} \langle S_{hh,back}^{(DB1)} S_{vh,back}^{(DB1)*} \rangle_{PolSAR} \quad (4.4.75)$$

$$\langle S_{hh,back}^{(DB1)} S_{hv,back}^{(DB1)*} \rangle_{PolSAR} = n_0 R_{hi} R_{hi}^* e^{-4Im(k_{ihz})d} A \int_{-d}^{0} dz' e^{i\beta_{zd} z'} e^{-(Im(k_{ihz}) - Im(k_{ivz}))z'}$$

$$\langle f_{hh}(\pi - \theta_i, \pi; \pi - \theta_i, 0) f_{hv}^*(\pi - \theta_i, \pi; \pi - \theta_i, 0) \rangle \quad (4.4.76)$$

$$\langle S_{hh,back}^{(DB1)} S_{hv,back}^{(DB1)*} \rangle_{PolInSAR} = e^{2i\beta_z d} \langle S_{hh,back}^{(DB1)} S_{hv,back}^{(DB1)*} \rangle_{PolSAR} \quad (4.4.77)$$

$$\langle S_{vh,back}^{(DB1)} S_{vh,back}^{(DB1)*} \rangle_{PolSAR} = n_0 A R_{vi} {R_{vi}}^* e^{-4Im(k_{ivz})d} \int_{-d}^{0} dz' e^{-2(Im(k_{ivz}) - Im(k_{ihz}))z'}$$

$$\langle f_{vh}(\pi - \theta_i, \pi; \pi - \theta_i, 0) f_{vh}^*(\pi - \theta_i, \pi; \pi - \theta_i, 0) \rangle \quad (4.4.78)$$

$$\langle S_{vh,back}^{(DB1)} S_{vh,back}^{(DB1)*} \rangle_{PolInSAR} = e^{2i\beta_z d} \langle S_{vh,back}^{(DB1)} S_{vh,back}^{(DB1)*} \rangle_{PolSAR} \quad (4.4.79)$$

$$\langle S_{vh,back}^{(DB1)} S_{hv,back}^{(DB1)*} \rangle_{PolSAR} = n_0 A R_{vi} R_{hi}^* e^{2i\beta_{zd} d} e^{-2(\, Im(k_{ivz}) + Im(k_{ihz}))d} \int_{-d}^{0} dz' e^{2i\beta_{zd} z'}$$

$$\langle f_{vh}(\pi - \theta_i, \pi; \pi - \theta_i, 0) f_{hv}^*(\pi - \theta_i, \pi; \pi - \theta_i, 0) \rangle \quad (4.4.80)$$

$$\langle S_{vh,back}^{(DB1)} S_{hv,back}^{(DB1)*} \rangle_{PolInSAR} = e^{2i\beta_z d} \langle S_{vh,back}^{(DB1)} S_{hv,back}^{(DB1)*} \rangle_{PolSAR} \quad (4.4.81)$$

$$\langle S_{hv,back}^{(DB1)} S_{hv,back}^{(DB1)*} \rangle_{PolSAR} = n_0 A R_{hi} R_{hi}^* e^{-4Im(k_{ihz})d} \int_{-d}^{0} dz' e^{-2(Im(k_{ihz}) - Im(k_{ivz}))z'}$$

$$\langle f_{hv}(\pi - \theta_i, \pi; \pi - \theta_i, 0) f_{hv}^*(\pi - \theta_i, \pi; \pi - \theta_i, 0) \rangle \quad (4.4.82)$$

$$\langle S_{hv,back}^{(DB1)} S_{hv,back}^{(DB1)*} \rangle_{PolInSAR} = e^{2i\beta_z d} \langle S_{hv,back}^{(DB1)} S_{hv,back}^{(DB1)*} \rangle_{PolSAR} \quad (4.4.83)$$

$$\langle S_{hv,back}^{(DB1)} S_{vh,back}^{(DB1)*} \rangle_{PolSAR} = n_0 A R_{hi} {R_{vi}}^* e^{-2i\beta_{zd} d} e^{-2\left(Im(k_{ihz}) + Im(k_{ivz}) \right) d} \int_{-d}^{0} dz' e^{-i2\beta_{zd} z'}$$

$$\langle f_{hv}(\pi - \theta_i, \pi; \pi - \theta_i, 0) f_{vh}^*(\pi - \theta_i, \pi; \pi - \theta_i, 0) \rangle \quad (4.4.84)$$

$$\langle S_{hv,back}^{(DB1)} S_{vh,back}^{(DB1)*} \rangle_{PolInSAR} = e^{2i\beta_z d} \langle S_{hv,back}^{(DB1)} S_{vh,back}^{(DB1)*} \rangle_{PolSAR} \quad (4.4.85)$$

Note that

$$\langle S_{vh,back}^{(DB1)} S_{hv,back}^{(DB1)*} \rangle_{PolSAR}^* = \langle S_{hv,back}^{(DB1)} S_{vh,back}^{(DB1)*} \rangle_{PolSAR} \quad (4.4.86)$$

$$\langle S_{vh,back}^{(DB1)} S_{hv,back}^{(DB1)*} \rangle_{PolInSAR}^* = e^{-2i\beta_z d} \langle S_{vh,back}^{(DB1)} S_{hv,back}^{(DB1)*} \rangle_{PolSAR}^*$$

$$\neq \langle S_{hv,back}^{(DB1)} S_{vh,back}^{(DB1)*} \rangle_{PolInSAR} \quad (4.4.87)$$

Besides, we also have

$$\langle S_{hh,back}^{(DB1)} S_{vv,back}^{(DB1)*} \rangle_{PolInSAR} = e^{2i\beta_z d} \langle S_{hh,back}^{(DB1)} S_{vv,back}^{(DB1)*} \rangle_{PolSAR} \quad (4.4.88)$$

$$\langle S_{vh,back}^{(DB1)} S_{vv,back}^{(DB1)*} \rangle_{PolInSAR} = e^{2i\beta_z d} \langle S_{vh,back}^{(DB1)} S_{vv,back}^{(DB1)*} \rangle_{PolSAR} \quad (4.4.89)$$

$$\langle S_{vh,back}^{(DB1)} S_{hh,back}^{(DB1)*} \rangle_{PolInSAR} = e^{2i\beta_z d} \langle S_{vh,back}^{(DB1)} S_{hh,back}^{(DB1)*} \rangle_{PolSAR} \quad (4.4.90)$$

Then we find the correlation

$$\langle S_{vv,back}^{(DB)} S_{hh,back}^{(DB)*} \rangle_{PolInSAR} = 4\langle S_{vv,back}^{(DB1)} S_{hh,back}^{(DB1)*} \rangle_{PolInSAR} = 4e^{2i\beta_z d} \langle S_{vv,back}^{(DB1)} S_{hh,back}^{(DB1)*} \rangle_{PolSAR}$$

$$= e^{2i\beta_z d} \langle S_{vv,back}^{(DB)} S_{hh,back}^{(DB)*} \rangle_{PolSAR} \quad (4.4.91)$$

$$\langle S_{vv,back}^{(DB)} S_{vv,back}^{(DB)*} \rangle_{PolInSAR} = 4\langle S_{vv,back}^{(DB1)} S_{vv,back}^{(DB1)*} \rangle_{PolInSAR} = 4e^{2i\beta_z d} \langle S_{vv,back}^{(DB1)} S_{vv,back}^{(DB1)*} \rangle_{PolSAR}$$

$$= e^{2i\beta_z d} \langle S_{vv,back}^{(DB)} S_{vv,back}^{(DB)*} \rangle_{PolSAR} \quad (4.4.92)$$

$$\langle S_{hh,back}^{(DB)} S_{hh,back}^{(DB)*} \rangle_{PolInSAR} = 4\langle S_{hh,back}^{(DB1)} S_{hh,back}^{(DB1)*} \rangle_{PolInSAR} = 4e^{2i\beta_z d} \langle S_{hh,back}^{(DB1)} S_{hh,back}^{(DB1)*} \rangle_{PolSAR}$$

$$= e^{2i\beta_z d} \langle S_{hh,back}^{(DB)} S_{hh,back}^{(DB)*} \rangle_{PolSAR} \quad (4.4.93)$$

$$\langle S_{vv,back}^{(DB)} S_{vh,back}^{(DB)*} \rangle_{PolInSAR} = 2\langle S_{vv,back}^{(DB1)} S_{vh,back}^{(DB1)*} \rangle_{PolInSAR} - 2\langle S_{vv,back}^{(DB1)} S_{hv,back}^{(DB1)*} \rangle_{PolInSAR}$$

$$= 2e^{2i\beta_z d}\langle S_{vv,back}^{(DB1)} S_{vh,back}^{(DB1)*}\rangle_{PolSAR} - 2e^{2i\beta_z d}\langle S_{vv,back}^{(DB1)} S_{hv,back}^{(DB1)*}\rangle_{PolSAR}$$

$$= e^{2i\beta_z d}\langle S_{vv,back}^{(DB)} S_{vh,back}^{(DB)*}\rangle_{PolSAR} \quad (4.4.94)$$

$$\langle S_{hh,back}^{(DB)} S_{vh,back}^{(DB)*}\rangle_{PolInSAR} = 2\langle S_{hh,back}^{(DB1)} S_{vh,back}^{(DB1)*}\rangle_{PolInSAR} - 2\langle S_{hh,back}^{(DB1)} S_{hv,back}^{(DB1)*}\rangle_{PolInSAR}$$

$$= 2e^{2i\beta_z d}\langle S_{hh,back}^{(DB1)} S_{vh,back}^{(DB1)*}\rangle_{PolSAR} - 2e^{2i\beta_z d}\langle S_{hh,back}^{(DB1)} S_{hv,back}^{(DB1)*}\rangle_{PolSAR}$$

$$= e^{2i\beta_z d}\langle S_{hh,back}^{(DB)} S_{vh,back}^{(DB)*}\rangle_{PolSAR} \quad (4.4.95)$$

$$\langle S_{vh,back}^{(DB)} S_{vh,back}^{(DB)*}\rangle_{PolInSAR}$$

$$= \langle S_{vh,back}^{(DB1)} S_{vh,back}^{(DB1)*}\rangle_{PolInSAR} - \langle S_{vh,back}^{(DB1)} S_{hv,back}^{(DB1)*}\rangle_{PolInSAR} - \langle S_{hv,back}^{(DB1)} S_{vh,back}^{(DB1)*}\rangle_{PolInSAR}$$
$$+ \langle S_{hv,back}^{(DB1)} S_{hv,back}^{(DB1)*}\rangle_{PolInSAR}$$

$$= e^{2i\beta_z d}\langle S_{vh,back}^{(DB1)} S_{vh,back}^{(DB1)*}\rangle_{PolSAR} - e^{2i\beta_z d}\langle S_{vh,back}^{(DB1)} S_{hv,back}^{(DB1)*}\rangle_{PolSAR}$$
$$-e^{2i\beta_z d}\langle S_{hv,back}^{(DB1)} S_{vh,back}^{(DB1)*}\rangle_{PolSAR} + e^{2i\beta_z d}\langle S_{hv,back}^{(DB1)} S_{hv,back}^{(DB1)*}\rangle_{PolSAR}$$

$$= e^{2i\beta_z d}\langle S_{vh,back}^{(DB1)} S_{vh,back}^{(DB1)*}\rangle_{PolSAR} - e^{2i\beta_z d} 2Re\left(\langle S_{vh,back}^{(DB1)} S_{hv,back}^{(DB1)*}\rangle\right)$$
$$+e^{2i\beta_z d}\langle S_{hv,back}^{(DB1)} S_{hv,back}^{(DB1)*}\rangle_{PolSAR}$$

$$= e^{2i\beta_z d}\langle S_{vh,back}^{(DB)} S_{vh,back}^{(DB)*}\rangle_{PolSAR} \quad (4.4.96)$$

For the coherency matrix

$$\bar{\bar{T}}_{3,PolInSAR} = \langle \bar{k}(f_1,\theta_{1i})\bar{k}^{\dagger}(f_2,\theta_{2i})\rangle = \begin{bmatrix} \langle k_1 k_1^*\rangle & \langle k_1 k_2^*\rangle & \langle k_1 k_3^*\rangle \\ \langle k_2 k_1^*\rangle & \langle k_2 k_2^*\rangle & \langle k_2 k_3^*\rangle \\ \langle k_3 k_1^*\rangle & \langle k_3 k_2^*\rangle & \langle k_3 k_3^*\rangle \end{bmatrix} \quad (4.4.97)$$

Note that

$$\langle k_m k_n^*\rangle_{PolInSAR} = e^{2i\beta_z d}\langle k_m k_n^*\rangle_{PolSAR} \quad (4.4.98)$$

Then

$$\bar{\bar{T}}_{3,PolInSAR}^{(DB)} = e^{2i\beta_z d}\bar{\bar{T}}_{3,PolSAR}^{(DB)} \quad (4.4.99)$$

4.4.3 Surface Scattering

Recall the correlation from (4.2.373)~(4.2.378)

$$\langle S_{vv,back}^{RV} S_{hh,back}^{RV*} \rangle_{PolSAR} = e^{2i[Re(k_{ivz})-Re(k_{ihz})+iIm(k_{ivz})+iIm(k_{ihz})]d} \langle S_{vv,back}^{R} S_{hh,back}^{R*} \rangle_{PolSAR} \quad (4.4.100)$$

$$\langle S_{vv,back}^{RV} S_{hh,back}^{RV*} \rangle_{PolInSAR} = e^{2i[\beta_z+\beta_{zd}+iIm(k_{ivz})+iIm(k_{ihz})]d} \langle S_{vv,back}^{R} S_{hh,back}^{R*} \rangle_{PolSAR}$$
$$= e^{2i\beta_z d} \langle S_{vv,back}^{RV} S_{hh,back}^{RV*} \rangle_{PolSAR} \quad (4.4.101)$$

$$\langle S_{vv,back}^{RV} S_{vv,back}^{RV*} \rangle_{PolSAR} = e^{-4Im(k_{ivz})d} \langle S_{vv,back}^{R} S_{vv,back}^{R*} \rangle_{PolSAR} \quad (4.4.102)$$

$$\langle S_{vv,back}^{RV} S_{vv,back}^{RV*} \rangle_{PolInSAR} = e^{2i\beta_z d} e^{-4Im(k_{ivz})d} \langle S_{vv,back}^{R} S_{vv,back}^{R*} \rangle_{PolSAR}$$
$$= e^{2i\beta_z d} \langle S_{vv,back}^{RV} S_{vv,back}^{RV*} \rangle_{PolSAR} \quad (4.4.103)$$

$$\langle S_{hh,back}^{RV} S_{hh,back}^{RV*} \rangle_{PolSAR} = e^{-4Im(k_{ihz})d} \langle S_{hh,back}^{R} S_{hh,back}^{R*} \rangle_{PolSAR} \quad (4.4.104)$$

$$\langle S_{hh,back}^{RV} S_{hh,back}^{RV*} \rangle_{PolInSAR} = e^{2i\beta_z d} e^{-4Im(k_{ihz})d} \langle S_{hh,back}^{R} S_{hh,back}^{R*} \rangle_{PolSAR}$$
$$= e^{2i\beta_z d} \langle S_{hh,back}^{RV} S_{hh,back}^{RV*} \rangle_{PolSAR} \quad (4.4.105)$$

$$\langle S_{vv,back}^{RV} S_{vh,back}^{RV*} \rangle_{PolSAR} = e^{i[Re(k_{ivz})-Re(k_{ihz})+3iIm(k_{ivz})+iIm(k_{ihz})]d} \langle S_{vv,back}^{R} S_{vh,back}^{R*} \rangle_{PolSAR} \quad (4.4.106)$$

$$\langle S_{vv,back}^{RV} S_{vh,back}^{RV*} \rangle_{PolInSAR} = e^{2i\beta_z d} e^{i[Re(k_{ivz})-Re(k_{ihz})+3iIm(k_{ivz})+iIm(k_{ihz})]d} \langle S_{vv,back}^{R} S_{vh,back}^{R*} \rangle_{PolSAR}$$
$$= e^{2i\beta_z d} \langle S_{vv,back}^{RV} S_{vh,back}^{RV*} \rangle_{PolSAR} \quad (4.4.107)$$

$$\langle S_{hh,back}^{RV} S_{vh,back}^{RV*} \rangle_{PolSAR} = e^{i[Re(k_{ihz})-Re(k_{ivz})+3iIm(k_{ihz})+iIm(k_{ivz})]d} \langle S_{hh,back}^{R} S_{vh,back}^{R*} \rangle_{PolSAR} \quad (4.4.108)$$

$$\langle S_{hh,back}^{RV} S_{vh,back}^{RV*} \rangle_{PolInSAR} = e^{2i\beta_z d} e^{i[Re(k_{ihz})-Re(k_{ivz})+3iIm(k_{ihz})+iIm(k_{ivz})]d} \langle S_{hh,back}^{R} S_{vh,back}^{R*} \rangle_{PolSAR}$$

$$= e^{2i\beta_z d}\langle S^{RV}_{hh,back} S^{RV*}_{vh,back}\rangle_{PolSAR} \quad (4.4.109)$$

$$\langle S^{RV}_{vh,back} S^{RV*}_{vh,back}\rangle_{PolSAR} = e^{-2[Im(k_{ivz})+Im(k_{ihz})]d}\langle S^{R}_{vh,back} S^{R*}_{vh,back}\rangle_{PolSAR} \quad (4.4.110)$$

$$\langle S^{RV}_{vh,back} S^{RV*}_{vh,back}\rangle_{PolInSAR} = e^{2i\beta_z d} e^{-2[Im(k_{ivz})+Im(k_{ihz})]d}\langle S^{R}_{vh,back} S^{R*}_{vh,back}\rangle_{PolSAR}$$

$$= e^{2i\beta_z d}\langle S^{RV}_{vh,back} S^{RV*}_{vh,back}\rangle_{PolSAR} \quad (4.4.111)$$

Again we notice every correlation term for PolInSAR differs by $e^{2i\beta_z d}$ from those from PolSAR. This is similar that in double bounce scattering. Then for the coherency matrix

$$\bar{\bar{T}}^{(Surf)}_{3,PolInSAR} = e^{2i\beta_z d}\bar{\bar{T}}^{(Surf)}_{3,PolSAR} \quad (4.4.112)$$

4.5 Cross-polarization and polarization ratio comparison for vegetated surface

To calculate coherency matrix at backscattering direction for polarimetry SAR and interferometric SAR, one needs to have accurate cross-polarization. Here we further verify the cross-polarization calculated from physical model of distorted Born approximation and multiple scattering model. Also polarization ratio will be more important as well. Here we show the comparison with data for HH/VV.

Figure 4.13 and Figure 4.14 show the validation of physical model with SMAPVEX12 corn data. This validation comes from the same physical parameters as that in chapter 3, however for VWC<=1, we consider only single scattering. This is because for small optical thickness as VWC is small, the multiple scattering effects are not important. As you can see from the comparison of co-polarization, the results are almost the same. Cross-polarization comparison shows good agreement for both root mean squared error and correlation. The polarization ratio, HH/VV, also shows good agreement.

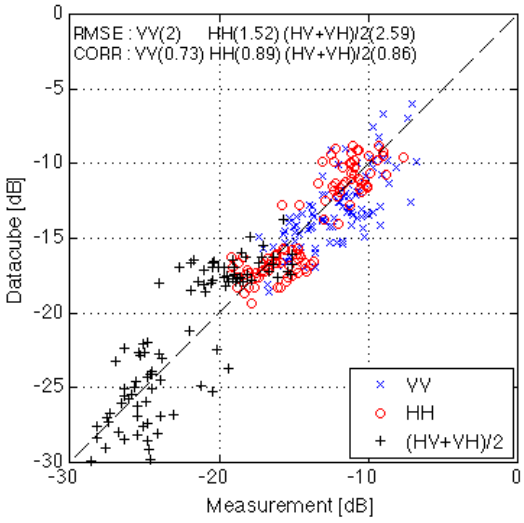

Figure 4.13 Validation of cross- and co-polarization using SMAPVEX12 corn data

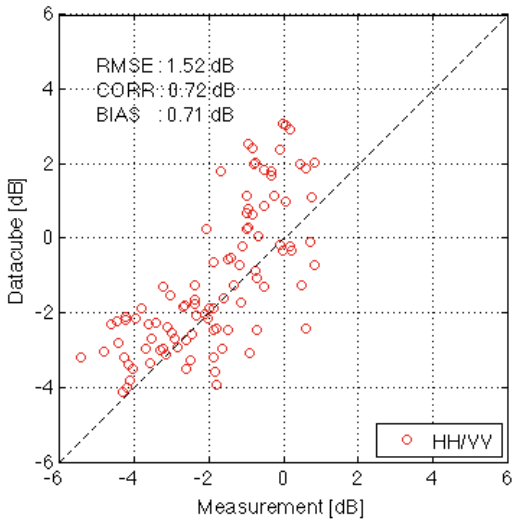

Figure 4.14 Validation of HH/VV using SMAPVEX12 corn data

Figure 4.15 and Figure 4.16 show the validation of physical model with SMAPVEX12 pasture data. Pasture is considered here using distorted Born approximation. Only cylinders are modeled for pasture. The comparison of co- and cross-polarization shows good agreement for both root mean squared error and correlation. The polarization ratio, HH/VV, is also shown with good root mean squared error, the lower correlation is because HH is close VV and the dynamic range is limited.

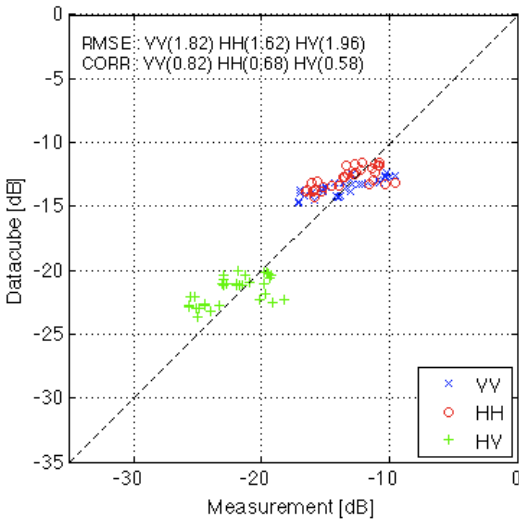

Figure 4.15 Validation of cross- and co-polarization using SMAPVEX12 pasture data

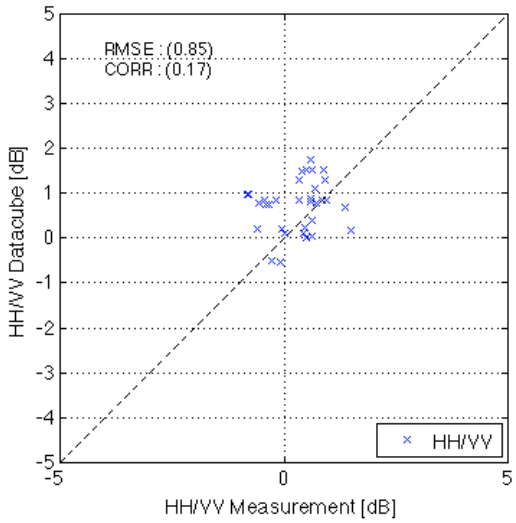

Figure 4.16 Validation of HH/VV using SMAPVEX12 pasture data

Chapter 5

Conclusion

In this thesis, we study the radar backscattering of soil and vegetated surface. Based on the distorted Born approximation and NMM3D, we extend the analysis to compute coherency matrix for polarimetry SAR and interferometry SAR. The cross-polarization and polarization ratio are addressed for their importance for PolSAR and PolIn SAR.

For soil surface, numerical Maxwell Method in 3D (NMM3D) was applied and the study covered L-, C-, X-, and Ku-bands for co- and cross-polarizations as well as polarization ratio. NMM3D is done with large scale computation using parallel computing on NSF XSEDE clusters. The key advancement in this study is the near field precondition. This method speeds up the convergence for the GMRES iterative solver and shorten the simulation time over 10 times for the case shown in chapter 2. To apply NMM3D for multi-angles and multi-frequencies, results from NMM3D were validated with POLARSCAT measurement data for L(1.25GHz), C(4.75GHz), and X(9.5GHz) with incident angles within 20 and 50 degrees. Various models are also included in the validation such as AIEM, SSA, SPM up to 4^{th} order. NMM3D shows good agreement for all 3 frequencies, especially for the cross-polarization. Polarization ratio is finally introduced to point out the frequency dependence of HH/VV, which can be the important index radar backscattering study for land surface. NMM3D shows the best dependence with POLARSCAT data for L-, C-, and X-bands. No dependence phenomenon for SPM is also pointed out due its formulation.

For vegetated surface, multiple scattering effects was studied and applied to physical model for corn fields. With the high optical thickness and high albedo, it is necessary to include multiple scattering effects, otherwise the attenuation will be overestimated and the scattering will be underestimated. The vector radiative transfer equation was formulated with the extinction theorem. The order of multiple scattering can be specified. The algorithm counts the scattering mechanism based on the scattering path. For those with cyclical path, the cyclical correction is applied. The

model is applied to corn field. Corn has thicker stalks which causes large attenuation as well as strong scattering for vertical polarization. In terms of vegetation water content (VWC) during the growth cycle, for large VWC(>1) multiple scattering starts to take effect. Results were validated with measurement data from SMAPVEX12 field campaign. Both co-and cross-polarization are in good agreement. This model is also applied to generate lookup table (datacube) for NASA SMAP mission for soil moisture retrieval. For this reason, we also validate the datacube with soil moisture measurement from SMAPVEX12. Both soil moisture and vegetation water content retrieval are in good agreement.

For the last part of this thesis, we derive the formulas for coherency matrix for vegetated surface applied to polarimetry SAR and interferometric SAR. Results from NMM3D are scattering matrix, however this can be quickly processed to coherency matrix. The speckle phenomenon is studied using NMM3D with results from many realizations. We compare the numerical results with theoretical distributions for PolSAR images. It shows excellent agreement for amplitude, phase difference, and amplitude ratio for L-band(1.26GHz) and C-band(5.4GHz).

Combined with NMM3D and distorted Born approximation, we give out the coherency matrix for 3 scattering mechanisms, including volume scattering, double bounce scattering, and surface scattering. We also correlate these quantity to previous study for radar backscatters. For polarimetry SAR, we consider one angle and one frequency for the correlation of two scattering matrix elements. The analysis of coherency matrix from PolSAR can help land surface classification. For interferometric SAR, we consider two slightly different angles as well as two slightly different frequencies. By doing this, there will be no horizontal phase shift. The vertical phase shift can then be analyzed to see how biomass changes. The correlation between coherency matrix from PolSAR and PolInSAR is also addressed. Correct cross-polarization and polarization ratio will be essential to apply these derivations. More validation for this method is necessary and here we show the validation for corn and pasture fields from SMAPVEX12.

The current study can be extended more to study the physical parameters dependence using coherency matrix from vegetated surface, even break down to the scattering mechanisms. Moreover, with the successful simulations of scattering matrix for bare soil using NMM3D, the study on vegetated surface can also move forward to fully numerical simulation. This will allows us to study the speckle phenomenon of vegetated surface. More interesting research can be conducted in wave rather than the ensembled intensity.

Appendix A

High Performance Computing

We have applied NMM3D extensively on high-performance computing(HPC) facility. For 3D rough surface with 512 by 512 discretized grid points in 2D projection, the surface unknowns involved are more than 1.5 million. NMM3D has been implemented in parallel computing with Message Passing Interface (MPI) which is familiar in HPC community for distributed memory infrastructure. We have run NMM3D on HPC clusters such as XSEDE Darter, Stampede, Trestles, Kraken, etc. Extreme Science and Engineering Discovery Environment (XSEDE) is an integrated service of NSF's high-performance computing and data resources. It provides a single user portal to access these resources. We have been using XSEDE of NSF under the proposal "Large Scale Simulations of Multiple Scattering of Waves in Random Media and Rough Surface" (TG-EAR100002) for the past 5 years. We were awarded 401k SUs on NICS Darter clusters and 1027k SUs on TACC Stampede during 2014. In 2015, our new proposal was awarded 977k SUs on TACC Stampede. Clusters are a set of computers, each equipped with multi-processors CPU and tens GB of memory connected with very high speed local network (LAN). If we consider each computer as a node, the cluster can be viewed as a single system with usually thousands of nodes. For example, TACC Stampede has 6400 nodes. By using MPI, we use many nodes at the same time to run NMM3D for large scale numerical problem. In the same 512 by 512 case, if we request 512 cores to run NMM3D, on Stampede these cores are actually assigned from at least 32 nodes.

Table AppendixA.I

Hardware spec for one node on Stampede

Network	56Gb/s
CPU	Two, 8-core E5-2680 at 2.7GHz
Memory	32GB
Filesystem	14-PB higher performance Lustre file system
Expandability	Space saved for expansion
Coprocessor	Intel Xeon Phi61-core for GPU

Table AppendixA.I shows detail spec for one node on stampede. Network interface is used to connect LAN in extremely high speed to minimize the transmitting delay among nodes. There are 16 processors (cores) for one node at 2.7GHz. There is 32GB memory for one node. We can increase the memory usage for one core by adjusting the request of number of cores for one node. For example, if we request 16 cores per node, we get 2GB memory in average for one core. However, if we request only 4 cores per node, we get 8GB memory in average for one core. This gives us flexibility to calculate problem which require larger memory for single core. Lustre file system is commonly used in cluster to keep very high speed of I/O while computing. On Stampede and some other clusters, there is also an option of running GPU to do parallel computing.

Table AppendixA.II

Realization done on XSEDE(previously TeraGrid) for NMM3D for different looking angle

NMM3D LUT	Realizations Per case	Cases	Total Realizations
40 degree	30,100,200	>170	>7340
20 degree	100	168	16800
30 degree	100	168	16800
50 degree	100	168	16800
5 degree	30	224	6720
10 degree	30	224	6720
17 degree	30	224	6720
55 degree	30	224	6720
		Total	>84620

There is another advantage of running simulation on cluster by exploitation of its high throughput. We usually calculate different combinations of physical parameters to study their dependence. This results in large amount of computation if we consider each with 200 realizations of Monte Carlo simulations. HPC is capable of doing this since all the realizations can be sent out as jobs to run at the same time. This leads to linear reduction in simulation time In Table AppendixA.II, we show part of realizations we have done with NMM3D for remote sensing. Each row corresponds to one looking angle with different parameters combination.

BIBLIOGRAPHY

[1] D. Entekhabi, S. Yueh, et al. SMAP Handbook, NASA Jet Propulsion Laboratory, Jul. 2014.

[2] D. Entekhabi, E.G. Njoku, P.E. O'Neill, K.H. Kellogg, W.T. Crow, W.N. Edelstein, J.K. Entin, S.D. Goodman, T.J. Jackson, J. Johnson, J. Kimball, J.R. Piepmeier, R.D. Koster, N. Martin, K.C. McDonald, M. Moghaddam, S. Moran, R. Reichle, J.C. Shi, M.W. Spencer, S.W. Thurman, L. Tsang, and J. Van Zyl,, " The Soil Moisture Active Passive (SMAP) Mission, " *Proceedings of the IEEE* , vol.98, no.5, pp.704-716, May 2010.

[3] S. O. Rice, "Reflection of electromagnetic waves from slightly rough surfaces." *Communications on Pure and Applied Mathematics*, vol.4, pp.351-378, 1951.

[4] A. Voronovich , "Small-slope approximation for electromagnetic wave scattering at a rough interface of two dielectric half-spaces." *Waves in Random Media*, vol.4, pp.337-367, 1994.

[5] T.-D. Wu, K.-S. Chen, J. Shi, H.-W. Lee, A. K. Fung. "A Study of an AIEM Model for Bistatic Scattering From Randomly Rough Surfaces." *IEEE Transactions on Geoscience and Remote Sensing*, vol.46, pp.2584-2598, 2008.

[6] Y. Oh, K. Sarabandi, F. T. Ulaby. "An empirical model and an inversion technique for radar scattering from bare soil surfaces." *IEEE Transactions on Geoscience and Remote Sensing*, vol.30, pp.370-381, 1992.

[7] Y. Oh, K. Sarabandi, F. T. Ulaby. "Semi-empirical model of the ensemble-averaged differential Mueller matrix for microwave backscattering from bare soil surfaces." *IEEE Transactions on Geoscience and Remote Sensing*, vol.40, pp.1348-1355, 2002.

[8] P. C. Dubois, J. vanZyl, T. Engman. "Corrections to "Measuring Soil Moisture with Imaging Radars". *IEEE Transactions on Geoscience and Remote Sensing*, vol.33, pp.1340, 1995.

[9] J. T. Johnson, L. Tsang, R. T. Shin, K. Pak, C. H. Chan, A. Ishimaru, and Y Kuga, "Backscattering enhancement of electromagnetic waves from two-dimensional perfectly conducting random rough surfaces: Comparison of Monte Carlo simulations with experimental data," *IEEE Transactions on Antennas and Propagation*, vol. 44, pp748-756, May, 1996.

[10] L. Zhou, L. Tsang, V. Jandhyala, Qin Li and C. H. Chan, "Emissivity simulations in passive microwave remote sensing with 3-dimensional numerical solutions of Maxwell equations", *IEEE Transactions on Geoscience and Remote Sensing*, vol. 42, pp. 1739-1748, 2004.

[11] S. Huang, L. Tsang, E. G. Njoku, and K.S. Chen, " Backscattering Coefficients, Coherent Reflectivities, and Emissivities of Randomly Rough Soil Surfaces at L-Band for SMAP Applications Based on Numerical Solutions of Maxwell Equations in Three-Dimensional Simulations, " *IEEE Transactions on Geoscience and Remote Sensing*, vol.48, no.6, pp.2557-2568, June 2010.

[12] S. Huang, and L. Tsang, " Electromagnetic scattering of randomly rough soil surfaces based on numerical solutions of Maxwell equations in 3 dimensional simulations using a hybrid UV/PBTG/SMCG method, " *IEEE Transactions on Geoscience and Remote Sensing*, vol. 50, pp. 4025-4035 , 2012.

[13] D. Xueyang and M. Moghaddam. "3-D Vector Electromagnetic Scattering From Arbitrary Random Rough Surfaces Using Stabilized Extended Boundary Condition Method for Remote

Sensing of Soil Moisture." *IEEE Transactions on Geoscience and Remote Sensing*, vol.50, pp.87-103, 2012.

[14] H. Lawrence, F. Demontoux, J. Wigneron, P. Paillou, Tzong-Dar Wu, Y. H. Kerr. "Evaluation of a Numerical Modeling Approach Based on the Finite-Element Method for Calculating the Rough Surface Scattering and Emission of a Soil Layer. " *IEEE Geoscience and Remote Sensing Letters*, vol.8, pp.953-957, 2011.

[15] S. B. Kim, L. Tsang, J.T. Johnson, S. Huang, J.J. vanZyl, and E.G. Njoku. " Soil moisture retrieval using time series radar observations over bare surfaces, " *IEEE Transactions on Geoscience Remote Sensing* , vol. 50, pp. 1853-1863 , 2012.

[16] S. B. Kim., S. Huang, L. Tsang, J. T. Johnson, E. G. Njoku. "Soil moisture retrieval over low-vegetation surfaces using time-series radar observations and a lookup table representation of forward scattering." *Geoscience and Remote Sensing Symposium (IGARSS), 2011 IEEE International*.

[17] L. Tsang, I.-S. Koh, T.-H. Liao, S. Huang, X. Xu, E. G. Njoku, and Y. H. Kerr. "Active and Passive Vegetated Surface Models With Rough Surface Boundary Conditions From NMM3D." *IEEE Journal of Selected Topics in Applied Earth Observations and Remote Sensing*, vol.6, pp.1698-1709, 2013.

[18] H. Huang, S.B Kim, L. Tsang, X. Xu, T.-H. Liao, T. Jackson, and S. Yueh. "Coherent model of L-band radar scattering by soybean plants : model development, validation, and retrieval" [submitted to IEEE Journal of Selected Topics in Applied Earth Observations and Remote Sensing]

[19] E. K. Miller, A. J. Poggio, G. J. Burke. "An integro-differential equation technique for the time-domain analysis of thin wire structures. I. The numerical method." *Journal of Computational Physics*, vol.12, pp.24-48, 1973.

[20] P. Naenna, and J. T. Johnson, "A Physically-Based Preconditioner for Quasi-Planar Scattering Problems", IEEE Transactions on Antennas and Propagation, vol.56, pp. 2421-2426, 2008.

[21] M. Carr, M. Bleszynski, J. L. Volakis. "A near-field preconditioner and its performance in conjunction with the BiCGstab(ell) solver." *IEEE Antennas and Propagation Magazine*, vol.46, pp.23-30, 2004.

[22] V. L. Mironov, M. C. Dobson, V. H. Kaupp, S. A. Komarov, V. N. Kleshchenko. "Generalized refractive mixing dielectric model for moist soils." *IEEE Transactions on Geoscience and Remote Sensing*, vol.42, pp.773-785, 2004.

[23] K.-S. Chen, L. Tsang, K.-L. Chen, T.-H. Liao, and J.-S. Lee, "Polarimetric Simulations of SAR at L-Band Over Bare Soil Using Scattering Matrices of Random Rough Surfaces From Numerical Three-Dimensional Solutions of Maxwell Equations." *IEEE Transactions on Geoscience and Remote Sensing*,, vol.52, pp.7048-7058, 2014.

[24] L. Tsang, J. A. Kong. *Scattering of Electromagnetic Waves, Vol. 3: Advanced Topics*. New York, Wiley Interscience, 2001.

[25] L. Tsang and A. Ishimaru, "Theory of backscattering enhancement of random discrete isotropic scatterers based on the summation of all ladder and cyclical terms," *J. Opt. Soc. Am. A*, vol. 2, no. 8, pp. 1331-1338, Aug. 1985.

[26] L. Tsang, J. A. Kong and R. T. Shin, *Theory of Microwave Remote Sensing*, Wiley-Interscience, New York, 1985.

[27] Y. Kuga and A. Ishimaru, "Retroreflectance from a dense distribution of spherical particles," *J. Opt. Soc. Am. A,* vol. 1, no. 8, pp. 831-835, Aug. 1984.

[28] L. Tsang and A. Ishimaru, "Backscattering enhancement of random discrete scatterers," *J. Opt. Soc. Am. A,* vol. 1, no. 8, pp. 836-1338, Aug. 1984.

[29] R. H. Lang and J. S. Sidhu, "Electromagnetic backscattering from a layer of vegetation: a discrete approach," *IEEE Trans. Geo. Remote Sensing*, vol. GE-21, no. 1, pp. 62-71, Jan. 1983.

[30] P. Ferrazzoli, L. Guerriero and D. Solimini, "Numerical model of microwave backscattering and emission from terrain covered with vegetation," *Appl. Comput. Electromagn. Soc. J.*, vol. 6, pp. 175-191, 1991.

[31] L. Tsang, J. Pan, D. Liang, Z. Li, D. W. Cline and Y. Tan, "Modeling active microwave remote sensing of snow using dense media radiative transfer (DMRT) theory with multiple-scattering effects," *IEEE Trans. Geosci. Remote Sens.*, vol. 45, no. 4, pp. 990-1004, Apr. 2007.

[32] H. McNairn, T.J. Jackson, G. Wiseman, S. Belair, A. Berg, P. Bullock, A. Colliander, M.H. Cosh, S.-B. Kim, R. Magagi, M. Moghaddam, E.G. Njoku, J.R. Adams, S. Homayouni, E.R. Ojo, T.L. Rowlandson, J. Shang, K. Goita, and M. Hosseini "The Soil Moisture Active Passive Validation Experiment 2012 (SMAPVEX12): Pre-launch Calibration and Validation of the SMAP Soil Moisture Algorithm", *IEEE Trans. Geoscience and Remote Sensing*, vol. 53, no. 5, pp. 2784 – 2801. 2015.

[33] S.-B. Kim, M. Moghaddam, L. Tsang, M. Burgin, X. Xu, and E. G. Njoku, "Models of L-band radar backscattering coefficients over the global terrain for soil moisture retrieval," *IEEE Trans. Geoscience and Remote Sensing*, vol. 52, pp. 1381-1396, 2014.

[34] L. Tsang, J. A. Kong and K. H. Ding, *Scattering of Electromagnetic Waves, vol. I. Theory and Applications*. Hoboken, NJ: Wiley-interscience, 2000.

[35] M. Kurum, "Quantifying scattering albedo in microwave emission of vegetated terrain," *Remote Sensing of Environment*, vol 129, pp. 66-74, 2013.

[36] L. Tsang, M. C. Kubacsi and J. A. Kong, "Radiative transfer theory for active remote sensing of a layer of small ellipsoidal scatterers," *Radio Science*, vol. 16, no. 3, pp. 321-329, May-June 1981.

[37] M. A. Karam, A. K. Fung and Y. M. M. Antar, "Electromagnetic Wave Scattering from Some Vegetation Samples," *IEEE Trans. Geoscience and Remote Sensing*, vol. 26, no. 6, pp. 799-808, Nov. 1988

[38] F. T. Ulaby and M. A. El-Rayes, "Microwave Dielectric Spectrum of Vegetation – Part II: Dual-dispersion Model," *IEEE Trans. Geoscience and Remote Sensing*, vol. GE-25, no. 5, pp. 550-557, Sep. 1987.

[39] L. Tsang, J. A. Kong, K-H. Ding, C. O. Ao, *Scattering of Electromagnetic Waves, vol. II. Numerical Simulations*. Hoboken, NJ: Wiley-interscience, 2000.

[40] N.S. Chauhan, D.M. Le Vine, and R.H. Lang: 'Discrete scatter model for microwave radar and radiometer response to corn: comparison of theory and data," *IEEE Trans. Geoscience and Remote Sensing*, vol.32, pp. 416-426, 1994.

[41] M.C. Dobson, F.T. Ulaby, M.T. Hallikainen, and M.A. El-Rayes, "Microwave Dielectric Behavior of Wet Soil-Part II: Dielectric Mixing Models," *IEEE Trans. Geoscience and Remote Sensing*, vol.GE-23, pp. 35-46, 1985.

[42] K. Sarabandi, Senior, T.B.A., and F.T. Ulaby: “Effect of Curvature on the Backscattering from a Leaf,” *Journal of Electromagnetic Waves and Applications*, vol.2, pp. 653-670, 1988.

[43] A.D. Vecchia, P. Ferrazzoli, and L. Guerriero: “A model study of leaf curvature effect on microwave vegetation scattering,” *IEEE International Geoscience and Remote Sensing Symposium(IGARSS)*, vol.2, pp.1341-1343, Toulouse, France, Jul.21-25, 2003.

[44] H. Huang, S.-B. Kim, L. Tsang, X. Xu, T.-H. Liao, T. J. Jackson, S. Yueh, “Coherent Model of L-band Radar Scattering by Soybean Plants : Model Development, Evaluation, and Retrieval,” submitted to JSTARS [under revision]

[45] J.-S. Lee and E. Pottier, Polarimetric Radar Imaging : From Basics to Applications. Boca Raton, FL, USA : CRC Press, 2009.

[46] K.-S. Chen, L. Tsang, K.-L. Chen, T.-H. Liao, and J.-S. Lee, "Polarimetric Simulations of SAR at L-Band Over Bare Soil Using Scattering Matrices of Random Rough Surfaces From Numerical Three-Dimensional Solutions of Maxwell Equations." IEEE Transactions on Geoscience and Remote Sensing,, vol.52, pp.7048-7058, 2014.

[47] F. T. Ulaby and C. Elachi, ed., *Radar Polarimetry for Geosceience Applications*, Artech House, 1990.

[48] S. Allain, L. Ferro-Famil, E. Pottier,I. Hajnsek, " Extraction of surface parameters from multi-frequency and polarimetric SAR data," *IEEE International Geoscience and Remote Sensing Symposium*, vol.1, pp. 426 - 428, 2002.

[49] I. Hajnsek, E. Pottier, and S. R. Cloude, “Inversion of Surface Parameters from Polarimetric SAR,” *IEEE Trans. Geosci. Remote Sens* , vol. 41, pp.727-745,2003

[50] I. Hajnsek, T. Jagdhuber, H. Schon, and K. P. Papathanassiou, "Potential of estimating soil moisture under vegetation cover by means of PolSAR," *IEEE Trans. on Geosci. Remote Sensing*, Vol. 47, No. 2, 442-454, 2009.

[51] T. Jagdhuber, I. Hajnsek, A. Bronstert, and K. P. Papathanassiou, "Soil moisture estimation under low vegetation cover using a multi-angular polarimetric decomposition," *IEEE Trans. on Geosci. Remote Sens*ing, Vol. 51, No. 4, 2201-2214, 2012.

[52] S. R. Cloude, *Polarisation: Applications in Remote Sensing*, Oxford University Press, 2009.